Photoluminescence Properties of Open and Closed Shell Uranium Compounds in Non-Aqueous Media

Emtithal Hashem

Doctor of Philosophy

University of Dublin, Trinity College

Supervisor: Robert Baker

Submitted to the University of Dublin, Trinity College

July 2013

Declaration

I hereby declare that this thesis has not been submitted as an exercise for a degree at this or any other university and it is entirely my own work.

I agree to deposit this thesis in the University's open access institutional or allow the library to do so on my behalf, subject to Irish Copyright Legislation and Trinity College Library conditions of use and acknowledgment.

Summary

Luminescence spectroscopy has been successfully applied to elucidate the photophysical properties of a family of uranium halides and pseudohalides, in two oxidation states (U^{IV} and U^{VI}) in non-aqueous media. The first example of the room temperature emission spectroscopy of uranium(IV) in non-aqueous media is reported and the limitations of the luminescence spectroscopic technique and the influence of the geometry on the photophysical properties were investigated. Such compounds were selected in order to avoid any possible quenching of the excited state, which may arise from an aromatic group or conjugated entities. Ligand centered charge transfer bands in the visible region were also important to avoid since they provide another quenching pathway.

From the absorption spectra, electronic transitions were assigned with the aid of a comprehensive computational study using CASSCF and CASPT2 techniques. In the case of uranium(IV) halide complexes, excitation into a band of charge transfer and *6d* orbital character led to inefficient electron transfer into the *f-orbital* manifold resulting in broad bands ranging from 360 – 520 nm. When "non-innocent" thiocyanate metal complexes were examined, excitation into the band of the ligand chromophore (230 - 340 nm) was again followed by inefficient electron transfer and subsequent de-excitation through the *f*-orbital manifold. In both cases featureless broad bands (360 - 520 nm) were observed in the emission spectral profile that have short-lived luminescence lifetime (~3 - 10 ns). Therefore the use of emission spectroscopy to fingerprint the U(IV) oxidation state has been proved for the first time. To prove the validity of this technique complexes containing a non-innocent ligand such as bipyridine in $[Et_4N][U(NCS)_5(bipy)_2]$ were examined. Electronic absorption and infrared spectroscopy corroborated the emission spectroscopy, and variable temperature magnetic measurements and theoretical calculations were used in order to confirm the oxidation states of both metal and ligand.

Probing the degree of covalency in the actinide-ligand bond by monitoring the $^1S_0$ state, using optical spectroscopy, was not straightforward and not possible in the case the uranium complexes studied in this thesis. This is due to the fact that the $^1S_0$ state is buried under the charge transfer bands. However, the charge transfer band can be used to sensitise the emission as an "antenna", commonly used in lanthanide luminescence spectroscopy, providing the ligand charge transfer bands are in the UV region.

Finally, the observation that emission spectra of U(IV) can be measured in the presence of uranyl species offers a substantial benefit for uranium detection in environmental samples, using luminescence spectroscopy, although a higher concentration sample of U(IV) complexes maybe required. In addition, the local coordination environment of closed shell uranyl complexes and the nature of ligand-to-metal charge transfer ands are explored and are related to the bond strength of these complexes. Overall, the work presented in this thesis provides a new diagnostic tool for the characterisation of uranium species in non-aqueous solutions using a combination of different spectroscopic techniques. This has the potential for creating a method for the *in situ* examination and identification of actinide/actinyl species during the extraction processes used during the nuclear waste reprocessing cycle.

Acknowledgments

I would like to thank my supervisor Ass. Prof. Robert Baker for all his support and guidance throughout this project. Thank you for the rather challenging project that kept my brain active during the four years.

I would also like to thank many people that without their help this project would not have seen the light. Thanks to Prof. Carola Schluzke (Greifswald University), Prof. John Kelly (TCD), Prof. Franti Hartle (Reading University), Ass. Prof. Rachel Evans (TCD), Dr. Munuswamy Venkatesan (TCD), Dr. Andrew Kerridge (UCL) and Dr. Jamie Platts (Cardiff University). I would also like to thank Dr. Louise Natrajan and her entire group for their help during my visit to Manchester and for having me in their Christmas party. I would like to thank the German Academic Exchange Service (DAAD) for funding me to have a good two months of hard work and fun in Germany. A big thank you to Prof. Karsten Meyer and his group at Friedrich Alexander University in Erlangen for allowing me to join their group and for looking after me during my visit.

I would like to thank Trinity College, Dublin for funding and all the staff in Trinity College for their friendliness. I would like to thank Dr. John O'Brien and Dr. Tom McCabe for all their help. Many thanks to Dr. Manuel Ruether for being the king of all the instruments I have had to use during my project in the college.

I would like to thank every person who had an impact on my life, many Irish people for their overwhelming hospitality, their kindness and sense of humor that put a smile on my face every day I spent in Ireland, in particular my dear friends Lyn and Aoife. Thanks to Ronan for helping me procrastinate during the long nights we spent in the write-up room, Paul Duffy for being Paul Duffy, Aurora Walshe for being a great lab mate.

I would like to thank two very special ladies that have been very kind to me during my study in Ireland; Phyllis for all the retail therapy trips and Mary for looking after me and for treating me like the daughter she never had.

Last but not least I would like to thank my family for their support, in particular my Mom and Dad.

Table of Contents

List of Appendices

List of Figures

List of Tables

List of Schemes

List of Abbreviations

α	alpha
β	beta
γ	gamma
°C	degrees Celsius
λ_{max}	wavelength of maximum absorption
λ_{ex}	excitation wavelength
λ_{em}	emission wavelength
δ	chemical shift in ppm
τ	lifetime
a.u	arbituary units
Å	Angstrom
AC	alternating current
AIM	atoms in molecules
An	actinide
BCP	bond critical points
Bipy	2,2'-bipyridine
ca.	circa
CASSCF	complete active space self-consistent field
CFT	crystal field theory
CT	charge transfer
DFT	density functional theory
EPR	electron paramagnetic resonance spectroscopy
EXAFS	extended X-ray absorption fine structure

HOMO	highest occupied molecular orbital
K	kelvin
LMCT	ligand to metal charge transfer
Ln	lanthanide
LUMO	lowest unoccupied molecule orbital
LS	Russell-Saunders
MeCN	acetonitrile
MLCT	metal to ligand charge transfer
mmol	millimoles
mg	miligram(s)
MPt	melting point
NBO	natural bonding orbital
NIR	near infrared-spectroscopy
nm	nanometer
NMR	nuclear magnetic spectroscopy
OTTLE	optically transparent thin layer electrochemical cell
ppm	parts per million
Py	pyridine
S	second
SMM	single molecular magnet
SQUID	superconducting quantum interference device
T	tesla
THF	tetrahydrofuran
TM	transition metal
TRLIFS	time-resolved laser induced fluorescence spectroscopy

Uv-Vis	ultraviolet-visible
V	volt
XANES	X-ray absorption near edge structure

Chapter 1

Introduction

1.1 Overview

The electronic and magnetic behaviour of almost every element of the d-block transition metals is by now well understood.[1] F-block metals however are still drawing researchers' attention due to their interesting physical and chemical behaviour.[2] The *4f* (lanthanide) and *5f* (actinide) series follow transition metals (TM) in some of their behaviour. For instance in the formation of coloured metal-ligand complexes due to *f-f* transition (*d-d* transition in TM), the existence of the metal ion in many oxidation states due to relatively low energy of *f*-orbitals (*d* in TM) and the formation of paramagnetic compounds due to the presence of unpaired *f* electrons (*d* in TM).[3] However, while the chemistry of lanthanides have seen great progress over the years,[2k-t] the chemistry of actinides is still lacking and despite all the studies there are still many questions to be answered and many debates over, for example, the number of electrons in valence states; magnetism; angular momentum coupling and the character of the metal-ligand bonding in actinide compounds.

All actinides are radioactive and release energy upon radioactive decay. They exist as either alpha emitters (Th, U, Np, Pu, Am, Cm, Es, Fm) or beta emitters (Ac, Bk, Pa, Cf). However, Thorium and uranium are the only naturally occurring alpha emitters actinides and are the most amenable to experimental work.[4] The majority of reported studies of actinide chemistry were based upon the chemistry of uranium as the toxic and radioactive nature of the later actinides makes it difficult and expensive to investigate and study experimentally. The absence of sufficient experimental data has therefore led to increased theoretical work on actinide chemistry.[5] Regardless, the lack of a healthy body of experimental data from which to validate the theory and the difficulty of the physics involved somewhat hinders real progress in understanding the chemistry of actinide ions and their compounds.[6]

Actinides form the basis of nuclear energy and are used as fuel in a nuclear reactor. In 2011, nuclear power provided 10% of the world's electricity[7] which fell by 4.3% after the Fukushima nuclear disaster.[7] Debates about the use of nuclear fission to generate heat and electricity is ongoing and radioactive waste comprising of actinides and other material from nuclear reactors remains a major environmental concern due to their radiotoxicity as alpha emitters with very long half-lives.[8] This makes understanding the chemical and physical behavior of actinides and their ion complexes is both environmentally and scientifically important and originate the driving force for the ongoing research. Spectroscopically, investigations of the chemical and physical properties of actinides have witnessed significant progress in research activities over the past few years.[2a-j] The accessibility to more reliable and highly sensitive techniques made it possible to study the unique properties of the actinide compounds and their interaction mechanism in aqueous, mineral and organic phases. Spectroscopic investigation using techniques such as X-ray Photoelectron Spectroscopy (XPS)[9], Diffuse Reflectance Infrared Fourier Transform Spectroscopy (DRIFT)[10], X-ray Absorption Spectroscopy (XAS)[11], Extended X-ray Absorption Fine Structure (EXAFS)[11,12] and X-ray Absorption Near Edge Structure (XANES)[12b] allow good basis to understanding the structural difference of actinide metal ions and their compounds leading to a better approach of radioactive waste treatment. Quantum chemistry, theoretical calculation and prediction of orbitals participation in bonding have also received great attention in the field of actinide chemistry and have been used extensively to support experimental verdicts.[5,13] Using theoretical studies such as the Hartee-Fock method, Density Functional Theory (DFT)[14] and the Complete Active Space Self-consistent Field (CASSAF)[15] method, one can determine the ground state wave function[16] taking into account core electrons and predict the contribution of the *f* electrons in chemical bonding.[17]

More recently, luminescence spectroscopy has been applied to study the electronic properties of a number of well-defined actinide complexes.[2a-j] Although, in theory, all actinide ions are emissive, it is only recently that their emission properties in solution and at different oxidation states have begun to be explored.[18] In comparison with their lanthanide[2k-u] and transition metal[1] counterparts, actinides luminescence properties are poorly understood. Their significant role in nuclear power production makes it important to understand their electronic structure and chemical behaviour. Furthermore, the sensitivity of the luminescence spectroscopic techniques makes it a desirable choice for the characterisation of highly radioactive materials in very small quantities. In this thesis, for the first time the photoluminescence properties of some simple uranium(IV) coordination compounds are investigated, and with the help of computational theory, their electronic structure is studied.

1.2 Actinides in Nuclear Energy

Nuclear energy production is considered to be a clean energy supply and it is predicted that if nuclear energy is to become the prime source of energy supply for the next 50 years, then the earth's carbon dioxide emissions could be halved.[19] However, there remains to be many environmental concerns with regards to the safety of nuclear power plants and the radioactive waste produced as a result of nuclear fission process.[19] Nuclear waste is often divided into different catagories. For example in the UK there are three types of nuclear fission waste: Low-Level Waste (LLW) in the form of contaminated material,[20] Intermediate-Level Waste (ILW) and the more problematic High-Level Waste (HLW) including Spent Nuclear Fuels (SNF), Transuranic Waste (TRU) and by-products of nuclear reprocessing, which consist of different isotopes of highly radioactive material, such as neptunium-237 and plutonium-239 with very long half-lives.[20] Table 1.1 lists the different isotopes of each actinide metal and the half-life of the most long-lived isotope.

Early Actinides							
Metal	**Ac**	**Th**	**Pa**	**U**	**Np**	**Pu**	**Am**
Isotopes	225, 227-228	226-232, 234-235	231, 233-236	232-240	237-240	238-240, 242, 244	241-245
Longest-lived Isotope	227	232	231	238	237	244	243
Half-life /year	21.8	14b	32500	4.47b	2.14m	80.8m	7370
Later Actinides							
Metal	**Cm**	**Bk**	**Cf**	**Es**	**Fm**	**Md**	**No**
Isotopes	242-249	249-250	249-253	252	257	258	259
Longest-lived Isotope	247	247	251	252	257	258	259
Half-life /year	15.6m	1400	900	1.29	100.5	52days	58min

Table 1.1: The mass of existing isotopes of actinide metals and the half-life of the most long-lived isotope (shown in year for Ac - Fm, m: million and b: billion)[21]

After Neutron irradiation, Spent Nuclear Fuel (SNF) consists of a large amount of radioactive isotopes that can no longer be used in sustaining the nuclear reaction. It typically consists of 95 % ^{238}U, 1 % ^{235}U, 1-2 % Pu isotopes, 2-3 % radioactive fission products and less than 0.1 % of other trans-uranic elements.[7] Management of spent nuclear fuel is a major concern and waste can either be disposed of or reprocessed. Currently, nuclear waste in the United States is stored in cooling pools of nitric acid and in dry storage casks at nuclear power plants.[22] This waste remains a hazard for tens of thousands of years.[23] Moreover, the pools are running out of space and with the United States government decision to drop the plan of burying the waste deep underground in the Yucca Mountains left the U.S. without a path that could eventually lead to a permanent place to store radioactive waste.[24] An alternative route to deal with spent nuclear fuel is to reprocess and re-use the fissile material to ultimately reduce both the volume and the activity of high level radioactive nuclear waste. However, in the U.S., concerns of nuclear weapon proliferation led to suspending indefinitely the commercial reprocessing and recycling of plutonium. Processing is still the chosen route for reducing nuclear waste in Europe. It currently takes place at Sellafield in the UK and waste generated from

the reprocessing method is then vitrified and sealed in stainless steel containers for dry storage above the ground at the Sellafield site.[25] Reprocessing can potentially recover up to 95% of the fissile material in spent nuclear fuel.[26] However, reprocessing requires to chemically isolate fissionable material in the spent fuel by separation processes such as the PUREX solvent extraction[27] (Plutonium and Uranium Reduction EXtraction) which is used to separate uranium and plutonium from the SNF that are then reused for nuclear energy production. After the PUREX separation, the remaining product is a highly radioactive raffinate and contains over 99.9% of the fission product such as lanthanide isotopes, ^{137}Cs, ^{90}Sr, and ^{99}Tc, and the minor actinides ^{237}Np, ^{243}Am, and ^{247}Cm.[28] These must also be separated in order to recycle nuclear fuel as proposed in the "Partitioning and Transmutation" strategy.[29] One important separation task is the isolation of fission product lanthanides.[30] The high neutron absorption cross-section of some of the lanthanide ions present in the SNF means the lanthanide ions effectively compete with the actinides for neutrons during irradiation.[30] Achieving this separation is extremely difficult because of the chemical similarities between the lanthanides and the actinides.[31] A few extraction processes have been established for the separation of material in the PUREX raffinate; those are summarised in Figure 1.1. The UREX[32] (URanium Extraction) process is used for the extraction of the remaining uranium and technetium from the nitric acid solution of the dissolved PUREX raffinate; the UNEX[33] process (UNiversal EXtraction) has the ability to simultaneously extract caesium, strontium and actinides from acidic raffinate solutions, and finally the SANEX[29e,d] (Selective ActiNide Extraction), the TRUEX[34] (TRansUranic Extraction) and the DIAMEX[35] (DIAMide Extraction) solvent extraction processes aim to separate the trivalent actinides (americium and curium) and lanthanide from a high acidity PUREX raffinate solutions.

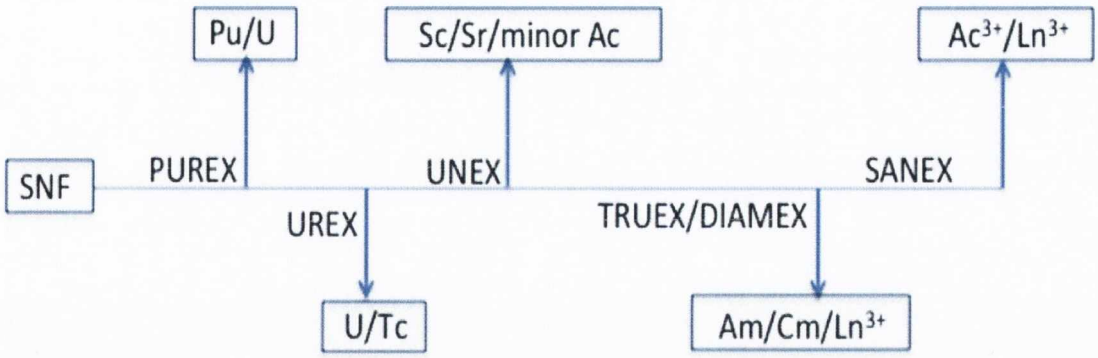

Figure 1.1: Schematic diagram summarising the separation process of SNF

The majority of the available techniques focus on the liquid separation using selective binding of an actinide and/or lanthanide to specific ligands. For example the tridentate N-donor 2,6'-bis-(1,2,4-triazin-3-yl)pyridine ligand[36] (BTP; Figure 1.2a) and its modified tetradentate forms, the 6,6'-bis-(5,5,8,8-tetramethyl-5,6,7,8-tetrahydro-1,2,4 benzotriazin-3-yl)-2,2'-bipyridine ligand[37] ($CyMe_4$-BTBP; Figure 1.2b) and 2,9-bis-(5,5,8,8-tetramethyl-5,6,7,8-tetrahydro-1,2,4-benzotriaz-in-3-yl)-1,10-phenanthroline ligand[38] ($CyMe_4$-BTPhen; Figure 1.1c) showed high selectivity for trivalent actinides over trivalent lanthanides with no alteration to lanthanide speciation[39] and despite problems they may suffer such as poor stability, slow extraction kinetics, and inefficient back-extraction due to high actinides affinities,[40] they demonstrated high potential for selective separation after modification.[38]

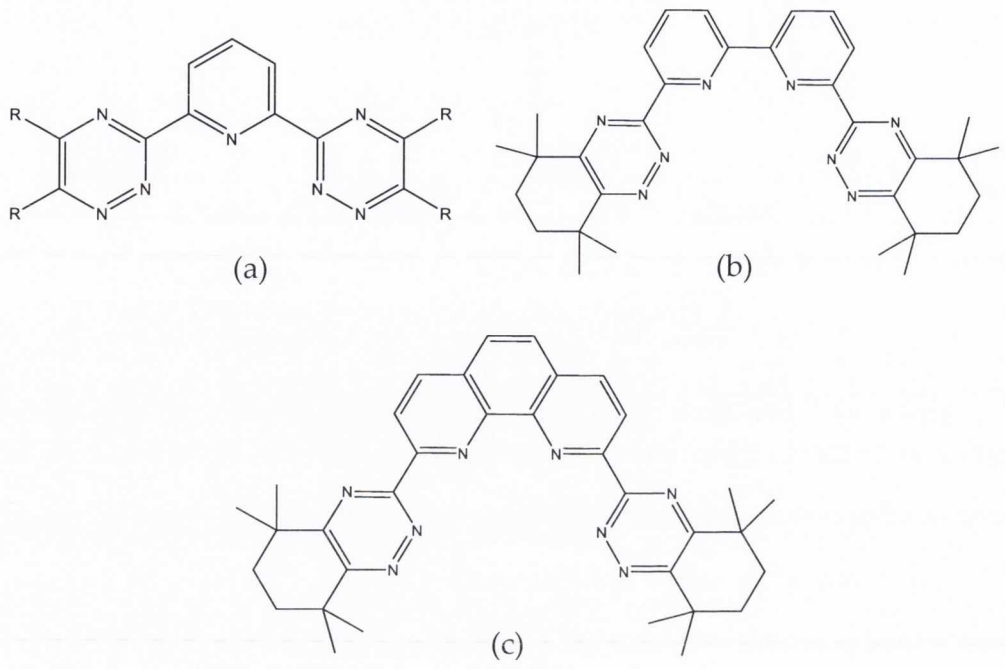

Figure 1.2: Structure of BTP (a), CyMe$_4$BTBP (b) and CyMe$_4$BTPhen (c) ligands

The high charge density of the lanthanides making them "hard" ions results in the selective coordination of a "soft" donor ligand onto the "softer" actinide ions over their lanthanide counterparts.[30] Therefore systems such as the BTP ligand contain softer nitrogen donor and have a higher affinity for trivalent actinides such as Am^{3+} and Cm^{3+} over trivalent lanthanides. The enhanced selectivity is also thought to be due, in part, to a greater covalent character to the actinide-ligand bond[41] arising from orbital overlap of the BTP ligands with the *5f* orbital of actinides. However, recent computational studies cast some doubt on the origins of this perceived covalency and suggest that enhancements in separation factors for the isoelectronic pair Am(III)/Eu(III) in particular are due to the coincidental match of ligand and metal orbitals and not enhanced overlap of the *f*-orbitals. This has been termed "near-degeneracy driven covalency".[42] Therefore, the type of interaction between the *4f* and *5f* ions and the extractant ligands plays a key role in their selectivity and understanding the nature of metal-ligand bonding and chemical behaviour of both actinides and lanthanides towards the extractant is important for further enhancement in the efficiency and selectivity of the extraction ligand, and must be well understood.

1.3 Electronic Structure of Actinide Metals

The f-block elements have unusual electronic configurations which play an important part in their chemical and physical behavior. The similarities of the electronic structure of the actinide and lanthanide is a matter of keen interest and the differences between the actinide and lanthanide metals and their behaviour can be explained with a comparison between the *4f* and *5f* electron shells.[43] Actinides exhibit large ionic radii with degenerate *f* electrons and a small energy gap between *7s*, *6d* and *5f* orbitals supporting a wide range of oxidation states in actinides (+3 to +6) (Figure 1.3) compared to lanthanides (mostly +3) and a higher coordination number than observed in the transition metal elements.[3] For example, thorium is most stable in the +4 oxidation state, and uranium can be found in the +3 to +6 oxidation state.

				+7	+7	+7								
			+6	+6	+6	+6								
		+5	+5	+5	+5	+5	+5							
	+4	+4	+4	+4	+4	+4	+4	+4	+4					
+3	+3	+3	+3	+3	+3	+3	+3	+3	+3	+3	+3	+3	+3	+3
						+2			+2	+2	+2	+2	+2	
Ac	Th	Pa	U	Np	Pu	Am	Cm	Bk	Cf	Es	Fm	Md	No	Lr

An = only found in solid state

An = most stable oxidation state in aqueous solution

Figure 1.3: Actinides oxidation states[3]

OS	Early Actinides						
+2							Am^{2+}
+3	Ac^{3+}	Th^{3+}	Pa^{3+}	U^{3+}	Np^{3+}	Pu^{3+}	Am^{3+}
+4		Th^{4+}	Pa^{4+}	U^{4+}	Np^{4+}	Pu^{4+}	Am^{4+}
+5			$[PaO_2]^+$	$[UO_2]^+$	$[NpO_2]^+$	$[PuO_2]^+$	$[AmO_2]^+$
+6				$[UO_2]^{2+}$	$[NpO_2]^{2+}$	$[PuO_2]^{2+}$	$[AmO_2]^{2+}$
+7					$[NpO_2]^{3+}$	$[PuO_2]^{3+}$	$[AmO_2]^{3+}$
	Later Actinides						
+2			Cf^{2+}	Es^{2+}	Fm^{2+}	Md^{2+}	No^{2+}	Lr^{2+}
+3	Cm^{3+}	Bk^{3+}	Cf^{3+}	Es^{3+}	Fm^{3+}	Md^{3+}	No^{3+}	Lr^{3+}
+4	Cm^{4+}	Bk^{4+}	Cf^{4+}					

Table 1.2: Oxidation states of actinide ions and their approximate colour in aqueous solution[3,44]

It has been suggested that as well as the ionic bonding observed in the metal-ligand interaction in organoactinide complexes, a covalent type bonding can also be observed.[41] This is usually rationalised by the "lanthanide and actinide contraction"; the *5f*-orbitals in the actinide have a large radial extension and are less shielded by *6s* and *6p* electrons than the *4f* orbitals in lanthanides by *5s* and *5p* (Figure 1.4)[45], thus the *5f* orbitals participate more readily in covalent bonding than the *4f* orbitals in lanthanides. In addition, valence electrons in early actinides are less tightly bound and more readily available for bonding, while lanthanides have their *4f* electrons so tightly held as to be chemically inaccessible and therefore only exhibit ionic metal-ligand bonds.[3] However, this covalency decreases with increasing the atomic number, *i.e.* across the series. As a consequence of the large atomic radii of actinides relative to transition metals the filled metal *f*-orbitals in actinides contract making them too deeply hidden beneath the existing upper *s*- and *d*-orbitals to overlap with the ligand orbitals.[3] Thus, for some actinides such as uranium, neptunium and plutonium, the *5f* orbitals are accessible leading to metal-ligand orbital overlap and covalent character. Later actinides (Bk – Lr) possess more contracted *f*-orbitals and behave

like lanthanides in their chemical behaviour and ionic bonding is the only type seen.[46]

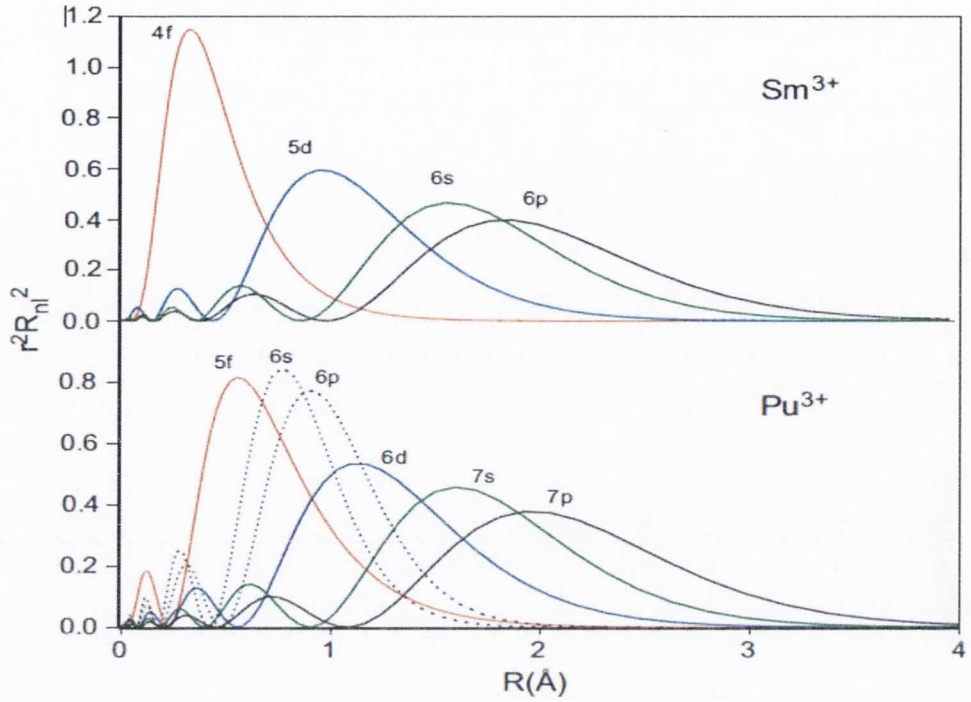

Figure 1.4: The probability of finding an electron at a distance, R, for *f*, *d*, *s* and *p* orbitals[45]

Furthermore, the *5f* and the *6d* orbitals in early actinides are very close in energy and elements can use either the *5f* or *6d* orbitals or both in bonding and therefore the early actinides elements (Ac - Pu), where the atomic ground state can occupy both *5f* and *6d* orbitals (Table 1.3), follow the d-block elements in their chemical behaviour.[47] However across the series the heavier metals have an increased nuclear charge due to addition of electrons in *f*-orbitals. The gap between the *5f* and *6d* orbitals begins to increase in energy until the orbital energies invert, with the *5f*'s becoming lower in energy than the *6d*'s, as a consequence of the localised *f*-orbital only ionic bonding is observed.[47] This has been shown theoretically by Bursten *et al.*[47] as illustrated in Figure 1.5 for the "base free" tris(η^5-cyclopendienyl) actinide complexes Cp_3An.

Actinide	Electronic Configuration	Actinide	Electronic Configuration
Actinium	$6d^1 7s^2$	Curium	$5f^7 6d^1 7s^2$
Thorium	$6d^2 7s^2$	Berkelium	$5f^9 7s^2$
Protactinium	$5f^2 6d^1 7s^2$	Californium	$5f^{10} 7s^2$
Uranium	$5f^3 6d^1 7s^2$	Einsteinium	$5f^{11} 7s^2$
Neptunium	$5f^4 6d^1 7s^2$	Fermium	$5f^{12} 7s^2$
Plutonium	$5f^6 7s^2$	Mendelevium	$5f^{13} 7s^2$
Americium	$5f^7 7s^2$	Nobelium	$5f^{14} 7s^2$
		Lawrencium	$5f^{14} 6d^1 7s^2$

Table 1.3: Ground state electronic configuration of actinides

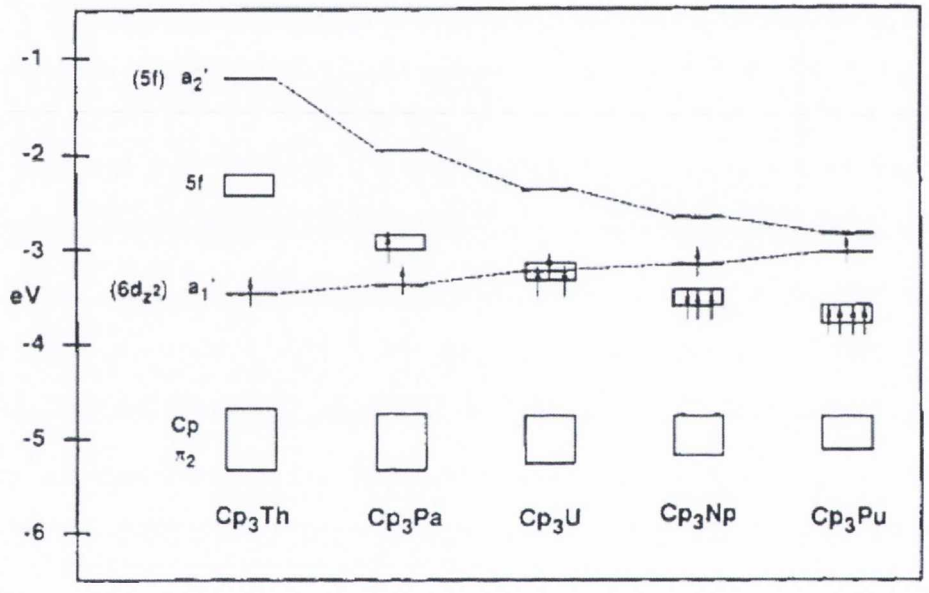

Figure 1.5: Metal-based orbital energies for the $5f^{n-1}6d^1$ ground state electron configurations of planar Cp_3An (An = Th, Pa, U, Np, Pu) complexes[47]

Experimental observations describing the covalency in *5f* metals from optical spectra, thermodynamics of complexation and early separation studies all concluded that the degree of orbital overlap and covalency is highly dependent on the oxidation state and the nature of the ligand.[48] Spectroscopic methods were very successful in quantifying covalency in transition metals.[49] However, matters are more complicated for actinide metals and a number of different experimental techniques along with computational studies usually complement each other in order to provide an insight and a good understanding to covalency by understanding the role the *5f* and *6d* orbitals play in metal-ligand bonding.

Examples of such techniques include Electron Paramagnetic Resonance (EPR) Spectroscopy, which can directly measure the delocalisation of the electron spin density into the ligand valence orbitals and quantify covalency[50] and PhotoElectron Spectroscopy (PES) which provides information on the energies of the occupied molecular orbitals of a complex and the atomic orbitals that constitute the molecular orbitals of the metal complex.[51] Mössbauer Spectroscopy and X-ray absorption spectroscopy (XAS) have also been employed to examine actinides; Mössbauer Spectroscopy can provide information on the shielding of s-orbitals by valence electrons, thereby providing insight into the participation of ligand orbitals in bonding and metal–ligand covalency.[52] However, this technique is only applicable to certain elements of Mössbauer-active nuclei such as ^{237}Np.[52] XAS provides a direct probe of the covalency of a metal–ligand bond by quantifying the amount of ligand *p* character in the primarily metal-based anti-bonding orbitals.[53]

1.4 Photophysical Properties of Actinides

The photophysical properties of lanthanide and transition metals and their complexes have been well defined and their electronic structure, bonding and chemical behaviour have been well understood.[54] The luminescence properties of transition metals and the lanthanides have in particular been extensively explored; studies of the excited state and intermolecular light-induced electron transfer of transition metal complexes are well established for the purpose of their value in solar energy,[55] and in applications such as optical imaging techniques,[56] light emitting devices[57] and protein biology.[58] Understanding both the absorption and the emission spectroscopy of the actinides is believed to help understand their electronic properties and allow access to more efficient separation processes of SNF.

The absorption spectra of both lanthanides and actinides exhibit a lower extinction coefficient than their counterparts of transition metals. However, *f-f* transitions are observed in the absorption spectra of actinides, although *5f–6d* transitions are allowed and are more intense and broad than the *f–f* transitions. Ligand-metal charge transfer (LMCT) transitions are observed in the ultraviolet and visible region and are very intense. Because of the larger vibronic coupling in actinide complexes, one can recognise that actinide compounds have a higher extinction coefficient than lanthanides. Solvation has a significant effect on the optical spectra of actinides and the relative energies of the *5f* and *6d* electrons; for example, charge transfer bands for U(III) in solid state are observed around 30000 cm^{-1} (333.3 nm) and shift significantly to 24000 cm (416 nm) for aqueous U(III).[59]

For many years, emission spectroscopy has been applied in the field of actinide chemistry and the most well defined is the green emission of the uranyl $[UO_2]^{2+}$ ion.[60] However, understanding the photophysical properties of actinide ions and their compounds in solution remain to be a challenge due to their complicated spectroscopic properties when compared to their counterparts of lanthanides and transition metals. For example, while in lanthanide the spin orbit coupling dominates over crystal field effect, in actinides both the spin orbit coupling and electrostatic repulsion must be taken into consideration and therefore an intermediate between both Russell-Saunders (*LS*) coupling and the *j-j* coupling must be used to calculate the energies in actinides[61] (see section 1.4.1).

1.4.1 Spin Orbit Coupling

Spin–orbit coupling and electron correlation effects are extremely important, particularly for understanding spectroscopic properties of metal ions.[62] As discussed above (Section 1.3), ligand-metal bonding in actinides can take place through ligand interactions with the *6d* orbitals of the metal which are strongly split by the presence of a ligand field, but the more contracted *5f* orbitals show only weak splitting.[63] The ground state electron configurations are therefore generally governed by the occupation of these closely spaced *5f* orbitals, which leads to many unpaired electrons that may couple to the open shell ground states.[62] In the Hamiltonian used for electronic structure calculation, angular momenta of multi-electronic system can be coupled by *LS* and/or *j-j* coupling. In transition metals where the spin orbit coupling is weak, the *LS* coupling holds well and atoms exhibit the Hund's rule ground state with maximum *L* and *S* states.[64] The total orbital angular momentum *L* (sum of orbital angular momentum of individual electrons ℓ) couples to the total spin angular momenta, *S* (sum of spin angular momenta of individual electrons) to give the total angular momentum *J*. For heavier elements, spin orbit coupling is much stronger and both *LS* and the *j-j* coupling must be taken into consideration.[3] However, spin-orbit coupling in lanthanides is still weak and the *LS* coupling makes a good model to calculate electronic transitions. In elements with large nuclear charge such as the *5f* actinides elements, the high kinetic energies of the core electrons result in high relativistic effects.[65] An increase in the atomic radii result in an increase in the *s-* and *p-* orbital contractions and in the *d-* and *f*-orbital expansion and will therefore increase the magnitude of the relativistic effects, hence relativistic effects are more pronounced for actinides than in lanthanides and the valence *5f* electrons are very weakly bound and chemically more active than their counterparts *4f* electrons.[65] Relativistic effects give rise to large spin-orbit interaction and thus the *j-j* coupling, where each electron orbital, ℓ, and spin angular momenta, s, couple to form individual electron angular momenta *j*,

which then couples to other electron angular momenta to give the total angular momentum *J*.[65] However, for actinide ions this is not straight forward and the *LS* coupling and *j-j* coupling depend so much on the electronic configuration of the ion. For example, uranium is considered to be the heaviest element that falls into the *LS* coupling curve. Its strong spin-orbit coupling is masked by the degree of localisation of the *5f* orbitals and therefore uranium in its +4 and +6 oxidation state exhibits *LS* coupling to about 80% and 90% respectively.[66] Progressing across the table the spin-orbit interaction becomes large enough to mix higher *L* and *S* states into the ground state, yielding intermediate coupling. It is important to note that if the spin-orbit value falls on the *j-j* curve, then the atom has *j-j* coupling, because this is the only way to create a large spin-orbit interaction. However, if the spin-orbit value falls on the *LS* coupling curve, the atom does not necessarily need to have *LS* coupling and an intermediate coupling is used to calculate the energies in actinides.[67]

1.4.2 Photophysical Properties of Actinyl(VI) Ions

Of all the actinide ions the uranyl ion, $[UO_2]^{2+}$, has been the most thoroughly studied due its role in nuclear fuel cycle.[2] The uranyl ion is the most universally existing form of natural uranium in the environment.[7,8] The molecular orbital description of the uranyl ion $[UO_2]^{2+}$, shown in Figure 1.6 is both experimentally and theoretically well understood.[68] Uranyl has a bond order of three arising from interactions of matching symmetries (e.g. σ and π); a U-O σ bond is formed by interaction of the O $2p\sigma$ orbitals with the uranium $6d_{z^2}$ orbitals (σ_g), and a hybrid metal orbital formed by mixing uranium $5f_{z^3}$ with the semi-core $6p_z$ (σ_u). A U–O π bond is formed by interaction of O $2p\pi$ orbitals with U $6d\pi$ (π_g) and $5f\pi$ (π_u) orbitals. The *5f* δ_u and φ_u are non-bonding *5f* orbitals as they have no symmetry match with the ligand orbitals and are the Lowest Unoccupied Molecular Orbitals (LUMO).[68] The π orbitals are lower in energy than the σ orbitals, which have been proved experimentally,[68] due to a small destructive overlap of the *2p* and σ_u orbitals. This molecular orbital structure also

explains the bonding in $[NpO_2]^{n+}$, $[PuO_2]^{n+}$ and $[AmO_2]^{n+}$ (n = 1, 2) ions and 1, 2, and 3 electrons are found in the non-bonding orbitals.[68]

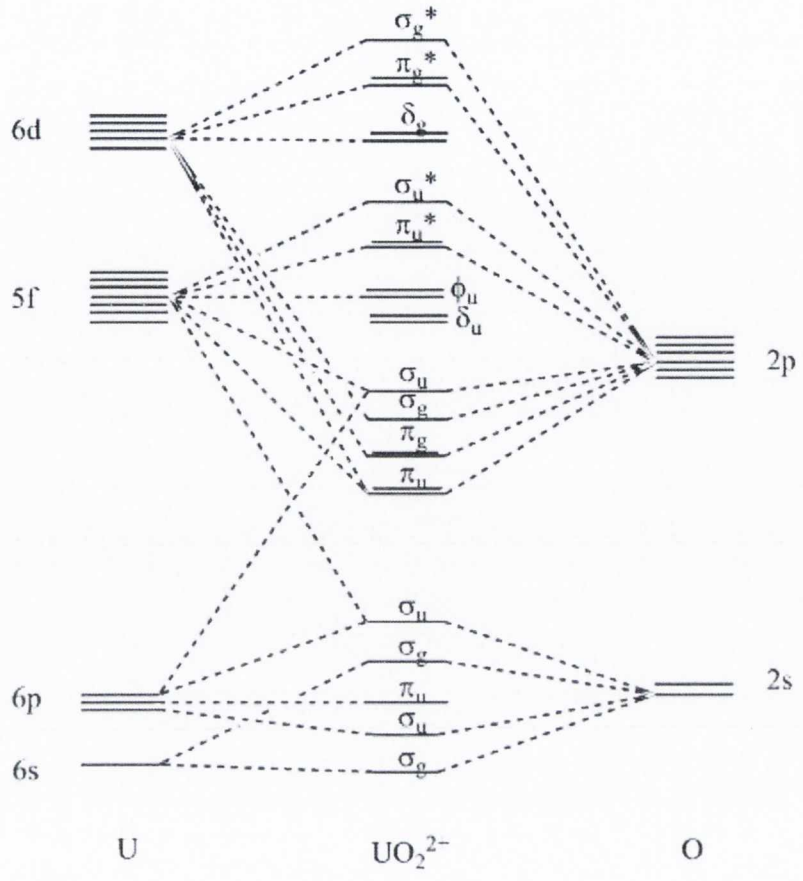

Figure 1.6: Qualitative molecular orbital diagram for $[UO_2]^{2+}$[68]

The photophysical properties of the uranyl ion can be explained by a ligand-to-metal charge-transfer transition involving the promotion of an electron from a bonding oxygen orbital to a non-bonding δ_u and ϕ_u orbital.[2j] $[UO_2]^{2+}$ displays bright green, vibrationally resolved ligand-metal charge transfer emission in aqueous solution and in solid state. The absorption spectra of uranyl(VI) ions show maximum of 12 transitions[69] with the vibrationally resolved band at 420- 500 nm that has been assigned to be a ligand-to-metal charge transfer transition from a bonding oxygen orbital (σ_u, σ_g, π_u and π_g) to a non-bonding uranium *5f*$_\delta$ and *5f*$_\phi$ orbital.[68a] The emission spectra show up to six "hot bands" in both solution and solid state arising from deactivation of the excited triplet state and are centered at about 520 nm.[70] The electronic excited

stated of uranyl(VI) ions are long lived with a lifetime of orders of hundreds of microseconds in solid state and tens of microseconds to nanoseconds in solutions.[71] The ground state Raman active symmetric vibrational O=U=O (ν_1) mode, generally observed between 780 and 900 cm^{-1}, coupled with the $^3\Pi_u$ electronic triplet excited state give rise to the vibrational progression observed in the spectrum of a uranyl(VI) ion.[72]

A number of examples that look at the chemical behaviour of uranyl ions using luminescence spectroscopy have been reported in the literature. For instance, the uranyl(VI) aqua ion has shown to undergo hydrolysis at different pH values forming monomeric hydroxides, dimeric hydroxides and oligomers.[70] Employment of spectroscopic techniques has been proven to be very powerful in identifying different component species present in aqueous solution.[70a] In aqueous solution the aqua ion $[UO_{2(aq)}]^{2+}$ has an absorption maximum at 413.8 nm, and an emission of 488 nm with lifetime of about (τ = 0. 9 ± 0.3 μs), the hydroxide $[UO_2(OH)_2]$ at 421.8 nm and emission of 497 nm with a lifetime (τ = 2.9 ± 0.3 μs) and the oligomer $[(UO_2)_3(OH)_5]^+$ at 429 nm.[70] similarly, speciation of aqueous uranyl(VI) carbonate[70] and sulfates[73] were reported to give both the monomeric $[UO_2(CO_3)]_{(aq)}$, $[UO_2(CO_3)_2]^{2-}{}_{(aq)}$ and $[UO_2(CO_3)_3]^{4-}{}_{(aq)}$ and the trimeric compound $[(UO_2)_3(CO_3)_6]^{6-}{}_{(aq)}$ in the case of the carbonate compounds and mono-$[UO_2SO_4]_{(aq)}$, bis- $[UO_2(SO_4)_2]^{2-}{}_{(aq)}$ and tris-sulfate species $[UO_2(SO_4)_3]^{4-}{}_{(aq)}$ in the case of the latter.[73]

While the electronic properties of aqueous solutions of uranyl(VI) ion have been well explored, the luminescence of uranyl in organic media remains a challenge due to its complexity.[74] The majority of actinide ions in organic solutions are known to be non-emissive at room temperature.[75] This is usually rationalised by the short lived electronic transitions as a result of different coordination organic ligands and solvents which govern the nature of the electronic properties and the radiative lifetime of actinide ions. However, in 1994 Yayamura et al[76] studied the influence of different coordination environment of a series of $[UO_2]^{2+}$ β-diketonate complexes in organic solvent on the energy of the

LMCT excited state.[76] The group concluded that at room temperature the absorption bands of the uranyl(VI) LMCT transitions were masked by the intra-ligand CT absorption bands of the di-ketonate ligands themselves, and that the lifetime of the emission bands depend on the nature of the ligand and the solvent. For example a reduced lifetime from 484 ns to 0.9 ns was observed when replacing the hexafluoroacetylacetone ligand in $[UO_2(hfac)_2THF]$ with acetylacetone in $[UO_2(acac)_2THF]$ which suggest that the nature of the emission spectra with the bands at 500-600 nm are assigned to the uranyl moiety and that the intermolecular energy transfer is LMCT based. Moreover, the significant reduction in the emission intensity and lifetime observed was in accordance to the complexing ability (pK_a value) of the bi-dentate ligand. For example, as the U=O bond distance decreases, the interaction between the atomic orbitals of oxygen and uranium in the forming uranyl molecular orbitals (Figure 1.6) increases, and hence the energy gap between the occupied orbitals, which are localised mainly on the *2p* orbitals of uranyl oxygen, and the unoccupied orbitals, localised mainly on uranium *5f* orbitals, decreases. Consequently, the increasing donation strengthens the uranyl U-O bond, and lowers the energy of the lowest excited state.[76]

The remarkable sensitivity of the LMCT and radiative decay in such compounds to the surrounding environment such as pH in aqueous solutions[68a] and/ or coordinating solvent in organic media,[18a] makes luminescence spectroscopy a suitable tool that would allow following chemical processes that may occur in solutions. For example, in spent nuclear fuel the separation process and the choice of the extractant ligand would highly depend on the nature of the aqueous solution and the chemistry of the metal cation. Understanding the chemical and physical properties of actinyl(VI) compounds and ultimetalty the type of bonding involved in metal-ligand interaction would make a significant contribution to the extraction process in nuclear fuel cycle. As well as being photo-luminescent, the uranyl ion is also photo-reactive and the photo-excited uranyl ion, $[UO_2]^{2+*}$, is highly oxidising as well as reducing,[77] and can readily

undergo photo-reduction in protic solutions. However, the photo excited U(V) radical pair, $[UO_2]^{+*}$, formation is more favourable than the photo-reduced uranyl(V) and the LMCT emission is partially precluded by electron transfer processes of the photo-excited radical pair.[78] Some examples of the luminescence spectroscopy of uranyl(VI) ions are reported in this thesis and the influence of the coordinating ligands and media on the energy of the LMCT bands is studied.

1.4.3 Photophysical Properties of Actinyl(V) Ions

Understanding the chemical behaviour of actinides in their +5 oxidation state is of a great interest for their presence in the environment as a result of their isolation and storage of nuclear waste.[8] For example, the most stable oxidation state of neptunyl in aqueous solution is the +5 oxidation state. The +6 valence state often reduces to the pentavalent state.[79] Other actinides such as U(V) and plutonium(V) are not very common as they are unstable and undergo disproportionation to U(IV) and $[UO_2]^{2+}$ and Pu(IV) and $[PuO_2]^{+}$ in protic media.[80] However, the uranyl $[UO_2]^{+}$ cation can be prepared by chemical, electrochemical and/or photochemical reduction of U(VI),[81] which when monitored spectroelectrochemically[82] shows the formation of $[UO_2]^{+}$ upon photo-reduction of $[UO_2]^{2+}$, seen as a disappearance of the charge transfer bands in the UV-Vis region and the evolution of a broad feature at higher energy, accompanied by a series of sharper *f-f* transition bands at approximately 1818, 1600, 1400, 990 and 760 nm.[83]

The first luminescence study of pentavalent uranyl $[UO_2]^{+}$ ion was reported by Steudner *et al.*[84] Irradiation of U(VI) in aqueous perchlorate solution with a mercury-vapour lamp at λ_{ex} = 245 nm and monitoring with absorption spectroscopy over time showed the formation of a new band at 255 nm which was assigned to be U(V). The corresponding fluorescence emission spectrum, measured using Time-Resolved Laser Induced Fluorescence Spectroscopy (TRLIFS), revealed a band at 440 nm with a radiative lifetime of 1.1 μs.

Grossmann *et al*[85] also investigated the surface alteration of uraninite UO_2 and UCl_4 under aerobic conditions using a combined technique of laser induced fluorescence spectroscopy and confocal laser scanning microscopy. The group reported that excitation at 408 nm resulted in an emission characteristic of U(V) as a result of the one electron oxidation process of UO_2 to $[UO_2]^+$. A second electron oxidation process gave $[UO_2]^{2+}$ as a result of exposure to air and laser source. The lack of examples of luminescence spectroscopy studies of pentavalent actinides and in particular uranium(V) highlights the complexity of the synthesis and characterisation of such species. Moreover the non-stability of the material demands the use of expensive techniques in order to study comprehensively. An example of spectroelectrochemical analysis of an attempt to access the +5 oxidation states of uranium ion via reduction of uranyl(VI) is discussed in Chapter 3.

1.4.4 Photophysical Properties of Actinide(IV) Ions

In contrast with the actinyl(VI) ions, where the participitation of the *5f* orbitals in oxo bonding leaving only non-bonding *5f* orbitals accessible to accommodate the unpaired electrons, in the open shell tetravalent actinide ions, the possibility of participation of *5f* orbitals in the chemical reactions make the electronic structure much more complex and challenging in terms of assigning and predicting transitions observed by the luminescence spectroscopy.[2j] The spin orbit Russell-Saunders coupling derived for trivalent lanthanide ions makes a good starting point for the assignment of electronic transitions for tetravalent actinides. However, unlike the lanthanides, due to the greater radial extension of the *5f* orbital, the position and the character of *f-f* absorption bands are dependent on the coordinated ligands, the coordinated solvent and to some extend the symmetry in actinide complexes.[3] The effect of the symmetry is illustrated in Figure 1.7 where the electronic energies of the free U(IV) ion change considerably for an octahedral symmetry.

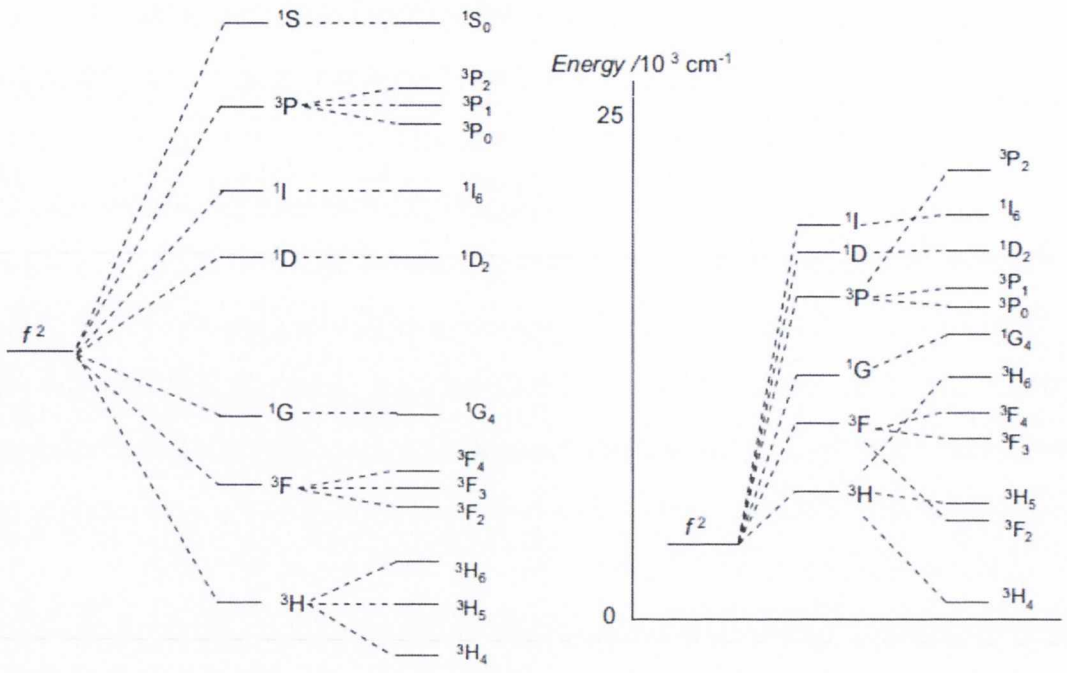

Figure 1.7: A qualitative molecular orbital diagram of the free U(IV) ion showing the effect of electrostatic repulsion and spin orbit coupling (left) and an energy level diagram for the U(IV) ion in an octahedral crystal field (right)[86]

In contrast with actinyl(VI) and An(III), there are only few examples of spectroscopic studies of actinide(IV) in solid state, and only one example of the emission of uranium(IV) in aqueous solution published by Kirishima *et al.* in 2003.[18a,b] The reason for this is that the absolute assignment for electronic transitions in an open shell *5f* compounds is not straightforward. Uranium makes an interesting yet challenging model for its complicated electronic structure; while it has a strong spin orbit interaction, the *5f* states in the metal are delocalised enough to create an *LS* like situation due to mixing of the $j = 5/2$ and 7/2 levels, which are split due to relativistic effect in the *5f* metals.[67] The spin-orbit splitting causes the 5*f* electrons to tend toward a *j-j* coupling mechanism, where the early actinide metals preferentially fill the $j = 5/2$ level and the later actinides fill the $j = 7/2$ level.[87] Hybridisation results in increased mixing of $j = 7/2$ character, and hence reduced spin-orbit interaction Thus, while uranium metal exhibits *LS* coupling, it does in fact have strong spin-orbit interaction, which is

masked by the degree of delocalisation bandwidth of the 5*f* states.[87] The complexity of this makes it challenging to study and characterise experimentally.

Most uranium(IV) compounds are known to be non-emissive, and at room temperature organometallic complexes of uranium compounds usually consist of a coordinating organic ligand and possess low energy broad charge transfer absorptions that mask any weaker *f-f* transitions. However, there are a few examples in the literature that describe the electronic structure of tetravalent actinides. In solid state, for example in the cubic geometry of the doped system U^{4+} in $LiYF_4$,[88] $ThCl_4$,[89] $ThSiO_4$,[89] and Cs_2ZrBr_6,[90] the charge transfer bands in the UV-Vis region and the corresponding emission bands in the visible region were assigned as $5f^16d^1 \rightarrow 5f^2$ electronic transitions from the lowest excited state to different levels of the $5f^2$ manifold, arising from redistribution of valence electrons in the 5*f* sub-shell, with a radiative lifetime of tens of nanoseconds at both room temperature and low temperature (77 K). In the single crystals of $LiYF_4:U^{4+}$, an absorption band observed at 240 nm had seven corresponding emission bands at 262, 282, 304, 328, 334, 438 and 492 nm.[88] They were assigned as transitions between the $^3F_2$ ($5f^16d^1$) excited state and $^3H_4$ ($5f^2$ manifold) ground state and possessed radiative lifetimes of approximately 17 ns at both 300 and 77 K.[88] In solution the only example of luminescence of tetravalent uranium(IV) reported by Kirishima[18a,b] assigned the only band observed in the absorption spectrum to be a charge transfer from $^3H_4 \rightarrow {}^1S_0$ transition and the corresponding emission bands at 525, 409, 394, 345, 338, 320, 318, 291 and 289 nm as transitions from $^1S_0$ highest lying state to lower lying levels $^1I_0$, $^1G_4$, $^3P_0$, $^1D_2$, $^3F_3$, $^3F_4$ and $^3H_5$ with a radiative lifetime of all bands of less than 20 ns at room temperature and 149 ns at liquid nitrogen temperature (77 K).

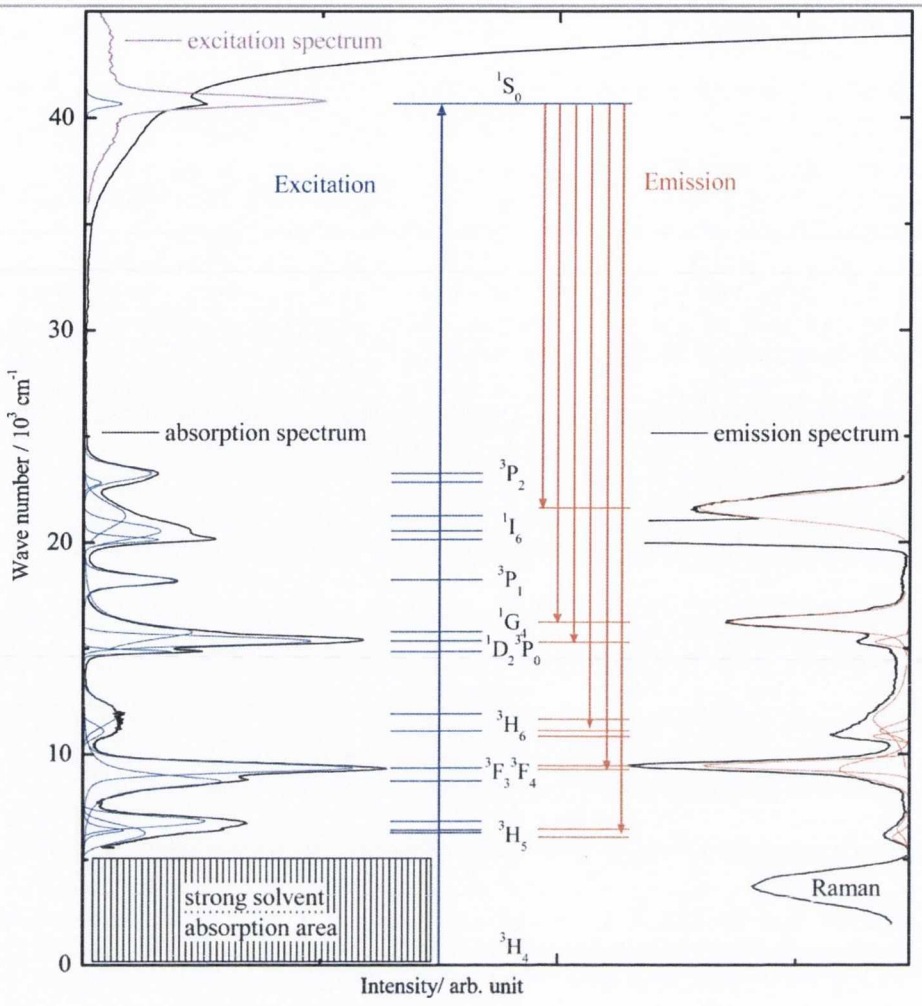

Figure 1.8: Transition energies of the U^{4+} ion in aqueous perchlorate medium reported by Kirishima[18b]

The absorption and emission profile for aqueous U^{4+} ion in acidic solution reported by Kirishima is shown in Figure 1.8.[18b] The emission bands mirrored the absorption bands and the excitation spectra of all emission bands was identical, suggesting that emission arises from de-excitation of the $^1S_0$ state only. It is important to note that this is the only example of fluorescence of uranium(IV) in solution. It highlights the fact that changing the nature of the anion (perchloride, chloride and sulphate) results in a small difference in the emission spectra as a result of a change in local symmetry and crystal field effect. This illustrates that the spectroscopic properties of uranium(IV) complexes are highly dependent on the coordinating environment and solvent. More details on the fluorescence of open shell tetravalent uranium compounds in solutions are discussed in Chapter

2 of this thesis including the first example of comprehensive experimental and computational study of uranium(IV) compounds in organic solvents.

1.4.5 Photophysical Properties of Actinide(III) Ions

The absorption spectra of trivalent *5f* ions are dominated by intra-configurational *f-f* transitions.[91] Those are Laporte forbidden by the electric dipole operator, but some are magnetic dipole and/or electric quadruple allowed as a result of the mixing of the *f* and *d* states and mixing of spin orbit coupled states.[91] The increased spin orbit interaction and mixing of the *J* states in actinides result in a reduction of the overall range of energy for transitions between different states in the *5f* series relative to the *4f* series.[92] The energy gaps between the *J* states are very small in actinides compared to lanthanides and the radiative lifetime of the emissive states in actinides are reduced by fast non-radiative transitions through the *5f* manifold mediated by photons.[18]

Luminescence spectroscopy showed great success in the analysis and detection of trivalent actinides in environmental samples. Trivalent actinides are common radioactive products of nuclear fuel cycle and their physical and chemical similarities with their trivalent lanthanides counterparts, another major product of spent nuclear fuel, make understanding their electronic behaviour of great interest and importance. For example, one very important Time Resolved Laser Induced Spectroscopy (TRLIFS) study reported beneficial to the extraction process of spent nuclear fuel is the determination of the hydration number of Cm^{3+} and lanthanide(III) complexes of the organic CYANEX ligands carried out by Rao and co-workers.[93] Based on the number of inner-sphere water molecules, it was possible to determine the composition of the extracted species, and hence the number of water molecules bound in each complex.

The most extensive investigations of actinide luminescence spectra have been carried out for the +3 actinide ions doped into single crystal $LaCl_3$.[92] A few examples of trivalent actinide luminescence spectroscopy were reported in the literature with the first TRLIFS of Am^{3+} in aqueous solution reported by Beitz *et al.*[94] and Yusov *et al.*[95] They both reported four emission bands between 570 and 1100 following the excitation at λ_{ex} = 503 nm that were assigned to *f-f* transitions originating from the $^5D_1$ state of Am^{3+} to $^7F_0$, $^7F_1$, $^7F_2$ and $^7F_3$. Many examples of time resolved fluorescence spectroscopy followed on for Cm^{3+} in different systems,[96] all of which reported an emission band at 590 nm following the excitation at ca. 380 nm with radiative lifetime of tens of microseconds depending on the system and media. To date, there is no emission spectrum reported for U(III) compounds. However, the developments of faster laser sources and more detection systems will undoubtedly lead to studies of the weaker near infrared transitions and the much shorter-lived emission bands in the future.

1.5 Magnetic Properties of Actinide Ions

The magnetic properties of actinide ions and compounds arise from the spin and orbital angular momenta of the unpaired electrons;[61] in 1932 Van Vleck provided the theoretical basis of understanding magnetic properties of actinides.[97] When accompanied with optical spectroscopic data, where the properties of the energy level in a magnetic field can be calculated, magnetic susceptibility data can be used to determine information on energy levels and their wave functions. For example, using optical data one can calculate the symmetry and crystal field splitting of the ground state. Information on the ground crystal field state, the low lying states, and possibly the first excited state, can then be determined using magnetic data such as temperature-dependent magnetic susceptibility measurements and electronic paramagnetic resonance (EPR) measurements. Moreover, the nature of the metal-ligand bond can be probed by looking at the ligand superhyperfine coupling[98] using double

resonance (electron nuclear double resonance, ENDOR) and pulsed (electron spin echo envelope modulation, ESEEM) EPR methods. Using such methods the delocalisation of the electron spin density into the ligand valence orbitals can be directly measured from the amplitude and anisotropy of the resulting superhyperfine coupling, hence covalency can be quantified.[98]

1.5.1 Magnetic Susceptibility of Actinide Ions

Superconducting QUantum Interference Device (SQUID) has recently been widely used to study the magnetic properties of actinide ions.[99] Variable temperature magnetic susceptibility measurements are very important and are very informative when investigating the magnetic field effect on the electronic structure of actinide ions. For example, the thermal population of different energy sublevels is highly dependent on the temperature due to the electronic complexity and low temperature depopulation of sublevels leads to a concomitant decrease in the magnitude of the angular momentum vector which manifests as a decrease in the magnetic susceptibility.[89]

Magnetic susceptibility measurements have been utilised in this thesis of a way of confirming the oxidation state of uranium compounds. Magnetic susceptibility data are usually presented by a plot of the molar magnetic susceptibility, χ_M, vs. the inverse of the temperature in Kelvin, 1/T, which is often linear over a particular range of temperature, and the effective moment can ultimately be calculated ($\mu_{eff} = 2.828\ (\chi_M T)^{1/2}$). Interpretation of the magnetic data for actinide compounds, in particular for open shell systems, is complicated and the literature lacks good theoretical foundation for accurately modeling the complex interactions that govern the magnetic properties of actinide compounds. This can be reasoned to the fact that the spin-only approximation that works well for the first row transition metals loses its validity due to the large spin-orbit coupling and relativistic effect in actinide compounds.[100] This is because neither the Russell-Saunders' method nor the *j-j* coupling method alone

accurately describes the electronic structure of actinides, so an intermediate coupling scheme is used when interpreting their magnetic properties. For an f^n configuration the ground state is determined from both the spin orbit coupling, and the total angular momentum, $^{2s+1}L_J$. Spin-orbit coupling produces an energy splitting based on the total angular momentum, J, (where $J = L + S, L + S - 1, ..., L - S$) and each J level has a $2J+1$ degeneracy which is split by the crystal field effect. The effect of mixing the J states by the crystal field effect and the degeneracy of the levels is usually determined by the symmetry.

Temperature-dependent paramagnatism for actinides in open shell systems such as uranium(IV) compounds ($5f^2$, $^3H_4$ ground state) is also dependent on the symmetry of the compounds. For example, in an octahedral geometry, only the second-order Zeeman term is observed and mixing of the $^3T_{1g}$ excited state into the ground state results in temperature-independent paramagnetism. When the symmetry of an octahedral uranium(IV) ($5f^2$ and $^3H_4$ ground state) is lowered e.g. from O_h to D_{4h}, a splitting of the $^3T_{1g}$ excited state, is observed and both first and second order Zeeman effects contribute to the susceptibility and temperature-paramagnetism depends on the splitting of the $^3T_{1g}$ excited state, the value of ΔE and the thermal population of these excited states.[59] Figure 1.9 shows the effect of crystal field interactions of the $5f^2$ configuration of two different symmetries.[59]

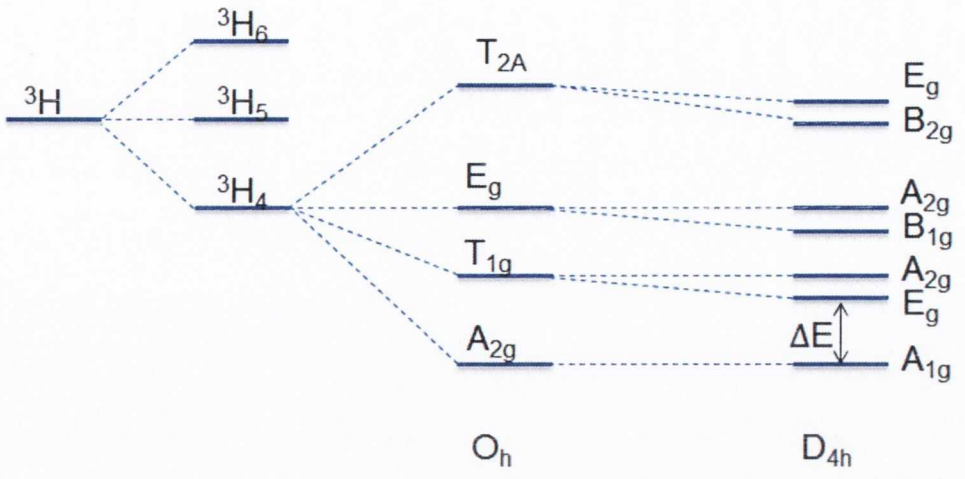

Figure 1.9: Energy level diagram showing crystal field splitting effect on the ground state only for an O_h symmetry and D_{4h} symmetry

For a $5f^1$ system, the absence of electron repulsion makes the magnetic data easy to interpret and the magnetic susceptibility value for $5f^1$ ions is generally reduced by the mixing effect and the covalency observed in the metal-ligand bonding. For example values of 1.2 μ_B in Na_3UF_8 0.71 μ_B in $CsUF_6$ and 0.403 μ_B in $Th(C_5H_5)_3$.[101] The closed shell system of actinide compounds ions such as $[UO_2]^{2+}$, U^{6+}, Th^{4+} and Pa^{5+} have $^1S_0$ ground state ($5f^0$) and is typically diamagnetic. However, complexes such as uranyl and UF_6 compounds exhibit temperature-independent paramagnetism due to covalent type metal-ligand bonding. Magnetic susceptibility measurement reported by Eisenstein and Pryce[102] concluded that the bonding in UF_6 is partially covalent and that coupling of higher energy excited states into the ground state by magnetic field results in paramagnetism. Similarly, the weak paramagnetism reported by Denning and co-worker for $[UO_2]^{2+}$ was attributed to the coupling of states and nature of the U-O bonding[103] (see MO description in Section 1.4.2).

1.6 References

[1] J. B. Berscker, *Electronic Structure and Properties of Transition Metal Compounds*, Wiley, New York, 1996

[2] For example see a) R. J. Baker, *Coord. Chem. Rev.*, 2012, **256**, 2843; b) O. P. Lamb and K. Meyer, *Polyhedron.*, 2012, **32**, 1; c) P. L. Arnold, *Chem. Commun.*, 2011, **47**, 9005; d) O. T. Summerscales and F. G. N. Cloke, *Struct. Bonding.*, 2008, **127**, 87; e) O. P. Lam, C. Anthon and K. Meyer, *Dalton Trans.*, 2009, 9677; f) T. W. Hayton, *Dalton Trans.*, 2010, **39**, 1145; g) S. T. Liddle and D. P. Mills, *Dalton Trans.*, 2009, 5592; h) S. T. Liddle, *Proc. R. Soc. A.*, 2009, **465**, 1673; i) I. Castro-Rodriguez and K. Meyer, *Chem. Commun.*, 2006, 1353; j) M. Ephritikhine, *Dalton Trans.*, 2006, 2501; j) L. S. Natrajan, *Coord. Chem. Rev.*, 2012, **256,** 1583; k) C. M. Sturza, R. Boscencu and V. Nacea, *Farmacia*, 2008, **3**, 326; l) A. K.Gschneider and L. Eyring: *Handbook of the Physics and Chemistry of Rare Earths*, 1978, Vol I , North-Holland, Amsterdam; m) W. K. Wong, X. Zhu and W. X, *Coord. Chem. Rev.*, 2007, **251**, 2386; n) I. Kostova, G. Momekov, T. Tzanova and M. Karaivanova, Bioinorg. *Chem. Appl.*, 2006, 25651; o) J.–C. G. Bünzli, *Chem. Rev.*, 2010, **110**, 2729; p) K. N. Allen and B. Imperiali, *Curr. Opin. Chem. Biol.*, 2010, **14**, 247; q) E. G. Moore, A. P. S. Samuel and K. N. Raymond, *Acc. Chem. Res.*, 2009, **42**, 542; r) C. M. G. dos Santos, A. J. Harte, S. J. Quinn and T. Gunnlaugsson, *Coord. Chem. Rev.*, 2008, **252**, 2512; s) J. –C. G. Bünzli and S. V. Eliseeva, *J. Rare Earths*, 2010, **28**, 824; t) J. Rocha, L. D. Carlos, F. A. Almeida Paz, and D. Ananias, *Chem. Soc. Rev.*, 2011, **40**, 926; u) M. D. Ward, *Coord. Chem. Rev.*, 2010, **254**, 2634; v) S. Faulkner, L. S. Natrajan, W. S. Perry and D. Sykes, *Dalton Trans.*, 2009, 3890

[3] N. Kaltsoyannis and P. Scott, *The f- elements*, Oxford Primer, 1999

[4] M. E. Weeks, *J. Chem. Ed.*, 1932, **9**, 459

[5] a) G. Schreckenbach and G. A. Shamov, *Acc. Chem. Res.*, 2010, **43**, 19; b) L. Gagliardi and B. O. Roos, *Chem. Soc. Rev.*, 2007, **36**, 893; c) N. Kaltsoyannis, *Chem. Soc. Rev.*, 2003, **32**, 9; d) I. Kirker and N. Kaltsoyannis, *Dalton Trans.*, 2011, **40**, 124; e) M. J. Tassell and N. Kaltsoyannis, *Dalton Trans.*, 2010, **39**, 6719; f) P. L. Arnold, Z. R. Turner, N. Kaltsoyannis, P. Pelekanaki, R. M. Bellabarba and R. P. Tooze, *Chem. Eur. J.*, 2010, **16**, 9623; g) D. Wang, W. F. van Gunsterenb and Z. Chai, *Chem. Soc. Rev.*, 2012,

41, 5836; h) A. E. Clark, J. L. Sonnenberg, P. J. Hay and R. L. Martin, *J. Chem. Phys.*, 2004, **121**, 2563; i) L. Petit, L. Joubert, P. Maldivi and C. Adamo, *J. Am. Chem. Soc.*, 2006, **128**, 2190; j) V. Vallet, U. Wahlgren and I. Grenthe *J. Phys. Chem. A.*, 2012, **116**, 12373; k) B. M. Gardner, D. Patel, A. D. Cornish, J. McMaster, W. Lewis, A. J. Blake and S. T. Liddle, *Chem. Eur. J.*, 2011, **17**, 11266

[6] a) J. Hafner, and D. Hobbs, *Phys. Rev. B.*, 2003, **68**, 014408; b) R. G. Haire, S. Heathman, M. Idiri, T. Le Bihan, A. Lindbaum and J. Rebizant, *Phys. Rev. B.*, 2003, **67**, 134101; c) P. Söderlind and B. Sadigh, *Phys. Rev. Lett.*, 2004, **92**, 185702; d) A. B. Shick, J. Havela, V. D Kolorenc, T. Gouder, and P. M. Oppeneer, *Phys. Rev. B.*, 2006, **73**, 104415

[7] Key World Energy Statistics 2012 Publication

[8] A. W. Murphy, *Q. Rev. Biol.*, 1977, **52**, 467

[9] a) J. Terry, R. K. Schulze, J. D. Farr, T. Zocco, K. Heinzelman, E. Rotenberg, D. K. Shuh, G. van der Laan, D. A. Arena and J. G. Tobin, *Surf. Sci.*, 2002, **499**, L141; b) K. I. Maslakov, A. Y. Teterin, K. E. Ivanov, S. V. Yudintsev and S. V. Stefanovskii, *Radiochemistry*, 2012, **54**, 115

[10] a) C. Zeine and J. Grobe, *Microchimica. Act.*, 1997, **125**, 279; b) M. M. Herron, S. Herron, A. Charsky and R. Akkurt, *From PCT. Int. Appl.*, 2013, WO 2013025679 A2 20130221; c) R. A. Zehnder, D. L. Clark, B. L. Scott, R. J. Donohoe, P. D. Palmer, W. H. Runde and D. E. Hobart, *Inorg. Chem.*, 2010, **49**, 4781

[11] a) D. C. Konningsberger and R. Prins, *X-Ray Absorption: Principles, Application, Techniques of EXAFS, SEXAFS, XANES*, John Wiley and Sons, USA 1988; b) G. Bunker, *Introduction to XAFS: A Practical Guide to X-ray Absorption Fine Structure Spectroscopy*, Cambridge University Press, 2010

[12] a) Gilberto Vlaic and Luca Olivi, Croat. *Chem. Acta.*, 2004, **77**, 427; b) B. K. Teo, *EXAFS: Basic Principles and Data Analysis, Inorganic Chemistry Concepts*, Vol. 9, Springer-Verlag, Berlin, 1986

[13] A. Marjolin, C. Gourlaouen, C. Clavaguera, P. Y. Ren, J. C. Wu, N. Gresh, J. P. Dognon and J. P. Piquemal, *Theor. Chem. Acc.*, 2012, **131**, 1198

[14] a) P. Pyykko and J. P. Desclaux, *Acc. Chem. Res.*, 1979, **12**, 276; b) P. Pyykko, *Chem Rev.*, 1988, **88**, 563

[15] a) B. O. Roos, P. R. Taylor and P. E. M. Siegbahn, *Chem. Phys.*, 1980, **48**, 157; b) K. Andersson, P. A. Malmqvist and B. O. Roos, *J. Chem. Phys.*, 1992, **96**, 1218

[16] W. Koch and M. C. Holthausen. *A Chemist's Guide to Density Functional Theory*, Second Ed., Wiley, New York, 2001

[17] K. T. Moore, *Rev. Mod, Phys.*, 2009, **81**, 235

[18] a) E. Hashem, A. N. Swinburne, C. Schulzke, R. C. Evans, J. A. Platts, A. Kerridge, L. S. Natrajan and R. J. Baker, *RSC Adv.*, 2013, **3**, 4350; b) Kirishima, T. Kimura, O. Tochiyama and Z. Yoshida, *Chem. Commun.*, 2003, **910**; c) A. Kirishima, T. Kimura, R. Nagaishi and O. Tochiyama, *Radiochim. Acta.*, 2004, **92** (Migration 2003, 705); d) R. Bradshaw, D. Sykes, L. S. Natrajan, R. J. Taylor, F. R. Livens and S. Faulkner, *Mater. Sci. Eng.*, 2010, **9**, 012047; e) T. Eeckelaars, S. J. A. Pope, A. J. Hynes, R. Copping, R. J. Taylor, S. Faulkner, D. Sykes, F. R. Livens and I. May, *J. Am. Chem. Soc.*, 2007, **129**, 2442

[19] H. Nifenecker, *Rep. Prog. Phys.*, 2011, **74**, 12

[20] M. Lenzen, *Energ. Convers. Manag.*, 2008, **49**, 2178

[21] J. Emsley. *Nature's Building Blocks: An A-Z Guide to the Elements*, New ed., New York, Oxford University Press, 2011

[22] J. Gray, S. Jones and A. Smith, *J. Radiol. Prot.*, 1995, **15**, 99

[23] V. M. Efremenkov, *An overview of the types of low- and intermediate-level wastes and how they are handled*, IAEA BULLETIN, 1989, **4**, 36

[24] J. Johnson, *Talk, No Action on Nuclear Waste Plan;* in C&EN, 2012, **40**, 44

[25] a) J. Johnson, *Reprocessing Key to Nuclear Plan*; in C&EN, 2007, **85**, 48; b) http://www.environment-agency.gov.uk

[26] N. Baldwin, *Remediating Sellafield* , WM'03 Conference, Tucson, AZ, 2003

[27] J. Mathur, M. Murali and K. Nash, *Solvent Extr. Ion Exc.*, 2001, **19**, 357

[28] I. S. Denniss and A. P. Jeapes, *in The Nuclear Fuel Cycle;* Wilson, P.D., Ed.; Oxford University Press: Oxford, U.K., 1986; 116

[29] a) A. P. Paiva and P. J. Malik, *Radioanal. Nucl. Chem.*, 2004, **261**, 485 b) D. Warin, *IOP Conf. Ser. Mater. Sci. Eng.*, 2010, **9**, 012063; c) Heino Nitsche, *Chem. Rev.*, 2013, **113**, 855; d) C. Madic, M. J. Hudson, J. O. Liljenzin, J. P, Glatz, R. Nannicini, A. Facchini, Z. Kolarik and R. Odoj, *Prog. Nucl. Energy.*, 2002, **40**, 523; e) C. Madic, B. Boullis, P. Baron, F. Testard, M. J. Hudson, J.-O. Liljenzin, B. Christiansen, M. Ferrando, A. Facchini, A. Geist, G. Modolo, A. G. Espartero and J. De Mendoza, *J. Alloys Compd.*, 2007, **444**, 23; f) M. J. Hudson, L. M. Harwood, D. M. Laventine and F. W. Lewis, *Inorg. Chem.*, 2013, **52**, 3414; g) J. P Grouiller, S. Pillon, C. de Saint Jean, F. Varaine, L. Leyval, L, G. Vambenepe and B. Carlier, *J. Nucl. Mater.*, 2003, **320**, 163

[30] a) M. Nilsson and K. Nash, Solvent Extr. Ion Exc., 2007, **25**, 665, b) M. P. Jensen and A. H. Bond, *J. Am. Chem. Soc.*, 2002, **124,** 9870; c) M. Mazzanti, R. L. Wietzke, J. Pecaut, J. M. Latour, P. Maldivi and M. Remy, *Inorg. Chem.*, 2002, **41,** 2389; d) T. Mehdoui, J. C. Berthet, P. Thuery and M. Ephritikhine, *Dalton Trans.*, 2004, 579; e) G. R. Choppin and M. P. Jensen, in: L. Morss, N. M. Edelstein, J. Fuger (Eds.), *The Chemistry of the Actinide and Transactinide Elements*, vol. **4**, Springer, Berlin, 2006, 2562. f) A. J. Gaunt, B. L. Scott and M. P. Neu, *Angew. Chem. Int. Ed.*, 2006, **45**, 1638

[31] a) S. Cotton, in *Comprehensive Coordination Chemistry II*, ed. J. A. McCleverty and T. J. Meyer, Elsevier, Oxford, 2004, vol. **3**, 93–188; b) C. J. Burns, M. P. Neu, H. Boukhalfa, K. E. Gutowski, N. J. Bridges and R. D. Rogers, in *Comprehensive Coordination Chemistry II*, ed. J. A. McCleverty and T. J. Meyer, Elsevier, Oxford, 2004, vol. **3**, 189–332; c) J. J. Katz, L. R. Morss, N. M. Edelstein and J. Fuger, in *The Chemistry of the Actinide and Transactinide Elements*, II ed. J. J. Katz, L. R. Morss, N. M. Edelstein and J. Fuger, Springer, Dordrecht, 2006, vol. **1**, 1–17.

[32] F. Poineau, J. Du Mazaubrun, D. Ford, J. Fortner, J. Kropf, G. Silva, N. Smith, K. Long, G. Jarvinen and K. Czerwinski, *Radiochim. Acta.*, 2008, **96**, 527; b) C. Gong, W. Lukens, F. Poineau and K. Czerwinski, *Inorg. Chem.*, 2008, **47**, 6674

[33] J. Law, S. Herbst, T. Todd, V. Romanovskiy, V. Babainb, V. Esimantovskiy, I. Smirnov and B. Zaitsev, *Solvent Extr. Ion Exc.*, 2001, **19**, 23

[34] E. Horwitza, D. Kalinaa, H. Diamonda, G. Vandegrifta and W. Schulzb, *Solvent Extr. Ion Exc.*, 1985, **3**, 75

[35] D. Serrano-Purroy, P. Baron, B. Christiansen, R. Malmbeck, C. Sorel and J. Glatz, *Radiochim. Acta.*, 2005, **93**, 351

[36] J. C. Berthet, Y. Miquel, P. B. Iveson, M. Nierlich, P. Thuery, C. Madic, and M. Ephritikhine, *J. Chem Soc, Dalton Trans.*, 2002, **16**, 3265

[37] M. G. B. Drew, M. R. S. Foreman, C. Hill, M. J. Hudson, C. Madic, *Inorg. Chem. Commun.*, 2005, **8**, 239

[38] F. W. Lewis, L. M Harwood, M. J. Hudson, M. G. B. Drew, J. F. Desreux, G. Vidick, N. Bouslimani, G. Modolo, A. Wilden, M. Sypula, T. H. Vu and J. P. Simonin, *J. Am. Chem. Soc.*, 2011, **133**, 13093

[39] D. M. Whittaker, T. L. Griffiths, M. Helliwell, A. N. Swinburne, L. S. Natrajan, F. W. Lewis, L. M. Harwood, S. A. Parry, and C. A. Sharrad, *Inorg. Chem.*, 2013, **52**, 3429

[40] a) D. Magnusson, B. Christiansen, M. R. S. Foreman, A. Geist, J. P. Glatz, R. Malmbeck, G. Modolo, D. Serrano-Purroy and C. Sorel, *Solvent. Extr. Ion. Exc.*, 2009, **27**, 97; b) D. Magnusson, B. Christiansen, R. Malmbeck, J. P. Glatz, *Radiochim. Acta.*, 2009, **97**, 497

[41] N. Kaltsoyannis, *Inorg. Chem.*, 2013 **52**, 3407

[42] M. L. Neidig, D. L. Clark, R. L. Martin, *Coord. Chem. Rev.*, 2013, **257**, 394

[43] J. C. Sullivan, L. R. Morss, K. H. Schmidt, W. A. Mulac and S. Gordon, *Inorg. Chem.*, 1982, **22**, 2338

[44] W. T. Carnell and H. M. Crosswhite, in *The Chemistry of The Actinide Elements* (J. Katz, G. Seaborg and L. Morss) V II second Ed., 1986, 1235

[45] G. Schreckenbach, P. J. Hay, R. L. Martin, *J. Comput. Chem.*, 1990, **20**, 70

[46] A. F. Cotton and G. Wilkinson, *Advanced Inorganic Chemistry* 1988, 5th ed., New York: Wiley-Interscience, 776- 955

[47] B. E. Bursten, L. F. Rhodes and R. J. Strittmatter, *J. Am. Chem. Soc.*, 1989, **111**, 2151

[48] a) G. R. Choppin, *J. Alloys Compd.*, 2002, **344**, 55; b) R. M. Diamond, K. Street and G. T. Seaborg, *J. Am. Chem. Soc.*, 1954, **76**, 1461; c) S. G. Thompson, B. G. Harvery, G. R. Choppin and G. T. Seaborg, *J. Am. Chem. Soc.*, 1954, **76**, 6229

[49] V. Balzani and F. Scandola. In Comprehensive Supermolecular Chemistry, J. L. Atwood, J. E. D Davis. D. D. Macnicol and F. Vogtle (eds.), Pergamon, Oxford, 1996, 16 b) V. Balzani , A. Credi and M. Venturi , Chem. Sus. Chem 2008, **1**, 26

[50] B. M. McGarvey, *Electron Spin Resonance of Transition-Metal Complexes*, in: R. L. Carlin (eds.), *Trans. Met. Chem.*, vol. **3**, Marcel-Dekker, 1967, 89

[51] J. P. Clark and J.C. Green, *J. Chem. Soc., Dalton Trans.*, 1977, 505

[52] G. M. Kalvius, *J. Less-Common Met.*, 1986, **121**, 353

[53] E. I. Solomon, B. Hedman, K. O. Hodgson, A. Dey and R. K. Szilagyi, *Coord. Chem. Rev.*, 2005, **249**, 97

[54] For example a) C. Lincheneau, J. P. Leonard, T. McCabe and T. Gunnlaugsson, *Chem. Comm.*, 2011, **47**, 7119; b) X. Sun, Y. Bian, M. Bai, C. Ma, N. Kobayashi and J. Jiang, *Dyes and Pigments* 2005, **65**, 145; c) G. Zucchi, R. Scopelliti, P-A. Pittet, J. C. G Bunzli and R. D. Rogers, *J. Chem. Soc., Dalton. Trans.*, 1999, **6**, 931

[55] a) V. Balzani, F, Bolletta, M. T. Gandolfi and M. Maestri, *Top. Curr. Chem.*, 1978, **75**, 1; b) T. J. Meyer, *Acc. Chem. Res.*, 1978, **11**, 94; c) N. Sutin and C. Creutz, *Pure. Appl. Chem.*, 1980, **52**, 2717; d) T. J Meyer, *progr. Inorg. Chem.*, 1983, **30**, 389; d) N. Sutin and C. Creutz, *J. Chem. Ed.*, 1983, **60**, 809; N. Serpone: in *Photoinduced electron transfer* (M.A. Fox and M. Chanon, eds.), 1988. Elsevier, Amsterdam, part d , p 47; e) V. Balzani and F. Scandola: in *Photoinduced electron transfer* (M.A. Fox and M Chanon, eds.), 1988, Elsevier, Amsterdam, part d , p 148; f) C. Gianotti, S. Gaspard and P. Kransz: In Photoinduced electron transfer (M.A. Fox and M Chanon, eds.), 1988) Elsevier, Amsterdam, part d , p 200

[56] J.-C. G. Bunzli, *Chem. Rev.*, 2010, **110**, 2729

[57] H. You, J. Fang, L. Wang, X. Zhu, W. Huang and D. Ma, Opt. Mater., 2007, **29**, 1514

[58] P. Brossier, G. Jaouen, B. Limoges, M. Salmain, A. Vessieres-Jaouen and J.P. Yvert, Ann. Biol. Clin., 2001, **59**, 677

[59] S. Cotton, *Electronic and Magnetic Properties of Actinides*, in: Lanthanide and Actinide Chemistry, John Wiley and Son Ltd, 2006, p 201

[60] E. Rabinowitch and R. L. Bedford, *Spectroscopy and Photochemistry of Uranyl Compounds*, Pergamon Press, Oxford, 1964, 112

[61] K.T. Moore and G. Van der Laan, *Rev. Modern Phys.*, 2009, **81**, 235

[62] a) B. E. Bursten, R. J. Strittmatter, *Angew. Chem., Int. Ed. Engl.*, 1991, **30**, 1069; b) R. G. Denning, *Struct. Bond.*, 1992, **79**, 215; c) M. Pepper, B. E. Bursten, *Chem. Rev.*, 1991, **91**, 719; e) S. Matsika, Z. Zhang, S. R. Brozell, J. P. Blaudeau, Q. Wang, R. M. Pitzer, *J. Phys. Chem. A.*, 2001, **105**, 3825

[63] N. Kaltsoyannis, P. J. Hay, J. Li, J. P. Blaudeau, B. E. Bursten, in: L. Morss, N.M. Edelstein, J. Fuger (Eds.), *The Chemistry of the Actinide and Transactinide Elements*, vol. **3**, Springer, Berlin, 2006, 1893

[64] M. J. Winter, *d-Block Chemistry*, Oxford Primer, 1994

[65] M. Seth, M. Dolg, P. Fulde, and P. Schwerdtfeger, *J. Am. Chem. Soc.*, 1995, **117**, 6597

[66] Y. Baer, and J. K. Lang, *Phys. Rev. B.*, 1980, **21**, 2060 b) S.B Nornes, and R. G. Meisenheimer, *Surf. Sci.*, 1979, **88**, 191; c) P. Söderlind, and K. T. Moore, *Scr. Mater.*, 2008, **59**, 1259

[67] G. van der Laan, *J. Phys. Condens. Matter.*, 1991, **3**, 7443. B) G. van der Laan, *Phys. Rev. B.*, 1995, **51**, 240

[68] R. G. Denning, *J. Phys. Chem. A.*, 2007, **111**, 4125; b) R. J. Baker, *Chem. Eur. J.* 2012, **18**, 16258

[69] V. V. Syt'ko and D. S. Umreiko, *J. Appl. Spectrosc.*, 1998, **65**, 857

[70] a) G. Meinrath, *Freiburg On-line Geosci.*, 1998, **1**, 1; b) C. K. Jorgenson and R. Reisfeld, *Struct. Bond.*, (Heidelberg) 1982, **50**, 122; c) J. L. Sessler, P. Melfi and G.D. Pantos, *Coord. Chem. Rev.*, 2006, **250**, 816; d) R. Ghosh, J. A. Mondal, H. N. Ghosh and D. K. Palit, *J. Phys. Chem. A.*, 2010, **114,** 5263; e) G. K Liu, *J. Phys. Chem. A.*, 2011, **115,** 12419

[71] I. Billard and G. Geipel, *Luminescence Analysis of Actinides: Instrumentation Application, Quauntifications, Future Trend and Quality Assurance:* in Springer Series, Fluorescence, Springer-Verlag Berlin Heidelberg, 2008, **5,** 465

[72] J. R. Plaisier, D. J. W. Ijdo, C. de Mello Donega and G. Blasse, *Chem. Mater.*, 1995, **7,** 738

[73] T. Vercouter, P. Vitorge, B. Amekraz and C. Moulin, *Inorg. Chem.*, 2008, **47**, 2180

[74] Z. Hnatejko, S. Lis and Z. Stryla, *J. Therm. Anal. Calorim.*, 2010, **100**, 253

[75] a) F. de Maria Ramirez, S. Varbenev, J. Padilla and J. C. G. Búnzli, *J. Phys. Chem. B.*, 2008, **112,** 10976; b) S. Kannan, M. A. Moody, C. L. Barns and P. B. Duval, *Inorg. Chem.*, 2006, **45**, 9206; c) A. E. Vaughn, D. B. Bassil, C. L. Barnes, S. A. Tucker and P. B. Duval, *J. Am. Chem. Soc.*, 2006, **128,** 10656

[76] T. Yayamura, S. Iwata, S. I. Iwamaru, and H. Tomiyasu, *J. Chem. Soc. Faraday Trans.*, 1994, **90,** 3253

[77] a) H. D. Burrows, *Inorg. Chem.*, 1990, **3**, 139; b) H. D. Burrows and T. Kemp, *J. Chem. Soc. Rev.*, 1974, **3**, 139; c) C. Görller-Walrand and K. Servaes, *Helv. Chim. Acta.*, 2009, **92**, 2304; d) R. Ghosh, J. A. Mondal, H. N. Gosh and D. K. Palit, *J. Phys. Chem. A.*, 2010, **114**, 5263; e) R. Nagaishi, Y. Katsumura, K. Ishigure, H. Aoyagi, Z. Yoshida, T. Kimura and Y. Kato, *J. Photochem. Photobiol. A.*, 2002, **146**, 157;

[78] a) S. J. Formosinho, H. D. Burrows, M. G. M. Miguel, M. E. D. G. Azenha, I. M. Saraiva, A. Catarina, D. N. Ribeiro, I. V. Kholyakov, R. G. Gasanov, M. Bolte and M. Sarakhad, *Photochem. Photobiol. Sci.*, 2003, **2**, 569; g) S. Tsushima, *Inorg. Chem.*, 2009, 48, 4856; b) S. Tsushima, C. Gótz, K. Fahmy, *Chem. Eur. J.*, 2010, 16, 8029

[79] D. Cohen, B. Taylor, *J. Inorg. Nucl. Chem.*, 1961, **22**, 151

[80] D. J. Cohen. Inorg. Nucl. Chem., 1970, **32,** 3525; Claude Degueldre, *The Chemistry of the Actinide and Transactinide Elements*, Springer, New York, 2006, Vol **5**, 3013

[81] a) T. I. Docrat, J. F. W. Mosselmans, J. M. Charnock, M. W. Whiteley, D. Collison, F. R. Livens, C. Jones and M. J. Edmiston, *Inorg. Chem.*, 1998 **38,** 1879; b) K. Mizuoka and Y. Ikeda, *Radiochim. Acta.*, 2004, **92**, 631; c) M. S. Sidhu, W. Schabel, J. Radioanal. *Nucl. Chem.*, 1996, **211**, 375

[82] I. B. Polovov, V. A. Volkovich, J. M. Charnock, B. Kralj, R. G. Lewin, H. Kinoshita, I. May, and C. A. Sharrad, *Inorg. Chem.*, 2008, **47**, 7474

[83] K. Mizunka, S. Tsushima, M. Hasegawa, T. Hoshi and Y. Ikeda, *Inorg. Chem.*, 2005, **44,** 6211; b) A. Ikeda, C. Hennig, S. Tsushima, K. Takao, Y. Ikeda, A. C. Scheinost and G. Bernhard, *Inorg. Chem.*, 2007, **46**, 4212

[84] R. Steudner, T. Arnold, K. Großmann, G. Giepel and V. Brendler, *Inorg. Chem. Commun.*, 2006, **9,** 939

[85] a) K. Grossman, T. Arnold, R. Steudtner, S. Weiss and G. Bernhard, *Naturwissenschaften.*, 2009, **96**, 963; b) T. Arnold, K. Grossmann and N. Baumann, *Anal. Bioanal. Chem.*, 2010, **396**, 1641

[86] a) H. Hirose, C. Miyake, L. G. H. Du Preez, B. Zeelie, *Inorg. Chim. Acta.*, 1988, **150**, 293; b) W. T. Carnall, G. K. Liu, C. W. Williams, M. F. Reid, *J. Chem. Phys.*, 1991, **95**, 7194; c) H. Hubert, E. Simoni, M. Genet, *J. Less. Common Met.*,1986, **122**, 81; d) A. I. Komyak, A. P. Zazhogin, D. S. Umreiko, A. A. Lugovsky, *J. Appl. Spectrosc.*, 2009, **76**, 167

[87] a) P. Söderlind, O. Eriksson, B. Johansson, J. M. Wills, and A. M.Boring, *Nature*, 1990, **374**, 524; b) K. T. Moore, G. van der Laan, R. G. Haire, M. A. Wall, A. J. Schwartz, and P. Söderlind, *Phys. Rev. Lett.*, 2007, **98**, 236402

[88] a) S. V. Godbole, A. G. Page, Sangeeta, S. C. Sabharwal, J. Y. Gesland and M. D. Sastry, *J. Lumin.*, 2001, **93**, 213; b) S. Hubert, E. Simoni, M. Louis, W. T. Zhang and J. Y. Gestland, *J. Lumin.*, 1994, **60**, 245

[89] a) L. Morss, N Edelsein and J. Fuger, *The Chemistry of the Actinide and Transactinide Elements*, Springer, New York, 2006, Vol **1**, 52 b) M. Genet, P. Delamoye, N. Edelstein and J. Conway, *J. Chem. Phys.*, 1977, **67**, 1620

[90] E. Simoni, S. Hubert and M. Genet, *J. Chem. Phys.*, 1988, **49**, 1425; c) C. K Malek, J. C. Krupa, P. Delamoye and M. Genet, *J. Chem. Phys.*, 1986, **47**, 1763; d) C. D. Flint and P. A. Tanner, *Mol. Phys.*, 1984, **53**, 429; e) C. K. Mallek and J. C. Krupa, *J. Chem. Phys.*, 1986, **84**, 6584; f) B. Ordejón, V. Vallet, J.-P. Flament, L. Seijoa and Z. Barandiarána, *J. Lumin.*, 2007, **126**, 779; g) B. Ordejón, M. Karbowiak, L. Seijo and Z. Z. Barandiarána, *J. Chem. Phys.*, 2006, **125**, 074511

[91] a) G. V. Inova and G. A. Gerasimova, *Russ. Chem. Rev.*, 1992, **62**, 907; b) J. Su, and J. Li, *Prog. Chem.*, 2011, **23**, 1329

[92] N. Edelstein, *Lanthanide and Actinide Chemistry and Spectroscopy*, ACS symposium Series, 1980; V. T. Carnell, H. M. Crosswhite, ANL-84 Argonne National Laboratory, Argonne, Illinois, 1985

[93] G. Tian, T. Kimura, Z. Yoshida and Y. Zhu and L. Rao, *Radiochim. Acta.*, 2004, **92**, 495

[94] J. V. Beitz, G. Jursich and G. Sullivan. *J. Less. Common. Met.*, 1986, **126**, 301

[95] A. B. Yusov, *J. Radioanal. Nucl. Chem.*, 1990, **143**, 287

[96] a) A. B. Yusov and A. M. Fedoseev, *J. Radio. Nucl. Chem.*, 1991, **147**, 201; b) T. Fanghänel and J. I. Kim, *J. Alloys Compd.*, 1998, **728**, 217; c) A. Skerencak, P. J. Panak, W. Hauser, V. Neck, R. Klenze, P. Lindqvist-Reis and T. Fanghänel, *Radiochim. Acta.*, 2009, **97**, 385; d) T. Stumpf, T. Fanghänel and I. Grenthe, *J. Chem. Soc., Dalton Trans.*, 2002, **20**, 3799; e) M. Morgensten, R. Klenze and J. I. Kim, *Radiochim. Acta.*, 2000, **88**, 7; f) H. Moll and G. Bernhard, Polyhedron, 2012, **31**, 759; f) D. Girnt, P. W. Roesky, A. Geist, C. M. Ruff, P. J. Panak and M. A. Denecke, *Inorg. Chem.*, 2010, **49**, 9627; g) P. Lindqvist-Reis, C. Walther, R. Klenze, A. Eichhofer and T. Fanghänel, *J. Phys. Chem. B.*, 2006, **110**, 5279

[97] J. H. Van Vleck, *The theory of Electric and Magnetic Susceptibilities*, Oxford University Press, London 1932

[98] B. M. McGarvey, *Electron Spin Resonance of Transition-Metal Complexes*, in: R. L. Carlin (Ed.), Trans. Met. Chem., vol. **3**, Marcel-Dekker, 1967, 89

[99] For example: a) O. P. Lam, F. W. Heinemann and K. Meyer, *Chem. Sci.*, 2011, **2**, 1538; b) O, P. Lam, F. W. Heinemann, and K. Meyer, *Angew. Chem. Int. Ed.*, 2011, **50**, 5965; c) F. Moro, D. P. Mills, S, T. Liddle, and J. v. Slageren, *Angew. Chem. Int. Ed.*, 2013, **52**, 3430

[100] a) B. G. Wybourne, *Spectroscopic Properties of Rare Earths*; Wiley: New York, 1965; b) T. H. Siddall, *Theory and Applications of Molecular Paramagnetism;* Wiley: New York, 1976; c) B. Kanellakopulos, in *Organometallics of the f-Elements*; c) T. J. Marks, and R.D. Fischer, Eds.; NATO Advanced Study Institutes Series; D. Reidel, Dordrecht, The Netherlands, 1978; d) A. F. Orchard, *Magnetochemistry*; Oxford University Press Inc.: New York, 2003; e) N.M. Edelstein and G.H. Lander, in *The Chemistry of the Actinide and Transactinide Elements*, 3rd ed.; L. R. Morss, N.M. Edelstein and J. Fuger, Eds.; Springer: Dordrecht, The Netherlands, 2006, **4**, 2225.

[101] B. Kanellakopulos, E. Dornberger and F. Baumgartner, *Inorg. Nucl. Chem. Lett.*, 1974, **10**, 155

[102] J. C. Eisestein and M. H. L. Pryce, *Proc. R. Soc., A.*, 1960, **255**, 181

[103] R. G. Denning, T. R. Snellgrove and D.R. Woodmark, *Mol. Phys.*, 1979, **37**, 1109

Chapter 2

Fluorescence Spectroscopy of Uranium(IV) Halide Complexes in Non-Aqueous Media

2.1 Introduction

Studies aimed at understanding the photophysical properties of actinides can provide a better understanding of their electronic structure and, hence, an insight into the degree of participation of the *5f* and *6d* orbitals in forming metal-ligand bonding. In 2006, Maldivi[1] reported a comprehensive theoretical characterisation of trivalent actinide compounds. The authors state that absorption spectroscopy can provide insight into the degree of covalency in metal-ligand bonding in actinides, particularly the participation of the *5f* and *6d* orbitals in forming this type of bond. For example, a stronger absorption profile was observed for the chloro complexes than the aquo complexes, and the red shift observed going from $[M(H_2O)_9]^{3+}$ to $[M(Cl)_2(H_2O)_7]^{+}$ was ascribed to a slight increase in covalency within the metal-chloride bond.[2] The presence of a covalent type character in actinide metal-ligand bonding is now of great experimental and theoretical interest.[3] Enhancement of covalency in actinide metal-ligand bonding is believed to be a key area of research into future methodologies for the separation of minor actinides in particular Am^{3+} and Cm^{3+} from lanthanide in nuclear waste streams.[4]

To date, there are very few examples reported for the photoluminescence spectroscopy studies on uranium(IV) in solid state,[5] with only one example of U(IV) photoluminescence spectroscopy in fluid solutions.[6] In the solid state, for example, for cubic U^{4+} doped into $LiYF_4$ crystals,[7] there are a number of studies that show strong bands observed in the emission spectrum, that were assigned to the $5f^1 6d^1 \rightarrow 5f^2$ electronic transition. This arises from a redistribution of valence electrons in the *5f* sub-shell, in particular transition in between the $^3F_2$ ($5f^1 6d^1$) excited state and the $^3H_4$ ground state ($5f^2$). For a very long time and for no obvious reason, U(IV) in solution was considered to have no luminescence properties,[8] except for phosphate complexes in concentrated phosphoric acid solution.[9] In phosphoric acid solutions of U(IV) complexes, the ligand allows a

different radiative and non-radiative decay from low energy charge transfer absorption that does not involve the *f*-orbitals.[9]

In 2008, Kiplinger[10] reported the first example of luminescence studies on the metallocene ketimide system $[Cp^*_2U\{N=C(Ph)(CH_2Ph)\}_2]$ and found that upon photoexcitation, decay from the ligand centred singlet state is non-radiative and proceeds directly through the *5f*-electrons manifold giving no *5f*-centred emission properties. However, for much simpler complexes of aqueous U(IV) species, Kirishima *et al.*[6] reported the first observations of photoluminescence properties for tetravalent uranium in aqueous solutions. In aqueous perchloric acid solution of uranium(IV) compounds, a peak at 245 nm in the absorption spectrum was assigned to a transition from the $^3H_4$ Russell-Saunders coupled ground state to the highest excited state, $^1S_0$, and is about 2800 cm^{-1} lower in energy than in the free ion AnO_2^{2+}.[11] The bands observed at a higher energy were identified as $5f^2 \rightarrow 5f^16d^1$ transition or charge transfer excitations.[12] Photoexcitation at $^1S_0$ ground state (λ_{ex} = 245 nm) gave rise to ten emission bands in UV-Vis region that mirrored the absorption bands and were assigned as a transition from $^1S_0$ (highest lying state of the $5f^2$ manifold) to lower lying levels: $^1S_0 \rightarrow {}^1I_6$, $^1G_4$, $^3P_0$, $^1D_2$, $^3F_3$, $^3F_4$ and $^3H_5$. However, in open shell uranium complexes the intra *5f* electronic transitions are very sensitive to the coordination environment, crystal field and to symmetry.[6] For example, the UV absorption spectra for octahedral uranium complexes, such as the 6-coordinate $[UX_6]^{2-}$, differ significantly from that observed for $U^{4+}(aq)$[13] suggesting that the coordination number for the uranium is higher than six, in stark contrast to the hydrated transition metals.[14] EXAFS and NMR studies estimated a coordination number between 8 and 11, while DFT calculations suggested the presence of 9 water molecules.[15] Theoretical calculations aimed at assigning the transition bands for aqueous U^{4+} compounds highly depend on the model chosen and has shown to change considerably when the highest energy term is corrected for a large Stokes' shift (*i.e.* solvation effects).[15] This makes the assignment of absorption

and emission bands challenging, although analysis based upon the Russell-Saunders coupling scheme can be used as a good approximation.[16] As discussed in Chapter 1 (Section 1.4.1), because spin-orbit coupling is masked by the degree of localisation of the *5f* orbitals, the contribution of the Russell- Saunders coupled ground state term is about 80% in U^{4+}.[17]

In this chapter photoluminescence spectroscopy, supported by the theoretical approaches of DFT (Density Functional Theory), AIM (Atoms-In-Molecules) and CASSCF (Complete Active Space Self-Consistent Field), was used to study the electronic structures of tetravalent uranium ions. The contributions of valence *5f* orbitals in metal-ligand bonding and their participation in forming covalent bonds were also studied. This is the first example of a comprehensive photoluminescence and computational study of tetravalent uranium in non-aqueous solution. Simple model compounds such as $[Li(THF)_4][UX_5(THF)]$ (X = Cl (**1**), Br (**2**) and I (**3**)), $[Li(THF)_4]_2[UCl_6]$ (**4**) and $[UCl_4(THF)_3]$, were used for our studies. Such compounds were selected in order to avoid any possible quenching of the excited state, which may arise from an aromatic group or conjugated entities. Ligand centred charge transfer bands in the visible region were also important to avoid since they provide another quenching pathway as shown by Kiplinger.[10] Furthermore, compounds such as **1**, **2** and **3** provide a reduction in symmetry around the uranium metal ion, allowing for any formally symmetry forbidden *f-f* bands to be observed. Based on Crystal Field Theory (CFT), changing the symmetry from O_h for $[UCl_6]^{2-}$ to C_{4v} for $[UCl_5(THF)]^-$ to C_{2v} for $[UCl_4(THF)_3]$ should have an impact on the spectroscopic properties.[6] Assigning the absorption spectroscopy bands of these compounds should provide a good starting point for identifying transitions associated with the *5f* and *6d* orbitals and their contributions in metal-ligand bonding.

2.2 Uranium(IV) Halide Complexes

2.2.1 Synthesis and Structural Characterisation

Uranium halide of the type $[Li(THF)_4][UX_5(THF)]$ (X = Cl (**1**), Br (**2**) and I (**3**)) **1** were synthesised and studied. $[Li(THF)_4][UX_5(THF)]$ (**1**) was synthesised by treating UCl_4 with one equivalent of anhydrous LiCl in anhydrous THF at room temperature (Scheme 2.1), which, following filtration and crystallisation, was obtained as an air sensitive green crystalline solid in 74% yield.

$$UCl_4 + LiCl \xrightarrow[24hrs,\ RT]{THF} \underset{\mathbf{1}}{[Li(THF)_4][UCl_5(THF)]}$$

Scheme 2.1: Synthesis of **1**

The corresponding halides $[Li(THF)_4][UBr_5(THF)]$ (**2**), and $[Li(THF)_4][UI_5(THF)]$ (**3**), were also prepared. These were synthesised from the reaction of **1** with excess Me_3SiX (X = Br, I) (Scheme 2.2 and 2.3) to give pure green crystals of **2** and a mixture of **3** and $[UO_2I_4]^{2-}$ as the iodide was substantially more air sensitive, as observed by UV-Vis absorption spectroscopy (*vide infra*), even under rigorous anhydrous and oxygen-free conditions.

$$\underset{\mathbf{1}}{[Li(THF)_4][UCl_5(THF)]} \xrightarrow[THF,\ 24hrs,\ RT]{Me_3SiBr\ (excess)} \underset{\mathbf{2}}{[Li(THF)_4][UBr_5(THF)]}$$

$$\underset{\mathbf{1}}{[Li(THF)_4][UCl_5(THF)]} \xrightarrow[THF,\ 24hrs,\ RT]{Me_3SiI\ (excess)} \underset{\mathbf{3}}{[Li(THF)_4][UI_5(THF)]} + [UO_2I_4]^{2-}$$

Scheme 2.2 **and** Scheme 2.3: **Synthesis of** 2 **and** 3

Pale green crystals of **1** suitable for X-ray diffraction were isolated (Figure 2.1), but during the course of this study **1** was reported as the by-product formed during the preparation of the triamidoamine uranium(IV) complex [U(Tren^{TMS})(Cl)(THF)] (Tren^{TMS}={N(CH$_2$CH$_2$NSiMe$_3$)$_3$}$_3$) from UCl_4 and [Li$_3$(Tren^{TMS})] in THF.[18] [Li(THF)$_4$][UCl$_5$(THF)] **1** was formed from the reaction of excess UCl_4 with the LiCl produced during the salt metathesis reaction. An analogous compound [^{n}Bu$_4$N][UCl$_5$(THF)] has also been previously reported.[19] Characterisation data and metric parameters around the uranium agree with those determined here (see appendix A for crystallographic data).

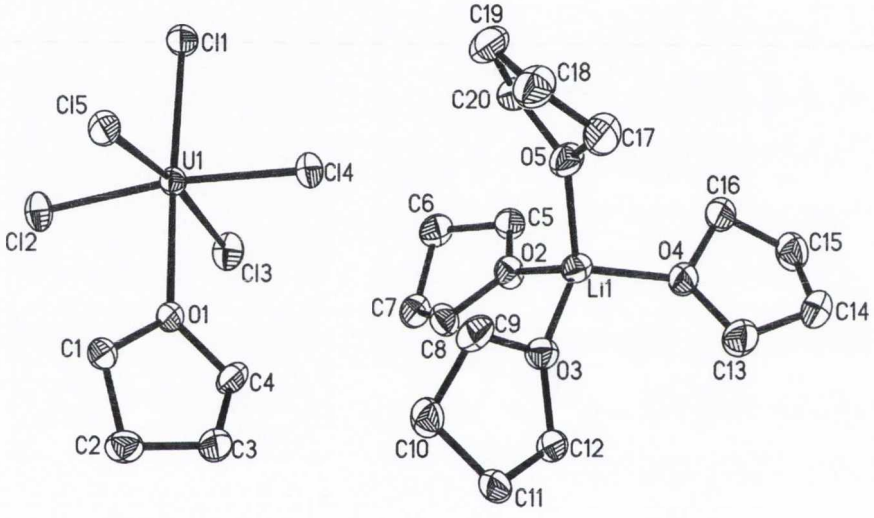

Figure 2.1: Molecular structure of **1**; bond length (Å) and angles (·): U(1)-O(1) 2.402(5), U(1)-Cl(1) 2.5919(19), U(1)-Cl(2) 2.6149(18), U(1)-Cl(3) 2.6033(19), U(1)-Cl(4) 2.6148(18), U(1)-Cl(5) 2.6136(18), Cl$_{eq}$-U-O 85.3, Cl$_{ax}$ -U-O 176.89

Compound **1** is present as solvent separated ion pairs, in which a lithium cation is coordinated by four THF molecules and a uranium pentachloride anion is coordinated to one THF molecule. The lithium centre adopts a distorted tetrahedral geometry and the uranium centre exhibits a slightly distorted octahedral geometry. The Cl$_{eq}$-U-O angles are 85.3° (average) as the uranium atom sits slightly above the equatorial plane by 0.2 Å. The U-Cl bond distances are within the ionic radii and range from 2.5919(19)–2.6136(18) Å with the shortest U-Cl bond length trans to the coordinated THF molecule. The average

bond length (2.60 Å) can be compared to U(III) compound K_2UCl_5 (2.80 Å)[20] and U(V) compound $[UCl_5(OPPh_3)]$ (2.47-2.50 Å).[21] The expected bond lengths, on the basis of the 6-coordinate ionic radii, are 2.43 Å, 2.56 Å and 2.695 Å for U(V), U(IV) and U(III) respectively,[22] suggesting that bonding in **1** is primarily ionic.

Raman spectroscopy shows the THF molecule stretch in the range of 1000 – 3000 cm^{-1} and the U-Cl stretch appears at 305 cm^{-1} as shown in Figure 2.2.

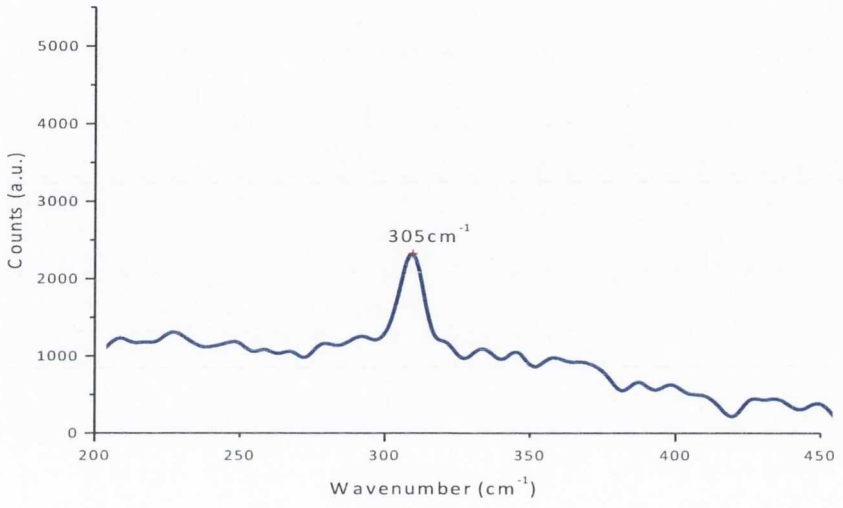

Figure 2.2: Experimental Raman spectrum for **1**

In order to ensure the symmetry around the uranium did not change due to an "-ate" formation in solution, $^7Li\{^1H\}$ NMR spectroscopy was used to probe the solution state structure of **1** and **2**. The $^7Li\{^1H\}$ NMR spectra for **1** and **2** (Figure 2.3) exhibit a single resonance at δ_{Li} = -2.64 ppm for **1** in THF and -0.97 ppm for **2** in THF, which shift to -20.42 ppm and -6.32 ppm in C_6D_6 respectively. The single resonance of **1** and **2** in THF confirms that both are present as solvent separated ion pairs. The observed shift in the $^7Li\{^1H\}$ NMR spectra for **1** and **2** in non-coordinating C_6D_6 indicates an interaction between the uranium metal centre and the Li atom *via* two bridging chloride atoms to give an "ate" complex. This is common for uranium complexes and Hayton reported a thorough study for such behaviour.[23] For example, upon the decomposition of the U(IV) complex $[Li(THF)_2][UO(^tBu)_6]$ to give the dinuclear U(IV) complex $[Li(THF)][U_2O(^tBu)_9]$

the single resonance at δ_{Li} = 2.72 ppm exhibits an upfield shift in the $^{7}Li\{^{1}H\}$ NMR to -28.0 ppm.

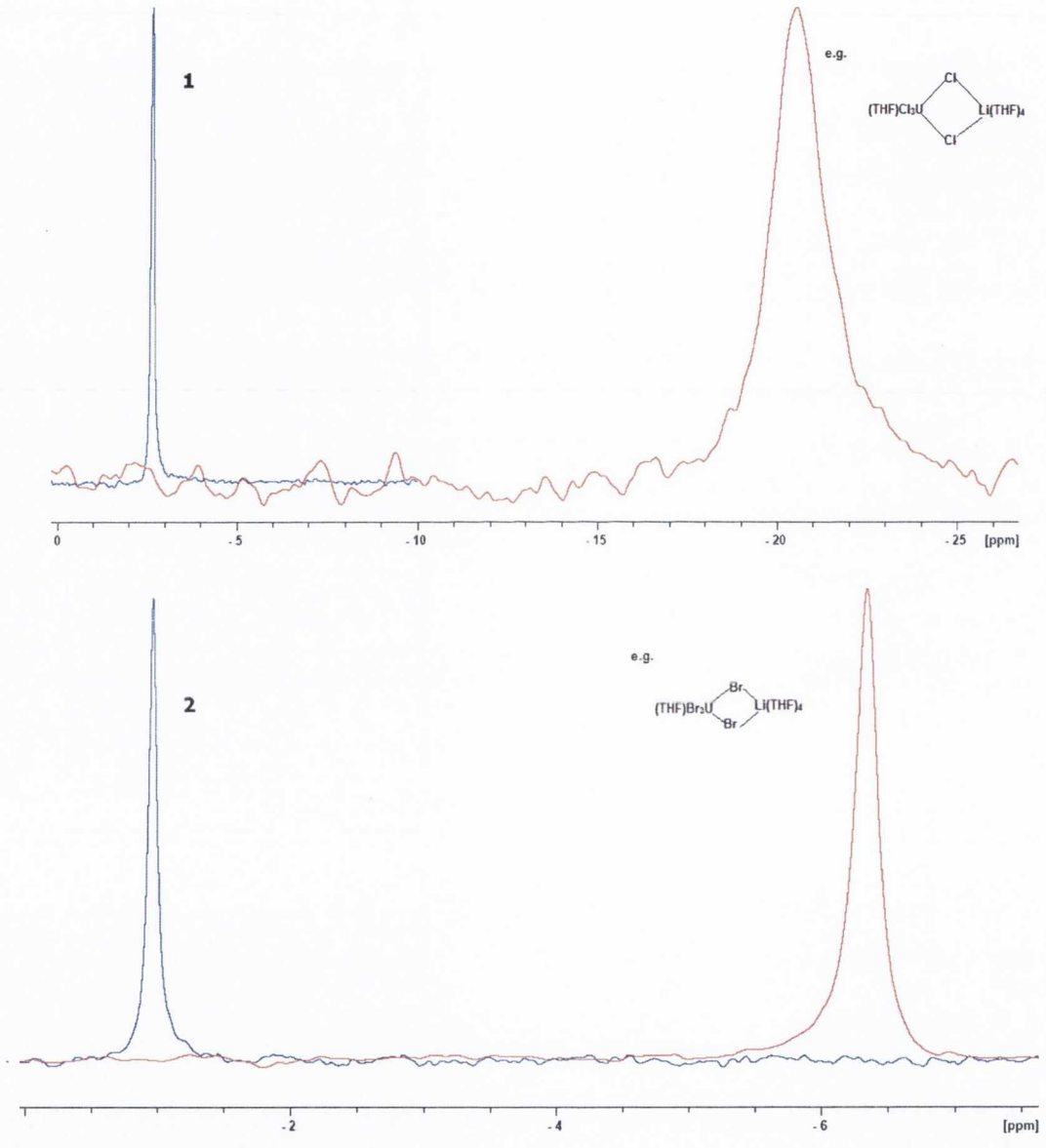

Figure 2.3: $^{7}Li\{^{1}H\}$ NMR Spectrum of **1** (top) and **2** (bottom) in THF (blue) and C_6D_6 (red)

Furthermore, the ^{1}H NMR spectra of **1** and **2** in a coordinating pyridine-d_6 solvent shows two peaks at 3.64 ppm and 1.80 ppm corresponding to free THF, suggesting it is labile. Changing the solvent to the non-coordinating C_6D_6 causes an upfield shift of the THF peaks from 3.64 ppm to -1.9 ppm and 1.80 ppm to -4.64 ppm, suggesting the THF is coordinated to the uranium metal.[23]

2.2.2 Magnetic Properties

Magnetic susceptibility indicates the degree of magnetisation of a material in response to an applied field.[24] It gives information on the degree of interaction with the magnetic field and therefore the oxidation state of the metal centre in a compound.[24] Uranium(VI) compounds are expected to be diamagnetic ($5f^0$ and $^1S_0$ ground state) while uranium(V) compounds are expected to be paramagnetic ($5f^1$ and $^3F_2$ ground state). Uranium(IV) ($5f^2$ and $^3H_4$ ground state) magnetism are much more complicated and depend on the symmetry of the compounds (discussed in Chapter 1 (Section 1.5.1)).

The magnetic susceptibility profile is a well-established method used for the characterisation of actinide ions and magnetic susceptibility values, while the use of temperature dependent magnetism profile and field dependant magnetism profile can be very informative and provide an insight on the oxidation state, the ground state and possibly spin orbit coupling of the actinide ions. For example, while U(IV) and U(III) compounds have similar magnetic moment at room temperature, the oxidation state in these compounds can be distinguished from their different low temperature magnetism profile and their variable field magnetism profile. Using high sensitivity Superconducting Quantum Interference Device (SQUID) variable temperature and variable field magnetic susceptibility measurements were conducted and used as a method of confirmation of U(IV) oxidation state of **1** as shown in Figure 2.4. Three samples of **1** were independently synthesised and measure to check for reproducibility.

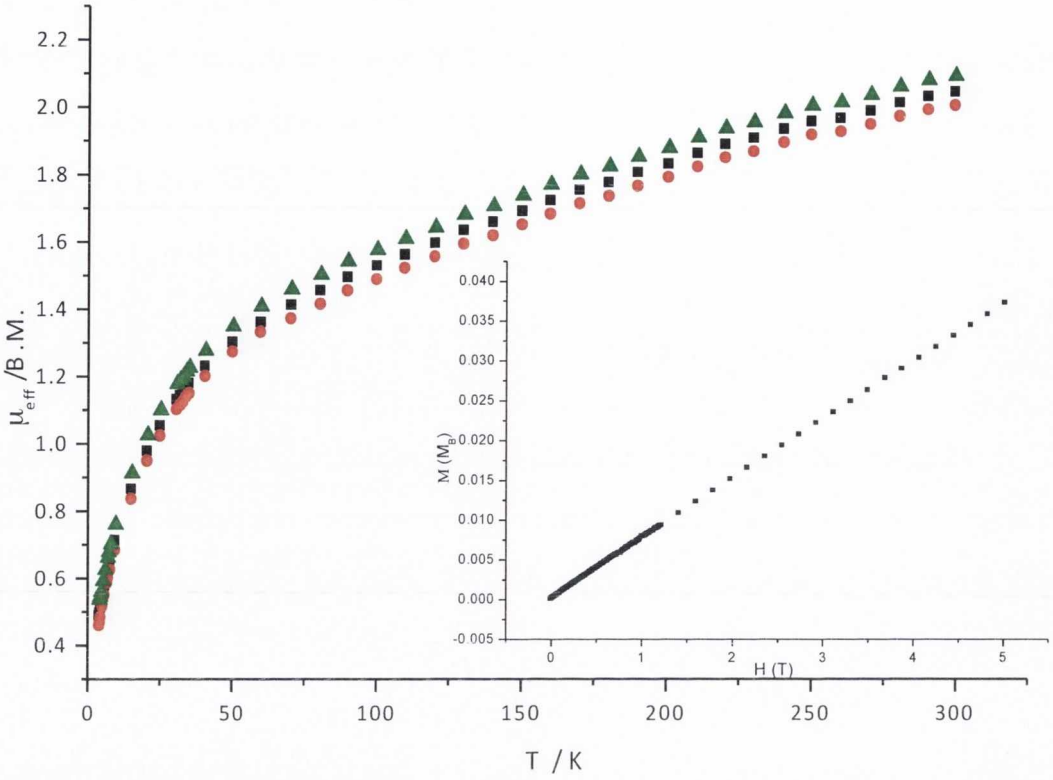

Figure 2.4: Temperature-dependent SQUID magnetisation data for **1** at 0.1 T plotted as a function of magnetic moment (μ_{eff}) *vs.* temperature (K). The plot shows three data sets measured of three independently synthesised samples. (inset shows field dependant magnetisation for **1** at 10 K plotted as a function of magnetism χM *vs.* field T)

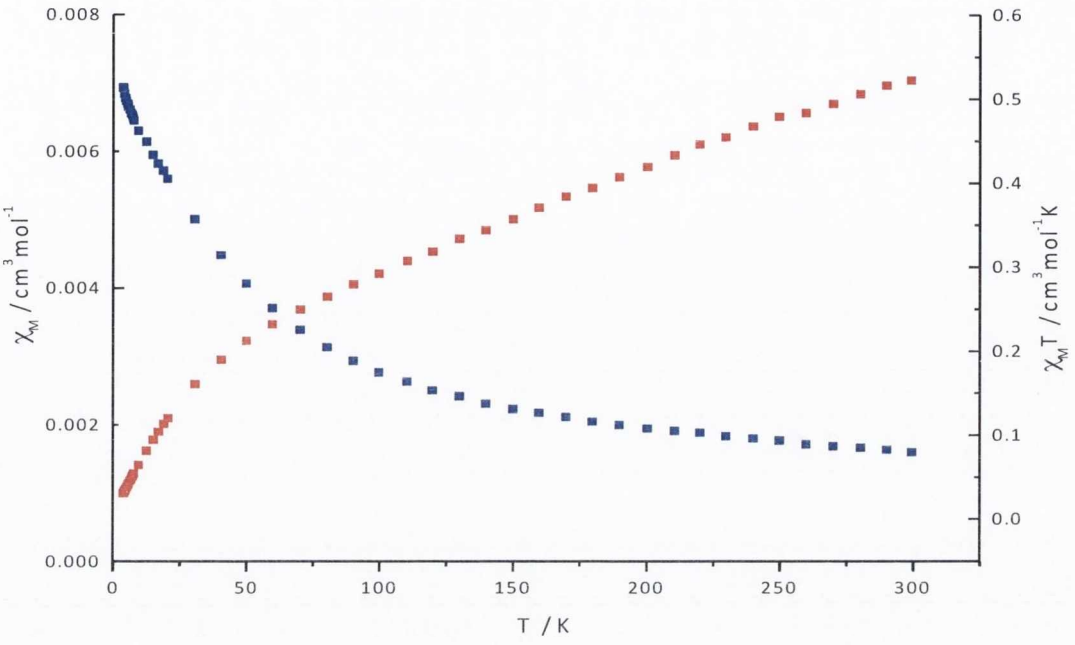

Figure 2.5: Magnetic susceptibility plots for **1** at 0.1 T plotted as a function of χM *vs.* T (red) and χMT *vs.* T (blue)

The variable temperature SQUID magnetisation data are characteristic of U(IV),[25] where an effective magnetic moment of 0.40 μ_B at 2 K is measured.[25] The magnetic moment value of 2.04 μ_B at 300 K compares well to the magnetic susceptibility recorded for $[Ph_3PBu]_2[UCl_6]$ (2.22 μB at 295 K),[3] and lower than the value of 3.38 μB at 300 K which is expected for a pure $^3H_4$ ground state.[25] The reduction in effective moment compared to the free ion at room temperature is common in U(IV) compounds and has been ascribed to the quenching of spin-orbit coupling, which is thought to be caused by a degree of covalency due to metal-ligand interactions. Furthermore, the dependence of the magnetic susceptibility on the intensity of the magnetic field was measured in the range from 0.1 to 5 T to allow distinction of U(IV) and U(III).

2.2.3 Density Functional Theory Calculations

Geometry optimisation of triplet $[UCl_5(THF)]^-$ at a number of levels of theory resulted in a distorted octahedral geometry with very similar features to the experimental data. The complex adopts a C_{2v} symmetry with bond lengths U-O (2.512 Å), U-Cl_{ax} (2.594 Å), UCl_{eq} 2.614 Å and 2.611 Å) and bond angles Cl-U-O (180.0°, 82.6°, 82.8°). The DFT geometries generally reproduce the solid state geometry, with one short U-Cl bond and Cl-U-O angle of less than 90°, but overestimate the U-O bond length. A comparison of the experimental and theoretical values is shown in Table 2.1.

	Experiment	BP86-TZVP	BP86-TZVPP	PBE-TZVP	B3LYP-TZVP	PBE0-TZVP
U-O	2.402(5) Å	2.512	2.527	2.519	2.542	2.507
U-$Cl_{(ax)}$	2.5919(19) Å	2.594	2.589	2.589	2.606	2.577
U-$Cl_{(eq)}$	2.614(18) Å	2.614, 2.611	2.615	2.609	2.627	2.598
Cl-U-O	84.5 - 86.8°	82.6, 82.8	82.3 - 83.3	82.1 - 82.9	82.2 - 82.9	81.9 - 82.9

Table 2.1: DFT calculated *vs.* experiment values of geometry optimisation of **1**

Furthermore, density functional theory (DFT) was used to theoretically calculate the frequencies of the U-Cl stretch and found that the most intense bands are 289.8 cm^{-1} using BP86 functional (Figure 2.6a) and 294.5 cm^{-1} with B3LYP functional (Figure 2.6b). Both computed values agree with the experimental value of 305.7 cm^{-1}, with the B3LYP in slightly better agreement.

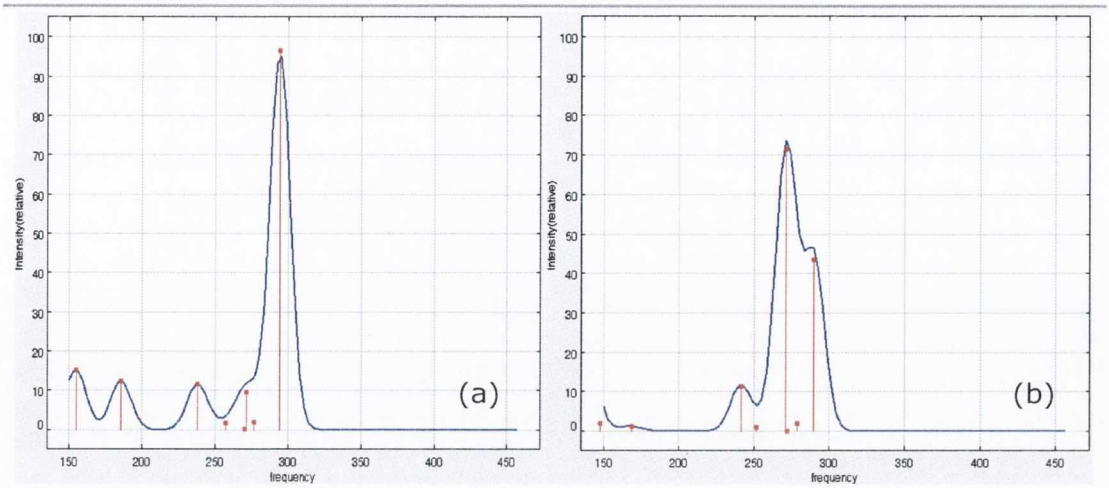

Figure 2.6: Calculated Raman spectrum of **1** at a) BP86 functional and at b) B3LYP functional

2.2.3.1 Natural Bonding Orbitals

In order to probe the degree of covalency in **1**, further theoretical studies such as natural bonding orbitals (NBO) were conducted. NBO analysis, in Gaussian09 by default, assigns *5f*, *6d*, *7s* and *7p* orbitals as valence. This definition leads to an electron configuration on U of [core] $7s^{0.2}\ 75f^{3.04}\ 6d^{1.68}\ 7p^{0.50}$, and an overall atomic charge of -0.033. Charges on Cl vary slightly between -0.244 and -0.230, and the overall charge on THF is +0.202. This NBO analysis indicates significant charge transfer from THF to U, and much smaller atomic charges than the formal U(IV) assignment would suggest. Comparisons of α- and β-spin NBOs demonstrate that the two unpaired electrons in the triplet state reside in orthogonal f-orbitals on U, thus giving rise to a highly localised distribution of spin density (Figure 2.7).

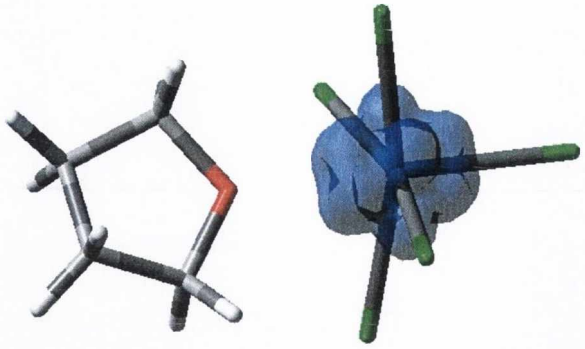

Figure 2.7: DFT spin density representation of *f*-orbital on U in **1** at the BP86 level

One or more natural bonding orbitals are found between U and each Cl, and within the THF unit, but no such overlap is located between U and O. A single NBO is located between U and the chloride *trans*- to THF, weighted heavily (83%) in favour of Cl and involving both *s*- and *p*-orbitals on Cl interacting with *s*-, *p*-, *d*- and *f*-orbitals on U. Table 2.2 summarises the NBO contribution from U and each Cl.

	U / Cl	**U s / p / d / f**	**Cl s / p**
U—Cl$_1$ [a]	16.9 / 83.1	20 / 26 / 41 / 14	54 / 46
U—Cl$_2$ [b]	17.5 / 82.5	15 / 17 / 35 / 32	52 / 48
U—Cl$_2$	10.6 / 89.4	0 / 10 / 47 / 43	1 / 99
U—Cl$_3$ [b]	17.5 / 82.5	16 / 17 / 35 / 32	52 / 48
U—Cl$_3$	10.8 / 89.2	0 / 10 / 47 / 43	1 / 99

Table 2.2: NBO analysis of symmetry unique U-Cl bonds in **1** (%) [a] axial; [b] equatorial

An isosurface representation of this orbital is shown in Figure 2.8. Orbitals with similar make-up are found between U and all four equatorial chlorides, but here are also found a second set of orbitals with *p*-symmetry that consist of Cl *p*-orbitals donating into U *d*- and *f*-orbitals.

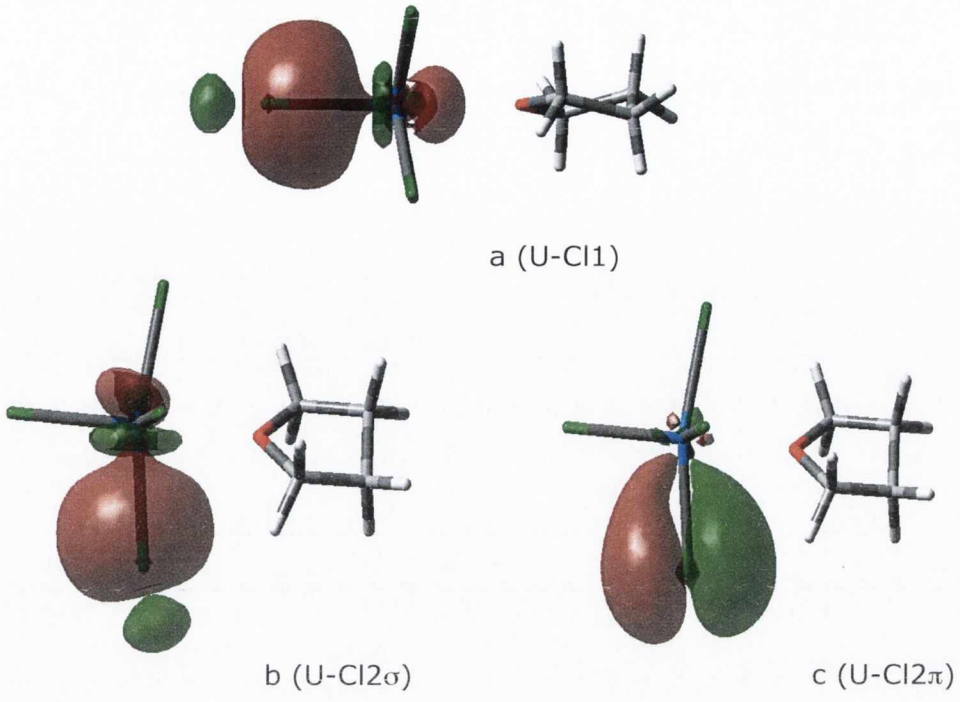

Figure 2.8: Isosurface representation for (a) σ-natural bonding orbital in U-Cl_{ax}, and σ-natural bonding orbital (b) and π-natural bonding orbitals (c) in U-Cl_{eq} of the anionic component of **1** at the BP86 level

NBO analysis proceeds by first defining a Lewis structure that best describes the molecule, and then reporting deviations from this in terms of donor-acceptor interactions between formally occupied and vacant NBOs. This 2nd-order perturbation theory analysis indicates significant overlap between U and O, despite the lack of a formal orbital for this interaction. This consists of donation from a *p*-type lone pair on O into a mixture of *d*- and *f*-orbitals on U, whose bond energy is estimated at 49.6 kcal/ mol. This perturbation analysis also identifies numerous weak donor-acceptor interactions from the chloride lone pairs into the formally empty *d*- and *f*-orbitals on U. These are present for all five chlorides, but their sum is noticeably larger for U—Cl_{ax} (55 kcal/ mol) than the four equatorial chlorides (39–43 kcal/ mol). Furthermore, the HOMO was calculated to consist of an *f*-orbital localised on the uranium centre with an anti-bonding contribution to the axial chloride, whilst the LUMO is a different *f*-

orbital with an anti-bonding contribution to the equatorial chlorides (Figure 2.9). The HOMO-LUMO gap of the α spin is calculated to be 3.83 eV (30891 cm^{-1}); the corresponding gap for the β spin is 3.41 eV (39572 cm^{-1}).

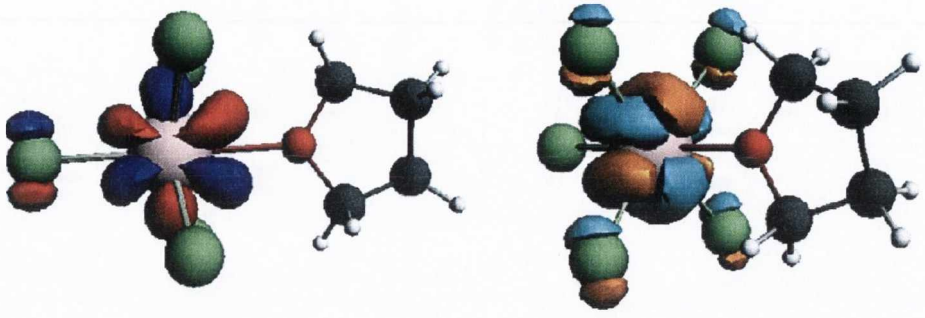

Figure 2.9: HOMO and LUMO α-spin orbitals of **1** at the BP86 level

2.2.3.2 Atoms in Molecules

Atoms in molecules (AIM) analysis concentrates on the topology of the electron density, giving complementary information to that from NBO analysis, and is increasingly utilised for actinide compounds.[26] AIM analysis looks for bond critical points (BCP) between two atoms, and the chemical bonding can be characterised by the properties of these BCPs. Table 2.3 reports properties evaluated at bond critical point for U-X bonds, which are located between U and all six complexed atoms and for comparison $ThCl_4$ and $LaCl_3$. Electron density with a value $\rho>0.2$ for an open shell system and $\rho<0.1$ in a closed shell indicates covalency; the Laplacian ($\nabla\rho$) value can determine the degree of covalency with a negative value indicating π-bond character and a positive value indicating σ-bond. The electron density (ρ) in the U-O bond is significantly less than in all U-Cl bonds. Further evidence for the relative weakness of this bond comes from the zero value of H (total energy density), indicating a balance of kinetic and potential energies, and the low value of the integrated bond order.

Compound	bond	ρ	∇ρ2	ε	*H*	Bond Order	Ref.
1	U-Cl_{ax}	0.072	+0.165	0.004	-0.019	0.78	
	U-Cl_{eq}	0.070	+0.142	0.090	-0.017	0.75	[27]
	U-Cl_{eq}	0.071	+0.143	0.096	-0.08	0.76	
	U-O	0.046	+0.132	0.132	0.000	0.31	
Cp_4U	U-C	0.034	+0.089	2.11	0.001	n.r.	[28]
Cp_3U	U-C	0.040	+0.115	1.31	-0.003	n.r.	[28]
$ThCl_4$	Th-Cl	0.081	+0.157	0.011	-0.024	n.r.	[28]
$LaCl_3$	La-Cl	0.066	+0.159	0.009	-0.011	n.r.	[28]
[(Tren)U-$RuCp(CO)_2$]	U-Ru	0.0425	+0.0605	n.r.	-0.008	n.r.	[29]

Table 2.3: Bond critical point properties for **1** *vs.* selected compounds (values in a.u.)

Variations in density within symmetry-unique U-Cl bonds are small, but more significant changes are apparent in Laplacian (∇ρ) and elliplicity (ε) values between axial and equatorial bonds. This reflects the significant π-character of the latter, which reduces the overall curvature but increases the symmetry of the density at the bond critical point, but by symmetry, cannot directly affect the total density in the bond. However, energy density does not show the expected increase in strength of the equatorial bonds relative to the axial bonds, perhaps reflecting the importance of the greater second-order interactions in the latter. AIM also gives an alternative definition of atomic charge from numerical integration of the electron density within the basin of each atom. Values are significantly different to those from NBO and suggests much great iconicity: U was found to have an overall charge of +2.26 by this definition, and chlorides varied from -0.66 to -0.67. THF is found to be very close to neutral and has an overall charge of +0.04. Overall, based on AIM description the bonding can be described as being principally ionic, but NBO shows some evidence for a dative covalent character.

2.2.4 Photophysical Properties

2.2.4.1 Absorption Spectroscopy

The UV-Vis/NIR absorption spectra of ~0.36 mmol THF solution of **1, 2** and **3** were measured in an inert atmosphere. The spectrum of **1** shows two broad, intense bands in the UV-Vis region at λ_{max} = 277 nm and 303 nm and a shoulder at 331 nm. The UV-Vis spectrum of **2** shows two broad bands at λ_{max} = 277 nm and 325 nm and a shoulder at 350 nm. The UV-Vis spectrum of **3** shows three bands at λ_{max} = 252 nm, 295 nm and 365 nm. Furthermore, $[R_4N][UCl_5(THF)]$ (R = Et, Bu) were synthesised according to the literature procedure[30] and lack of interaction between the uranium and the counter ions in **1** and **2** (as seen in $^7Li\{^1H\}$ NMR) resulted in identical absorption spectra for all three $[UCl_5(THF)]^-$ anions. The observed bands must be Laporte allowed transitions with large molar absorption coefficients (ε) arising from transitions of either ligand to metal charge transfer (LMCT) resulting from either halide or THF to uranium charge transfer, LMCT or $f \rightarrow d$ transitions.

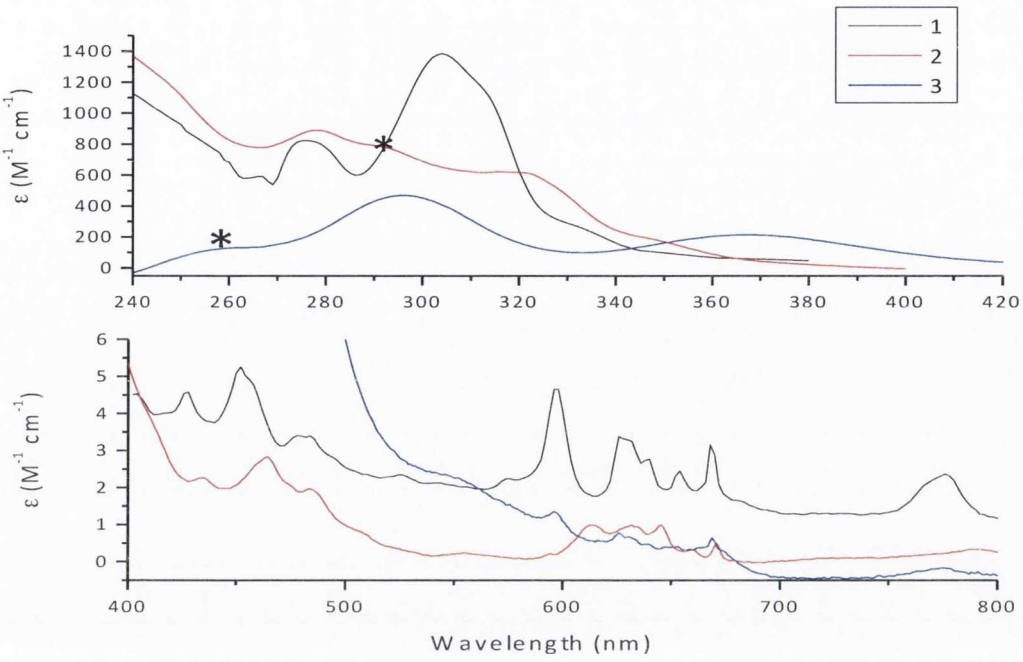

Figure 2.10: UV-Vis absorption spectra of **1** (black line), **2** (red line), and **3** (blue line) in THF at ~0.36 mmol showing CT (top) and *f-f* transitions (bottom); (* indicates uranyl impurity)

Comparison of the absorption spectra of **1** and **2** indicates that upon substitution of halides from Cl (**1**) to Br (**2**) the band at λ_{max} = 303 nm for **1** exhibit a bathochromic shift to 325 nm in **2**, and 295 nm in **3**, which indicates that this is likely to be a charge transfer (CT) band containing a contribution from a halide to uranium or uranium to halide charge transfer process. The band at λ_{max} = 277 nm remains at the same position for **1** and **2** and thought to be buried under the uranyl band at λ_{max} = 250 nm in **3**. It can therefore be assigned as an $f \rightarrow d$ transition from the ground $^3H_4$ state into the $^3F_2$ Russell-Saunders coupled state (*6d* t_{2g} orbitals).[31] The band at λ_{max} = 331 nm in **1**, 350nm in **2** and 370 nm in **3** can be another CT, but it is not possible to conclusively prove this.

The *f-f* transitions for all three compounds are also almost identical. Sixteen bands were observed in the visible and near infrared region at λ_{max} = 404, 428, 452, 484, 599, 627, 655, 667, 778, 909, 1098, 1227, 1356 , 1571, 1843, 1970 nm with molar absorption of 5-40 M^{-1} cm^{-1} (Figure 2.10 bottom) These bands are formally Laporte forbidden *f*→*f* transition and are typical for U(IV). It must be noted that due to high air and moisture sensitivity of **3**, it was not possible to synthesise the pure format of the complex and its absorption spectra shows a combination of both **3** and the uranyl moiety $[UO_2I_4]^{2-}$. It was therefore not possible to determine an accurate extinction coefficient value for **3**. Using previously published energy level diagrams derived from experimental data[32] and computational studies (*vide infra*) the *f-f* transitions in **1** can be fully assigned. The highest energy *f-f* transition to the $^1S_0$ state is likely to be buried under the more intense bands in the UV region. This band is significantly lowered upon solvation ($U^{4+}_{(g)}$, 221 nm {45316 cm^{-1}}; $U^{4+}_{(aq)}$, 245 nm {40820 cm^{-1}}),[33,34] and suggests it may be sensitive to the coordination environment. The *f-f* transitions for **2** and **3** are rather similar. This is expected as the crystal field effects are small resulting in negligible perturbation of the *5f* manifold. It is also worth noting that transitions seen for octahedral actinide complexes are usually broader than those observed in the absorption spectra of lanthanide complexes[13] due to a larger crystal field splitting effect resulting in the sensitivity of actinides to the coordination environment.

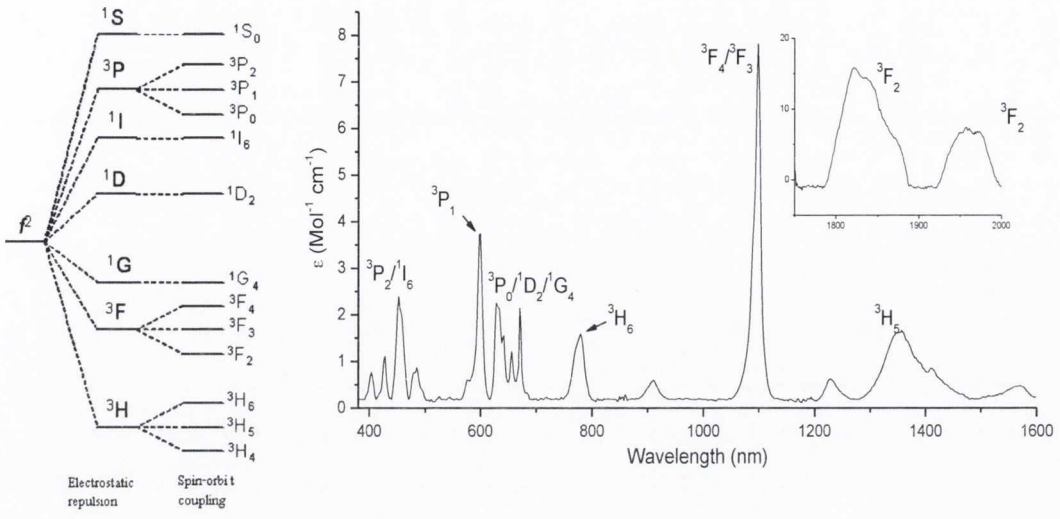

Figure 2.11: A qualitative energy level diagram for U^{4+} ion and the UV-Vis/NIR absorption spectrum of **1** showing the assignment of intra-configurational *f-f* transitions (insert shows bands in the region 1750 - 2000 nm)

In order to help ascertain the presence and direction of the charge transfer bands (i.e. LMCT or MLCT) cyclic voltammetry was used. The observed electrochemical behaviour of **1** (Figure 2.12 (left)) was identical to the previously reported in $[Et_4N][UCl_5(THF)]$,[19] showing an irreversible reduction process with a reduction potential of -2.75 V (*vs.* Fe/Fe^+ at 298 K) and no observable oxidation wave suggesting a reduction of U(IV) to U(III). Similarly, the electrochemical behaviour of **2** (Figure 2.13 (left)) shows one reduction peak at a potential of -2.03 V (*vs.* Fe/Fe^+ at 298 K) and no oxidation wave.

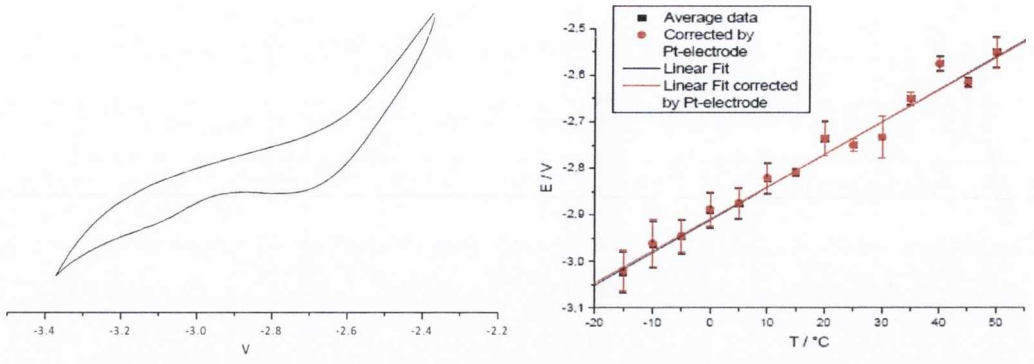

Figure 2.12: Room Temperature cyclic voltammetry and variable temperature cyclic Voltammetry for the redox process in **1** *vs.* Fc/Fc^+ in THF with 0.1 M $[^nBu_4N]BPh_4$ as a supporting electrolyte and a scan rate of 0.1 V/ s

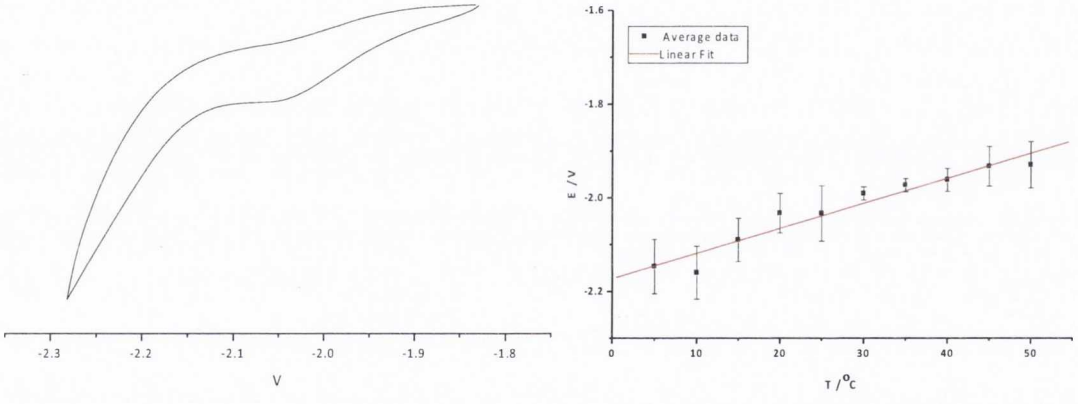

Figure 2.13: Room Temperature cyclic voltammetry and variable temperature cyclic Voltammetry for the redox process in **2** *vs.* Fc/Fc^+ in THF with 0.1 M $[^nBu_4N][BPh_4]$ as a supporting electrolyte and scan rate of 0.1 V/ s

A small decrease in the reduction potential is observed for **2** compared to that for **1**. Of note is that under no experimental conditions U(IV)/U(V) oxidation in either **1** or **2** was observed. The lack of an oxidation potential has commonly been observed in previous systematic reports of CV investigations of U(IV) compounds with σ-donating ligands[35] as the U(V) species formed is unstable with respect to disproportionation on the CV timescale. Important exceptions to this observation are $[Cp_3U(NEt_2)]$,[36] and $[(C_5H_4R)_3UCl]$ (R = H, Me, ^{t}Bu, $SiMe_3$).[37] Except for the mono(amide) complex, the U(IV)/U(V) couple is proposed to be

linked to a subsequent chemical reaction, which presumably involves disproportionation of the U(V) species.

Furthermore, variable temperature cyclic voltammetry measurements were conducted in order to determine thermodynamic parameters of the redox process observed in **1**. Thus, a plot of the redox potential *vs.* temperature allows entropy ΔS to be directly measured and enthalpy ΔH to be relatively measured.[38] **1** shows well-defined temperature dependence with thermodynamic parameters of 464 kJ mol^{-1} for ΔH and 666 J mol^{-1} K^{-1} for ΔS (Figure 2.12 (right)). The large enthalpy is to be anticipated as the redox potential of -2.75 V suggests that **1** is difficult to reduce. Similarly the thermodynamic parameters of **2** were obtained (Figure 2.13 (right)) with values of ΔH = 336 kJ mol^{-1} and ΔS = 471 J mol^{-1} K^{-1}, in keeping with the less negative redox potential observed in **1**.

Compounds **1** - **3** are highly air and moisture sensitive and any decomposition would be observed in the UV-Vis/NIR spectrum. The sensitivity of the techniques and the air sensitivity of the compounds allowed for a simple experiment to be carried out to confirm the assignments of the bands observed in the UV-Vis region. Compound **1** and **2** were exposed to air to form the uranyl salts $[UO_2Cl_4]^{2-}$ and $[UO_2Br_4]^{2-}$ respectively and the UV spectra for both salts were measured over time (Figure 2.14 and 2.15). It is clear that the band at λ_{max} = 303 nm for **1**, which shifts to 325 nm for **2** is a halide-uranium charge transfer band that also shifts upon exposure to air and oxidation of U^{4+} to $[UO_2]^{2+}$. Spectroscopic properties of uranyl are discussed in Chapter 4. The vibronically coupled bands at λ_{max} = 420 - 450 nm characteristic of uranyl are also observed and increase in intensity over time which confirms the loss of f-f transition due to oxidation of U(IV) $5f^2$ to U(VI) $5f^0$. It was not possible to synthesise a pure form of compound **3** due to its high instability. However, the UV-Vis spectrum shows a CT band at λ_{max} = 295 and two other bands that can be related to its uranyl salt $[UO_2I_4]^{2-}$.

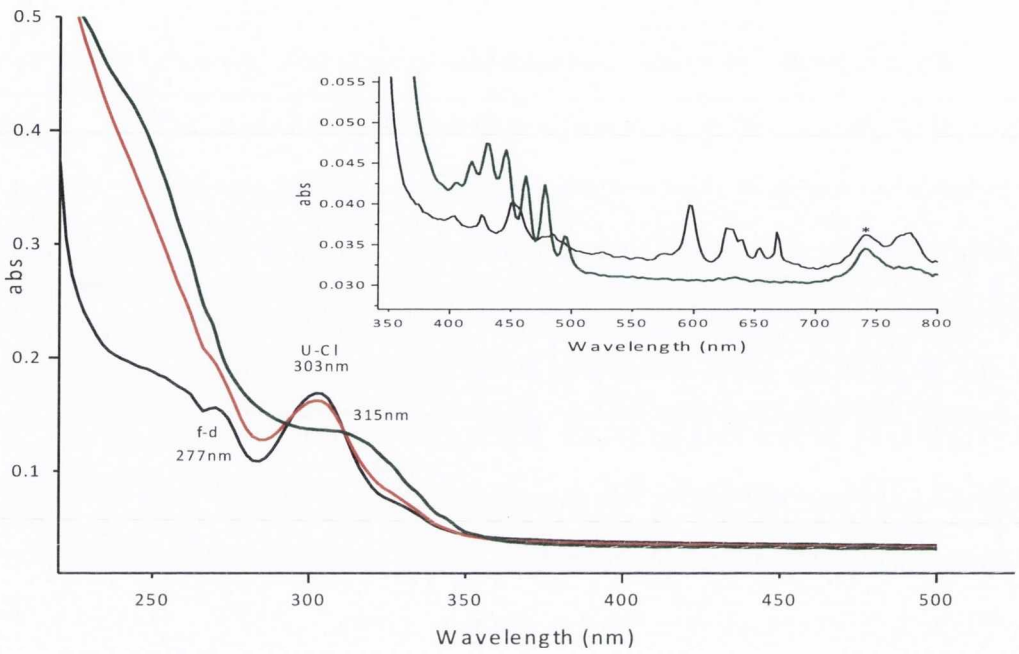

Figure 2.14: UV-Vis absorption spectra (220 – 500 nm) of 0.36 mmol THF solution of **1** in an inert atmosphere (black line), in air after 5 min (red line) and in air after 24hrs (green line) (insert is an expansion of the main spectra showing the loss of *f-f* transition (black line) and the growth of U=O vibronic coupling (green line)

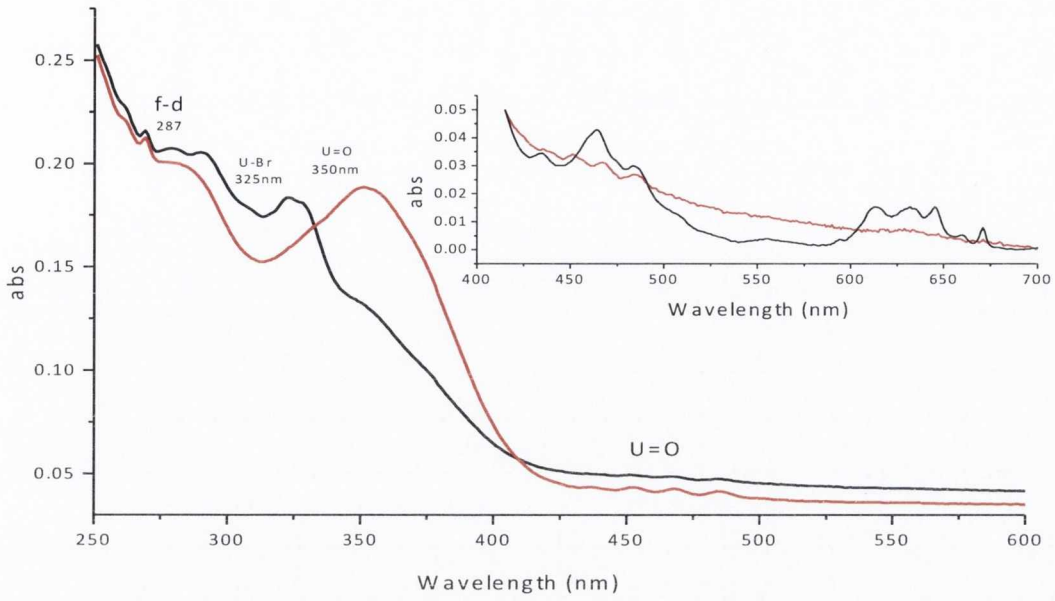

Figure 2.15: UV-Vis absorption spectra of 0.36 mmol of **2** in an inert atmosphere (black line) and in air (red line) (inset is an expansion to show the growth of U=O vibronic coupling (red line))

2.2.4.2 Effect of Symmetry on Absorption Profile of 1

$[A]_2[UCl_6]$ (A = $Li(THF)_4$, Et_4N, Bu_4N) allow a good comparison of the effect of geometry on the photophysical properties. Recent studies (e.g. using Cl K-edge XAS absorption spectroscopy)[31] showed spectroscopic involvement of both *5f* and *6d* orbitals in metal-ligand bonding. $[Li(THF)_4]_2[UCl_6]$ (**4**) was synthesised from the reaction of one equivalent of UCl_4 with two equivalents of LiCl followed by filtration and crystallisation to afford the thermally unstable green crystals in a good yield. $^7Li\{^1H\}$ NMR spectroscopy showed the lack of interaction between the uranium and the lithium in coordinating solvent such as THF, seen as a single resonance band at -1.98 ppm which shifts to -16.80 ppm in C_6D_6 as seen in Figure 2.16.

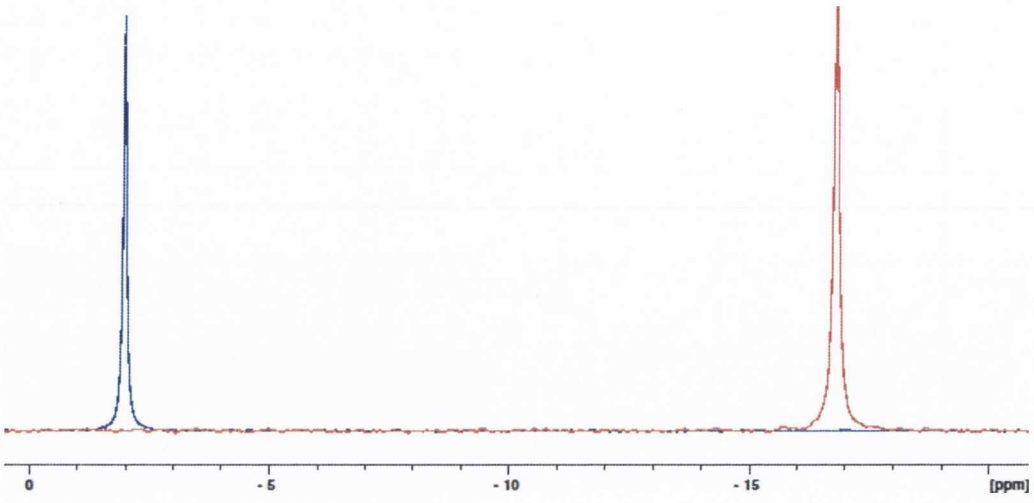

Figure 2.16: $^{7}Li\{^{1}H\}$ NMR Spectrum of **4** in THF (blue) and C_6D_6 (red)

Furthermore, $[R_4N]_2[UCl_6]$ (R = Et,[39] Bu[30]] were prepared according to previously reported procedure. The absorption spectrum of **4**, $[Et_4N]_2[UCl_6]$ and $[Bu_4N]_2[UCl_6]$ are all remarkably identical to each other and to that observed for **1** (Figure 2.17) and display absorption maxima at λ_{max} = 280 nm, 307 nm and 337 nm. There appears to be little difference in the energy of the bands for both **1** and **4**, which suggests that the local symmetry is not as important as the coordination geometry and THF to uranium charge transfer band can be discounted. In addition, when THF was replaced with acetonitrile or pyridine no significant change on the absorption spectra was observed. Unexpectedly the molar extinction coefficient for **4** is measured to be higher than that for **1** as the latter has a reduced symmetry of C_{4v} compared to **4** (O_h). This unexpected difference in molar extinction coefficient could be due to possible errors in determining the accurate concentration associated with the air sensitivity and instability of these compounds. However, the higher absorptivity of **4** can be explained by its intense colour when compared to an equimolar solution of **1** in THF as seen in Figure 2.18.

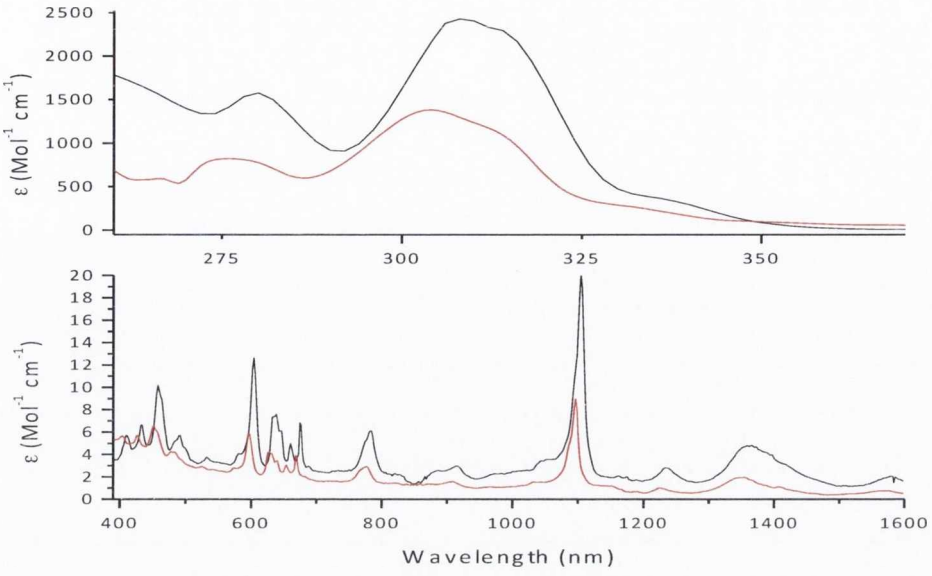

Figure 2.17: UV-Vis/NIR absorption spectra for **4** (black line) compared with **1** (red line)

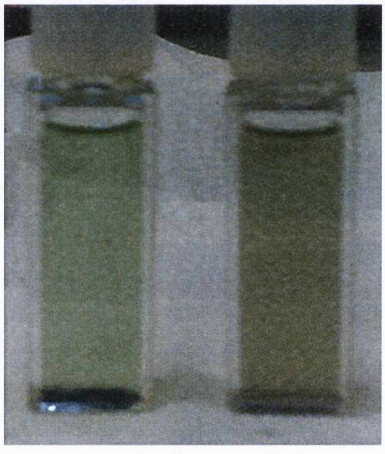

Figure 2.18: Picture of equimolar solutions of **1** (left) and **4** (right) in THF

$[UCl_4(THF)_3]$ was also prepared according to previously reported procedure[40] and its absorption spectrum in THF was similar to that observed for compound **1** and **4** with absorption maxima at λ_{max} = 272 nm, 300 nm and 330 nm. This again confirms that change in symmetry from C_{4v} for **1** to O_h for **4** and C_{2v} for $[UCl_4THF_3]$ does not have a noticeable effect on the absorption transitions and that the only charge transfer bands observed are LMCT resulting from halide-uranium charge transfer.

2.2.4.3 Emission Spectroscopy

Kirishima *et al.*[6] reported the first emission spectra of tetravalent uranium compounds in aqueous solution. The excitation wavelength of λ_{max} = 245 nm corresponds to the transition energy of $^3H_4 \rightarrow {}^1S_0$ of U^{4+} in 1M $HClO_4$ solution gave rise to emission spectrum with 12 different bands at 289, 292, 313, 319, 321, 335, 339, 346, 394, 410, 447 and 525 nm. Those bands were assigned to transitions of $^1S_0 \rightarrow {}^1I_6$, $^1S_0 \rightarrow {}^3P_1$, $^1S_0 \rightarrow {}^1G_4$, $^1S_0 \rightarrow {}^3P_0\ {}^1D_2$, $^1S_0 \rightarrow {}^3H_6$, $^1S_0 \rightarrow {}^3F_4$, $^1S_0 \rightarrow {}^3F_3$ and $^1S_0 \rightarrow {}^3H_5$.

Here, the emission spectroscopy of U(IV) in non-aqueous media is studied for the first time and compared to that of aqueous U(IV) reported by Kirishima. The photoluminescence spectroscopic measurements were conducted for solutions of an absorbance of ~0.2 – 0.5 absorbance units; whilst this is generally higher than ideally required for photoluminescence measurements, the weak U(IV) emission and the difficulties associated in the handling of these challenging samples, made this unavoidable. Furthermore, when lowering the concentration of the samples the emission spectra were dominated by the presence of uranyl due to rapid oxidation of U(IV) to U(VI) and consequently quantitative data of quantum yield for such compounds was not possible to determine.

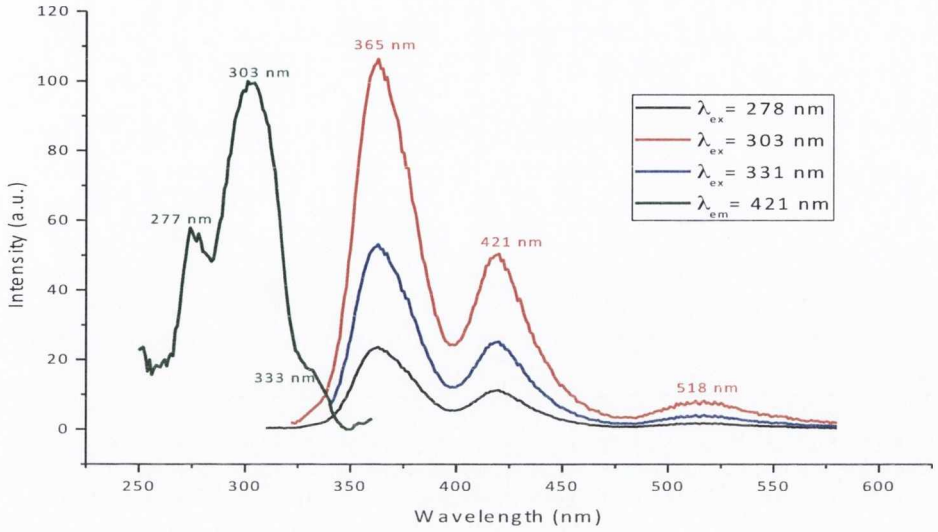

Figure 2.19: Emission and excitation spectra of **1** in THF excited at (λ_{ex} = 278 nm; black line), (λ_{ex} = 303 nm; red line) and (λ_{ex} = 331 nm; black line) and emitted at (λ_{em} = 367 nm; green line); slit width = 2.5 nm

Starting with compound **1,** the emission spectrum is noted to be wavelength independent and excitation into any UV-Vis absorption band of solutions **1** in THF (e.g. λ_{ex} = 277, 303 and 331 nm) produces identical emission spectra with three, featureless bands observable in the UV and visible region centred at 365 nm, 421 nm and 518 nm at different intensities (Figure 2.19). Changing the coordinated halide, the counter ion, the symmetry and the solvent showed no significant effect on the emission profile and compounds **2**, **3**, **4** and $[UCl_4(THF)_3]$ were shown to exhibit similar emission profile with a small shift in **2** and **3** that matches the red shift observed in the UV absorption spectrum as seen in Figure 2.20.

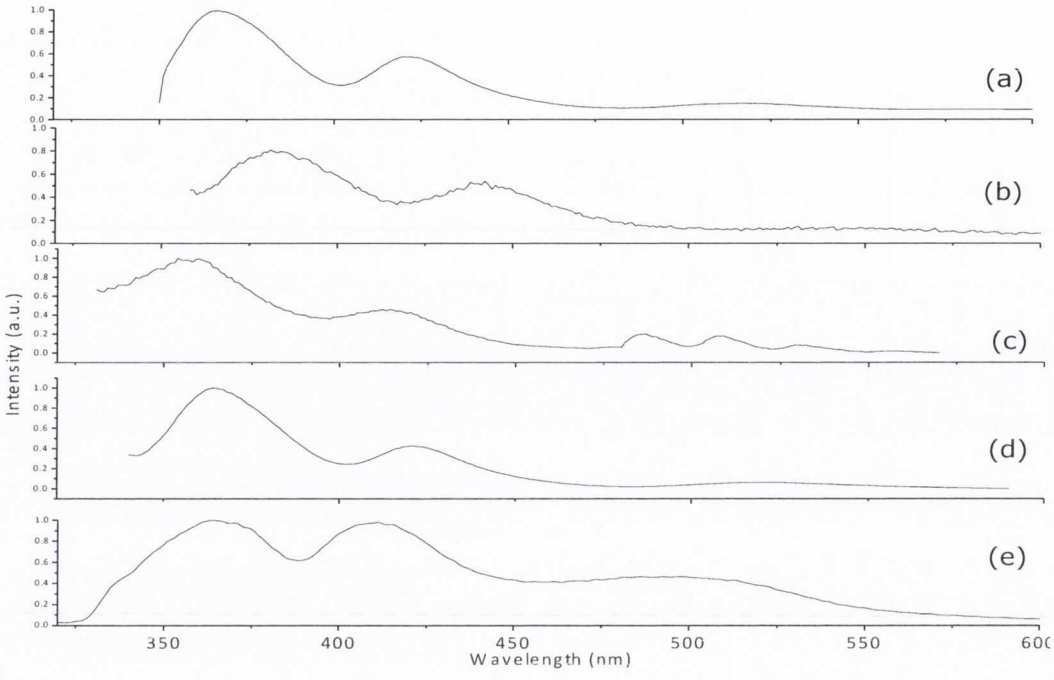

Figure 2.20: Emission spectrum of a) **1** in THF (λ_{ex} = 303 nm); b) **2** in THF (λ_{ex} = 325 nm); c) **3** in THF (λ_{ex} = 295 nm); d) **4** in THF (λ_{ex} = 303 nm) and e) $[UCl_4(THF)_3]$ in THF (λ_{ex} = 300 nm); all measured at 298 K

The consistent observation of three identical broad bands in the emission spectrum suggest that excitation into the highest energy absorption band results in excitation into vibrationally coupled states of the $5f^16d^1$ configuration, followed by relaxation into a lower energy level arising from the same electronic configuration resulting in emission at *ca.* 360 nm. The two remaining lower energy transitions at 421 and 518 nm are likely to terminate on successively higher energy Russell-Saunders coupled states in the $5f^2$ ground state configuration. From the absorption bands and the emission bands the three transition maybe assigned to $^3F_2 \rightarrow {}^3H_4$, $^3F_2 \rightarrow {}^3H_5$ and $^3F_2 \rightarrow {}^3H_6$. This is in agreement with the U(IV) doped solid state system U:$LiYF_4$,[7] although the photoluminescence spectra are considerably more resolved; an effect of increased vibrational coupling of the excited electronic states in fluid solution. In order to ascertain that the emission arises from the *f*-orbitals on U(IV), $[ThCl_4(DME)_2]$[41] was examined[42] and no photoluminescence spectra was

observed. The f-orbitals on the closed shell Th(IV) ion are known to be much higher in energy and generally not involved in bonding.[43]

The excitation spectra measured at the three emission wavelengths, λ_{em} = 360, 420 and 518 nm corresponding to the peaks of the emission spectrum shows the same excitation bands at 274, 303, 331 nm strongly suggesting that the emission bands originate from a common excited state. These bands were also observed to exhibit a "Stoke shift" when increasing sample concentration as illustrated in Figure 2.21. The emission spectrum for a sample with absorbance of 0.2 abs show three bands at 274, 303 and 331 nm which shift to 284, 314, and 343 nm respectively for a sample of higher concentration, an indication of higher concentration of impurities in the smaple.

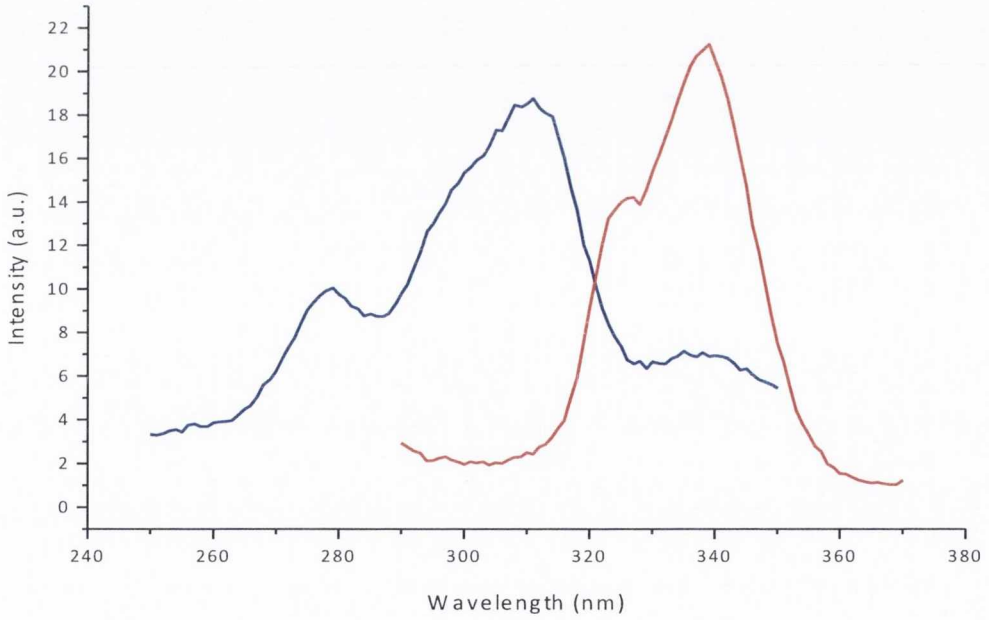

Figure 2.21: Excitation spectrum of **1** in THF at λ_{em} = 418 nm showing Stokes' shift as a result of increased solution concentration from absorbance unit of 0.2 for the CT band (red line) to 0.8 (blue line)

The room temperature emission spectroscopy gives very broad featureless emission bands. In order to obtain high resolution emission spectra to enable assign transitions to individual energy levels, low temperature (77 K) emission experiments were conducted. Compound **1** was measured in THF at liquid nitrogen temperature and the emission spectrum was consistently observed to be a mixture of U(IV) and a uranyl moiety U(VI), assigned on the basis of the diagnostic vibronically coupled uranyl peak centred at 520 nm (Figure 2.22).

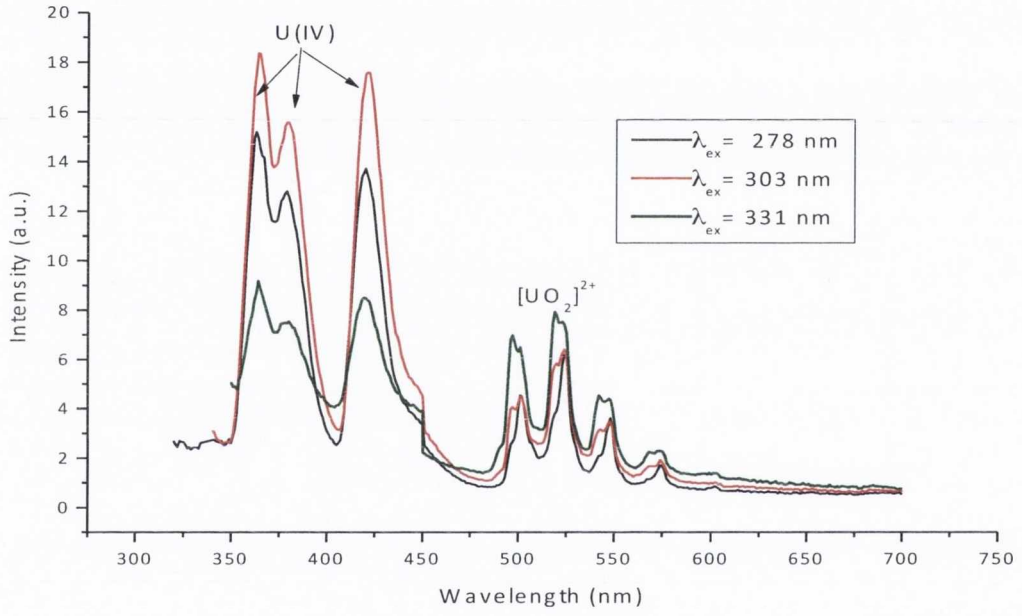

Figure 2.22: Liquid nitrogen temperature (77K) emission profile for **1** (λ_{ex} = 278, 303 and 331 nm)

The emission spectra obtained from the low temperature measurements promote an important argument that questions the nature of the emission spectra obtained for compounds **1 - 4**. In order to investigate the nature of the emission spectra, a solution of **1** in THF was exposed to air and the room temperature emission spectrum was recorded over 20 minutes intervals (Figure 2.23). The emission spectra clearly show a decrease in bands intensity of U(IV) species and an increase in the vibronically coupled $[UO_2]^{2+}$ band.

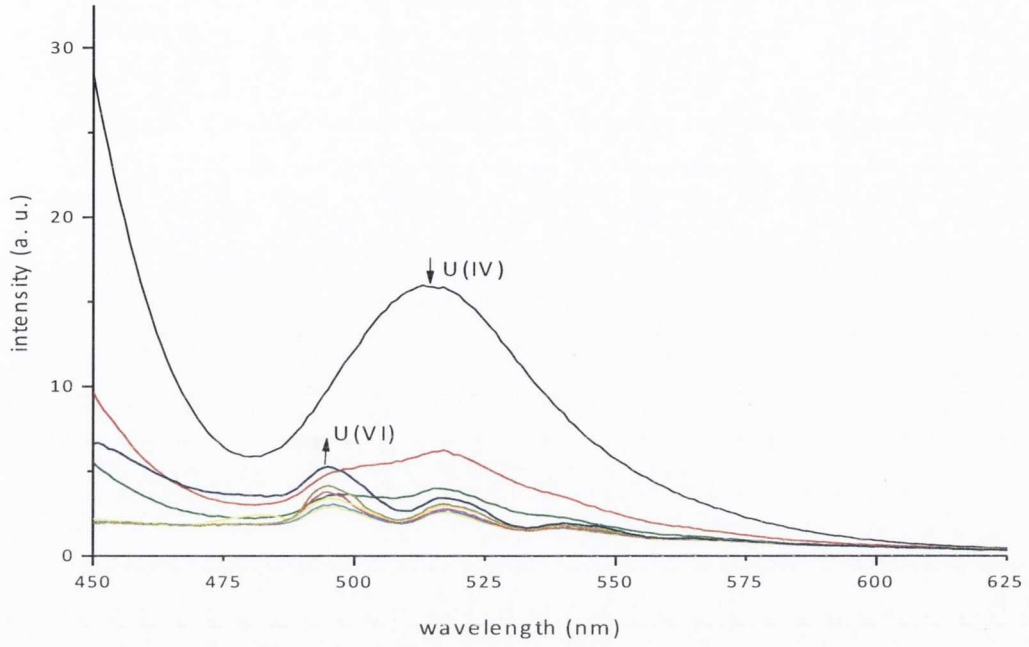

Figure 2.23: Oxidation of THF solution of **1** in air monitored by the emission band at 518 nm over time (λ_{ex} = 303 nm; 298 K)

After complete oxidation of **1** in air, monitored by emission spectroscopy, the compound was crystallised from a mixture of THF and pyridine. Small yellow crystals suitable for X-ray analysis were grown and the structure was determined to be $[PyH]_2[UO_2Cl_4]$; the structure is unremarkable, with metric parameters typical for this ion.[44] This structure determination proved the hypothesis that the spectrum is due to the uranyl(VI) ion as the low temperature emission spectrum of these crystals dissolved in THF show features that are identical to that observed for uranyl $[UO_2]^{2+}$ ions.[45] The chemical structure and the photophysical properties of this compound are discussed in Chapter 4.

2.2.4.4 Lifetime Measurements

Excitation at the CT bands λ_{ex} = 294 nm, multi-exponential de-convolution of the kinetic data of **1** showed emission of all three bands observed 365, 421 and 518 nm have the same radiative decay with a value of ~4 ns (Figure 2.24) indicating that each band originates from the same emissive state. Comparable emission lifetimes are observed for **2, 3, 4** and $[UCl_4(THF)_3]$ (value 2 – 10 ns). The kinetic decay profile of all complexes was fitted to multi-exponential decay suggesting multiple radiative processes occurring in fluid solution and the radiative decay involves more than one excited state. This behaviour is also observed in the broadening of the emission bands indicating mixing of more than one excited state.

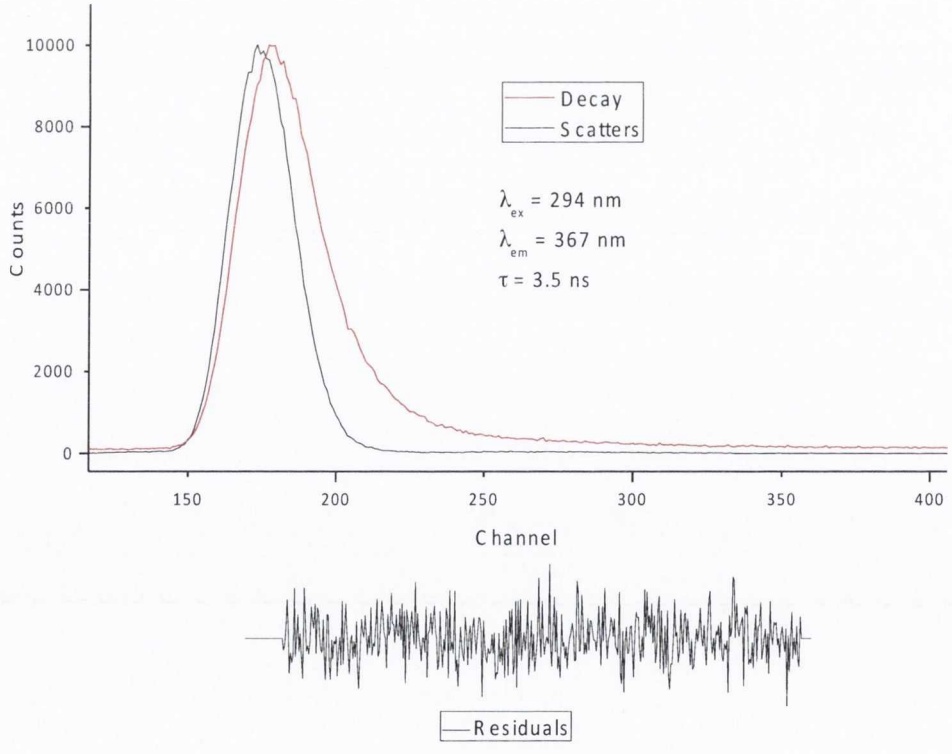

Figure 2.24: Typical kinetic traces obtained for **1** in THF recorded at 298 K following 294 nm excitation (red trace) and the instrument response function (using water as the scatterer, black trace); λ_{em} = 367 nm

The lifetime observed is comparable with the lifetime observed for the seven bands resolvable $5f^16d^1 \rightarrow 5f^2$ charge transfer bands in the system U:$LiYF_4$ (17 ns) and in the macrocyclic complex [U(DO3A)]Br (DO3A = [4,7,10-tris-carboxymethyl-,1,4,7,10-tetraaza-cyclododec-1-yl]-acetic acid) (8-12 ns).[7] It is therefore thought that photo-induced electron transfer from halide eg. Cl ions in complexes **1**, **4** and $[UCl_4(THF)_3]$ may act to quench the emission to a certain degree and/or bimolecular deactivation with labile THF solvent molecules may increase the rate of radiative decay. This makes sense when compared to organometallic compound in the metallocene ketimide system $[Cp^*_2U\{NC(Ph)(CH_2Ph)\}_2]$ (Cp^* = C_5Me_5) where the lifetime is very short.[10] Furthermore, direct excitation into the visible and near infra-red *f-f* U(IV) transitions (e.g. at *ca.* 420, 640, 880 and 980 nm) showed no emission indication of a very short lived transitions and therefore CASSCF calculations were performed to help characterise the emissive states in **1**.

2.2.5 Theoretical Analysis

2.2.5.1 Complete Active Space Self Consistent Field

State averaged CASSCF (complete-active-space self-consistent-field)[46] calculations were performed using version 7.6 of the MOLCAS code.[47] Dynamic correlation was included *via* multiconfigurational 2nd order perturbation theory (CASPT2).[48] All possible $5f^2$ and $5f^16d^1$ configurations were considered, resulting in 119 states in the absence of spin orbit coupling, which was included using the RASSI formalism.[49] This resulted in a total of 231 spin-orbit coupled states. Although the reduced symmetry of the complexes considered in this study means that atomic term symbols cannot be rigorously defined, the weak ligand field experienced by the uranium ion means that those dominated by $5f^2$ configurations can be approximated, and these approximate term symbols are quoted here. A comparison of the calculated transitions energies and states for **1**, **4** and $[UCl_4(THF)_3]$ is shown in the Figure 2.25 and values are listed in Table 2.4

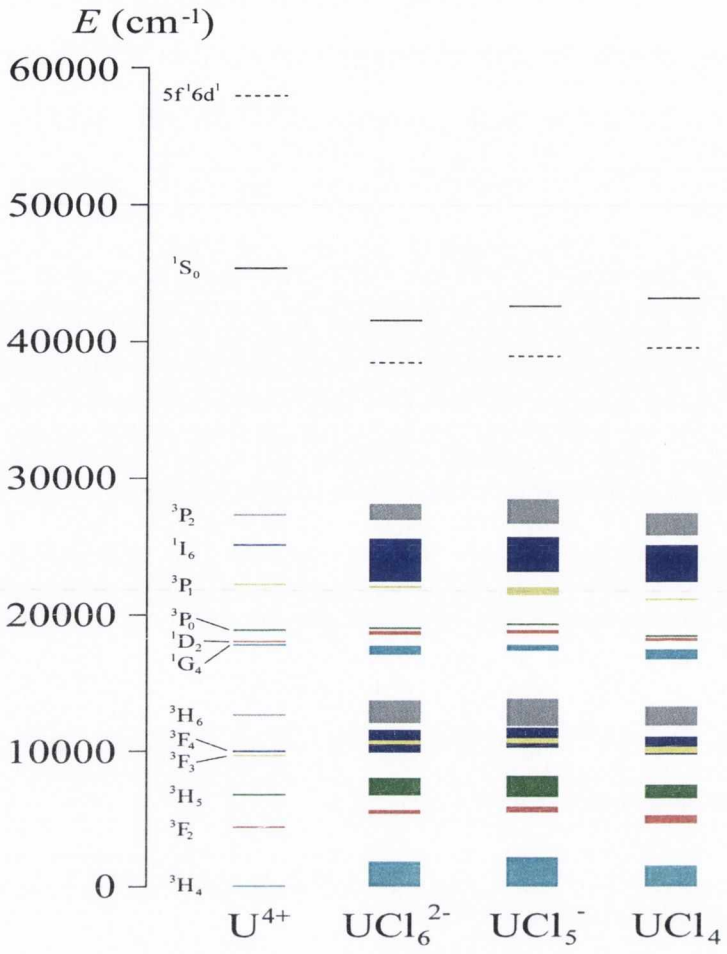

Figure 2.25: Computed mean ground and excited state energy levels and assignments for U^{4+} in H_2O, **4**, **1** and $[UCl_4(THF)_3]$. Note a PCM solvent continuum of H_2O was used in the calculations of U^{4+}, but no explicit water molecules ligated to the U(IV) centre were included, meaning the $^1S_0$ state may be artificially high in energy

$5f^2$ State	λ(nm) $[UCl_6]^{2-}$	λ(nm) $[UCl_5{\cdot}THF]^-$	λ(nm) $[UCl_4{\cdot}THF_3]$
$^3H_4$	256 (1)	251 (1)	241(1)
$^3F_2$	291 (0.33)	290 (0.29)	275 (0.38)
$^3H_5$	304 (0.14)	292 (0.16)	284 (0.17)
$^3F_4$	310 (0.14)	310 (0.086)	319 (0.17)
$^3F_3$	337 (0.14) **364**	334 (0.14) **365**	323 (0.12) **365**
$^3H_6$	325 (0.04)	334 (0.029)	327 (0.030)
$^1G_4$	439 (0.017) **424**	428 (0.018) **421**	413 (0.026) **408**
$^1D_2$	468 (5.3×10^{-3})	453 (5.0×10^{-3})	388 (0.01)
$^3P_1$	600 (2.7×10^{-3}) **510**	554 (3.2×10^{-3}) **518**	494 (5.0×10^{-3}) **500**

Table 2.4: CASPT2 calculated $5f^16d^1 \rightarrow 5f^2$ transitions for **1**, **4** and $[UCl_4(THF)_3]$. Values in parentheses are intensities, relative to the most intense $^3H_4$ transition; values in bold are the experimentally determined transitions

The CASPT2 calculations reveal that the $5f^2$ and $5f^16d^1$ manifolds interact only very weakly in the presence of spin orbit coupling, with the exception of the high energy $^1S_0$ state. In the absence of any $5f^16d^1$ contribution this state is calculated to lie 49500 cm^{-1} (202 nm) above the ground state; inclusion of the $5f^16d^1$ states results in significant stabilisation, to 42600 cm^{-1} (235 nm). The extent of the mixing is revealed when the contribution of the $5f^2$ spin-orbit free terms to the latter states is considered; this contribution is 24%. The lowest lying $5f^16d^1$ state is calculated to lie at 38600 cm^{-1} (259 nm; c.f. 278 nm experimental value) and so clearly, the $5f^16d^1$ manifold begins at a lower energy than the $^1S_0$ state. Of the other $5f^2$ states the highest in energy is calculated to lie at 28500 cm^{-1} (351 nm) and analysis of the calculated emission spectrum strongly supports the view that the observed emissions are due to $5f^16d^1 \rightarrow 5f^2$ transitions. Furthermore, the excitation wavelength (λ_{ex} = 260 to 390 nm) implies that the observed transitions originate from the lower part of the $5f^16d^1$ manifold, most probably the $^3F_2$ state.

Bearing this in mind, a subgroup of all calculated transitions was used in order to interpret the observed emission spectra. This subgroup consisted only of transitions originating from states in the $5f^16d^1$ manifold lying ≤ 44400 cm^{-1} (≥ 225 nm) above the ground state (i.e. just above the calculated position of the $5f^2$ $^1S_0$ state) and having an oscillator strength $f \geq 10^{-5}$. This reduced the number of considered transitions from 24627 to 915. The analysis reveals that the effect of the ligand environment is to significantly broaden all transitions, and so the positions quoted here are obtained as the peak value of all transitions to a given $5f^2$ state combined.

An intense peak is calculated at 251 nm and corresponds to a transition into the $^3H_4$ ground-state of the $5f^2$ manifold. Two strong peaks are calculated at 290 and 292 nm and correspond to transitions into the $^3F_2$ and $^3H_5$ states, respectively. An intense peak is calculated at 334 nm and is primarily due to a transition into the $^3F_3$ state, with a small component corresponding to a transition into $^3H_6$. Since there are no other transitions calculated to be in this energy range, we assigned the experimentally observed transition at 365 nm to the $^3F_3$ state. A weaker transition into the $^1G_4$ state is calculated at 428 nm and is assigned to the observed transition at 421 nm. There is also a very weak contribution to this peak from a transition into the $^1D_2$ state at 453 nm. At longer wavelengths, transitions become very broad and weak; the strongest transition is into the $^3P_1$ state at 554 nm, which we assign to the observed transition at 518 nm. No significant peaks are calculated at longer wavelengths.

2.3 Conclusions

On the basis of the experimental and computational results presented herein, it can be concluded that excitation into a band of charge transfer and *6d* orbital character leads to electron transfer into the *f*-orbital manifold. Notably, the absorption, excitation and emission spectra for all the halides complexes studied are similar, which supports the argument that in fluid solution at least, the geometry and local symmetry at the U(IV) ion has a minor effect on the optical properties of the complex. However, the CASPT2 data indicate that the energies and the relative ordering of the Russell-Saunders coupled levels derived from the $5f^2$ configuration show a degree of sensitivity to site symmetry and crystal field effects as might be anticipated for this *5f* ion. The observation that emission spectra of U(IV) can be measured in the presence of $[U^{VI}O_2]^{2+}$ may be of substantial benefit in environmental applications. Importantly, the relatively large quantum yield of uranyl(VI) emission in a frozen glass, means that trace quantities can be detected alongside U(IV). Furthermore, computational chemistry played an important rule to gain further insight into the electronic structure and is no doubt seeing a great progress in actinide chemistry.[50]

The charge transfer bands were confirmed using UV-Vis absorption spectroscopy and cyclic voltammetry. Notably the UV-Vis absorption spectra of the compounds **4** and $[UCl_4(THF)_3]$ in anhydrous THF are remarkably similar to **1** and display absorption maxima at 280 nm, 307 nm, 331 nm for **4** and 260, 290 and 334 nm for $[UCl_4(THF)_3]$[51] respectively, confirming that the change in symmetry does not have a noticeable effect and that the only charge transfer band observed was a halide-uranium charge transfer. Using the assignments from the absorption spectra and CASPT2 calculations, the bands in the emission spectra were assigned as transitions from the $5f^16d^1$ state to the $^2F_3$ (**1,** 365 nm; **2,** 384 nm; **4,** 364 nm; $[UCl_4(THF)_3]$, 365 nm), $^1G_4$ (**1,** 421 nm; **2,** 420 nm; **4,** 424 nm; $[UCl_4(THF)_3]$, 408 nm) and $^3P_1$ (**1,** 518 nm; **2,** 541 nm; **4,** 510 nm; $[UCl_4(THF)_3]$, 500 nm) $5f^2$ states. However, as the bands are quite broad the emissions are most

probably due to an envelope of energy levels; this is borne out to a certain extent by analysis of the CASPT2 calculated transitions and comparison to the assignments in earlier reports on doped systems.

Finally, whilst DFT calculations show a small degree of covalency in the U-Cl bond, the bonding is essentially ionic. Moreover, the assumption that the $^1S_0$ state could be used to investigate the degree of covalency was not successful as the $^1S_0$ is buried under the CT bands in **1**. However, the CT bands can be used to sensitise the emission, as an "antenna", commonly used in lanthanide spectroscopy, providing the ligand CT bands are in the UV region. For example, in the ketimide system,[10] where the CT bands are in the visible region and no emission from the *f*-orbital manifold is seen. This type of chemistry is discussed in detail in the uranium thiocyanate system in Chapter 3.

2.4 Experimental

All manipulations were carried out using standard Schlenk and glove box techniques under an atmosphere of high purity argon. ^{1}H and $^{7}Li\{^{1}H\}$ NMR spectra were recorded on a Bruker AV400 spectrometer operating at 400.23 MHz and 155.54 MHz respectively, and were referenced to the residual ^{1}H resonances of the solvent used or external LiCl. Raman spectra were obtained using 785 nm excitation on a Renishaw 1000 micro-Raman system in sealed capillaries. X-ray crystallography was measured on a Rigaku Saturn diffractometer. The crystals were mounted and the structures were resolved by Prof. Carola Schulzke (Greifswald University). The structures were solved by direct methods and refined on F^2 by full matrix least squares (SHELX97)[52] using all unique data. Crystal data, details of data collections and refinement are given in appendix A. Magnetic susceptibility measurements were carried out by Dr. M unuswamy Venkatesan (TCD). Thermal scans of magnetization in a 100 mT field from 4-300 K were carried out using a 5T Quantum Design MPMS XL SQUID magnetometer in a field of 100 mT. Powdered samples were mounted in gel caps, which have a temperature–independent diamagnetic susceptibility, in a glove box and the gel caps were placed in sample straws for the measurement. Diamagnetic corrections were made using Pascal's constants.[53] Multiple measurements were taken to ensure reproducibility. UV-Vis/NIR measurements were made on either a Perkin Elmer Lambda 1050 spectrometer or a double–beam Cary Varian 500 scan UV–Vis/NIR spectrophotometer over the range 300–1300 nm using fused silica cells with a path length of 1 cm. Steady-state emission spectra were recorded in screw-cap quartz cuvettes on a Horiba-Jobin-Yvon Fluorolog-3 spectrometer. Lifetime data were recorded following 294 nm and 340 nm excitation wavelength with a NanoLED. Lifetimes were obtained by tail fit on the data obtained or by a reconvolution fit using water as the scatterer, and quality of fit judged by minimisation of reduced chi-squared and residuals squared. Electrochemical measurements were undertaken with an AUTOLAB PGSTAT12

potentiostat/galvanostat using a platinum disc electrode with a reaction surface of 1 mm^2 as working electrode. A platinum rod electrode (together with internal referencing versus $[Cp_2Fe]^{0/+}$) was used as a reference electrode and a platinum knob electrode as auxiliary electrode. All measurements took place in a glove box under an atmosphere of high purity nitrogen, $[^nBu_4N][BPh_4]$ (0.1 M) was used as electrolyte.

Uranium stocks were obtained from TCD's stocks of U_3O_8, which was used to make the starting material UCl_4. THF and MeCN were distilled over potassium whilst d_5-pyridine, CD_3CN, and C_6D_6 were dried over Na, distilled and degassed immediately prior to use. Spectroscopic measurements used spectroscopic grade THF or MeCN solvents which were purchased from commercial sources and dried over potassium and molecular sieves and thoroughly degassed before use. $[UCl_4(THF)_3]$,[40] $[Et_4N][UCl_5(THF)]$[30] and $[Et_4N]_2[UCl_6]$[39] were made by previously reported methods whilst all other reagents were obtained from commercial sources. LiCl was dried by refluxing in freshly distilled $SOCl_2$ overnight, washing with copious CH_2Cl_2 and finally drying under vacuum. Me_3SiX (X = Br, I) was dried over 4Å Molecular Sieves and freeze-pump-thaw degassed immediately prior to use.

2.4.1 Synthesis of $[Li(THF)_4][UCl_5(THF)]$ (1)

To a suspension of LiCl (11 mg, 0.26 mmol) in THF (10 cm^3) was added a solution of UCl_4 (100 mg, 0.26 mmol) in THF (10 cm^3) and this was stirred for 24 hours at room temperature. The resulting green solution was filtered and the solvent reduced in volume. Placement at -30 °C overnight gave pale green crystals suitable for X-ray diffraction (150 mg, 0.19 mmol, 74%). ^1H NMR (CD_3CN; ppm): δ 3.64 (m, 4H, THF); 1.80 (m, 4H, THF); ^1H NMR (C_6D_6, ppm) δ -1.90 (b, 4H, THF), -4.69 (b, 4H, THF); $^7Li\{^1H\}$ NMR (THF, ppm) δ_{Li} -2.64; $^7Li\{^1H\}$ NMR (C_6D_6, ppm) δ_{Li} -20.42. MPt: 145-148 °C; Raman (cm^{-1}): 1185, 1138, 1027, 997, υ(THF) 305, υ(U-Cl); UV-Vis/NIR (ε (mol dm^{-3} cm^{-1}): (THF, ~0.36 mmol) 277 (832),

303 (1384), 331 (258); (THF, ~3.6 mmol) 404 (0.76), 428 (1.11), 452 (2.39), 484 (0.87), 599 (3.72), 627 (2.25), 655 (1.21), 667 (2.14), 778 (1.59), 909 (0.59), 1098 (7.81), 1227 (0.62), 1356 (1.60), 1571 (0.80), 1843 (15.83), 1970 (7.14) nm.

2.4.2 Synthesis of [Li(THF)$_4$][UBr$_5$(THF)] (2)

To a solution of **1** (50 mg, 0.064 mmol) in THF (5 cm^3) was added Me$_3$SiBr in excess (97.9mg, 0.64 mmol). The solution was stirred for 24 hours at room temperature and the solvent removed *in vacuo*. Dissolution in THF and placement at -30 °C overnight yielded dark green powder of **2** (42 mg, 0.042 mmol, 66 %) ^{1}H NMR (CD_3CN, 298 K): δ 3.50 ppm (m, 4H, THF), 1.62 ppm (m, 4H, THF); ^{1}H NMR (C_6D_6, 298 K) δ = -0.56 ppm (b, 4H, THF), -5.08 ppm (b, 4H, THF); ^{7}Li{^{1}H} NMR (THF, 298 K) δ_{Li} = -0.97 ppm; ^{7}Li{^{1}H} NMR (C_6D_6) δ_{Li} -6.32 ppm; UV-Vis/NIR (ε (mol dm^{-3}cm^{-1}): (THF, ~0.36 mmol): 277 (889), 325 (617), 350 (170); (THF, ~3.6 mmol) 433 (0.22), 464 (1.05), 483 (0.37), 554 (0.11), 614 (0.98), 632 (1.05), 664 (0.31), 670 (0.56), 795 (0.36) nm.

2.4.3 Synthesis of [Li(THF)$_4$][UI$_5$(THF)] (3)

To a solution of **1** (50 mg, 0.064 mmol) in THF (5 cm^3) was added Me$_3$SiI in excess (128mg, 0.64 mmol). The solution was stirred for 24 hours at room temperature to give a pale yellow solution. The solvent removed *in vacuo* and dissolution in THF followed placement at -30 °C overnight yielded a yellow powder that contained **3** and [Li(THF)$_4$]$_2$[UO_2I_4] which could not be separated. Spectroscopic data were obtained on this mixture. UV-Vis: 252, 295, 365, 597, 626, 653, 669, 776 nm; Emission spectrum (THF, 298K): 354, 412, 508 nm.

2.4.4 Synthesis of $[Li(THF)_4][UCl_6]$ (4)

To a suspension of LiCl (22 mg, 0.52 mmol) in THF (10 cm^3) was added a solution of UCl_4 (100 mg, 0.26 mmol) in THF (10 cm^3) and this was stirred for 24 hours at room temperature. The resulting green solution was filtered and the solvent removed under vacuum to give dark green crystalline powder (221 mg, 0.21 mmol, 82%). $^7Li\{^1H\}$ NMR (THF) δ_{Li} -1.98 ppm; $^7Li\{^1H\}$ NMR (C_6D_6) δ_{Li} -16.80 ppm; UV-Vis/NIR (ε (mol $dm^{-3}cm^{-1}$): (THF, ~0.36 mmol) 280 (1560), 307 (2400), 337 (350); (THF, ~3.6 mmol) 410 (1.05), 434 (1.80), 458 (3.05), 490 (1.31), 606 (5.22), 634 (4.10), 662 (1.51), 674 (4.06), 782 (3.27), 914 (1.02), 1105 (16.23), 1232 (1.02), 1361 (3.20), 1578 (1.10) nm.

2.4.5 Computational Details

DFT geometry optimisation was carried out by Dr. Jamie Platts (Cardiff University). It was performed on a single molecule of $[UCl_5(THF)]^-$, extracted from the crystal structure, at the unrestricted BP86/def2-TZVP[54,55] level using Turbomole[56] within C_2 symmetry. Scalar relativistic effects in uranium were included through use of effective core potentials, as defined for this basis set. Spin contamination was not significant, with values of S^2 within 1% of the anticipated value of 2.00. Further single-point DFT calculations were performed in Gaussian09[57] using the BP86 and B3LYP[58] functionals. The (27 s 24p 18d 14f 6 g)/[8s 7p 5d 3f 1g] all-electron ANO-RCC basis sets of DZP quality was used for uranium,[59] with 6-31+G(d,p) on C, O, H and Cl.[60] Scalar relativistic effects were included *via* the second-order Douglas-Kroll-Hess Hamiltonian.[61] Natural bond orbital (NBO) analysis[62] was performed using Gaussian09; Atoms-in-Molecules (AIM) analysis used AIMAll.[63] Topological analysis of the electronic density (ρ) is based upon those points where the gradient of the density, $\nabla\rho$, vanishes.[64] Points where one curvature (in the inter-nuclear direction) are considered positive and two (perpendicular to the bond direction) are negative, termed (3, -1) or bond critical points. Properties evaluated at such points characterise the

bonding interactions present. The second derivative of ρ or Laplacian, $\nabla^2\rho$, and the bond ellipticity, the ratio of the two negative curvatures, are reported, as is the local energy density, H, defined as the sum of the kinetic and potential energy densities. This reveals whether accumulation of electronic density is stabilising ($E<0$) or destabilising ($E>0$). Integrated properties of atoms were checked for numerical accuracy *via* the basin integral of the Laplacian, which should vanish for properly defined atomic basins (all values 10^{-4} or less), and also by comparison of the sum of all atomic integrals with directly calculated molecular values. Integration of the overlap matrix over atomic basins can be used to derive covalent bond order, as set out by Angyan *et al.*[65]

State averaged CASSCF (complete-active-space self-consistent-field)[46] calculations were carried out by Dr. Andrew Kerridge (UCL). The calculations were performed using version 7.6 of the MOLCAS code.[66] Calculations were performed using the all-electron ANO-RCC basis set,[67] of polarised triple-zeta quality, and scalar relativistic effects were included via the Douglas-Kroll-Hess Hamiltonian.[68] In these calculations, the two open shell uranium electrons were explicitly correlated in an active space of thirteen orbitals, comprising the *5f*, *6d* and *7s* uranium orbitals. Dynamic correlation was included via multiconfigurational 2nd order perturbation theory (CASPT2).[69] All possible $5f^2$ and $5f^16d^1$ configurations were considered, resulting in 119 states in the absence of spin orbit coupling, which was included using the RASSI formalism.[70] This resulted in a total of 231 spin-orbit coupled states. Although the reduced symmetry of the complexes considered in this study means that atomic term symbols cannot be rigorously defined, the weak ligand field experienced by the uranium ion means that those dominated by $5f^2$ configurations can be approximated, and these approximate term symbols are quoted here.

2.5 References

[1] L. Petit, A. Borel, C. Dual, P. Maldivi and C. Adamo, *Inorg. Chem.*, 2006, **45**, 7382

[2] E. Y. Wong, O. M. Stafsudd, D. R. Johnston, *J. Chem. Phys.*, 1963, **39**, 786

[3] a) P. L. Arnold, Z. Turner, N. Kaltsoyannis, P. Pelekanaki, R. Bellabarba and R. Tooze, *Chem. Eur. J.*, 2010, **16**, 9623; b) M. J. Tassell and N. Kaltsoyannis, *Dalton Trans.*, 2010, **39**, 6719; c) J. A. Bradley, S. SenGupta, G. T. Seidler, K. T. Moore, M. W. Haverkort, G. A. Sawatzky, S. D. Conradson, D. L. Clark, S. A. Kozimor and K. S. Boland, *Phys. Rev. B.*, 2010, **81**, 193104; d) S. A. Kozimor, P.Yang, E. R. Batista, K. S. Boland, C. J. Burns, D. L. Clark, S. D. Conradson, R. L. Martin, M. P. Wilkerson and L. E. Wolfsberg, *J. Am. Chem. Soc.*, 2009, **131**, 12125; e) L. Maron, O. Eisenstein and R. A. Andersen, *Organometallics*, 2009, **28**, 3629; f) K. I. M. Ingram, M. J. Tassell, A. J. Gaunt and N. Kaltsoyannis, *Inorg. Chem.*, 2008, **47**, 7824; g) R. G. Denning, *J. Phys. Chem. A.*, 2007, **111**, 4125; h) I. D. Prodan, G. E. Scuseria and R. L. Martin, *Phys. Rev. B.*, 2007, **76**, 33101; i) K. I. M. Ingram, N. Kaltsoyannis, A. J. Gaunt and M. P. Neu, *J. Alloys Compd.*, 2007, **444-445**, 369; j) A. J. Gaunt, S. D. Reilly, A. E. Enriquez, B. L. Scott, J. A. Ibers, P. Sekar, K. I. M. Ingram, N. Kaltsoyannis and M. P. Neu, *Inorg. Chem.*, 2002, **46**, 29; k) C. J. Burns, and M. S. Eisen, in *The Chemistry of the Actinide and Transactinide Elements*, 3rd ed.; L. R. Morss, N. M. Edelstein and J. Fuger, Eds.; Springer: Dordrecht, The Netherlands, 2006, **5**, 2799; l) R. G. Denning, J. C. Green, T. E. Hutchings, C. Dallera, A. Tagliaferri, K. Giarda, N. B. Brookes and L. J. Braicovich, *Chem. Phys.*, 2002, **117**, 8008; m) M. Mazzanti, R. L. Wietzke, J. Pecaut, J. -M. Latour, P. Maldivi and M. Remy, *Inorg. Chem.*, 2002, **41**, 2389; n) B. B. Iversen, F. K. Larsen, A. A. Pinkerton, A. Martin, A. Darovsky and P. A. Reynolds, *Inorg. Chem.*, 1998, **37**, 4559; o) J. Li and B. E. Bursten, *J. Am. Chem. Soc.*, 1997, **119**, 9021; p) J. G. Brennan, R. A. Andersen and J. L. Robbins, *J. Am. Chem. Soc.*, 1986, **108**, 335; q) M. L. Neidig, D. L. Clark and R. L. Martin, *Coord. Chem. Rev.*, 2012, **137**, 154707

[4] a) M. J. Hudson, L. M. Harwood, D. M. Laventine and F. W. Lewis, *Inorg. Chem.*, 2013, **52**, 3414; b) A. E. V. Gorden, M. A. DeVore and B. A. Maynard, *Inorg. Chem.*, 2012, **49**, 1578; c) D. Girnt, P. W. Roesky, A. Geist, C. M. Ruff, P. J. Panak and M. A. Denecke, *Inorg. Chem.*, 2010, **49**, 9627; d) Z. Kolarik, *Chem. Rev.*, 2008, **108**, 4208; e) C. Madic, B.

Boullis, P. Baron, F. Testard, M. J. Hudson, J. -O. Liljenzin, B. Christiansen, M. Ferrando, A. Facchini, A. Geist, G. Modolo, A. G. Espartero and J. De Mendoza, *J. Alloys Compd.*, 2007, **444-445**, 23; f) L. Petit, C. Daul, C. Adamo and P. Maldivi, *New J. Chem.* 2007, **31**, 1738; g) L. Petit, C. Adamo and P. Maldivi, *Inorg. Chem.*, 2006, **45**, 8517; h) G. R. Choppin and K. L. Nash, *Radiochim. Acta*, 1995, **70-71**, 225

[5] a) S.V. Godbole, A.G. Page, Sangeeta, S.C. Sabharwal, J.Y. Gesland and M.D. Sastry, *J. Lumin.*, 2003, **93**, 213; b) S. Hubert, E. Simoni, M. Louis, W.T. Zhang and J.Y. Gestland, *J. Lumin.* 1994, **60**, 245; c) M. Genet, P. Delamoye, N. Edelstein and J. Conway, *J. Chem. Phys.*, 1977, **67**, 1620; d) E. Simoni, S. Hubert and M. Genet, *J. Phys.*, 1988, **49**, 1425; e) C. Khan Malek, J. C. Krupa, P. Delamoye and M. Genet, *J. Phys.*, 1986, **7**, 1763; f) C. D. Flint and P. A. Tanner, *Mol. Phys.*, 1984, **53**, 429; g) C. K. Mallek and J. C. Krupa, *J. Chem. Phys.*, 1986, **84**, 6584; h) B. Ordejón, V. Vallet, J.-P. Flament, L. Seijoa and Z. Barandiarána, *J. Lumin.*, 2007, **126**, 779; i) B. Ordejón, M. Karbowiak, L. Seijo and Z. Barandiarána, *J. Chem. Phys.*, 2006, **125**, 74511

[6] A. Kirishima, T. Kimura, O. Tochiyama and Z. Yoshida, *Chem. Commun.*, 2003, 910; b) A. Kirishima, T. Kimura, R. Nagaishi and O. Tochiyama, *Radiochim. Acta.*, 2004, **92**, 705

[7] M. Kirm, J.C. Krupa, V. N. Makov, E. Negodin, G. Zimmerer, and J. Y. Gesland. *J. Lumin.*, 2003, **104**, 85

[8] W. T. Carnall, Gmelin *Handbook of Inorganic Chemistry 8th Edition*, Uranium. Supplement Volume **A5**, Chapter 2; Absorption and Luminescence Spectra, Springer-Verlag, Berlin Heidelberg, 1982

[9] V. A. Perfil'ev, D. V. Demeshko and V. T. Mishchenko, *Radiokhimiya*, 1991, **33**, 32.

[10] D. J. Hilton, R. P. Prasankumar, E. J. Schelter, V. K. Thorsmølle, S. A. Trugman, A. P. Shreve, J. L. Kiplinger, D. E. Morris and A. J. Taylor, *J. Phys. Chem. A.*, 2008, **112**, 7840

[11] J. F. Wyart, V. Kaufman and J. Sugar, *Phys. Scr.*, 1980, **22**, 389; b) C. H. H. Van Deurzen, K. Rajnak and J. G. Conway, *J. Opt. Soc. Am. B.*, 1984, **1**, 45

[12] J. L. Ryan, *Inorg. Chem.*, 1964, **3**, 211

[13] Lanthanide and Actinide Chemistry, Chapter **12**, *Electronic and Magnetic properties of the Actinide*, S. Cotton 2006

[14] D. M. Gruen and R. L. Macbeth, *J. Inorg. Nucl. Chem.*, 1959, **9**, 297

[15] C. Danilo, V. Vallet, J. -P. Flament and U. Wahlgren, *Phys. Chem. Chem. Phys.*, 2010, ***12***, 1116

[16] G. Liu and J.V. Beitz in *The Chemistry of the Actinide and Transactinide Elements*, L. R. Morss, N. M. Edelstein and J. Fuger (Eds), 2010, *Springer*, Dordrecht, The Netherlands

[17] Y. Baer, and J. K. Lang, *Phys. Rev. B.*, 1980, **21**, 2060 b) S. B. Nornes, and R. G. Meisenheimer, *Surf. Sci.*, 1979, **88**, 191; c) P. Söderlind, and K. T. Moore, *Scr. Mater.*, 2008, **59**, 1259

[18] B. M. Gardner, W. Lewis, A. J. Blake and S. T. Liddle, *Inorg. Chem.*, 2011, **50,** 9631

[19] O. Maury, M. Ephritikhine, M. Nierlich, M. Lance and E. Samuel, *Inorg. Chim. Acta.*, 1998, **279**, 210

[20] K. Krämer, H. U. Güdel, G. Meyer, T. Heuer, N. N. Edelstein, B. Jung, L. Keller, P. Fischer, E. Zych and J. Drozdzynski, *Z. Anorg. Allg. Chem.*, 1994, **620**, 1339

[21] G. Bombieri, D. Brown and C. Mealli, *J. Chem. Soc., Dalton Trans.*, 1976, 2025

[22] R. D. Shannon, *Acta Cryst.*, 1976, **A32**, 751

[23] S. Fortier, G. Wu and T. Hayton. *Inorg. Chem.*, 2008, **47**, 4752

[24] J. H. Van Vleck, *The Theory of Electric and Magnetic Susceptibilities*, Oxford University Press, London 1932

[25] a) B. S. Newell, T. C. Schwaab and M. P. Shores, *Inorg. Chem.*, 2011, **50**, 12108; b) I. Castro-Rodríguez, K. Olsen, P. Gantzel and K. Meyer, *J. Am. Chem. Soc.*, 2003, **125**, 4565; c) J. D. Rinehart, T. D. Harris, S. A. Kozimor, B. M. Bartlett and J. R. Long, *Inorg. Chem.*, 2009, **48**, 3382; d) O. P. Lam, C. Anthon, F. W. Heinemann, J. M. Connor and K. Meyer, *J. Am. Chem. Soc.*, 2008, **130,** 6567; e) M. J. Monreal, C. T. Carver and P. L. Diaconescu, *Inorg. Chem.*, 2007, **46**, 7226; f) Y. L. Lai, R. K. Chiang, K. H. Lii and S. L. Wang, *Chem. Mater.*, 2008, **20**, 523; g) L. Salmon, P. Thuery, E. Riviere, S. Miyamoto, T. Yamato and M. Ephritikhine, *New J. Chem.*, 2006, **30,** 1220; h) G. Nocton, F. Burdet, J. Pecaut and M. Mazzanti, *Angew. Chem., Int. Ed.*, 2007, **46,** 7574; i) G. Nocton, J. Pecaut and M. Mazzanti, *Angew. Chem., Int. Ed.*, 2008, **47**, 3040; j) S. Fortier, B. C. Melot, G. Wu and T. W. Hayton,

J. Am. Chem. Soc., 2009, **131**, 15512; k) E. J. Schelter, D. E. Morris, B. L. Scott, J. D. Thompson and J. L. Kiplinger, *Inorg. Chem.*, 2007, **46,** 5528

[26] a) P. L. Arnold, Z. R. Turner, N. Kaltsoyannis, P. Pelekanaki, R. M. Bellabarba and R. P. Tooze, *Chem. Eur. J.*, 2010, **16**, 9623; b) A. E. Clark, J. L. Sonnenberg, P. J. Hay and R. L. Martin, *J. Chem. Phys.*, 2004, **121**, 2563; c) L. Petit, L. Joubert, P. Maldivi and C. Adamo, *J. Am. Chem. Soc.*, 2006, **128**, 2190; d) I. Kirker and N. Kaltsoyannis, *Dalton Trans.*, 2011, **40**, 124; e) B. M. Gardner, D. Patel, A. D. Cornish, J. McMaster, W. Lewis, A. J. Blake and S. T. Liddle, *Chem. Eur. J.*, 2011, **17**, 11266; f) V. Vallet, U. Wahlgren and I. Grenthe *J. Phys. Chem. A*, 2012, **116**, 12373

[27] E. Hashem A. N. Swinburne, C. Schulzke, R. C. Evans, J. A. Platts, A. Kerridge, L. S. Natrajan and R. J. Baker, *RSC Adv.*, 2013, **3**, 4350

[28] a) A. E. Clark, J. L. Sonnenberg, P. J. Hay and R. L. Martin, *J. Chem. Phys.*, 2004, **121**, 2563; b) I. Kirker and N. Kaltsoyannis, *Dalton Trans.*, 2011, **40**, 124; c) B. M. Gardner, D. Patel, A. D. Cornish, J. McMaster, W. Lewis, A. J. Blake and S. T. Liddle, *Chem. Eur. J.*, 2011, **17**, 11266; d) V. Vallet, U. Wahlgren and I. Grenthe *J. Phys. Chem. A*, 2012, **116**, 12373

[29] L. Petit, L. Joubert, P. Maldivi and C. Adamo, *J. Am. Chem. Soc.*, 2006, **128**, 2190

[30] O. Mauray, M. Ephritikhine, M. Nierlich, M. Lance and E. Samuel, *Inor Chem Acta*, 1998, **279**, 210

[31] S. G. Minasian, J. M. Keith, E. R. Batista, K. S. Boland, D. L. Clark, S. D. Conradson, S. A. Kozimor, R. L. Martin, D. E. Schwarz, D. K. Shuh, G. L. Wagner, M. P. Wilkerson, L. E. Wolfsberg and P. Yang, *J. Am. Chem. Soc.*, 2012, **134**, 5586

[32] a) R. A. Satten, C. L. Schreiber and E. Y Wong, *J. Chem. Phys.*, 1965, 42, 162; b) W. Wagner, N. Edelstein, B. Whittaker and D Brown, *Inorg. Chem.*, 1977, **16,** 1021; c) M. Karbowiak, A. Mech and J. Drożdżyński, *J. Chem. Phys.*, 2005, **308**, 135

[33] C. Danilo, V. Vallet, J. -P. Flament and U. Wahlgren, *Phys. Chem. Chem. Phys.*, 2010, **12**, 1116

[34] a) C. Danilo, V. Vallet, J. -P. Flament and U. Wahlgren, *J. Chem. Phys.*, 2008, **128**, 154310; b) I. Infante, E. Eliav, M. J. Vilkas, Y. Ishikawa, U. Kaldor and L. Visscher, *J. Chem. Phys.*, 2007, **127**, 124308

[35] D. E. Morris, R. E. Da Re, K. C. Jantunen and I. Castro-Rodríguez, *Organometallics*, 2004, **23**, 5142

[36] F. Ossola, P. Zanella, P. Ugo and R. Seeber, *Inorg. Chim. Acta*, 1988, **147**, 123

[37] C. Clappe, D. Leveugle, D. Hauchard and G. Durand, *J. Electroanal. Chem.*, 1998, **448**, 95

[38] C. Schulzke, *Dalton Trans.*, 2009, **34**, 6683

[39] D. Brown, *J. Chem. Soc. A.*, 1966, **766**

[40] J. L. Kiplinger, D.E. Morris, B.L. Scott and C.J. Burns, *Organometallics*, 2002, **21** 5978

[41] T. Cantat, B. L. Scott and J. L. Kiplinger, *Chem. Commun.*, 2010, **46**, 919

[42] P. O. Adelani and T. E. Albrecht-Schmitt, *Inorg. Chem.*, 2010, **49**, 5701

[43] B. A. Maynard, K. S. Lynn, R. E. Sykora and A. E. V. Gorden, *J. Radioanal. Nucl. Chem.*, 2013, **295**, 453; b) B. A. Maynard, R. E. Sykora, J. T. Mague and A. E. V. Gorden, *Chem. Commun.*, 2010, **46**, 4944

[44] R. J. Baker, E. Hashem, M. Motevalli, H. V. Ogilvie and A. Walshe, Z. *Inorg. Allg. Chem.*, 2010, **653**, 443

[45] M. P Redmond, S. M. Cornet, S. D. Woodall, D. Whittaker, D. Collison, M. Helliwell, and L. S. Natrajan, *Dalton Trans.*, 2011, **40**, 3914

[46] B. Roos, P. R. Taylor and P. E. M. Siegbahn, *Chem. Phys.*, 1980, **48**, 157

[47] G. Karlström, *Comp. Mater. Sci.*, 2003, **28,** 222

[48] K. Anderson, P.-Å. Malmqvist, B. O. Roos, A. J. Sadlej and K. Wolinskit, *J. Phys. Chem.* 1990, 5483

[49] P. -Å. Malmqvist, B. O. Roos and B. Schimmelpfennig, *Chem. Phys. Lett.*, 2002, **357**, 230

[50] a) G. Schreckenbach and G. A. Shamov, *Acc. Chem. Res.*, 2010, **43**, 19; b) L. Gagliardi and B. O. Roos, *Chem. Soc. Rev.*, 2007, **36,** 893; c) N. Kaltsoyannis, *Chem. Soc. Rev.*, 2003,

32, 9; d) I. Kirker and N. Kaltsoyannis, *Dalton Trans.*, 2011, **40,** 124; e) M. J. Tassell and N. Kaltsoyannis, *Dalton Trans.*, 2010, **39,** 6719; f) D. Wang, W. F. van Gunsterenb and Z. Chai, *Chem. Soc. Rev.*, 2012, **41,** 5836

[51] UCl4 dissolved in THF exists as the monomeric tris THF adduct in dilute conditions/optically dilute conditions. see: a) A. I. Komyak, A. P. Zazhogin, D. S. Umreiko and A. A. Lugovsky, *J. Appl. Spectr.*, 2009, **76,** 167; b) W. G. van der Sluys, J. M. Berg, D. Barnhardt and N. N. Sauer, *Inorg. Chim. Acta.*, 1993, **204**, 251

[52] G. M. Sheldrick, SHELXL-97, University of Göttingen, Göttingen, Germany, 1998

[53] G. A. Bain and J. F. Berry, *J. Chem. Edu.*, 2004, **84**, 532

[54] a) A. D. Becke, *Phys. Rev. A,* 1988, **38** 3098; b) J. P. Perdew, *Phys. Rev. B.*, 1986, **33**, 8822

[55] F. Weigend and R. Ahlrichs, *Phys. Chem. Chem. Phys.*, 2005, **7**, 3297

[56] Turbomole v5.10, R. Ahlrichs, M. Baer, M. Haeser, H. Horn, C. Koelmel, *Chem. Phys. Lett.*, 1989, **162,** 165

[57] Gaussian 09, Revision B.01, M. J. Frisch, G. W. Trucks, H. B. Schlegel, G. E. Scuseria, M. A. Robb, J. R. Cheeseman, G. Scalmani, V. Barone, B. Mennucci, G. A. Petersson, H. Nakatsuji, M. Caricato, X. Li, H. P. Hratchian, A. F. Izmaylov, J. Bloino, G. Zheng, J. L. Sonnenberg, M. Hada, M. Ehara, K. Toyota, R. Fukuda, J. Hasegawa, M. Ishida, T. Nakajima, Y. Honda, O. Kitao, H. Nakai, T. Vreven, J. A. Montgomery, Jr., J. E. Pera ta, F. Ogliaro, M. Bearpark, J. J. Heyd, E. Brothers, K. N. Kudin, V. N. Staroverov, T. Keith, R. Kobayashi, J. Normand, K. Raghavachari, A. Rendell, J. C. Burant, S. S. Iyengar, J. Tomasi, M. Cossi, N. Rega, J. M. Millam, M. Klene, J. E. Knox, J. B. Cross, V. Bakken, C. Adamo, J. Jaramillo, R. Gomperts, R. E. Stratmann, O. Yazyev, A. J. Austin, R. Cammi, C. Pomelli, J. W. Ochterski, R. L. Martin, K. Morokuma, V. G. Zakrzewski, G. A. Voth, P. Salvador, J. J. Dannenberg, S. Dapprich, A. D. Daniels, O. Farkas, J. B. Foresman, J. V. Ortiz, J. Cioslowski and D. J. Fox, Gaussian, Inc., Wallingford CT, 2010

[58] a) A. D. Becke, *J. Chem. Phys.*, 1993, **98**, 5648; b) C. Lee, W. Yang, and R. G. Parr, *Phys. Rev. B.*, 1988, **37,** 785

[59] B. O. Roos, R. Lindh, P.-Å. Malmqvist, V. Veryazov, and P.-O. Widmark, *J. Phys. Chem. A.*, 2008, **112**, 11431

[60] a) W. J. Hehre, R. Ditchfield and J. A. Pople, *J. Chem. Phys.*, 1972, **56,** 2257; b) T. Clark, J. Chandrasekhar, G. W. Spitznagel, P. V. R. Schleyer, *J. Comp. Chem.*, 1983, **4,** 294; c) P. C. Hariharan and J. A. Pople, *Theoret. Chimica. Acta.*, 1973, **28,** 213

[61] G. Jansen and B. A. Hess, *Phys. Rev. A.*, 1989, **39**, 6016 and references cited therein

[62] A. E. Reed and F. Weinhold, *J. Chem. Phys.*,1985, **83**, 1736

[63] T. Keith, AIMAll http://aim.tkgristmill.com

[64] R. F. W. Bader "Atoms in Molecules - A Quantum Theory" *Oxford University Press*, Oxford, 1990

[65] T. Kar, J. G. Angyan, A. B. Sannigrahi, *J. Phys. Chem. A*, 2000, **104**, 9953

[66] G. Karlström, MOLCAS: a program package for computational chemistry. *Computational Materials Science*, 2003, **28,** 222

[67] a) B. O. Roos, R. Lindh, P.-Å Malmqvist, V. Veryazov and P.-O. Widmark, *J. Phys. Chem. A.*, 2004, **108,** 2851; b) B. O. Roos, R. Lindh, P.-Å. Malmqvist, V. Veryazov and P.-O. Widmark, *Chem. Phys. Lett.*, 2005, **409,** 295

[68] a) M. Douglas and N. Kroll, *Annals of Physics* 1974, **155**, 89; b) B. Hess, *Phys. Rev. A.*, 1986, **33,** 3742

[69] K. Anderson, P.-Å Malmqvist, B. O. Roos, A. J. Sadlej and K. Wolinskit, *J. Phys. Chem.* 1990, 5483

[70] P.-Å Malmqvist, B.O. Roos and B. Schimmelpfennig, *Chem. Phys. Lett.*, 2002, **357,** 230

Chapter 3

Spectroscopic Properties of Pseudohalide Uranium Complexes in Multiple Oxidation States

3.1 Introduction

Actinide complexes of the thiocyanate ligand have received a substantial amount of interest due to their potential in the field of spent nuclear fuel separation.[1] This system provides a chloride-free extractant for liquid-liquid extraction process used during the separation of actinide and lanthanide fission products, in particular trivalent americium from trivalent europium.[1] Liquid-liquid extraction is the most preferred and applied method in actinides recovery and purification, and over the years chemists have worked to improve the process by developing systems with greater selectivity, better overall recovery, improved physical properties, less toxicity and lower cost. Chloride-free systems can therefore provide an alternative extractant as they are less vicious, and less corrosive in comparison to lithium chloride-hydrochloric acid system used in alternative liquid-liquid extractions.[2] Moreover, thiocyanate, system was reported to have higher efficiency as an extractant ligand than the azide and isocyanate system.[3] For example, in the BTP ligand extraction system, the extraction of the trivalent lanthanides Nd(III) and Eu(III) was reported to be much more efficient for the thiocyanate than for the azide coordinated species[4] and ions such as N_3^- and NCO^- prefer the formation of unextractable outer-sphere complexes while $NCSe^-$ and NCS^- ions form extractable inner-sphere complexes.

Chapter 2 discussed the use of photoluminescence spectroscopy to study the electronic structures of tetravalent uranium ions to determine the contributions of valence *5f* orbitals in metal-ligand bonding and the participation of the *5f* and *6d* orbitals in forming covalent type bonding. This was exemplified by studying the electronic properties of simple uranium(IV) compounds such as $[Li(THF)_4][UX_5THF]$ (X = Cl, Br and I), $[Li(THF)_4]_2[UCl_6]$ and $[UCl_4(THF)_3]$ in non-aqueous solutions, and comparing them to those in solid state and in aqueous media,[5] where the assignment of the emission bands was shown to change

considerably when the highest energy term is corrected for a large Stokes' shift.[6] In this chapter, the effect of the geometry on the emission profile is further investigated and the electronic properties of the high symmetry uranium(IV) thiocyanate in non-aqueous media is studied using both spectroscopic and computational techniques. The pseudohalide $[U(NCS)_8]^{4-}$ ion makes a good model to study as the ligand based bands are in the UV region, and the high symmetry will allow the influence of the geometry on the photoluminescence properties to be explored. The 2,2'-bipyridine (bipy) adducts of the thiocyanate compounds are also explored in this chapter. The solid-state structure of the known complex $[Et_4N][U(NCS)_5(bipy)_2]$ has been re-determined and photoluminescence spectroscopic techniques have been utilised in order to confirm the oxidation state of the uranium and hence the bipy ligand.

Furthermore, the spectroscopic properties of the uranyl thiocyanate, $[UO_2(NCS)_5]^{3-}$, in ionic liquids[7] has recently been reported and some recent structural and Raman spectroscopic data[8] have shed light on these species, which have important implications in nuclear fuel reprocessing. Herein, the spectroscopic properties of uranyl thiocyanate compounds in non-aqueous media are fully explored; a spectroelectrochemical investigation of the redox nature of these compounds is reported and a comprehensive computational study allows the bonding to be analysed in detail.

3.2 Uranium(IV) Thiocyanate Compounds

3.2.1 Synthesis and Structural Characterisation

Actinide thiocyanate compounds of the type $[Et_4N]_4[M(NCS)_8]$ (M= Th, Pa, Np, and Pu) were prepared in the 1960's[9] and structurally characterised in 1971 where the anion was shown to have a cubic (O_h) geometry.[10] However, X-ray diffraction showed that the size and the geometry of the cation affect the packing arrangement in the lattice and favour a particular symmetry of the anion. For example, the corresponding Cs salt $Cs_4[M(NCS)_8]$ (M= U and Pu) has a square-antiprismatic (D_{4h}) anion symmetry,[11] but in solution all compounds show the same geometry, namely square anti-prismatic, based on ^{13}C NMR and vibrational spectroscopic data.[12] The shape of the counter-ion is therefore energetically more important than the crystal field effect, and is responsible for the geometry adopted by the anion $[(U(NCS)_8]^{4-}$.[10-12]

$[Et_4N]_4[U(NCS)_8]$ (**5**)[9] and $Cs_4[U(NCS)_8]$ (**6**)[11] were synthesised according to previously reported procedure. $[Bu_4N]_4[U(NCS)_8]$ (**7**) was also synthesised accordingly with some modifications. UCl_4 (1 eq.) was added to a mixture of tetrabutylammonium chloride (4 eq.) and sodium thiocyanate (8 eq.) in anhydrous acetonitrile. After stirring and filtration, single green crystals of **7** suitable for X-ray diffraction were grown by cooling at -20 °C. The solid state crystal structure, is shown in Figure 3.1 and bond lengths and bond angles are listed in Table 3.1.

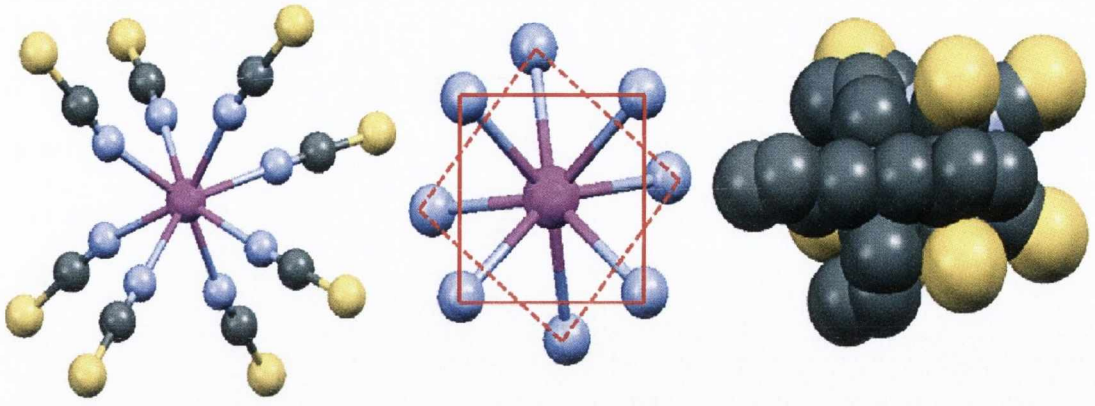

Figure 3.1: Solid state structure of the anion of **7** (left); depiction of the geometry of the anion (middle) and space filling diagram showing interaction of one cation with the anion (right)

U1-N2	2.406(4)	S6-C1	1.628(5)	N2-C1	1.163(7)
U1-N4	2.459(4)	S9-C6	1.631(8)	N4-C6	1.178(9)
U1-N5	2.439(5)	S10-C5	1.627(6)	N5-C5	1.168(7)
U1-N7	2.428(4)	S11-C7	1.635(5)	N7-C7	1.162(6)
U1-N9	2.429(4)	S14-C8	1.635(5)	N9-C8	1.148(7)
U1-N10	2.466(4)	S15-C9	1.648(6)	N10-C9	1.156(7)
U1-N26	2.425(4)	S31-C99	1.625(6)	N26-C99	1.153(7)
U1-N27	2.391(4)	S32-C204	1.606(6)	N27-C204	1.207(7)

N2-U1-N4	72.2(1)	N5-U1-N10	111.0(2)	U1-N5-C5	177.7(4)
N2-U1-N5	85.3(1)	N5-U1-N26	71.9(2)	U1-N7-C7	165.9(4)
N2-U1-N7	71.8(1)	N5-U1-N27	140.9(2)	U1-N9-C8	165.6(4)
N2-U1-N9	150.3(1)	N7-U1-N9	81.9(1)	U1-N10-C9	171.5(4)
N2-U1-N10	137.6(1)	N7-U1-N10	148.8(1)	U1-N26-C99	175.9(4)
N2-U1-N26	76.9(1)	N7-U1-N26	136.3(1)	U1-N27-C204	167.5(4)
N2-U1-N27	106.0(1)	N7-U1-N27	72.8(1)	S6-C1-N2	177.9(5)
N4-U1-N5	145.5(1)	N9-U1-N10	71.3(1)	S10-C5-N5	178.9(5)
N4-U1-N7	119.0(1)	N9-U1-N26	116.2(1)	S90C6-N4	177.7(6)
N4-U1-N9	134.7(1)	N9-U1-N27	78.1(1)	S11-C7-N7	178.8(5)
N4-U1-N10	73.4(1)	N10-U1-N26	72.1(2)	S14-C8-N9	179.1(5)
N4-U1-N26	77.7(1)	N10-U1-N27	86.0(2)	S15-C9-N10	178.1(5)
N4-U1-N27	72.0(1)	N26-U1-N27	146.6(2)	S31-C99-N26	178.1(5)
N5-U1-N7	75.7(1)	U1-N2-C1	165.4(4)	S32-C204-N27	179.0(5)
N5-U1-N9	75.0(1)	U1-N4-C6	174.9(5)		

Table 3.1: bond distances (Å) and bond angles (^{0}) in **7**

Compound **7** exhibits a distorted anti-prismatic symmetry (interplane N-U-N angles = 73 - 85°) with eight thiocyanate ligands coordinated to the uranium metal centre via the nitrogen atom. As expected, the unit cell parameters are similar to those observed for **5** and **6**. The U-N bond distances range from 2.391(4) to 2.466(4) Å with the average (2.43 Å) being close to that observed for **5** (2.38 Å)[9] and **6** (2.42 Å).[11] The average bond length for N=C and C=S are 1.16 Å and 1.63 Å respectively are very close to the average bond lengths in **5** and **6** (N=C 1.14 Å and C=S 1.61 Å for **5** And N=C 1.145 Å and C=S 1.60 Å for **6**). Whilst the bond lengths for **7** are similar (within error) to **5** and **6**, the geometry around the uranium and the subsequent packing of the anion are different. The less rigid butyl arms wrap around the voids in the uranium coordination sphere, and causes the U-N-C angle to bend to 165° creating a geometry is best described as a distorted square antiprism

For $[U(NCS)_8]^{4-}$ with cubic symmetry, two Raman active ν(C=N) stretches ($A_{1g} + T_{2g}$) appear at 2090 cm^{-1} and 2040 cm^{-1}, and one IR stretch at 2047 cm^{-1} (T_{1u}) are observed.[10] For $[U(NCS)_8]^{4-}$ with antiprismatic symmetry, three Raman-active ν(C=N) stretches ($A_1 + E_2 + E_3$) are observed at 2090 cm^{-1}, 2055 cm^{-1}, and 2045 cm^{-1}, and two IR stretches ($B_2 + E_1$) at 2047 cm^{-1} and 2090 cm^{-1}.[11] In the solid state, **7** shows three Raman bands at 2090 cm^{-1}, 2056 cm^{-1}, and 2045 cm^{-1} (Figure 3.2) and two IR stretches at 2047 cm^{-1} and a shoulder at 2090 cm^{-1} (Figure 3.3 (left)). This confirms its structural similarities with **6** in the solid state. In acetonitrile solutions, only one broad band at 2045 cm^{-1} was observed in the IR spectra (Figure 3.3 (right)) for compounds **5 - 7** with no free SCN^- from possible dissociation observed, seen by the absence of a band at 2060 cm^{-1}. The spectroscopic features of all compounds studied (**5 - 7**) are identical and for the purposes of the spectroscopic and theoretical discussion only **5** was studied in detail.

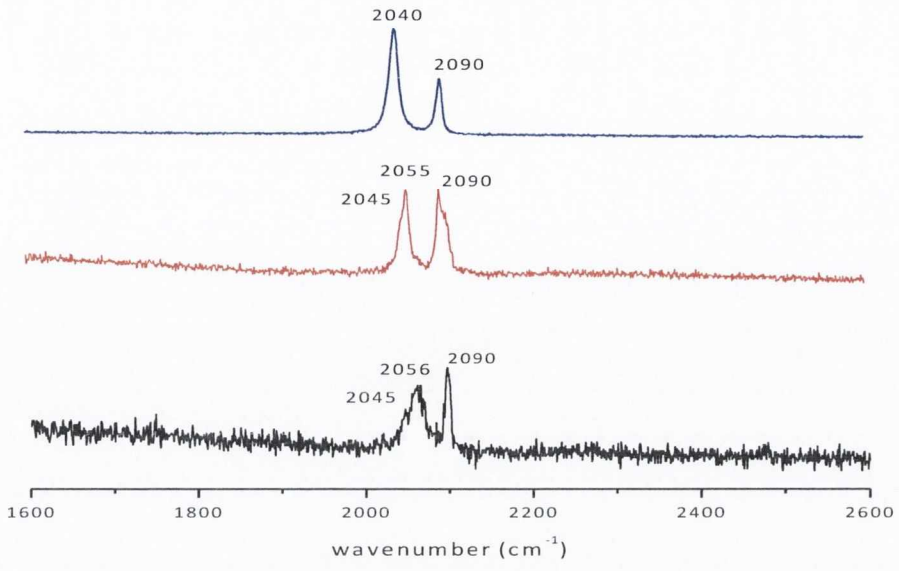

Figure 3.2: Raman spectrum of **5** (blue line), **6** (red line) and **7** (black line) in solid state showing the ν(C=N) vibrational stretch

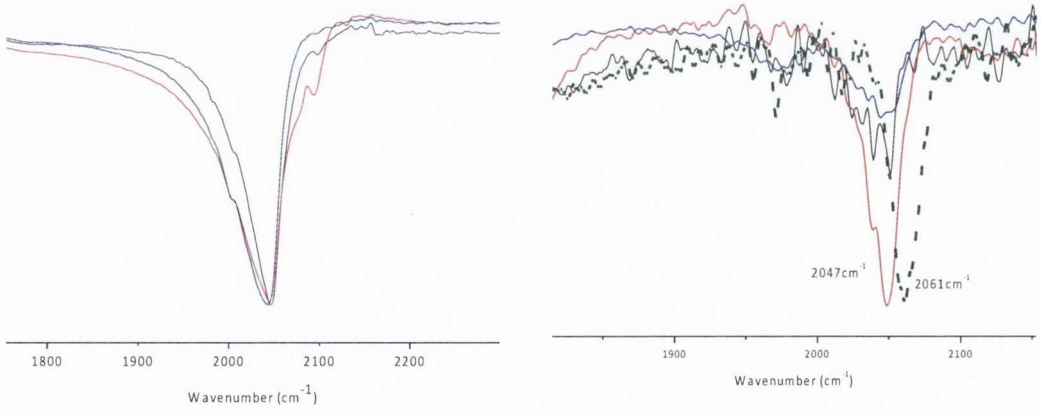

Figure 3.3: IR spectrum of **5** (blue line), **6** (red line) and **7** (black line), in solid state (left) and in acetonitrile solution (right). Dash line shows free NCS in acetonitrile

3.2.2 Magnetic Properties

Recent interest in uranium chemistry has come from the magnetic properties; in particular as a number of compounds show Single Molecular Magnetic (SMM) behaviour. For example, the U(III) species $[U(Ph_2BPz_2)_3]$,[13] $[U(H_2BPz_2)_3]$,[14] $[U(Tp)_3]$,[15] $[U(Tp^*)_2I]$,[16] $[U(Tp^*)_2(bipy)]I$,[17] $[(U(BIPMTMSH)(I))_2(\mu\text{-}\eta^6\text{:}\eta^6\text{-PhMe})]$,[18] and $[UO_2]^+$ complex $[\{[UO_2(salen)]_2Mn(Py)_3\}_6]$[19] all show SMM behaviour. Most interestingly it appears that SMM behaviour is an intrinsic property of U(III).[20] A recent computational study[21] has also suggested that U(IV) compounds could show unusual magnetic behaviour, particularly in tetragonal or trigonal prismatic geometries with the correct ground state. The magnetic properties of both the cubic, **5**, and the anti-prismatic, **6**, uranium(IV) thiocyanate compounds were investigated and are illustrated in Figure 3.4.

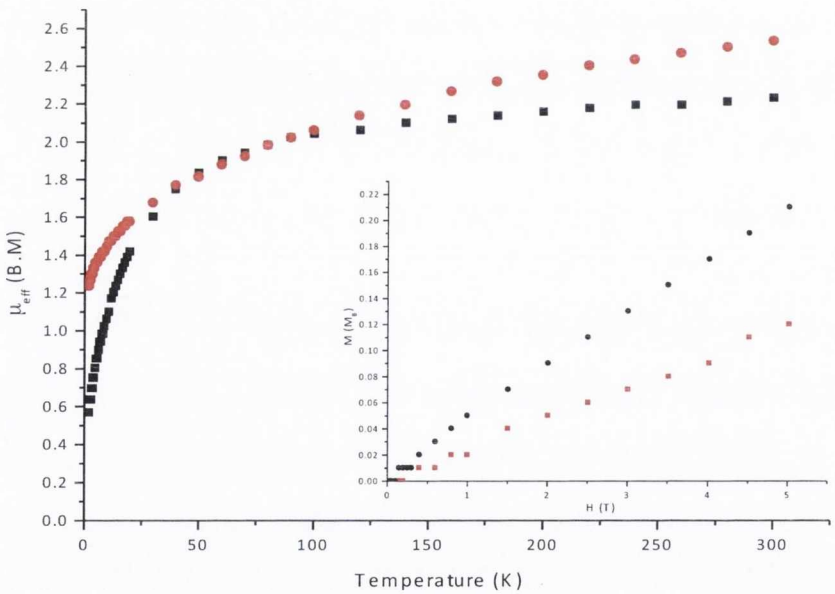

Figure 3.4: Temperature dependent magnetic susceptibility and field dependent magnetism for **5** (red) and **6** (black)

Variable temperature and variable field magnetic susceptibility are typical of U(IV) with a region of temperature independent paramagnetism followed by a precipitous drop at low temperatures for **6** compared to **5**, consistent with a singlet ground state with magnetic susceptibility value of 2.50 μB and 2.22 μB at room temperature and 1.2 μB and 0.5 μB at low temperature for **5** and **6** respectively. The low temperature magnetic susceptibility behaviour observed for **5** was previously related to the labile nature of the $[U(NCS)_8]^{4-}$ anion. The cubic configuration of **5** is only stabilised by the tetraethylammonium anion, while in **6** where the Cs+ salt is the cation, the $[U(NCS)_8]^{4-}$ anion exhibits a square anti-prismatic geometry. Furthermore the low temperature magnetic susceptibility value for **5** (1.2 μB) is within the range expected for uranium(V) complexes[22] and may be related to the degeneracy of the ground electronic state of the cubic $[U(NCS)_8]^{4-}$ anion. In order to obtain further information on the nature of this behaviour, alternating current (AC) susceptibility measurements were investigated but showed no unusual behaviour as illustrated in Figure 3.5.

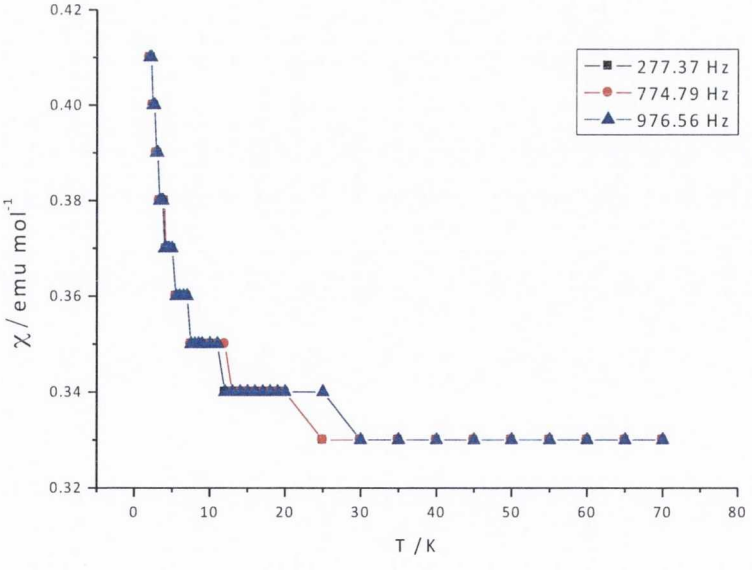

Figure 3.5: AC susceptibility for **5** showing its frequency dependence at 227.37 Hz (black line), at 774.79 Hz (red line) and at 976.56 Hz (blue line)

3.2.3 Photophysical Properties

3.2.3.1 Absorption Spectroscopy

The UV-Vis absorption spectrum of ~10^{-4} M acetonitrile solution of **5** was measured in an inert atmosphere. The electronic absorption spectra of **5** in acetonitrile in the UV-Vis region (Figure 3.6) display an intense band centered at 230 nm assigned to a Laporte allowed ligand centered n→π* transition within the thiocyanate chromophore. No *f-d* transitions were observed and are thought to be at higher energy than the solvent absorption (< 200 nm)

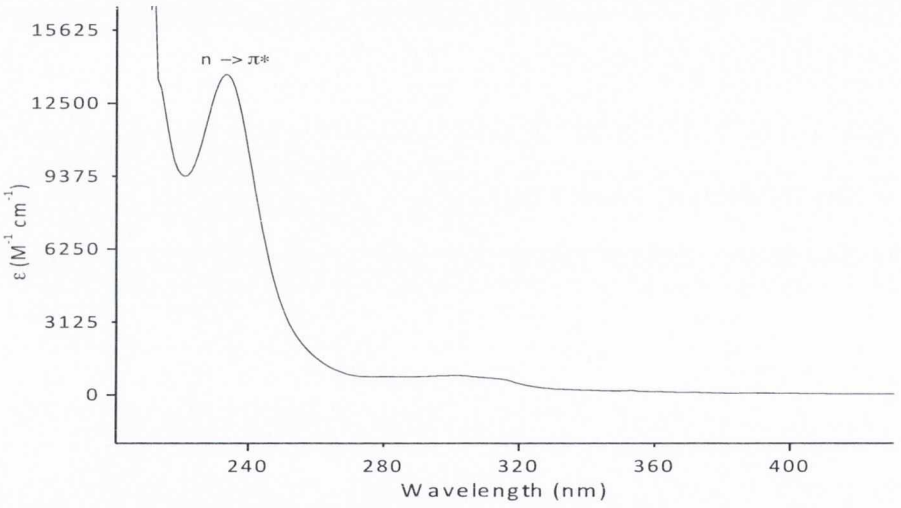

Figure 3.6: UV-Vis absorption spectrum of **5** in anhydrous MeCN at 298 K

In the Vis/NIR region (Figure 3.7) eight *f-f* bands were observed and are assigned to transitions from the Russell-Saunders coupled $^3H_4$ ground state to the states of higher energy.[12b] Those are: 475 nm (21050 cm^{-1}; $^3P_2$,), 505 nm (19840 cm^{-1}; $^1I_6$), 573 nm (17480 cm^{-1}; $^3P_1$), 691 nm (14490 cm^{-1}; $^3P_0$ $^1D_2$ $^1G_4$), 933 nm (10710 cm^{-1}; $^3H_6$), 1168 nm (8560 cm^{-1}; $^3F_4$), 1584 nm (6310 cm^{-1}; $^3F_3$ $^3H_5$), 1994 nm (5015 cm^{-1}; $^3F_2$), Since the geometry and crystal field effects are rather unimportant in the energy of the *f-f* transitions as shown from the uranium(IV) halide complexes in chapter 2,[23] theoretical values of $[U(H_2O)_8]^{4+}$ using CASPT2 techniques by Vallet.[24] an energy level diagram for **5** was constructed (Figure 3.7) and a direct

comparison of the observed experimental energies of the *f-f* transitions of different symmetry uranium(IV) compounds are obtained and are shown in Table 3.2.

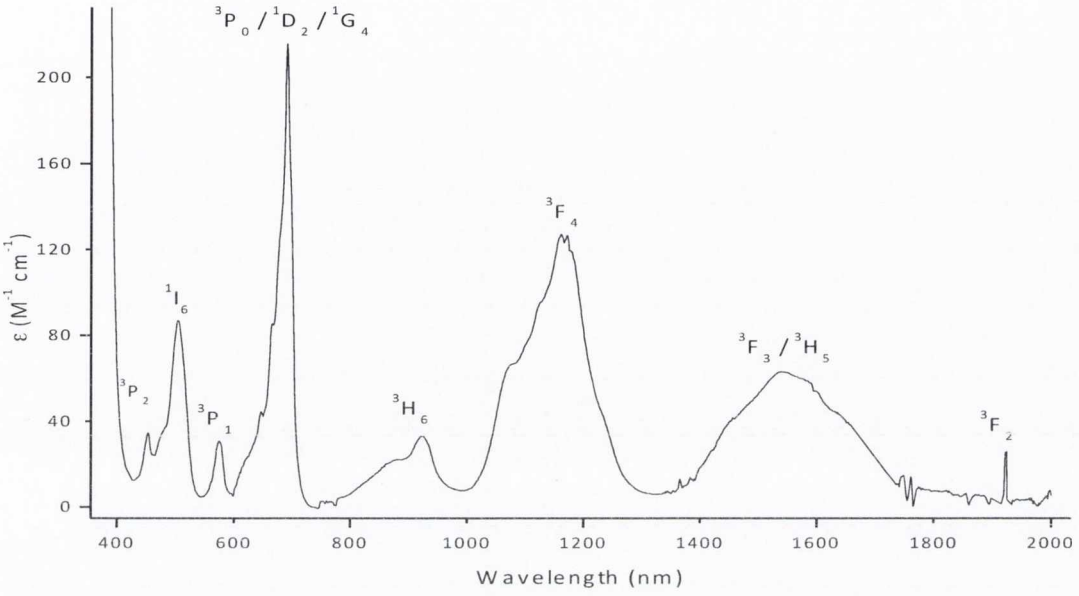

Figure 3.7: UV-Vis/NIR absorption spectrum of **5** in anhydrous acetonitrile, showing *f-f* transitions

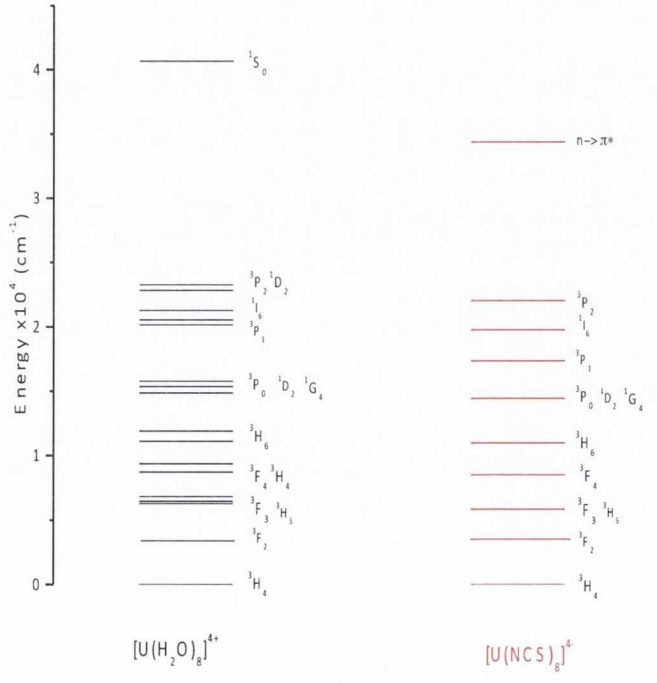

Figure 3.8: Energy level diagram of 8-coordinate U(IV) compounds[24]

Transition	Energy		
	$[U(H_2O)_8]^{4+}$ (a)	$[U(NCS)_8]^{4-}$ (b)	$[UCl_5(THF)]^{-}$ (b)
$^3F_2$	4161	5015	5076
$^3F_3$ / $^3H_5$	6137	6310	6365
$^3F_3$	8984		7374
$^3F_4$ / $^3H_4$	9434	8560	8149
$^3H_6$	11514	10710	1282
$^3F_4$ $^1G_4$	16656		14925
$^1D_2$ / $^3P_2$ / $^3F_2$	16465		15384
$^3P_0$ $^1D_2$ $^1G_4$	17128	14490	15948
$^3P_1$	19819	17480	16666
$^1I_6$	22276	19840	20661
$^3P_2$ $^1D_2$	24653	21050	22123
$^1S_0$	43614		
n-π^*		43478	
CT			30211 / 33003
f-d		>50000	35971

Table 3.2: Excitation energies in cm^{-1} for the $^3H_4$ ground state of U(IV) compounds in different geometries ((a) theoretical value; (b) experimental value)

3.2.3.2 Emission Spectroscopy

Attempts to obtain fluorescence profile of **5** by excitation into any of the absorption bands in MeCN gave no detectable signal. However, repeating the measurements in CD_3CN and exciting between 280 and 350 nm resulted in the observation of an emission spectrum as shown in Figure 3.9. A broad, weak band centred at 410 nm is observed and is consistent with the emission profile of the uranium halide complexes reported in Chapter 2, and the measured lifetime shown in Figure 3.10, of 10 ns is indicative of U(IV) species. The observation of an emission profile in deuterated solvents suggests that non-radiative processes are reduced on deuteration and possible quenching due to hydrogen bonding is eliminated.[25] Thus emission is observed due to an increased fluorescence quantum yield and lifetime of the excited state. Direct excitation into *f-f* transitions showed no emission in both MeCN and CD_3CN as the oscillator strengths are relatively weak.

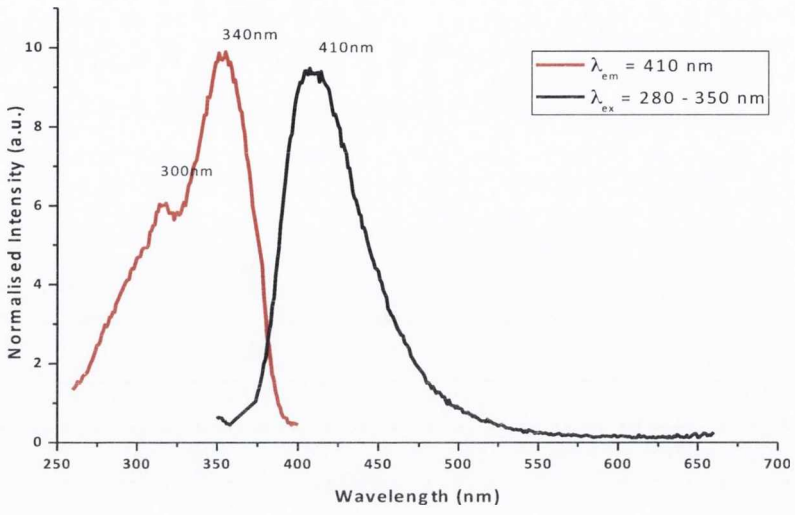

Figure 3.9: Excitation (black) and emission (red) spectra of **5** in CD_3CN at 298 K

The lifetime was measured at 294 nm excitation and the kinetic trace was best fitted to bi-exponential decay and subject to errors (χ^2 = 0.9847933). The second lifetime is less than 1 ns and the contribution from the second component is very small.

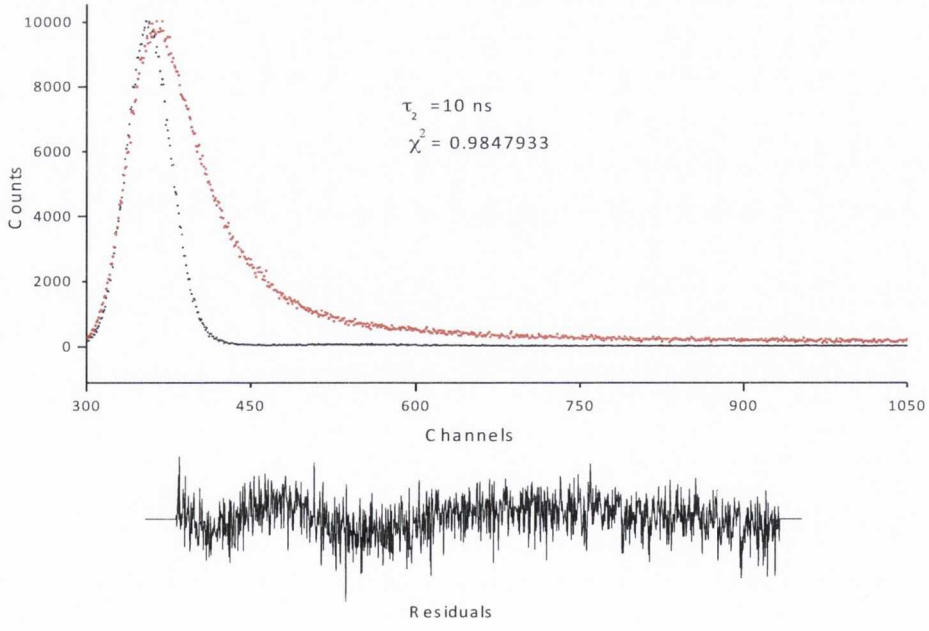

Figure 3.10: Typical kinetic traces obtained for **5** in CD_3CN recorded at 298 K following 340 nm excitation (red trace) and the instrument response function (using water as the scatterer, black trace); λ_{em} = 410 nm

It can be postulated that excitation into the ligand chromophore is followed by inefficient electron transfer and subsequent de-excitation through the *f*-orbital manifold. In effect, an 'antenna' effect is used to sensitise the emission of the U(IV) complex, which is reminiscent of lanthanide emission spectroscopy.[26] It is not possible to quantify the quantum yield for **5** as the emissions are weak, but the intensities of these emissions are comparable to the Raman bands from the solvent. Furthermore low temperature emission spectroscopy (Figure 3.11) shows the presence of both U(IV) thiocyanate and its oxidised form U(VI) thiocyanate.

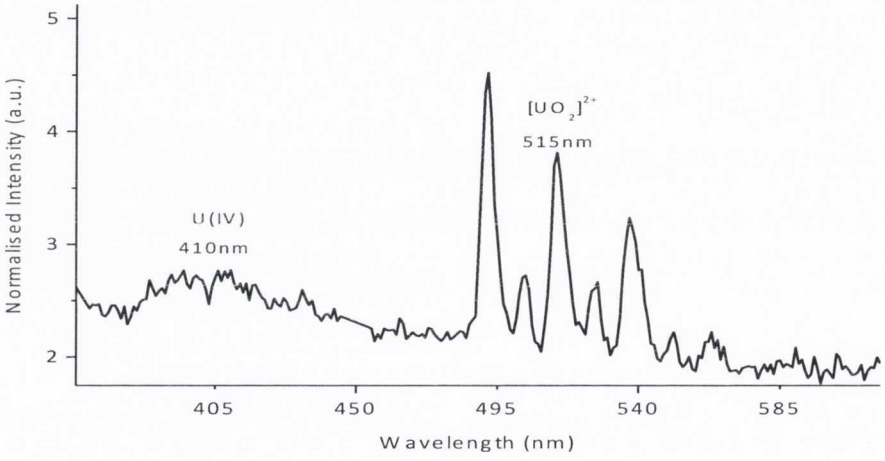

Figure 3.11: Emission profile of **5** at 77 K (λ_{ex} = 280 - 340 nm)

In order to eliminate the possibility that the emission profile is resulting from a uranyl impurity, two additional experiments were conducted; firstly, an authentic sample of $[Et_4N]_3[UO_2(NCS)_5]$, was prepared and measured in CD_3CN at 298 K, which gave vibronically coupled bands at *ca.* 520 nm with a lifetime of 1.5 μs this spectrum is essentially identical to that observed of this anion in ionic liquids and is discussed in Section 3.5.3.

Secondly, **5** was exposed to air and the emission profile was monitored over time. The decrease in intensity of the band at 410 nm and the ingrowth of the vibronically coupled bands at *ca.* 520 nm proves conclusively that the emission profile observed corresponds to U(IV) species (Figure 3.12). Final further evidence for the involvement of *f*-orbitals in the emission is that no emission from the corresponding $[Et_4N]_4[Th(NCS)_8]$[27] complex is observed where the *f*-orbitals in $[Et_4N]_4[Th(NCS)_8]$ are much higher in energy,[28] or from the free thiocyanate ligand (NaNCS) under identical conditions.

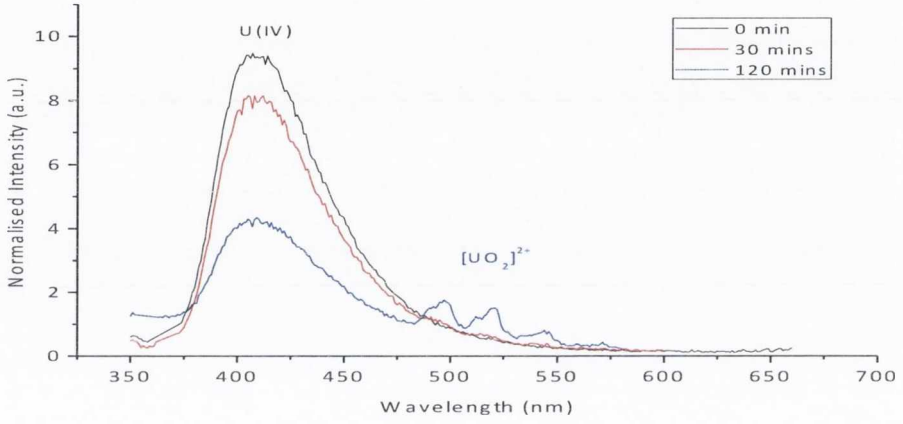

Figure 3.12: Emission profile of **5**, exposed to air at 298 K in CD_3CN (λ_{ex} = 280 - 350 nm) showing the emission profile of **5** in an inert atmosphere (black line), **5** in air after 30 mins (red line) and **5** in air after 120 mins (blue line)

3.2.3.3 Spectroelectrochemistry of 5

Compound **5** was further investigated using cyclic voltammetry. A solution of **5** in acetonitrile containing 0.1 M $[^nBu_4N][BPh_4]$ as a supporting electrolyte, measured at scan rate of 1 V/S shows two features (Figure 3.13 (left)): an irreversible reduction at -1.8 V *vs* Fc/Fc^+ ascribed to the U(IV)/U(III) redox couple, and a ligand based reversible oxidation at +0.22 V *vs* Fc/Fc^+. The observed values are comparable with the redox potential for An(IV)/An(III) and An(IV)/An(V) compounds as seen from Table 3.3. In order to confirm the U(IV)/U(V) redox couple, the analogue Th(IV) also compound was investigated.

Th(IV) does not have an accessible reduction to Th(III) and no available higher oxidation states. The cyclic voltammetry shows only the anodic wave at +0.22V Fc/Fc$^+$ (Figure 3.13 (right)). This electron transfer can therefore be ascribed to ligand based oxidation and suggests that the HOMO is predominantly ligand based, which has been borne out by DFT calculations (Section 3.6).

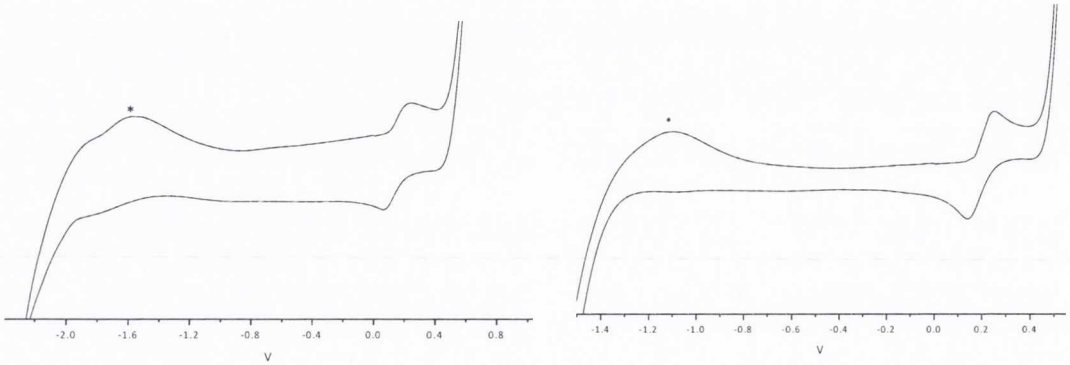

Figure 3.13: CV of compound **5** (left) and $[Et_4N]_4[Th(NCS)_8]$ (right) *vs.* Fc/Fc$^+$ in acetonitrile with $[^nBu_4N][BPh_4]$ as a supporting electrolyte recorded at 298 K and 1 V/s (* = impurity in electrolyte)

Complex	E/V *vs.* $[(C_5H_5)_2Fe]/Fe^+$		Ref
	An(IV)/An(III)	An(IV)/An(V)	
$[Et_4N]_4[U(NCS)_8]$ **5**	-1.8	0.22 (ligand based)	This work
$(C_5Me_5)_2UCl_2$	-1.85		29
$(C_5Me_5)_2U(CH_3)_2$	-2.41		30
$(C_5Me_5)_2U(\eta^2(N,N')$ $CH_3NN{=}CPh_2)(SO_3CF_3)$	-2.01	0.18	31
$(C_5Me_5)_2U[\eta^2(N,N')$-$CH_3NN{=}CPh_2]_2$	-2.78	-0.68	
$(C_5Me_5)_2U[\text{-}N{=}C(Ph)_2]_2$	-2.50	-0.48	
$(C_5Me_5)_2Th[\eta^2(N,N')$-$PhNN{=}CPh_2]_2$	-3.0		
$(C_5Me_5)_2Th[\text{-}N{=}C(Ph)_2]_2$	-2.8		

Table 3.3: Formal redox half potentials (*vs.* Fc/Fc$^+$) for the U(VI)/U(III) and (VI)/(V) couple of selected actinide complexes

Expanding the range for cyclic voltammetry and repeating at a lower scan rate showed a second oxidation feature at +0.52 V as seen in Figure 3.14.

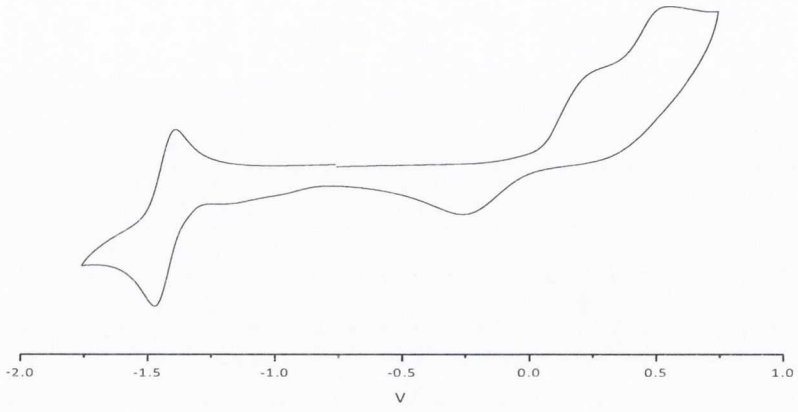

Figure 3.14: CV of compound **5** *vs.* Fc/Fc^+ in acetonitrile with $[^nBu_4N][PF_6]$ as a supporting electrolyte at 298 K and 0.1 V/ s

Spectroelectrochemistry was used to further investigate the chemistry of **5**. Spectroelectrochemical (SEC) measurements[32] are ideal for this type of system as the ν(N=C) and ν(C=S) frequencies of the thiocyanate ligand in the infrared spectrum and intraligand n-π* transition in the electronic absorption spectrum act as sensitive reporting parameters. The nature of the frontier orbitals and the chemical reversibility of the redox processes of **5** can be investigated. In addition, the *f-f* transitions in the uranium ion can also be used to monitor changes in its oxidation state, although, due to the high orbital symmetry these bands are rather weak.

The spectroelectrochemistry for **5** was carried out using controlled potential electrolysis in anhydrous acetonitrile containing ~0.1 M $[Bu_4N][PF_6]$ at 298K in an Optically Transparent Thin Layer Electrochemical (OTTLE) cell. Changes in the IR active ν(C=N) stretch and the ν(C=S) in the infrared spectral profile upon oxidation were examined and are shown in Figure 3.15. The one-electron ($1e^-$) oxidation process for **5** has been found to be fully reversible, in line with the recorded well-defined anodic wave and cathodic counter wave in the

corresponding thin-layer cyclic voltammogram (Figure 3.14) and a complete recovery of the parent complex after the potential cycle.

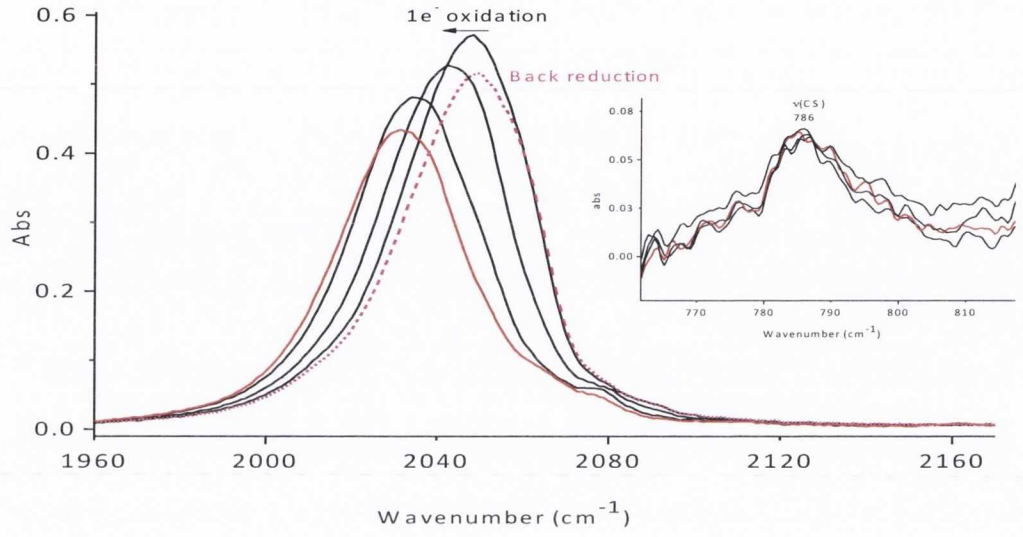

Figure 3.15: IR spectral changes in the ν(C=N) region and the ν(C=S) region (inset), accompanying the electrochemical reversible 1e⁻ oxidation of **5** in acetonitrile/ [^{n}Bu$_4$N][PF$_6$] at 298 K within an OTTLE cell showing the absorption bands for the parent complex **5** (black line), its oxidised form (red line) and the reproduction of the parent complex upon back reduction (dashed pink line)

The IR spectral profile in Figure 3.15 shows a reversible 1e⁻ oxidation of **5** in anhydrous acetonitrile solution; a shift of the ν(N=C) band from 2047 cm^{-1} (shown in black line) to 2031 cm^{-1} (shown in red line). The ν(C=S) band at 786 cm^{-1} (shown as an inset) remained unchanged and unaffected by this oxidation process suggesting little interaction with the uranium metal centre. The reversibility of the process was confirmed and the initial experimental spectral profile was reproduced upon back reduction (shown in dashed pink line). This confirms that the reversible oxidation profile observed in the voltammogram at +0.22 V is ligand based.

The corresponding UV-Vis spectral profile was also examined. The ligand-based 1e⁻ oxidation process of **5** shows a slight wavelength shift and small decrease in the intensity of the *f-f* transitions observed at 691 nm, 573 nm, and 505 nm (Figure 3.16) suggesting that the oxidation state of U(IV) in **5** remains unchanged, and further corroborates the ligand based oxidation.

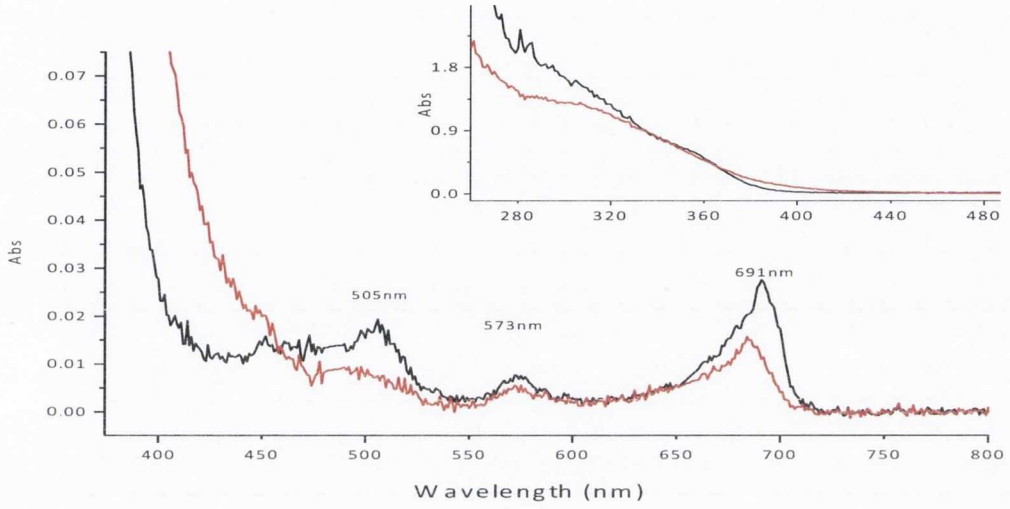

Figure 3.16: UV-Vis spectra of the 1e⁻ oxidation process of **5** recorded at 298 K in dry MeCN/ [^{n}Bu$_4$N][PF$_6$] with an OTTLE cell (ca. 0.2 mm optical path)

The subsequent two-electron (2e⁻) oxidation of **5** at +0.52 V was also investigated spectroelectrochemically (Figure 3.17) and shown to be electrochemically irreversible. The ν(C=N) band at 2031 cm^{-1} (shown in red) dropped in intensity and a new weak band at 2160 cm^{-1} grew in, which matches the vibrational bands for the NCS· radical.[33] Back reduction of the product at *ca.* +0.30 V (corresponding to a well-defined cathodic wave in the thin-layer CV) did not recover the parent compound **5**. Instead, it resulted in the appearance of a new ν(C=N) band at 2060 cm^{-1} (shown in black line) characteristic of NCS–SCN.[33] The UV-Vis spectra (Figure 3.18) corresponding to the secondary anodic product absorbing at 2160 cm^{-1} showed two bands characteristic of the chromophore at λ_{max} = 290 nm and 340 nm.[34] The disappearance of the *f-f* transitions reflects a decomposition of the U(IV) complex; although, the fate of the uranium compound is unknown.

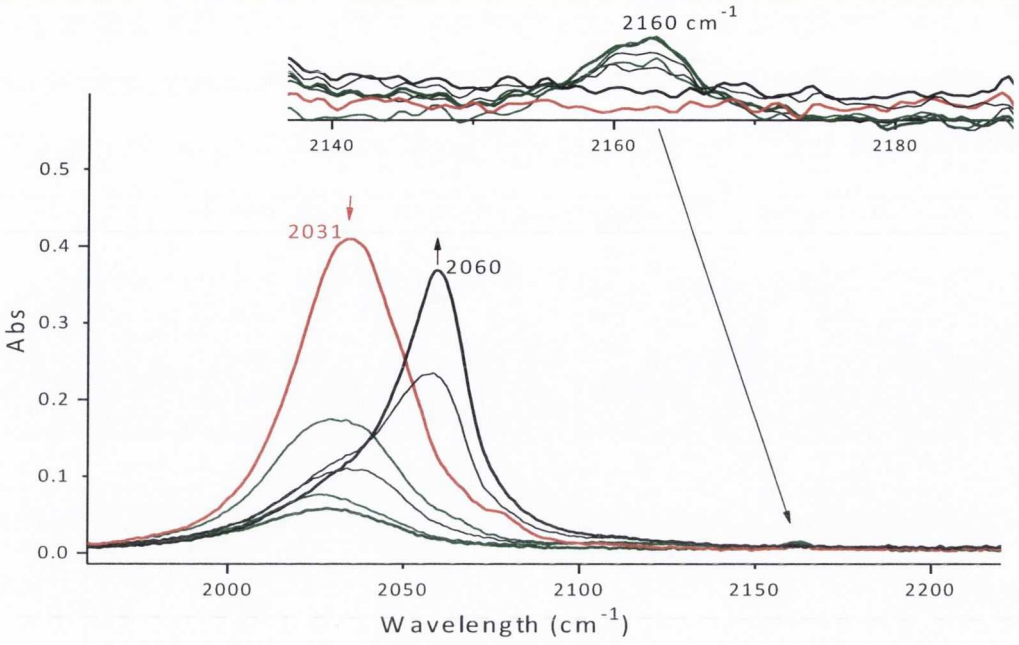

Figure 3.17: IR spectral changes in the ν(C=N) region accompanying the irreversible 2e⁻ oxidation of **5** in acetonitrile/ [^{n}Bu$_4$N][PF$_6$] at 298 K within an OTTLE cell showing the band for the parent complex (red line), its oxidised form (green line) and the back reduction (black line). Inset is expanded view of the band forming at 2160 cm^{-1}

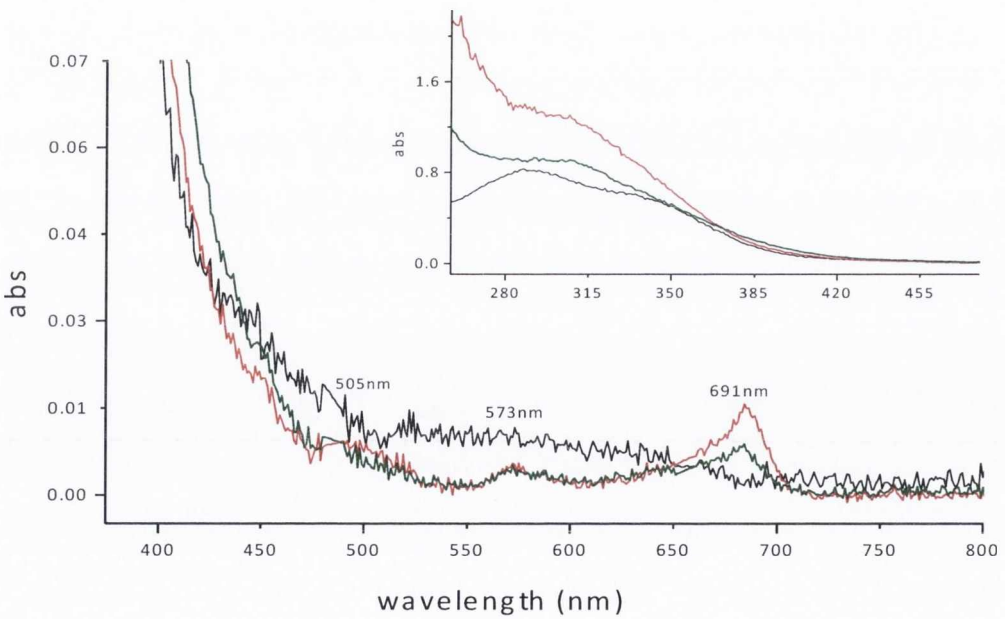

Figure 3.18: UV-Vis spectrum of 2e⁻ oxidation of **5** recorded at 298 K in dry MeCN containing [^{n}Bu$_4$N][PF$_6$] within an OTTLE cell

From this, it is postulated that whilst the 1e- oxidation of **5** is a reversible ligand based oxidation process, the 2e- oxidation process is irreversible and results in the formation of the free short lived radical coordinated U(IV) species $[Et_4N]_4[U(NCS)_8]^{\cdot}$, which then combine to form the dithiolate NCS-SCN species as illustrated in Scheme 3.1.

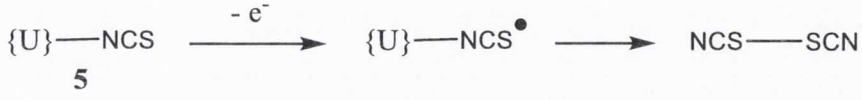

Scheme 3.1: Spectroelectrochemical oxidation process of **5**

Attempts to access the ligand-based oxidation chemically have not yielded tractable product. However, exposure of an acetonitrile solution of **5** to UV light over a period of time resulted in the growth of two bands in the UV-Vis region at λ_{max} = 290 nm and 340 nm (Figure 3.19) characteristic of the chromophore within the thiocyanate ligand and similar to those observed upon the 2e- oxidation process of **5**. The formation of those bands is thought to be associated with photochemical oxidation of **5** to give a radical coordinated thiocyanate compound $[Et_4N]_4[U(NCS)_8]^{\cdot}$ (**8**). Crystallisation from MeCN yielded orange crystals of **8** suitable for X-ray diffraction and the solid state structure is shown in Figure 3.20.

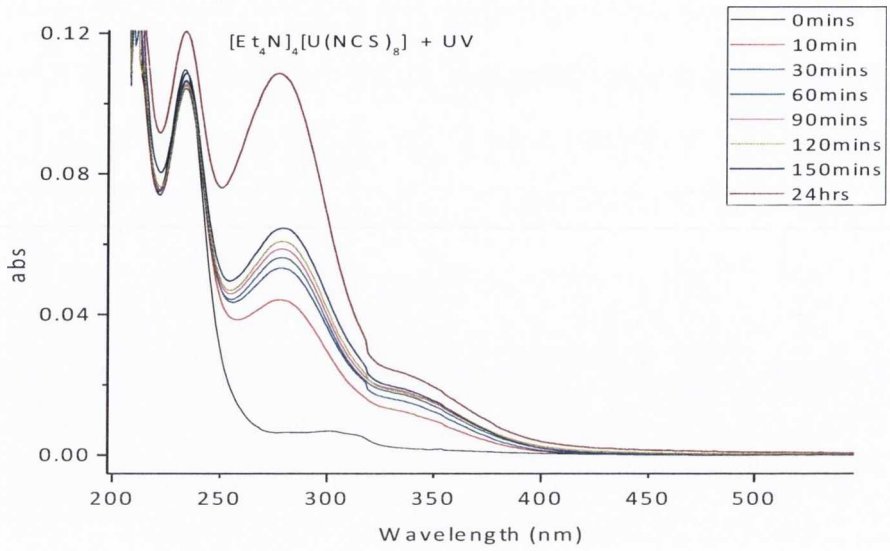

Figure 3.19: Change in UV-Vis spectrum of **5** in MeCN upon exposure to UV light (λ_{ex} = 340 nm)

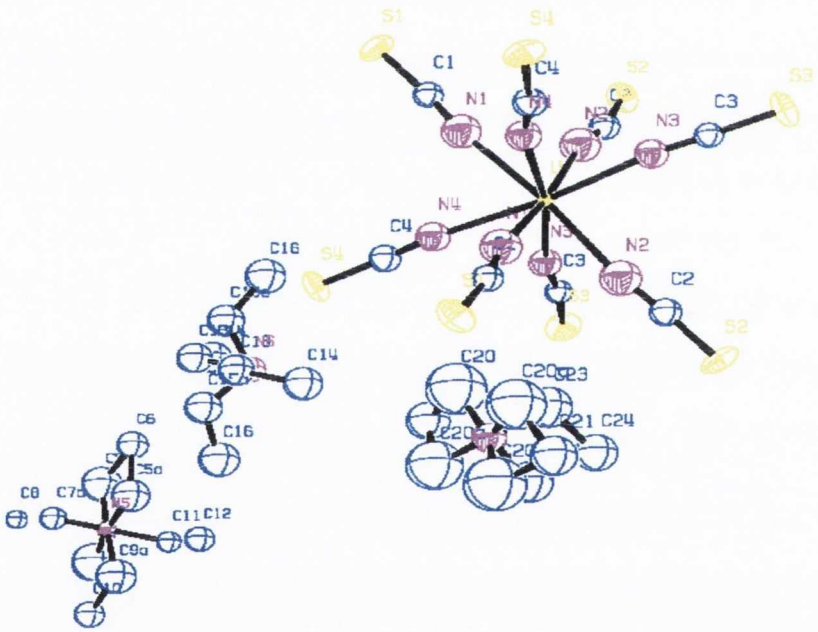

Figure 3.20: Solid state crystal structure of **8**

U1-N1	2.3924(1)	S3-C3	1.5893(1)
U1-N2	2.4341(1)	S4-C4	1.6033(1)
U1-N3	2.3996(1)	N1-C1	1.1990(1)
U1-N4	2.4034(1)	N2-C2	1.1938(1)
S1-C1	1.5852(1)	N3-C3	1.1974(1)
S2-C2	1.5814(1)	N4-C4	1.1888(1)

N1-U1-N2	70.24	N3-U1-N2	75.52	U1-N3-C3	166.83
N1-U1-N3	110.24	N3-U1-N3	119.04	U1-N4-C4	164.45
N1-U1-N4	67.66	N3-U1-N4	170.05	S1-C1-N1	170.18
N1-U1-N1	103.45	N4-U1-N1	64.97	S2-C2-N2	168.67
N1-U1-N2	172.77	N4-U1-N2	111.40	S3-C3-N3	170.10
N1-U1-N3	106.40	N4-U1-N3	170.05	S4-C4-N4	170.71
N1-U1-N4	64.97	N4-U1-N4	99.17	U1-N1-C1	168.23
N2-U1-N3	73.42	N1-U1-N2	70.24	U1-N2-C2	168.29
N2-U1-N4	108.63	N1-U1-N3	110.24	U1-N3-C3	166.83
N2-U1-N1	172.77	N1-U1-N4	67.66	U1-N4-C4	164.45
N2-U1-N2	116.28	N2-U1-N3	73.42	S1-C1-N1	170.18
N2-U1-N3	75.52	N2-U1-N4	108.63	S2-C2-N2	168.67
N2-U1-N4	111.40	N3-U1-N4	70.90	S3-C3-N3	170.10
N3-U1-N4	70.90	U1-N1-C1	168.23	S4-C4-N4	170.71
N3-U1-N1	106.40	U1-N2-C2	168.29		

Table 3.4: Bond length (Å) and bond angles (°) observed for **8**

The solid state crystal structure of **8** is very similar to **5** but due to the high symmetry it is impossible to distinguish the presence of one radical as each NCS ligand has 1/8 of a radical character and the geometry and metric parameters are identical to that seen in **5**. All bond lengths and bond angles are listed in Table 3.4 and match those reported for **5 - 7** with average bond length for U-N of 2.43 Å and bond angles of 113.1° and 70.45°. Furthermore, vibrational IR and Raman spectroscopy showed identical bands to those observed for **5** suggesting that **5** is photochromic and not photochemically oxidised. Further information could be obtained from magnetic properties, however, not enough sample was obtained at this stage. However, EPR spectroscopy on the Th(IV) analogue were conducted and gave no signal, another indication that the process is photochromic. Thermochromic type behaviour was reported for $[UO_2(NCS)_5]^{3-}$ compounds in ionic liquids[7] and acombined with a colour change from yellow to orange to red.

3.3 Spectroelectrochemistry of Free Thiocyanate Ligand

To help ascertain the nature of the oxidation process of **5**, it was necessary to study the spectroelectrochemical process of the free thiocyanate ligand under similar conditions. One-electron and two-electron oxidations of sodium thiocyanate were carried out in anhydrous acetonitrile containing $[^nBu_4N][PF_6]$, and the IR and UV-Vis spectra were recorded (Figure 3.21 and Figure 3.22, respectively). The initial asymmetric profile of the ν(N=C) is due to the fact that in acetonitrile, NaNCS exists as both inner (NaNCS) and outer sphere $[Na(MeCN)_nNCS]$ ion, seen at 2059 cm^{-1} and 2067 cm^{-1} respectively. Both the $1e^-$ and $2e^-$ oxidation processes were shown to be reversible and resulted in a decrease in the intensity of the band observed for the free ν(N=C) in NaNCS at 2059 cm^{-1} in the IR spectrum (Figure 3.21), and an increase in the band at λ_{max} = 320 nm in the UV-Vis spectrum (Figure 3.22). The $2e^-$ oxidation process gives rise to a new band at 2160 cm^{-1}, identical to that observed in the $2e^-$ oxidation process of **5** suggesting the formation of $NCS^·$ radical.[35] From this it can be postulated that both the $1e^-$ and $2e^-$ oxidation processes of **5** are ligand based and may result in the formation of the radical $NCS^·$ species. The latter has a very short lifetime and most likely recombines to form the dithiolate NCS-SCN bond.

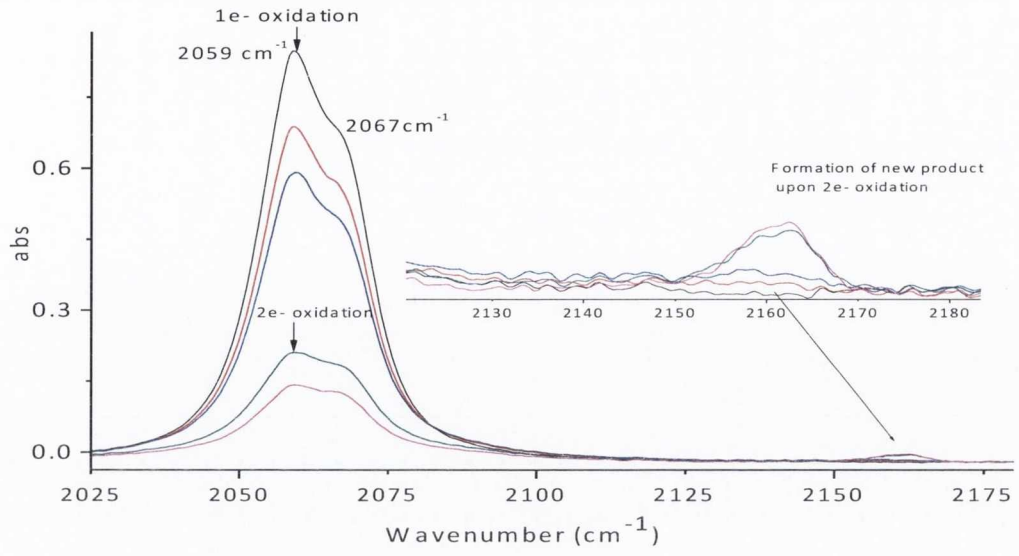

Figure 3.21: Reversible spectroelectrochemical 1e⁻ and 2e⁻ oxidation processes of NaNCS in acetonitrile containing [^{n}Bu$_4$N][PF$_6$] at 293K. Inset is an expanded view to show the growth of the band at 2160 cm^{-1}

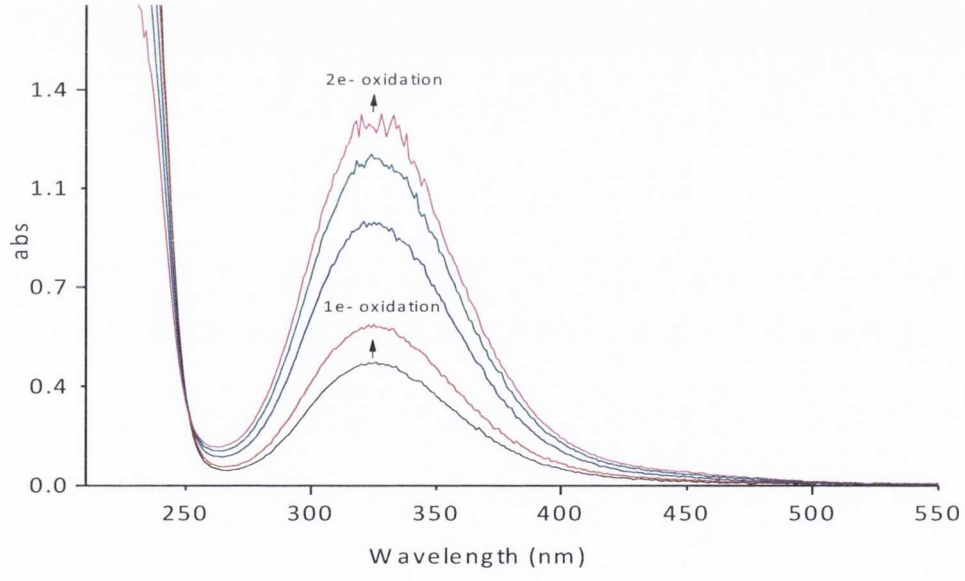

Figure 3.22: UV-Vis spectral profile of the reversible 1e⁻ and 2e⁻ oxidation processes of NaNCS in acetonitrile/ [^{n}Bu$_4$N][PF$_6$] at 293 K

3.4 Tetraethylammonium Pentakis(isothiocyanato)bis(2,2'bipyridine)uranate(IV) (9)

Emission spectroscopy is further utilised in an attempt to fingerprint the oxidation state of open shell uranium ions. The presence of redox active ligands in the coordination sphere can sometimes cause ambiguity in the metal oxidation state of d-and p-block complexes,[36] but actinide complexes featuring non-innocent ligands are scarce. One ligands that is known to display non-innocence is the 2,2'-bipyridine (bipy) ligand, as this can accept one or two electrons into the low lying LUMO and therefore can exist as $(bipy^{\cdot})^{-}$ and $(bipy)^{2-}$. The oxidation state of this ligand can be determined by the C1-C1' bond length from the solid state structures as well as magnetic and spectroscopic measurements.[37] For instance the absorption profile of the uncoordinated bipy radical anion, $(bipy^{\cdot})^{-}$, displays intense bands at *ca.* 820, 530 and 385 nm ($\varepsilon = 10^4\ M^{-1}\ cm^{-1}$) while the absorption profile for the bipy anion, $(bipy)^{2-}$, displays two intense bands at 610 and 373 nm.[38] Well characterised chromium[39] and group 5 metal complexes[40] featuring bipy radical anions display bands at *ca.* 1100 nm and 520 nm. However, actinide compounds containing non-innocent bipy ligands are not so well explored with few examples reported. The compounds $[Tp^*_2U(bipy)]$[41], (Tp*=hydrotris(3,5-dimethylpyrazolyl)borate); $[Cp^*(\eta^8\text{-}C_8H_8)U(R_2bipy)]$[42], ($R_2$bipy = bipy, 4,4'$Me_2$bipy); $[(\eta^5\text{-}1,2,4\text{-}(Me_3C)_3C_5H_2)_2An(bipy)]$, (An = U,[43] Th[44]); $[(\eta^5\text{-}1,3\text{-}(Me_3C)_2C_5H_3)_2Th(bipy)]$[45] and $[Et_4N][U(NCS)_5(bipy)_2]$[46] have all been assigned as containing a bipy radical anion on the basis of structural data, namely the C1-C1' bond length. The latter compound is intriguing in that it was reported as a U(IV) species, implying a neutral bipy ligand formulation but the structure has varying C1-C1' bond lengths that could suggest a bipy radical anion; if this were the case the oxidation state of the uranium would not be +4. In addition, all other compounds above, apart from $[Cp^*(\eta^8\text{-}C_8H_8)U(R_2bipy)]$, are formed in the presence of a reducing agent. Single electron transfer reactivity of bipy is known for transition metals such as Cr(II),[47] but without the presence of a reducing

agent neutral bipy species are commonly formed. For example reaction of $[Tp^*UI_2(THF)_2]$ with bipy gives the simple adduct $[Tp^*UI_2(bipy)]$.[41] In the $[Cp^*(\eta^8\text{-}C_8H_8)U(R_2bipy)]$ example it has been postulated that one of the COT dianions is the reducing agent.[42] However, diimine ligands such as dipp-BIAN (dipp-BIAN = 1,2-bis(2,6-diisopropylphenylimino)acenaphthylene) can facilitate single electron transfer to U(III),[48] whereas the α-diimine [(mes)N=C(Me)C(Me)=N(mes)] requires the use of external reducing agents to do this type of electron transfer chemistry.[49] $[Et_4N][U(NCS)_5(bipy)_2]$ (**9**) was synthesised and luminescence spectroscopy was utilised in order to investigate the oxidation state of uranium in this complex.

3.4.1 Synthesis and Structural Characterisation

The complex $[Et_4N][U(NCS)_5(bipy)_2]$ (**9**) was prepared in an analogous manner to that previously reported[46] to give green crystals upon crystallisation from anhydrous acetonitrile. The infrared data and Raman data for **9** show bands attributable to the NCS ligand with ν(N=C) seen at 2070 cm^{-1} and 2030 cm^{-1} and ν(C=S) at 831 cm^{-1} in the Raman spectrum and ν(N=C) at 2016 cm^{-1} and ν(C=S) = 763 cm^{-1} in the IR spectrum. There are no strong absorptions between 900 and 1000 cm^{-1} in the IR spectra, which would be typical of bipy radical ion, but bands at ca. 1600 cm^{-1} infer a neutral bipy. Finally, the bands for ν(C=C) and ν(C=N) associated with the bipy ligand show very little perturbation in the Raman spectrum and do not change significantly in the IR spectrum when compared to uncoordinated bipy shown in Figure 3.23 and Figure 3.24.

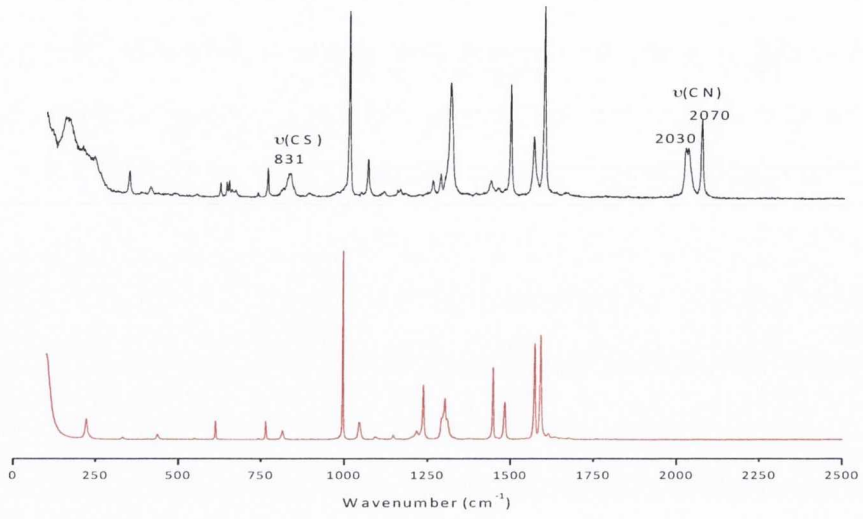

Figure 3.23: Raman spectral profile of **9** (top) plotted against Raman spectrum of bipy (bottom) for comparison

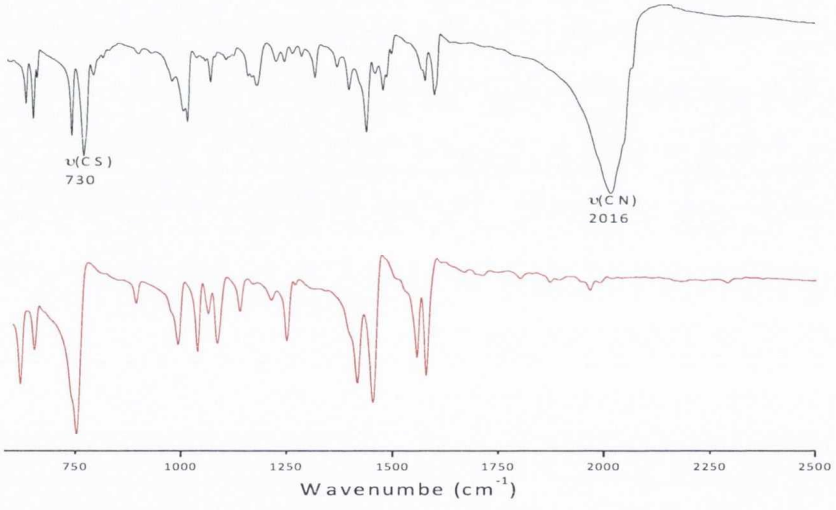

Figure 3.24: IR spectral profile of **9** (top) plotted against IR spectrum of bipy (bottom) for comparison

The solid state structure was resolved and is shown in Figure 3.25. It is worth noting that the cell parameters are identical to the original report, but the better refinement allows more precise metric parameters to be recorded. Thus, whilst the U-N, N=C and C=S bond lengths are similar to the earlier report, the C1-C1′ bond in the bipy are now 1.486(8) and 1.471(8) Å thus corroborating the assignment of the bipy as a neutral, innocent ligand. The crystal structure data are listed in Table 3.5. The average bond length for U-N is 2.4212(4) Å, C=S is

1.6182(5) Å, N-C(NCS) is 1.666(6) and U-N(bipy) is 2.642(4) Å. The measured bond angles for the two N-U-N in bipy are 61.25° and 137.55°, the bond angle for (bipy)N-U-N(NCS) range between 67.3 to 77.5° and 111.1 to 136.7°, and for N-U-N between 78.5° to 140.5°.

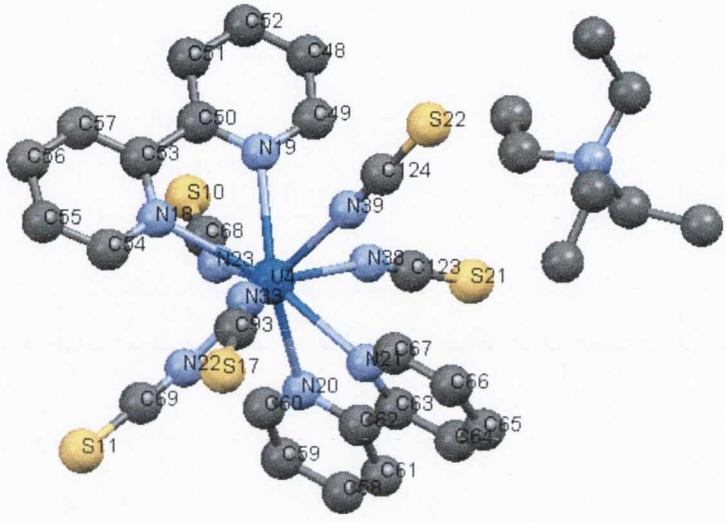

Figure 3.25: Solid state crystal structure of **9**

U4-N18	2.6446(1)	S10-C68	1.6232(1)	N20-C60	1.3410(1)
U4-N19	2.6321(1)	S11-C69	1.6148(1)	N20-C62	1.3639(1)
U4-N20	2.6372(1)	S17-C93	1.6153(1)	N21-C63	1.3565(1)
U4-N21	2.6247(1)	S21-C123	1.6198(1)	N21-C67	1.3545(1)
U4-N22	2.4288(1)	S22-C124	1.6180(1)	N22-C69	1.1792(1)
U4-N23	2.4276(1)	N18-C53	1.3460(1)	N23-C68	1.1626(1)
U4-N33	2.3920(1)	N18-C54	1.3451(1)	N33-C93	1.1607(1)
U4-N38	2.4265(1)	N19-C49	1.3462(1)	N38-C123	1.1645(1)
U4-N39	2.4317(1)	N19-C50	1.3586(1)	N39-C124	1.1665(1)

N18-U4-N19	61.20	N22-U4-N39	146.12	C49-C48-C52	119.34
N18-U4-N20	133.47	N23-U4-N33	141.08	C51-C50-C53	121.72
N18-U4-N21	145.66	N23-U4-N38	78.20	C50-C51-C52	118.92
N18-U4-N22	73.56	N23-U4-N39	131.51	C48-C52-C51	119.17
N18-U4-N23	74.64	N33-U4-N38	140.66	C50-C53-C57	121.55
N18-U4-N33	71.82	N33-U4-N39	73.29	C54-C55-C56	119.20
N18-U4-N38	136.73	N38-U4-N39	75.48	C55-C56-C57	118.81
N18-U4-N39	98.49	U4-N18-C53	121.63	C53-C57-C56	119.71
N19-U4-N20	133.23	U4-N18-C54	120.25	C59-C58-C61	118.19
N19-U4-N21	137.80	U4-N19-C49	119.81	C58-C59-C60	118.39
N19-U4-N22	128.77	U4-N19-C50	120.95	C58-C61-C62	120.43

N19-U4-N23	67.30	U4-N20-C60	120.96	C61-C62-C63	122.54
N19-U4-N33	111.12	U4-N20-C62	120.81	C62-C63-C64	121.82
N19-U4-N38	77.50	U4-N21-C63	120.96	C63-C64-C65	119.99
N19-U4-N39	67.67	U4-N21-C67	120.92	C64-C65-C66	118.79
N20-U4-N21	61.27	U4-N22-C69	159.36	C65-C66-C67	118.50
N20-U4-N22	66.45	U4-N23-C68	156.16	N19-C49-C48	122.75
N20-U4-N23	75.36	U4-N33-C93	159.83	N19-C50-C51	121.72
N20-U4-N33	115.61	U4-N38-C123	162.80	N19-C50-C53	116.49
N20-U4-N38	67.94	U4-N39-C124	176.80	N18C53C50	116.14
N20-U4-N39	128.00	S10-C68-N23	178.74	N18-C53-C57	122.16
N21-U4-N22	93.27	S11-C69-N22	179.54	N18-C54-C55	122.26
N21-U4-N23	135.00	S17-C93-N33	178.10	N20-C60-C59	124.07
N21-U4-N33	74.02	S21-C123-N38	179.24	N20-C62-C61	121.07
N21-U4-N38	75.14	S22-C124-N39	179.95	N20-C62-C63	116.33
N21-U4-N39	74.71	C53-N18-C54	117.82	N21-C63-C62	116.40
N22-U4-N23	79.13	C49-N19-C50	118.07	N21-C63-C64	121.67
N22-U4-N33	72.96	C60-N20-C62	117.78	N21-C67-C66	123.88
N22-U4-N38	132.75	C63-N21-C67	117.04		

Table 3.5: Bond lengths (Å) and bond angles (°) for **9**

Moreover ^{1}H NMR spectroscopy was used to investigate the solution structure of **9**. The ^{1}H NMR spectrum in CD_3CN is displayed in Figure 3.26 and shows a number of resonances at a slight upfield shift (9.0 - 10.6 ppm) when compared to the free bipy ligand (8.0 ppm) and can be related to a labile bipy ligand.

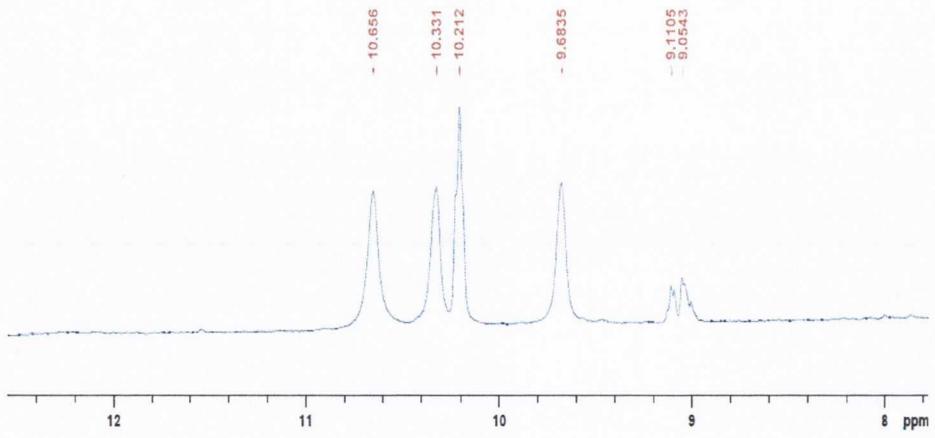

Figure 3.26: ^{1}H NMR for **9** in CD_3CN at 298 K

3.4.2 Photophysical properties of 9

The electronic absorption spectrum can be used to characterise the oxidation state of the bipy ligand. The uncoordinated bipy radical anion displays intense (ε ~10^4 M^{-1} cm^{-1}) bands at ~820, 530, and 385 nm, whilst two intense bands at ~610 and 373 nm are seen for $(bipy)^{2-}$.[50] The UV-Vis/NIR spectrum of **9** is shown in Figure 3.27 and bands at 236 nm and 305 nm can be assigned to the n-π^* transition of the NCS ligand and the π-π^* transition of the neutral bipy ligand respectively. There are no strong bands in the NIR region, which reinforces the spectroscopic assignment of a neutral bipy ligand. The bands that do appear in the visible and NIR region can be assigned to *f-f* transitions as the extinction coefficients are small. Therefore the electronic absorption spectrum suggests that the oxidation state of the uranium in **9** remains +4.

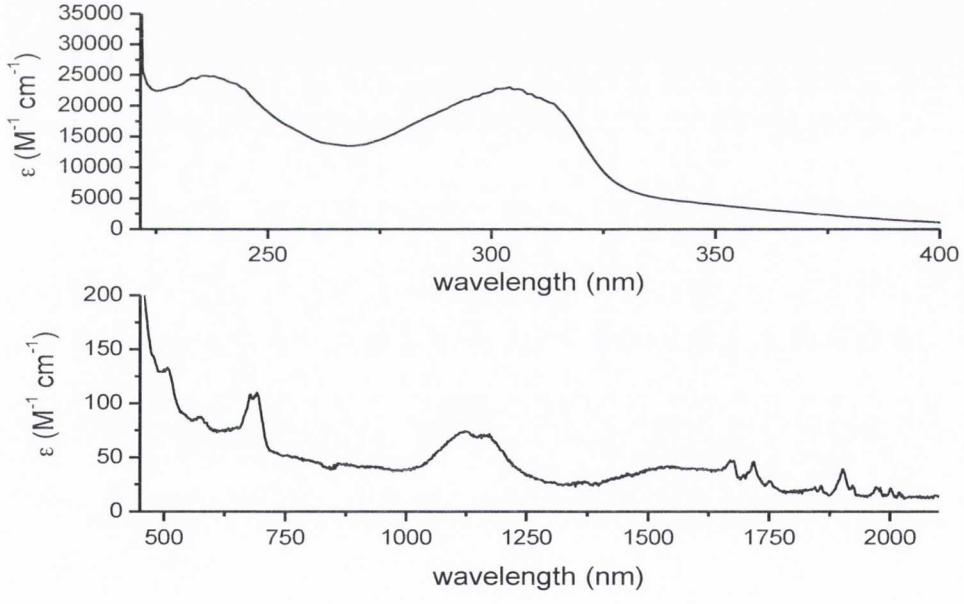

Figure 3.27: UV-Vis/NIR spectrum of **9** in MeCN

As discussed previously, emission spectroscopy can be used for fingerprinting the U(IV) oxidation state in compounds where ligand based charge transfer bands do not encroach into the visible region of the spectrum, as this affords a fast quenching mechanism and emission ending on *f*-orbitals are not observed. The excitation and emission spectra for **9** is shown in Figure 3.28. As the charge transfer bands in **9** are confined to the UV region, its emission profile is similar to the emission profile for **5**, and a broad band at 420 nm for **9** in acetonitrile is observed.

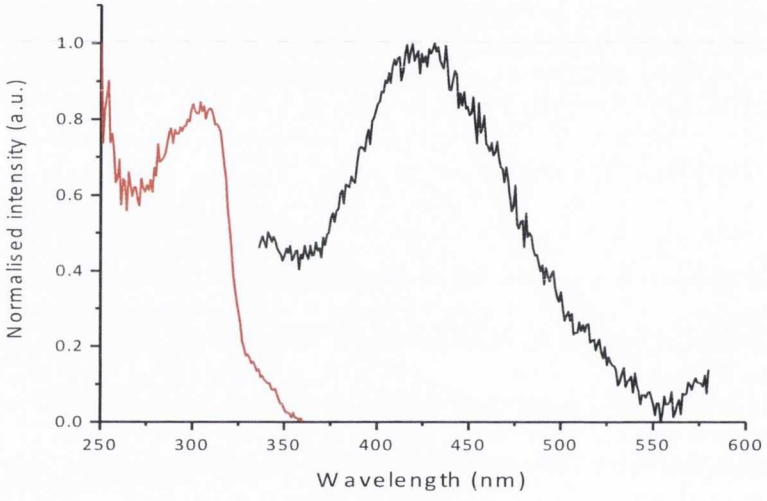

Figure 3.28: Excitation (red) and emission (black) of **9** in MeCN at 298 K (λ_{ex} = 420 nm; λ_{em} = 325 nm)

The lifetime for **9** (Figure 3.29) is measured to be 4 ns and can be compared to the lifetime of the uranium halide complexes discussed in Chapter 2[23] and [U(DO3A)]Br (DO3A = [4,7,10-tris-carboxymethyl-,1,4,7,10-tetraaza-cyclododec-1-yl]-acetic acid) (8-12 ns).[51] The observation of an emission profile for **9** in MeCN when compared to **5** in MeCN can be indicative of a longer lifetime for the bipy adduct as a result of its higher symmetry. The bipy ligand complex can exhibit a different packing ultimately reducing non-radiative quenching.

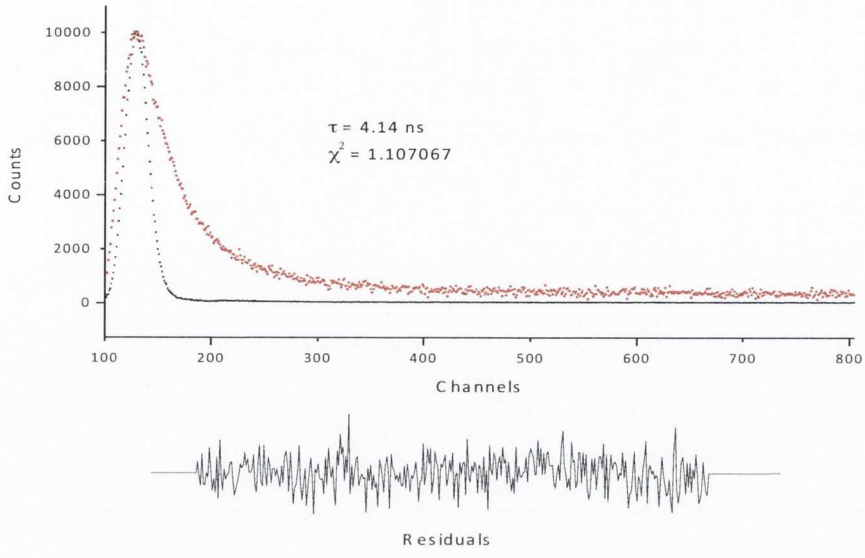

Figure 3.29: Typical kinetic traces obtained for **9** in MeCN recorded at 298 K following 294 nm excitation (red trace) and the instrument response function (using water as the scatterer, black trace); λ_{em} = 420 nm

3.4.3 Magnetic Properties of 9

In order to unequivocally confirm the oxidation state of the uranium metal, the variable temperature magnetic profile was examined using SQUID measurements (Figure 3.30). The magnetic moment at 300 K is 2.90 μ_B, significantly lower than expected for a $^3H_4$ ground state ion (3.58 μ_B); reduced magnetic moments are common in uranium(IV) compounds and sometimes ascribed to enhanced covalency which quenches the spin-orbit coupling, or the presence of strong field ligands.[22] Upon decreasing the temperature there is a precipitous drop to 0.35 μ_B at 2 K. This magnetic profile is typical for the +4 oxidation state of uranium as U(V) species typically have a room temperature magnetic moment of 1.9 to 2.5 μ_B at room temperature and *ca.* 1 μ_B at low temperatures.[52] The influence of the magnetization upon varying field (Figure 3.30(inset)) and lack of frequency dependence of the AC susceptibility as demonstrated in Figure 3.31 corroborates the assignment of a U(IV) ion.[22]

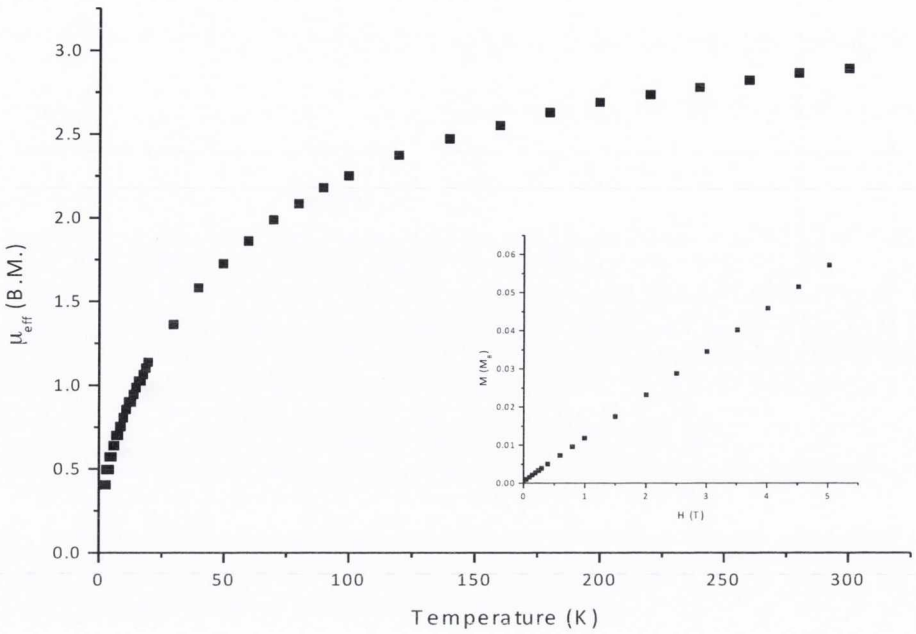

Figure 3.30: Temperature dependent magnetic susceptibility at 0.1 T for **9** from 4 to 300 K and inset shows the variable field magnetisation at 4 K

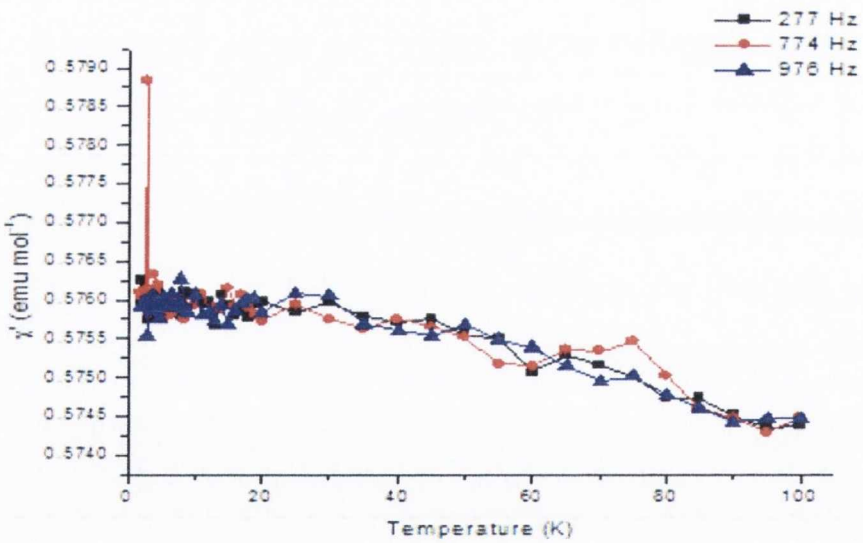

Figure 3.31: AC magnetic susceptibility of **9** showing its frequency dependence at 227 Hz (black line), 774 Hz (red line) and 976 Hz (blue line)

Given that the lower than expected room temperature magnetic susceptibility values could be ascribed to enhanced covalency, and the fact that N-heterocyclic donor ligands show promise in Ln/ An separation by overlap of the heterocyclic π* orbitals with uranium *6d*- or *5f*-orbitals, DFT and related methods to probe the bonding in **9** was used. DFT geometry optimisation at the BP86/SV(P) level results in C1-C1′ bond length of 1.482 Å in both ligands, in excellent agreement with solid state values (the equivalent value in free bipy is 1.499 Å). Calculation of harmonic vibrational frequencies at the same level identifies vibrations with substantial C1-C1′ character at 1593, 1468, 1464, 1302, and 1301 cm^{-1} (in free bipy such vibrations are found at 1594 and 1294 cm^{-1}). Thus, DFT adds further support for the assignment of a neutral bipy ligand that is only very slightly perturbed by coordination to U. For comparison, N=C stretches are found between 2037 and 2047 cm^{-1} and C=S stretches between 864 and 880 cm^{-1}. These values are somewhat higher than the experimental observations, but in the range expected for DFT calculations with medium-sized basis sets.

DFT data shows that the HOMO is mainly based on the bipy whilst the LUMO is of thiocyanate character (Figure 3.32). The lowest energy orbital that has bipy π* character is the LUMO+4, which is 1.69 eV higher in energy than the HOMO (α-spin). Natural bond orbital (NBO) analysis indicates a charge on U of +1.618, with an electronic configuration of [core] $7s^{0.24}$ $5f^{2.65}$ $6d^{1.07}$ $7p^{0.46}$. NBO analysis finds no evidence for bonding orbitals shared between U and bipy N. Instead, 2nd order orbital effects are present, corresponding to donation from lone pairs on bipy N into formally empty orbitals, with mainly *d* and *f* character, on U are located, which amount to 65 to 70 kcal/ mol of stabilisation in total. No evidence for significant back donation from U into formally empty bipy orbitals is found in NBO data.

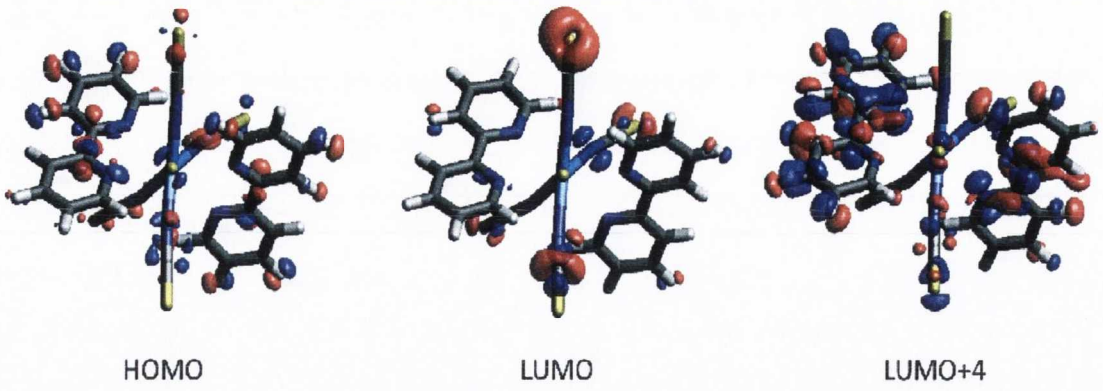

Figure 3.32: Selected molecular orbitals of **9** at the BP86/SV(P) level of theory

3.5 Uranyl Thiocyanate Complexes

3.5.1 $[Et_4N]_3[UO_2(NCS)_5]$ (10)

Given the facile ligand based one-electron oxidation of **5**, the redox chemistry of the uranyl thiocyanate species $[Et_4N]_3[UO_2(NCS)_5]$, **10** was explored. **10** was synthesised according to the literature procedure;[53] an aqueous solution of uranyl nitrate, tetraethylammonium chloride and sodium thiocyanate was allowed to stir overnight at room temperature. Following filtration and crystallisation from acetone, single yellow crystals of **10** were collected. Each ν(C=N) and ν(U=O) and ν(C=S) stretches are Raman and IR active and in the solid state give rise to three vibrational bands in the Raman spectrum observed at 2043, 2054 and 2090 cm^{-1} for ν(C=N), one vibrational band at 849 cm^{-1} for ν(U=O) and one vibrational band at 807 cm^{-1} for ν(C=S).[54] The IR spectrum shows a vibrational band at 2047cm^{-1} and a shoulder at 2090 cm^{-1} for ν(C=N), a vibrational band at 924 cm^{-1} for ν(U=O), and a vibrational band at 781 for ν(C=S). In solution however, both the IR and the Raman signals shift to a higher energy suggesting the formation of different symmetry of **10** in solution.[55]

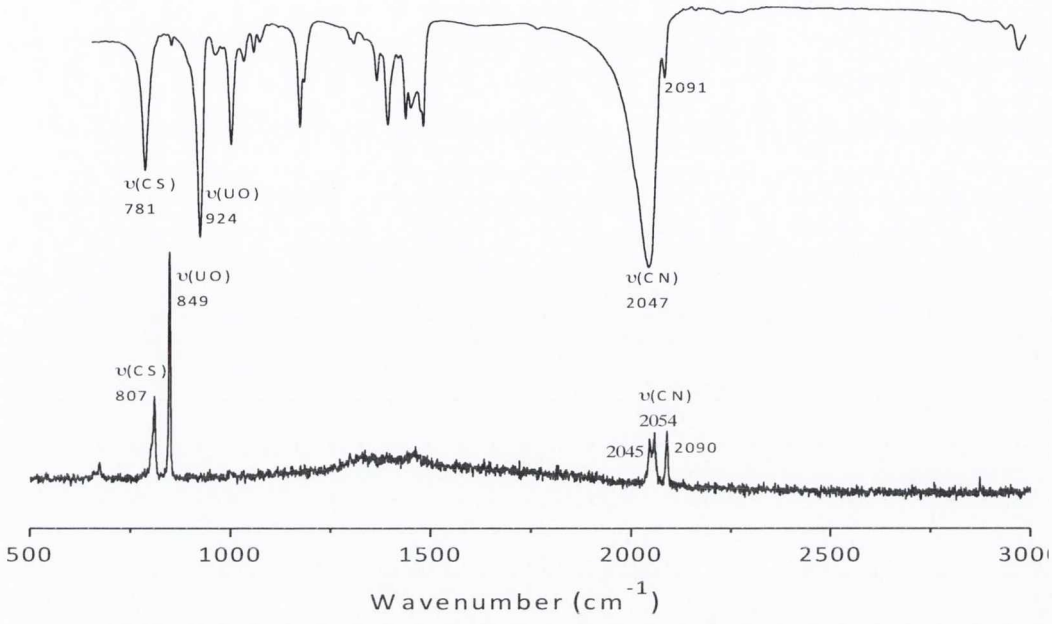

Figure 3.33: IR (top) and Raman (bottom) spectral profile of **10** in solid state

3.5.2 $Cs_3[UO_2(NCS)_5]$ (11)

The caesium analogue of uranyl thiocyanate was also synthesised from the oxidation of **6** in air. Crystallisation from acetonitrile gave dark yellow crystals of $Cs_3[UO_2(NCS)_5]$ (**11**). The solid state structure displays three vibrational bands in the Raman spectra observed at 2040, 2060 and 2095 cm^{-1} for ν(C=N), one vibrational band 849 cm^{-1} for ν(U=O) and one vibrational band at 821 cm^{-1} for ν(C=S). The IR spectrum shows a vibrational band at 2020cm^{-1} and a shoulder at 2104 cm^{-1} for ν(C=N), a vibrational band at 900 cm^{-1} for ν(U=O), and a vibrational band at 798 for ν(C=S). The slight shift of both the Raman and IR vibrational bands relative to the $[Et_4N]_4[U(NCS)_8]$ analogue might be attributed to a cation-cation interaction as seen from the solid state crystal structure shown in Figure 3.35.

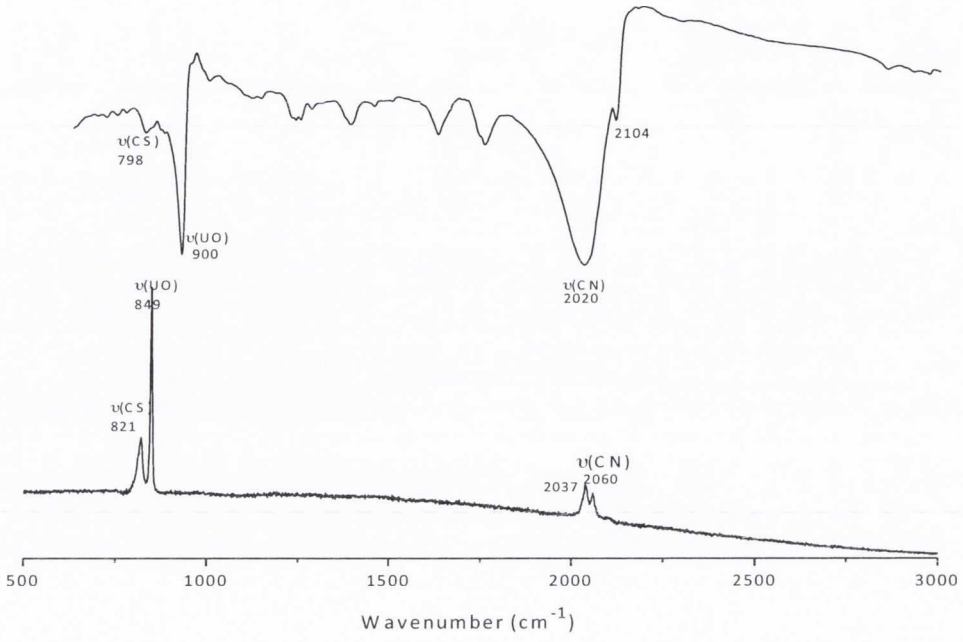

Figure 3.34: IR (top) and Raman (bottom) spectral profile for **11**

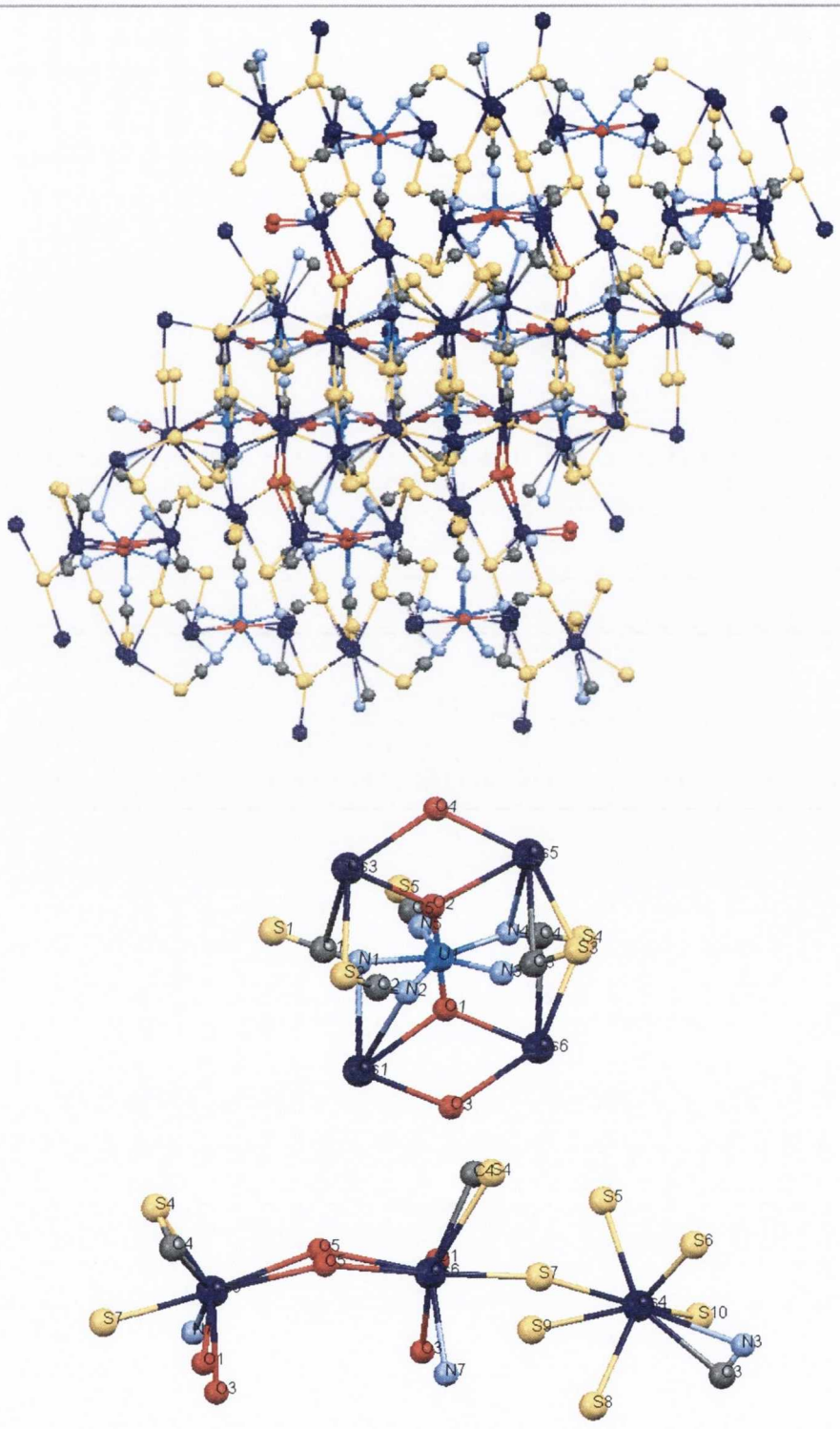

Figure 3.35: Solid state structure of **11** showing the packing structure (top), the uranyl coordination sphere (middle) and the caesium coordination sphere (U = blue; N = light blue; C = grey; S = yellow; Cs = purple; O = red

C1N1	1.15(2)	Cs3O4	3.285(9)	N8U2	2.41(1)	N4Cs5	3.42(1)
C1S1	1.64(1)	Cs3S1	3.609(5)	N9U2	2.42(1)	N5U1	2.40(1)
C1Cs3	3.70(1)	Cs5C6	3.59(3)	N9Cs1	3.61(1)	N6U2	2.46(1)
C2N2	1.15(2)	Cs5C7	3.48(1)	N9Cs3	3.41(1)	N7U2	2.43(1)
C2S2	1.63(2)	Cs5O4	3.182(8)	N10U2	2.43(1)	N7Cs6	3.24(1)
C3N3	1.15(2)	Cs5S4	3.624(4)	N10Cs3	3.63(1)	N8U2	2.41(1)
C3S3	1.63(2)	Cs5S6	3.56(3)	O1U1	1.77(1)	N9U2	2.42(1)
C3Cs5	3.44(1)	C1N1	1.15(2)	O1Cs6	3.17(1)	N9Cs1	3.61(1)
C3Cs4	3.39(2)	C1S1	1.64(1)	O2U1	1.76(1)	N9Cs3	3.41(1)
C4N4	1.21(2)	C1Cs3	3.70(1)	O2Cs3	3.29(1)	N1U2	2.43(1)
C4S4	1.61(1)	C2N2	1.15(2)	O2Cs5	3.341(9)	N1Cs3	3.63(1)
C4Cs6	3.44(1)	C2S2	1.63(2)	O3U2	1.78(1)	O1U1	1.77(1)
C5N5	1.17(2)	C3N3	1.15(2)	O3Cs1	3.25(1)	O1Cs6	3.17(1)
C5S5	1.64(2)	C3S3	1.63(2)	O3Cs6	3.216(9)	O2U1	1.76(1)
C6N6	1.19(3)	C3Cs5	3.44(1)	O4U2	1.768(9)	O2Cs3	3.29(1)
C6S6	1.95(3)	C3Cs4	3.39(2)	O4Cs3	3.285(9)	O2Cs5	3.341(9)
C6Cs5	3.59(3)	C4N4	1.21(2)	O4Cs5	3.182(8)	O3U2	1.78(1)
C7N7	1.18(2)	C4S4	1.61(1)	S1Cs3	3.609(5)	O3Cs1	3.25(1)
C7S7	1.62(1)	C4Cs6	3.44(1)	S2Cs3	3.629(9)	O3Cs6	3.216(9)
C7Cs5	3.48(1)	C5N5	1.17(2)	S3Cs5	3.652(5)	O4U2	1.768(9)
C8N8	1.15(2)	C5S5	1.64(2)	S4Cs2	3.596(4)	O4Cs3	3.285(9)
C8S8	1.63(2)	C6N6	1.19(3)	S4Cs6	3.730(4)	O4Cs5	3.182(8)
C9N9	1.17(2)	C6S6	1.95(3)	S4Cs5	3.624(4)	S1Cs3	3.609(5)
C9S9	1.62(1)	C6Cs5	3.59(3)	C10S10	1.62(2)	S2Cs3	3.629(9)
C9Cs1	3.42(1)	C7N7	1.18(2)	Cs1N1	3.33(1)	S3Cs5	3.652(5)
C10N10	1.16(2)	C7S7	1.62(1)	Cs1N2	3.53(1)	S4Cs2	3.596(4)
C10S10	1.62(2)	C7Cs5	3.48(1)	Cs1O1	3.272(9)	S4Cs6	3.730(4)
Cs1N1	3.33(1)	C8N8	1.15(2)	Cs1S9	3.684(4)	S4Cs5	3.624(4)
Cs1N2	3.53(1)	C8S8	1.63(2)	Cs1C9	3.42(1)	S5Cs2	3.330(5)
Cs1O1	3.272(9)	C9N9	1.17(2)	Cs1N9	3.61(1)	S5Cs4	3.646(5)
Cs1S9	3.684(4)	C9S9	1.62(1)	Cs1O3	3.25(1)	S6Cs1	3.57(3)
Cs1C9	3.42(1)	C9Cs1	3.42(1)	Cs1S6	3.57(3)	S6Cs5	3.56(3)
Cs1N9	3.61(1)	C10N10	1.16(2)	Cs2S2	3.55(1)	S8Cs4	3.636(5)
Cs1O3	3.25(1)	Cs4S5	3.646(5)	Cs2S8	3.369(5)	S9Cs4	3.706(4)
Cs1S6	3.57(3)	Cs4S8	3.636(5)	Cs2S4	3.596(4)	S10Cs4	3.641(4)
Cs2S2	3.55(1)	Cs4S9	3.706(4)	Cs2S5	3.330(5)	Cs3N9	3.41(1)
Cs2S8	3.369(5)	Cs4S10	3.641(4)	Cs4S6	3.41(3)	Cs3N10	3.63(1)
Cs2S4	3.596(4)	Cs6S7	3.604(4)	Cs4S7	3.598(4)	Cs3O4	3.285(9)
Cs2S5	3.330(5)	Cs6O5	3.64(1)	Cs4C3	3.39(2)	Cs3S1	3.609(5)
Cs4S6	3.41(3)	Cs6O5	3.58(1)	Cs4N3	3.48(1)	Cs5C6	3.59(3)
Cs4S7	3.598(4)	Cs6C4	3.44(1)	Cs4S5	3.646(5)	Cs5C7	3.48(1)
Cs4C3	3.39(2)	Cs6N7	3.24(1)	Cs4S8	3.636(5)	Cs5O4	3.182(8)
Cs4N3	3.48(1)	Cs6O1	3.17(1)	Cs4S9	3.706(4)	Cs5S4	3.624(4)
S5Cs2	3.330(5)	Cs6O3	3.216(9)	Cs4S10	3.641(4)	Cs5S6	3.56(3)
S5Cs4	3.646(5)	Cs6S4	3.730(4)	Cs6S7	3.604(4)	C3N3	1.15(2)
S6Cs1	3.57(3)	N1U1	2.45(1)	Cs6C4	3.44(1)	C4S4	1.61(1)
S6Cs5	3.56(3)	N2U1	2.48(1)	Cs6N7	3.24(1)	C6S6	1.95(3)
S8Cs4	3.636(5)	N3U1	2.47(1)	Cs6O1	3.17(1)	C9N9	1.17(2)
S9Cs4	3.706(4)	N3Cs4	3.48(1)	Cs6O3	3.216(9)	Cs2S4	3.596(4)
S10Cs4	3.641(4)	N4U1	2.43(1)	Cs6S4	3.730(4)	Cs4S6	3.41(3)
O5O5	1.04(1)	N4Cs5	3.42(1)	N1U1	2.45(1)	Cs4S5	3.646(5)

O5Cs6	3.58(1)	N5U1	2.40(1)	N2U1	2.48(1)	Cs6O3	3.216(9)
O5Cs6	3.64(1)	N6U2	2.46(1)	N3U1	2.47(1)	S4Cs5	3.624(4)
Cs3N9	3.41(1)	N7U2	2.43(1)	N3Cs4	3.48(1)		
Cs3N10	3.63(1)	N7Cs6	3.24(1)	N4U1	2.43(1)		

N1C1S1	179(1)	N3U1N5	142.7(4)	S7Cs6O3	79.4(2)
N1C1Cs3	94.1(9)	N3U1O1	89.5(4)	S7Cs6S4	68.73(8)
S1C1 Cs3	86.0(5)	N3U1O2	89.4(4)	C4Cs6N7	148.8(3)
N2C2S2	166(1)	N4U1N5	73.0(4)	C4Cs6O1	69.8(3)
N3C3S3	179(1)	N4U1O1	90.7(4)	C4Cs6O3	125.4(3)
N3C3Cs5	95(1)	N4U1O2	89.8(4)	C4Cs6S4	25.5(2)
N3C3Cs4	85(1)	N5U1O1	90.5(4)	N7Cs6O1	109.8(3)
S3C3Cs5	84.0(6)	N5U1O2	91.0(4)	N7Cs6O3	55.3(3)
S3C3Cs4	95.0(6)	O1U1O2	178.6(4)	N7Cs6S4	133.0(2)
Cs5C3Cs4	129.4(5)	N6U2N7	70.0(4)	O1Cs6O3	57.5(2)
N4C4S4	179(1)	N6U2N8	144.2(4)	O1Cs6S4	94.1(2)
N4C4Cs6	91.6(9)	N6U2N9	141.8(4)	O3Cs6S4	144.5(2)
S4C4Cs6	87.5(5)	N6U2N10	70.9(4)	C1N1Cs1	110(1)
N5C5S5	179(1)	N6U2O3	91.2(4)	C1N1U1	155(1)
N6C6S6	163(2)	N6U2O4	87.7(4)	Cs1N1U1	93.1(4)
N6C6Cs5	92(1)	N7U2N8	74.3(4)	C2N2Cs1	98(1)
S6C6Cs5	73(1)	N7U2N9	148.1(4)	C2N2U1	138(1)
N7C7S7	179(1)	N7U2N10	140.8(4)	Cs1N2U1	87.9(3)
N7C7Cs5	90.2(9)	N7U2O3	89.4(4)	C3N3U1	153(1)
S7C7Cs5	88.8(5)	N7U2O4	90.4(4)	C3N3Cs4	76(1)
N8C8S8	179(1)	N8U2N9	73.8(4)	U1N3Cs4	122.7(4)
N9C9S9	177(1)	N8U2N10	144.9(4)	C4N4U1	156(1)
N9C9Cs1	89.8(9)	N8U2O3	90.7(4)	C4N4Cs5	107.6(9)
S9C9Cs1	88.5(5)	N8U2O4	90.3(4)	U1N4Cs5	94.9(4)
N10C10S10	178(1)	N9U2N10	71.1(4)	C5N5U1	178(1)
N1Cs1N2	49.0(3)	N9U2O3	90.8(4)	C6N6U2	151(1)
N1Cs1O1	54.6(3)	N9U2O4	89.9(4)	C7N7U2	156(1)
N1Cs1S9	68.5(2)	N10U2O3	89.1(4)	C7N7Cs6	105.5(9)
N1Cs1C9	133.5(3)	N10U2O4	90.4(4)	U2N7Cs6	98.2(4)
N1Cs1N9	137.3(3)	O3U2O4	178.9(4)	C8N8U2	170(1)
N1Cs1O3	109.3(3)	Cs6O5O5	78.5(8)	C9N9U2	163(1)
N1Cs1S6	100.5(5)	Cs6O5Cs6	147.4(3)	C9N9Cs1	71.2(9)
N2Cs1O1	52.6(3)	O5O5Cs6	84.9(8)	C9N9Cs3	101.9(9)
N2Cs1S9	109.3(2)	Cs6O5O5	84.9(8)	U2N9Cs1	92.6(4)
N2Cs1C9	167.1(3)	Cs6O5Cs6	147.4(3)	U2N9Cs3	93.3(4)
N2Cs1N9	148.4(3)	O5O5Cs6	78.5(8)	Cs1N9Cs3	137.4(4)
N2Cs1O3	96.6(3)	C1Cs3O2	63.8(3)	C10N10U2	168(1)
N2Cs1S6	52.6(5)	C1Cs3S2	71.5(3)	C10N10Cs3	88(1)
O1Cs1S9	66.9(2)	C1Cs3N9	131.6(3)	U2N10Cs3	87.7(4)
O1Cs1C9	116.5(3)	C1Cs3N10	165.3(3)	Cs1O1U1	111.1(4)
O1Cs1N9	102.6(3)	C1Cs3O4	114.6(3)	Cs1O1Cs6	123.0(3)
O1Cs1O3	56.2(2)	C1Cs3S1	61.8(2)	U1O1Cs6	122.6(4)
O1Cs1S6	70.5(5)	O2Cs3S2	85.1(2)	U1O2Cs3	128.0(4)
S9Cs1C9	67.1(2)	O2Cs3N9	107.4(3)	U1O2Cs5	114.0(4)
S9Cs1N9	69.3(2)	O2Cs3N10	101.8(3)	Cs3O2Cs5	115.3(3)

S9Cs1O3	73.7(2)	O2Cs3O4	57.9(2)	U2O3Cs1	120.9(4)
S9Cs1S6	133.8(5)	O2Cs3S1	64.4(2)	U2O3Cs6	116.6(4)
C9Cs1N9	19.0(3)	S2Cs3N9	156.6(3)	Cs1O3Cs6	122.2(3)
C9Cs1O3	70.5(3)	S2Cs3N10	112.0(3)	U2O4Cs3	112.7(4)
C9Cs1S6	120.1(5)	S2Cs3O4	126.7(2)	U2O4Cs5	121.4(4)
N9Cs1O3	52.0(3)	S2Cs3S1	131.7(2)	Cs3O4Cs5	120.1(3)
N9Cs1S6	104.3(5)	N9Cs3N10	47.1(3)	C1S1Cs3	90.5(5)
O3Cs1S6	68.1(5)	N9Cs3O4	53.2(3)	C2S2Cs2	112.5(7)
S2Cs2S8	99.1(2)	N9Cs3S1	71.6(2)	C2S2Cs3	82.4(6)
S2Cs2S4	140.7(2)	N10Cs3O4	51.4(3)	Cs2S2Cs3	88.9(2)
S2Cs2S5	86.0(2)	N10Cs3S1	110.5(2)	C3S3Cs5	69.5(6)
S8Cs2S4	75.9(1)	O4Cs3S1	68.1(2)	C4S4Cs2	95.5(5)
S8Cs2S5	147.3(1)	C3Cs5N4	57.6(3)	C4S4Cs6	67.0(5)
S4Cs2S5	79.8(1)	C3Cs5O2	67.3(3)	C4S4Cs5	92.3(5)
S6Cs4S7	89.9(5)	C3Cs5S3	26.4(3)	Cs2S4Cs6	77.62(7)
S6Cs4C3	88.7(6)	C3Cs5C6	109.7(5)	Cs2S4Cs5	169.3(1)
S6Cs4N3	72.8(5)	C3Cs5C7	170.6(3)	Cs6S4Cs5	112.36(9)
S6Cs4S5	82.4(5)	C3Cs5O4	115.7(3)	C5S5Cs2	106.9(6)
S6Cs4S8	116.2(5)	C3Cs5S4	123.1(3)	C5S5Cs4	103.9(6)
S6Cs4S9	146.2(5)	C3Cs5S6	91.5(5)	Cs2S5Cs4	149.0(1)
S6Cs4S10	110.4(5)	N4Cs5O2	52.6(3)	C6S6Cs4	106(1)
S7Cs4C3	145.8(3)	N4Cs5S3	78.2(2)	C6S6Cs1	121(1)
S7Cs4N3	151.4(2)	N4Cs5C6	162.6(5)	C6S6Cs5	75(1)
S7Cs4S5	70.51(9)	N4Cs5C7	130.7(3)	Cs4S6Cs1	131.6(9)
S7Cs4S8	74.41(9)	N4Cs5O4	105.6(3)	Cs4S6Cs5	89.9(7)
S7Cs4S9	57.96(8)	N4Cs5S4	68.0(2)	Cs1S6Cs5	113.2(8)
S7Cs4S10	148.5(1)	N4Cs5S6	146.8(5)	C7S7Cs4	98.1(5)
C3Cs4N3	19.2(3)	O2Cs5S3	92.8(2)	C7S7Cs6	87.9(5)
C3Cs4S5	142.9(3)	O2Cs5C6	113.0(4)	Cs4S7Cs6	165.7(1)
C3Cs4S8	75.6(3)	O2Cs5C7	120.5(3)	C8S8Cs2	109.8(6)
C3Cs4S9	123.4(3)	O2Cs5O4	58.4(2)	C8S8Cs4	109.9(6)
C3Cs4S10	61.5(3)	O2Cs5S4	67.5(2)	Cs2S8Cs4	139.3(1)
N3Cs4S5	127.2(2)	O2Cs5S6	130.5(5)	C9S9Cs1	89.9(5)
N3Cs4S8	92.6(2)	S3Cs5C6	94.1(4)	C9S9Cs4	101.3(5)
N3Cs4S9	140.7(2)	S3Cs5C7	144.4(2)	Cs1S9Cs4	166.3(1)
N3Cs4S10	60.1(2)	S3Cs5O4	130.4(2)	C10S10Cs4	107.3(5)
S5Cs4S8	140.1(1)	S3Cs5S4	146.2(1)	N1U1N2	70.7(4)
S5Cs4S9	77.31(9)	S3Cs5S6	68.8(5)	N1U1N3	144.5(4)
S5Cs4S10	88.0(1)	C6Cs5C7	63.1(5)	N1U1N4	145.8(4)
S8Cs4S9	68.22(9)	C6Cs5O4	67.4(4)	N1U1N5	72.9(4)
S8Cs4S10	114.2(1)	C6Cs5S4	118.5(4)	N1U1O1	90.4(4)
S9Cs4S10	95.76(9)	C6Cs5S6	31.7(6)	N1U1O2	89.9(4)
S7Cs6O5	175.2(2)	C7Cs5O4	68.4(3)	N2U1N3	73.7(4)
S7Cs6O5	165.3(2)	C7Cs5S4	66.2(2)	N2U1N4	143.5(4)
S7Cs6C4	66.1(2)	C7Cs5S6	79.3(5)	N2U1N5	143.6(4)
S7Cs6N7	85.1(2)	O4Cs5S4	63.1(2)	N2U1O1	89.1(4)
S7Cs6O1	65.1(2)	O4Cs5S6	98.5(5)	N2U1O2	89.7(4)
S7Cs6O3	79.4(2)	S4Cs5S6	144.8(5)	N3U1N4	69.7(4)
S7Cs6S4	68.73(8)	N1C1S1	179(1)	N3U1N5	142.7(4)
O5Cs6O5	16.6(2)	N1C1Cs3	94.1(9)	N3U1O1	89.5(4)
O5Cs6C4	111.6(3)	S1C1Cs3	86.0(5)	N3U1O2	89.4(4)

O5Cs6N7	96.1(3)	N2C2S2	166(1)	N4U1N5	73.0(4)
O5Cs6O1	118.4(2)	N3C3S3	179(1)	N4U1O1	90.7(4)
O5Cs6O3	105.1(2)	N3C3Cs5	95(1)	N4U1O2	89.8(4)
O5Cs6S4	107.3(2)	N3C3Cs4	85(1)	N5U1O1	90.5(4)
O5Cs6C4	102.9(3)	S3C3Cs5	84.0(6)	N5U1O2	91.0(4)
O5Cs6N7	107.4(3)	S3C3Cs4	95.0(6)	O1U1O2	178.6(4)
O5Cs6O1	102.5(2)	Cs5C3Cs4	129.4(5)	N6U2N7	70.0(4)
O5Cs6O3	101.1(2)	N4C4S4	179(1)	N6U2N8	144.2(4)
O5Cs6S4	105.9(2)	N4C4Cs6	91.6(9)	N6U2N9	141.8(4)
C4Cs6N7	148.8(3)	S4C4Cs6	87.5(5)	N6U2N10	70.9(4)
C4Cs6O1	69.8(3)	N5C5S5	179(1)	N6U2O3	91.2(4)
C4Cs6O3	125.4(3)	N6C6S6	163(2)	N6U2O4	87.7(4)
C4Cs6S4	25.5(2)	N6C6Cs5	92(1)	N7U2N8	74.3(4)
N7Cs6O1	109.8(3)	S6C6Cs5	73(1)	N7U2N9	148.1(4)
N7Cs6O3	55.3(3)	N7C7S7	179(1)	N7U2N10	140.8(4)
N7Cs6S4	133.0(2)	N7C7Cs5	90.2(9)	N7U2O3	89.4(4)
O1Cs6O3	57.5(2)	S7C7Cs5	88.8(5)	N7U2O4	90.4(4)
O1Cs6S4	94.1(2)	N8C8S8	179(1)	N8U2N9	73.8(4)
O3Cs6S4	144.5(2)	N9C9S9	177(1)	N8U2N10	144.9(4)
C1N1Cs1	110(1)	N9C9Cs1	89.8(9)	N8U2O3	90.7(4)
C1N1U1	155(1)	S9C9Cs1	88.5(5)	N8U2O4	90.3(4)
Cs1NU1	93.1(4)	N10C10S10	178(1)	N9U2N10	71.1(4)
C2N2Cs1	98(1)	N1Cs1N2	49.0(3)	N9U2O3	90.8(4)
C2N2U1	138(1)	N1Cs1O1	54.6(3)	N9U2O4	89.9(4)
Cs1N2U1	87.9(3)	N1Cs1S9	68.5(2)	N10U2O3	89.1(4)
C3N3U1	153(1)	N1Cs1C9	133.5(3)	N10U2O4	90.4(4)
C3N3Cs4	76(1)	N1Cs1N9	137.3(3)	O3U2O4	178.9(4)
U1N3Cs4	122.7(4)	N1Cs1O3	109.3(3)	C1Cs3O2	63.8(3)
C4N4U1	156(1)	N1Cs1S6	100.5(5)	C1Cs3S2	71.5(3)
C4N4Cs5	107.6(9)	N2Cs1O1	52.6(3)	C1Cs3N9	131.6(3)
U1N4Cs5	94.9(4)	N2Cs1S9	109.3(2)	C1Cs3N10	165.3(3)
C5N5U1	178(1)	N2Cs1C9	167.1(3)	C1Cs3O4	114.6(3)
C6N6U2	151(1)	N2Cs1N9	148.4(3)	C1Cs3S1	61.8(2)
C7N7U2	156(1)	N2Cs1O3	96.6(3)	O2Cs3S2	85.1(2)
C7N7Cs6	105.5(9)	N2Cs1S6	52.6(5)	O2Cs3N9	107.4(3)
U2N7Cs6	98.2(4)	O1Cs1S9	66.9(2)	O2Cs3N10	101.8(3)
C8N8U2	170(1)	O1Cs1C9	116.5(3)	O2Cs3O4	57.9(2)
C9N9U2	163(1)	O1Cs1N9	102.6(3)	O2Cs3S1	64.4(2)
C9N9Cs1	71.2(9)	O1Cs1O3	56.2(2)	S2Cs3N9	156.6(3)
C9N9Cs3	101.9(9)	O1Cs1S6	70.5(5)	S2Cs3N10	112.0(3)
U2N9Cs1	92.6(4)	S9Cs1C9	67.1(2)	S2Cs3O4	126.7(2)
U2N9Cs3	93.3(4)	S9Cs1N9	69.3(2)	S2Cs3S1	131.7(2)
Cs1N9Cs3	137.4(4)	S9Cs1O3	73.7(2)	N9Cs3N10	47.1(3)
C10N10U2	168(1)	S9Cs1S6	133.8(5)	N9Cs3O4	53.2(3)
C10N10Cs3	88(1)	C9Cs1N9	19.0(3)	N9Cs3S1	71.6(2)
U2N10Cs3	87.7(4)	C9Cs1O3	70.5(3)	N10Cs3O4	51.4(3)
Cs1O1U1	111.1(4)	C9Cs1S6	120.1(5)	N10Cs3S1	110.5(2)
Cs1O1Cs6	123.0(3)	N9Cs1O3	52.0(3)	O4Cs3S1	68.1(2)
U1O1Cs6	122.6(4)	N9Cs1S6	104.3(5)	C3Cs5N4	57.6(3)
U1O2Cs3	128.0(4)	O3Cs1S6	68.1(5)	C3Cs5O2	67.3(3)
U1O2Cs5	114.0(4)	S2Cs2S8	99.1(2)	C3Cs5S3	26.4(3)

Cs3O2Cs5	115.3(3)	S2Cs2S4	140.7(2)	C3Cs5C6	109.7(5)
U2O3Cs1	120.9(4)	S2Cs2S5	86.0(2)	C3Cs5C7	170.6(3)
U2O3Cs6	116.6(4)	S8Cs2S4	75.9(1)	C3Cs5O4	115.7(3)
Cs1O3Cs6	122.2(3)	S8Cs2S5	147.3(1)	C3Cs5S4	123.1(3)
U2O4Cs3	112.7(4)	S4Cs2S5	79.8(1)	C3Cs5S6	91.5(5)
U2O4Cs5	121.4(4)	S6Cs4S7	89.9(5)	N4Cs5O2	52.6(3)
Cs3O4Cs5	120.1(3)	S6Cs4C3	88.7(6)	N4Cs5S3	78.2(2)
C1S1Cs3	90.5(5)	S6Cs4N3	72.8(5)	N4Cs5C6	162.6(5)
C2S2Cs2	112.5(7)	S6Cs4S5	82.4(5)	N4Cs5C7	130.7(3)
C2S2Cs3	82.4(6)	S6Cs4S8	116.2(5)	N4Cs5O4	105.6(3)
Cs2S2Cs3	88.9(2)	S6Cs4S9	146.2(5)	N4Cs5S4	68.0(2)
C3S3Cs5	69.5(6)	S6Cs4S10	110.4(5)	N4Cs5S6	146.8(5)
C4S4Cs2	95.5(5)	S7Cs4C3	145.8(3)	O2Cs5S3	92.8(2)
C4S4Cs6	67.0(5)	S7Cs4N3	151.4(2)	O2Cs5C6	113.0(4)
C4S4Cs5	92.3(5)	S7Cs4S5	70.51(9)	O2Cs5C7	120.5(3)
Cs2S4Cs6	77.62(7)	S7Cs4S8	74.41(9)	O2Cs5O4	58.4(2)
Cs2S4Cs5	169.3(1)	S7Cs4S9	57.96(8)	O2Cs5S4	67.5(2)
Cs6S4Cs5	112.36(9)	S7Cs4S10	148.5(1)	O2Cs5S6	130.5(5)
C5S5Cs2	106.9(6)	C3Cs4N3	19.2(3)	S3Cs5C6	94.1(4)
C5S5Cs4	103.9(6)	C3Cs4S5	142.9(3)	S3Cs5C7	144.4(2)
Cs2S5Cs4	149.0(1)	C3Cs4S8	75.6(3)	S3Cs5O4	130.4(2)
C6S6Cs4	106(1)	C3Cs4S9	123.4(3)	S3Cs5S4	146.2(1)
C6S6Cs1	121(1)	C3Cs4S10	61.5(3)	S3Cs5S6	68.8(5)
C6S6Cs5	75(1)	N3Cs4S5	127.2(2)	C6Cs5C7	63.1(5)
Cs4S6Cs1	131.6(9)	N3Cs4S8	92.6(2)	C6Cs5O4	67.4(4)
Cs4S6Cs5	89.9(7)	N3Cs4S9	140.7(2)	C6Cs5S4	118.5(4)
Cs1S6Cs5	113.2(8)	N3Cs4S10	60.1(2)	C6Cs5S6	31.7(6)
C7S7Cs4	98.1(5)	S5Cs4S8	140.1(1)	C7Cs5O4	68.4(3)
C7S7Cs6	87.9(5)	S5Cs4S9	77.31(9)	C7Cs5S4	66.2(2)
Cs4S7Cs6	165.7(1)	S5Cs4S10	88.0(1)	C7Cs5S6	79.3(5)
C8S8Cs2	109.8(6)	S8Cs4S9	68.22(9)	O4Cs5S4	63.1(2)
C8S8Cs4	109.9(6)	S8Cs4S10	114.2(1)	O4Cs5S6	98.5(5)
Cs2S8Cs4	139.3(1)	S9Cs4S10	95.76(9)	S4Cs5S6	144.8(5)
C9S9Cs1	89.9(5)	O5Cs6O5	16.6(2)	Cs4C3N3	85(1)
C9S9Cs4	101.3(5)	O5Cs6S7	165.3(2)	Cs4C3N3	85(1)
Cs1S9Cs4	166.3(1)	O5Cs6C4	102.9(3)	Cs6C4S4	87.5(5)
C10S10Cs4	107.3(5)	O5Cs6N7	107.4(3)	Cs6C4S4	87.5(5)
N1U1N2	70.7(4)	O5Cs6O1	102.5(2)	Cs5C6S6	73(1)
N1U1N3	144.5(4)	O5Cs6O3	101.1(2)	Cs5C6S6	73(1)
N1U1N4	145.8(4)	O5Cs6S4	105.9(2)	Cs1C9N9	89.8(9)
N1U1N5	72.9(4)	O5Cs6S7	175.2(2)	Cs1C9N9	89.8(9)
N1U1O1	90.4(4)	O5Cs6C4	111.6(3)	C9Cs1N9	19.0(3)
N1U1O2	89.9(4)	O5Cs6N7	96.1(3)	C9Cs1O3	70.5(3)
N2U1N3	73.7(4)	O5Cs6O1	118.4(2)	N9Cs1O3	52.0(3)
N2U1N4	143.5(4)	O5Cs6O3	105.1(2)	C9Cs1N9	19.0(3)
N2U1N5	143.6(4)	O5Cs6S4	107.3(2)	C9Cs1O3	70.5(3)
N2U1O1	89.1(4)	S7Cs6C4	66.1(2)	N9Cs1O3	52.0(3)
N2U1O2	89.7(4)	S7Cs6N7	85.1(2)	S5Cs2S4	79.8(1)
N3U1N4	69.7(4)	S7Cs6O1	65.1(2)	S5Cs2S4	79.8(1)
S5Cs4S9	77.31(9)	Cs4N3C3	76(1)	N9Cs3O4	53.2(3)
S5Cs4S10	88.0(1)	Cs4N3C3	76(1)	N9Cs3S1	71.6(2)

S9Cs4S10	95.76(9)	Cs1N9C9	71.2(9)	N10Cs3O4	51.4(3)
S5Cs4S9	77.31(9)	Cs1N9C9	71.2(9)	N10Cs3S1	110.5(2)
S5Cs4S10	88.0(1)	Cs1O3Cs6	122.2(3)	O4Cs3S1	68.1(2)
S9Cs4S10	95.76(9)	Cs1O3Cs6	122.2(3)	N9Cs3N10	47.1(3)
C3Cs4N3	19.2(3)	Cs3O4Cs5	120.1(3)	N9Cs3O4	53.2(3)
C3Cs4S5	142.9(3)	Cs3O4Cs5	120.1(3)	N9Cs3S1	71.6(2)
C3Cs4S6	88.7(6)	Cs2S4Cs6	77.62(7)	N10Cs3O4	51.4(3)
N3Cs4S5	127.2(2)	Cs2S4C4	95.5(5)	N10Cs3S1	110.5(2)
N3Cs4S6	72.8(5)	Cs2S4Cs5	169.3(1)	O4Cs3S1	68.1(2)
S5Cs4S6	82.4(5)	Cs6S4C4	67.0(5)	C6Cs5C7	63.1(5)
C3Cs4N3	19.2(3)	Cs6S4Cs5	112.36(9)	C6Cs5O4	67.4(4)
C3Cs4S5	142.9(3)	C4S4Cs5	92.3(5)	C6Cs5S6	31.7(6)
C3Cs4S6	88.7(6)	Cs2S4Cs6	77.62(7)	C6Cs5S4	118.5(4)
N3Cs4S5	127.2(2)	Cs2S4C4	95.5(5)	C7Cs5O4	68.4(3)
N3Cs4S6	72.8(5)	Cs2S4Cs5	169.3(1)	C7Cs5S6	79.3(5)
S5Cs4S6	82.4(5)	Cs6S4C4	67.0(5)	C7Cs5S4	66.2(2)
C4Cs6O1	69.8(3)	Cs6S4Cs5	112.36(9)	O4Cs5S6	98.5(5)
C4Cs6S4	25.5(2)	C4S4Cs5	92.3(5)	O4Cs5S4	63.1(2)
C4Cs6O3	125.4(3)	Cs5S4Cs2	169.3(1)	S6Cs5S4	144.8(5)
O1Cs6S4	94.1(2)	Cs5S4Cs2	169.3(1)	C6Cs5C7	63.1(5)
O1Cs6O3	57.5(2)	Cs2S5Cs4	149.0(1)	C6Cs5O4	67.4(4)
S4Cs6O3	144.5(2)	Cs2S5Cs4	149.0(1)	C6Cs5S6	31.7(6)
C4Cs6O1	69.8(3)	Cs5S6C6	75(1)	C6Cs5S4	118.5(4)
C4Cs6S4	25.5(2)	Cs5S6C6	75(1)	C7Cs5O4	68.4(3)
C4Cs6O3	125.4(3)	Cs1S6Cs4	131.6(9)	C7Cs5S6	79.3(5)
O1Cs6S4	94.1(2)	Cs1S6Cs4	131.6(9)	C7Cs5S4	66.2(2)
O1Cs6O3	57.5(2)	N7Cs6O3	55.3(3)	O4Cs5S6	98.5(5)
S4Cs6O3	144.5(2)	N7Cs6O3	55.3(3)	O4Cs5S4	63.1(2)
S6Cs5S4	144.8(5)	N9Cs3N10	47.1(3)		

Table 3.6: Bond lengths (Å) and bond angles (°) for **11**

The bond lengths of the U=O within the uranyl fragment (1.764 and 1.767 **Å)** are in the range expected for the uranyl moiety.[56] The Cs^+ cations form long contacts with the uranyl oxygen with an average distance of 3.342 **Å** agree reasonably well with similar Cs…O=U=O compounds.[57] It is worth noting that these types of cation-cation interactions are very rare and this is the fourth example in the literature that reports this type interaction.

3.5.3 Photophysical Properties of Uranyl Thiocyanate Complex

3.5.3.1 Absorption Spectroscopy

The UV-Vis absorption spectrum of ~10^{-6} M acetonitrile solution of **10** (Figure 3.36) displays three bands with extinction coefficient $\varepsilon = 10^4$ M^{-1} cm^{-1}: an intense band centered at $\lambda_{max} = 230$ nm identical to that observed in **5** assigned to a spin allowed ligand centered $n \rightarrow \pi^*$ transition within the thiocyanate chromophore; a band at $\lambda_{max} = 290$ nm and 340 nm assigned to $\pi \rightarrow \pi^*$ transitions within the thiocyanate chromophore and these are similar to those observed for **5** upon photochemical oxidation. The weaker O=U=O charge transfer band is observed at $\lambda_{max} = 440$ nm with an extinction coefficient $\varepsilon = 40$ M^{-1} cm^{-1}

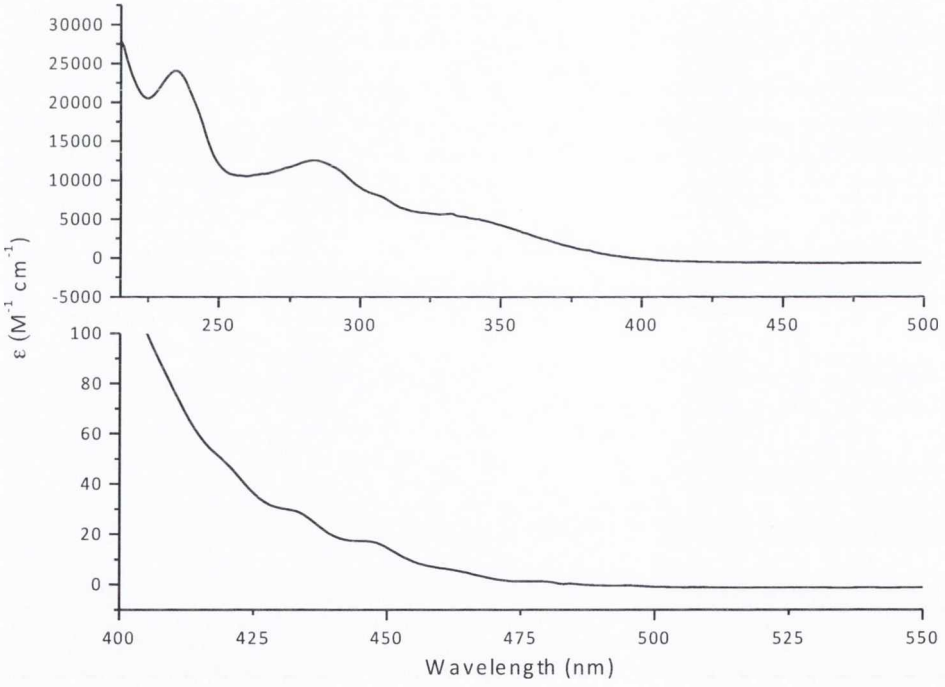

Figure 3.36: UV-Vis absorption spectrum of **10**

3.5.3.2 Emission Spectroscopy

The emission profile of **10** displays the characteristic vibrational fine structure with four "hot bands" being resolved centred at 520 nm (Figure 3.37) and corresponds to ligand-to-metal charge transfer emission. The luminescence lifetime was measured to be 1.4 μs following excitation at 340 nm using single exponential decay to fit the data (Figure 3.38).

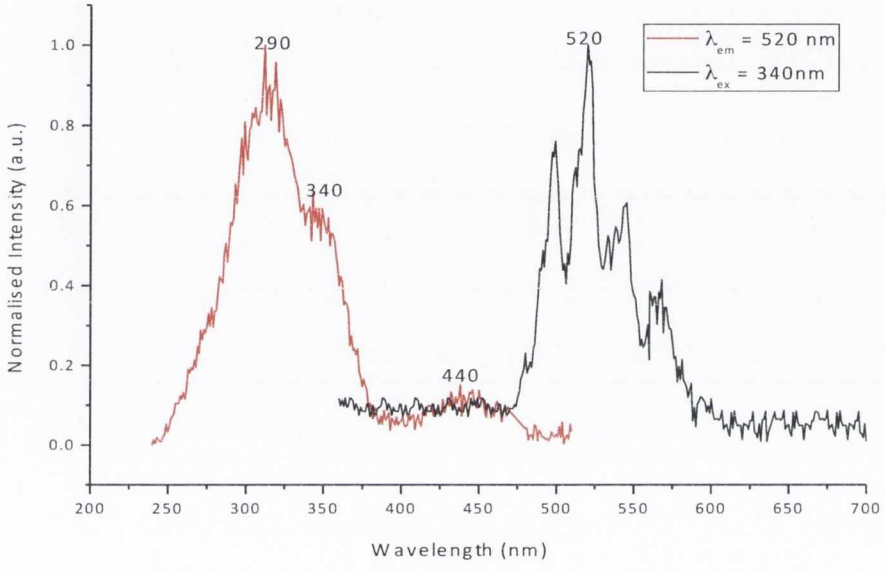

Figure 3.37: Emission (black line) and excitation (red line) profile of **8** in CD_3CN recorded at 298 K (λ_{ex} = 340 nm and λ_{em} = 520 nm)

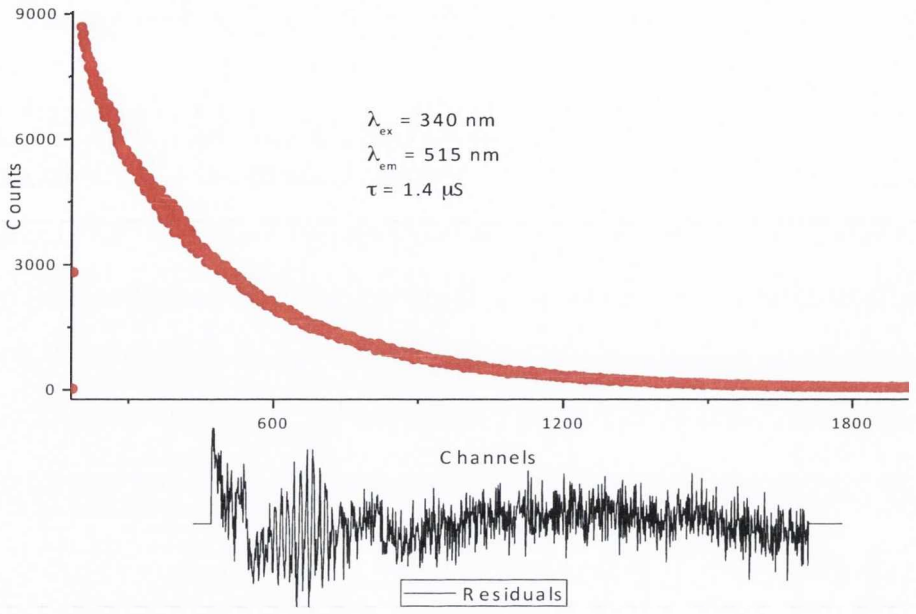

Figure 3.38: Typical kinetic traces obtained for **10** in MeCN recorded at 298 K (λ_{ex} = 340 nm and λ_{em} = 520 nm)

The lifetime was measured at 340 nm excitation and the kinetic trace was fitted to a single exponential decay with χ^2 value = 1.025.

3.5.3.3 Spectroelectrochemistry

Under the same SEC conditions as for **5**, cyclic voltammetry of a solution of **10** in acetonitrile containing 0.1 M [^{n}Bu$_4$N][PF$_6$] scaned at 0.1 V/S (Figure 3.39) shows a reversible one electron oxidation at +0.25 V *vs.* (Fc/Fc^+) and an irreversible one-electron reduction at -1.75 V *vs.* (Fc/Fc^+) ascribed to the $[UO_2]^{2+}/[UO_2]^+$ redox couple in line with known formal redox potentials of U(IV)/U(V) reduction listed in Table 3.7.

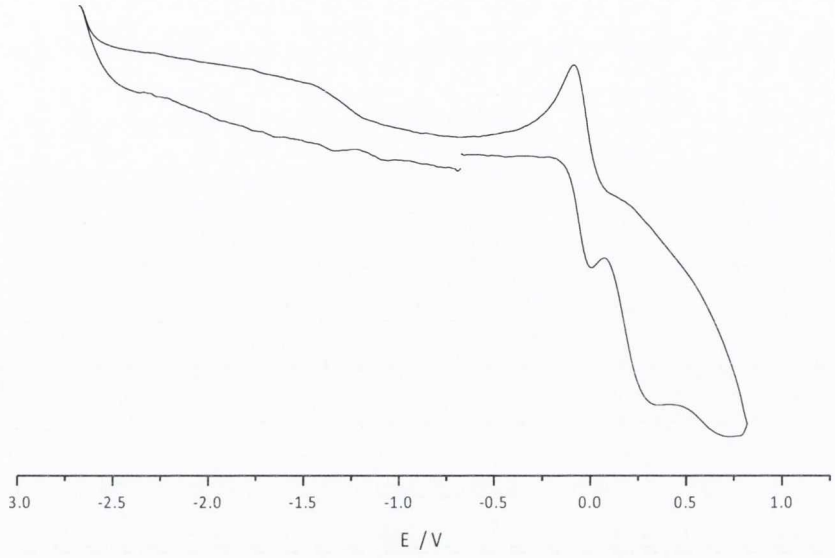

Figure 3.39: Cyclic voltammogram of **10** in MeCN *vs.* Fe/Fe^{+} using 0.1 M $[^{n}Bu_4N][PF_6]$ as a supporting electrolyte and recorded at 298 K and 0.1 V/ s

Complex	E/V *vs.* $[(C_5H_5)_2Fe]/Fe^{+}$	Ref
	An(IV)/An(III)	
$[UO_2(NCS)_5]^{3-}$ **11**	-1.80	This work
$[UO_2(OH)_5]^{3-}$	-1.11	58
$[UO_2Cl_4]^{2-}$	-0.24	58
$[UO_2(salmnt^{(Et2N)2})(py)]$	-1.81	59
[UO2(salen(py)]	-1.67	60
[UO2(salophen)(py)]	-1.626	60

Table 3.7: Formal redox half potentials (*vs.* Fc/Fc^{+}) for the U(VI)/U(V) couple of selected uranyl complexes; ($salmnt^{(Et_2N)_2}$ = 2,3-bis[(4-diethylamino-2-hydroxobenzylidene)amino] but-2-enedinitrile; salen = (*N,N'*-disalicylidene-1,2-ethylenediaminate) and salophen = (*N,N'*-disalicylidene-1,2-phenylenediaminate)

The one-electron oxidation process of **10** was investigated using spectroelectrochemistry and is shown in Figure 3.40.

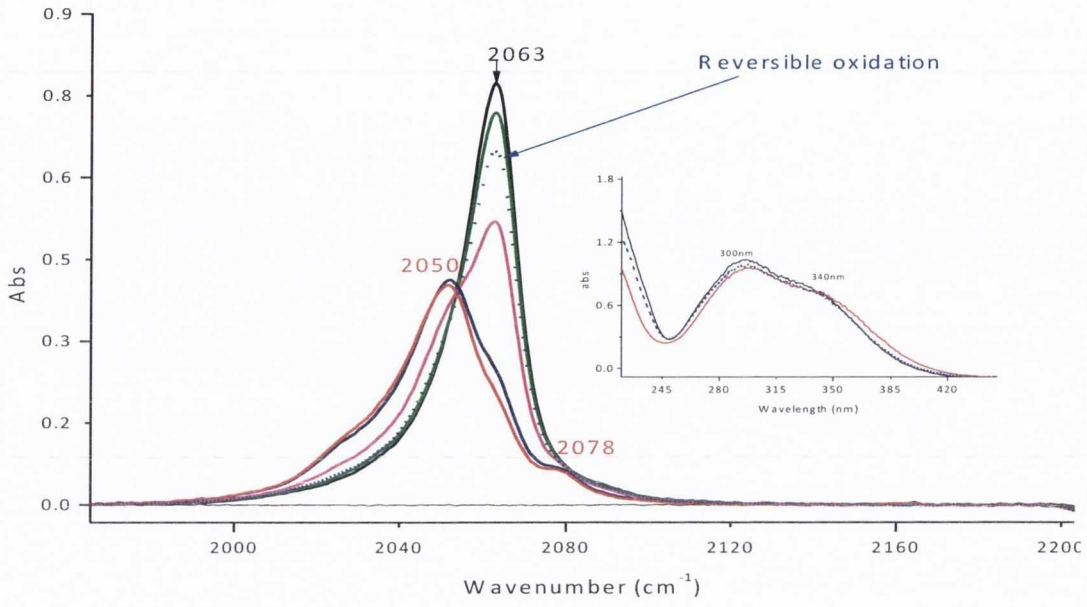

Figure 3.40: Spectroelectrochemical oxidation of **10** in MeCN containing ~0.1 M [^{n}Bu$_4$N][PF$_6$] recorded at 298 K, (inset shows the corresponding UV-Vis spectra of the parent and oxidised species)

In compound **10**, the parent band for ν(N=C) at 2063 cm^{-1} is rather symmetrical. Upon oxidation of **10**, the parent band at 2063 cm^{-1} (black line) firstly decreases in intensity (green and pink line) and secondly shifts to a lower energy (2050 cm^{-1}; red and blue line) to give a profile similar to that observed for **5**. The oxidation process is reversible and must be ligand based. Unfortunately, solvent bands have obscured the U=O stretch making it difficult to monitor this, but the UV-Vis spectra showed no distinguishable change and the only bands seen are at *ca.* 290 nm and 340 nm characteristic of the chromophore.

The spectroelectrochemical reduction process of **10** was also investigated and is shown in Figure 3.41.

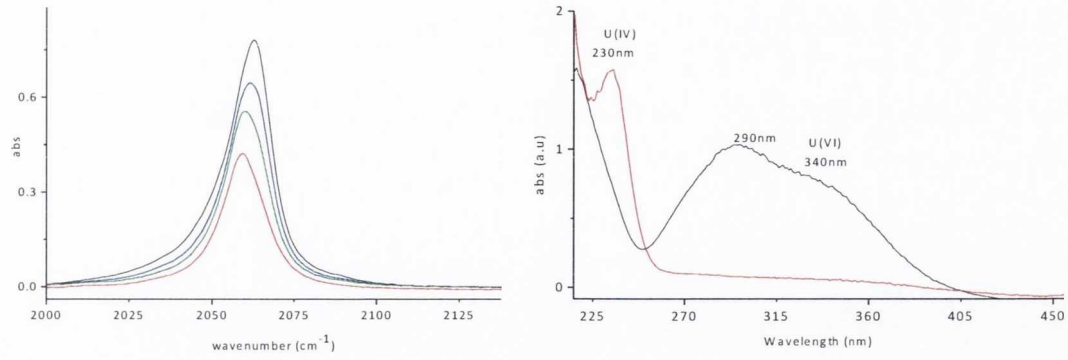

Figure 3.41: Spectroelectrochemical reduction of **10** in a MeCN containing 0.1 M [^{n}Bu$_4$N][PF$_6$] as a supporting electrolyte, showing the IR profile (left) and the UV-Vis profile (right) recorded at 298 K

The one-electron reduction process of **10** shows a decrease in intensity of the parent band at 2063 cm^{-1} as shown in Figure 3.41 (left). The UV-Vis spectrum (Figure 3.41 (right)) shows the disappearance of the chromophoric bands at 290 and 340 cm^{-1} and the growth of a band at 230 nm which matches the band observed for the U(IV) species in **5**. This can be postulated to the reduction of uranyl(VI) to give uranyl(V) followed by rapid disproportionation of the putative uranyl(V) species to **5** and the uranyl **10**, but as this measurement is conducted at a controlled potential, **10** is then further reduced to the unstable uranyl(V) species and the only complex observed in solution appears to be characteristic of **5**. The reduction process is thought to give uranyl(V) species [Et$_4$N]$_4$[UO$_2$(NCS)$_5$] which are predicted to be unstable as it is now quite well established that good π-donors and/or sterically bulky groups in the equatorial plane are required for stabilisation of this unusual oxidation state.[59,61] Ligand-to-metal σ and π bonding of the equatorial ligands increases the electron density on the uranium metal centre and increases electrostatic repulsion with the axial atoms to weaken the axial metal-ligand bond which in this case is the U=O bond in **10**. The production of unstable U(V) species would manifest itself in an irreversible reduction and the IR and UV spectra of the reduced product in the SEC measurement show only evidence of decomposition.

3.6 Density Functional Theory Calculations

In order to gain further insight into the electronic structure of the thiocyanate U(IV) and U(VI) compounds, especially the degree of covalency in the U-N bonds, density functional theory (DFT), which is increasingly being utilised in this field,[62] was used. Geometry optimisation of triplet $[U(NCS)_8]^{4-}$ using both pure (BP86) and hybrid (B3LYP) functionals with a TZVPP basis set resulted in square antiprismatic geometry. A comparison between the calculated and experimentally determined bond lengths and angles are reported in Table 3.8. The DFT geometries generally reproduce the solid-state geometry well; however, geometry optimisation of isolated **5** results in exactly linear NCS groups, supporting the observation that the non-linearity of these groups in the solid-state is due to crystal packing forces. Previous DFT studies of actinide complexes reported significant differences in the description of metal-ligand bonding between pure and hybrid DFT methods. Table 3.8 indicates that BP86 reproduces the U-N and C-S bond lengths determined by XRD within experimental error but overestimates the N-C length. In contrast, B3LYP performs well for N-C, but overestimates the U-N length. Given the apparent importance of crystal packing, it is not possible to deduce from this data whether one method gives a better description of bonding. Instead, the vibrational modes of the NCS group, especially N-C stretching modes, allow a more reliable test of the performance of these methods. Not only is this mode easily observed in IR and Raman spectra, but it should also be sensitive to the electronic character of U-N bonding. Table 3.8 clearly shows that BP86 yields a much better description of this mode than does B3LYP. Two IR active bands are found within 20 cm^{-1} of the experimental value, while the most intense Raman bands are centred on 2060 cm^{-1}, again slightly above the experimental value, with a less intense peak close to the experimental band at 2093 cm^{-1}. In contrast, B3LYP overestimates the energy of these bands by as much as 100 cm^{-1}.

	Bond Lengths (Å)			N-C vibration (cm^{-1})		C-S vibration (cm^{-1})	
	U-N	N-C	C-S	IR	Raman	IR	Raman
$[U(NCS)_8]^{4-}$							
Expt	2.466(4)	1.156(7)	1.648(6)	2048	2040	783	823
					2055		
					2093		
BP86	2.469	1.185	1.644	2067 (b_2)	2057 (e_2)	797	805
				2071 (e_1)	2060 (e_3)		
					2099 (a_1)		
B3LYP	2.485	1.171	1.644	2151 (b_2)	2139 (e_2)	803	811
				2154(e_1)	2144 (e_3)		
					2191 (a_1)		
$[U(NCS)_8]^{3-}$							
BP86	2.376	1.190	1.625	2044	2083	831	849
				2048			
$[Th(NCS)_8]^{4-}$							
BP86	2.538	1.185	1.644	2072	2107	800	809

Table 3.8: DFT geometry and vibrational modes using BP86 and B3LYP basis set

Since BP86 gave the best fit to the experiment, it was utilised to examine the bonding in **5** and related compounds. This method finds that the HOMO is ligand based and the LUMO is of *5f*-orbital character as shown in Figure 3.42. Natural bond order (NBO) analysis finds a single U-N bonding orbital, made up of 10.9% U and 89.1% N character, of which the U contribution is 12.34%*s*; 34.14%*p*; 38.01%*d* and 15.51%*f*. This can be compared to the U-Cl bond in $[UCl_5(THF)]^-$ (17% U and 83 % Cl, 20 %*s*, 26 %*p*, 41%*d* and 14% *f*). This analysis also locates one σ and two π bonding orbitals in N-C, and a single σ C-S bond, suggesting that the most appropriate resonance form of the coordinated thiocyanate ligand is $^-$N≡C-S with lone pairs of electrons on the sulfur that may be accessible for bonding to soft transitional metals. NBO indicates a charge on U in **5** of just +0.26, much less than the formal charge of +4, with corresponding charges of -0.18, +0.07 and -0.16 on N, C and S, respectively.

DFT simulation of oxidised $[U(NCS)_8]^{3-}$ for **5** are also reported in Table 3.8. Despite not having formal D_{4d} symmetry this complex retains approximate square-antiprismatic coordination, with U-N bond lengths between 2.365 and 2.385 Å, *i.e.* substantial shortening on loss of an electron which was not observed in the crystal structure of **8** suggesting the resulting product is not the $[U(NCS)_8]^{4-}$ radical. NBO analysis supports the assignment of oxidation as being ligand-based, indicating a loss of 0.18 electrons from each NCS ligand, primarily from S. For comparison, data for $[Th(NCS)_8]^{4-}$ indicates slightly longer Th-N bonds than in the U complex but identical N-C and C-S geometry and vibrational data, with a much more ionic complex with a charge on Th of +1.20. All complexes of this form have the same resonance structure of one U/Th-N, three N-C and one C-S bonding orbital.

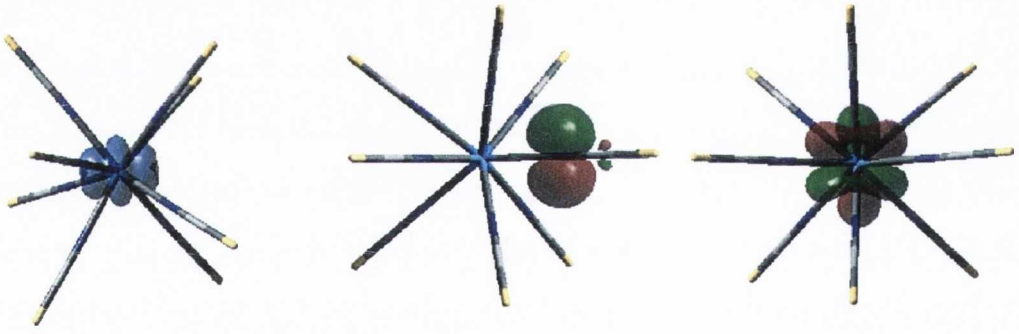

Figure 3.42: Spin density (left), HOMO (middle) and LUMO (right) of **5** ion at BP86 level of theory

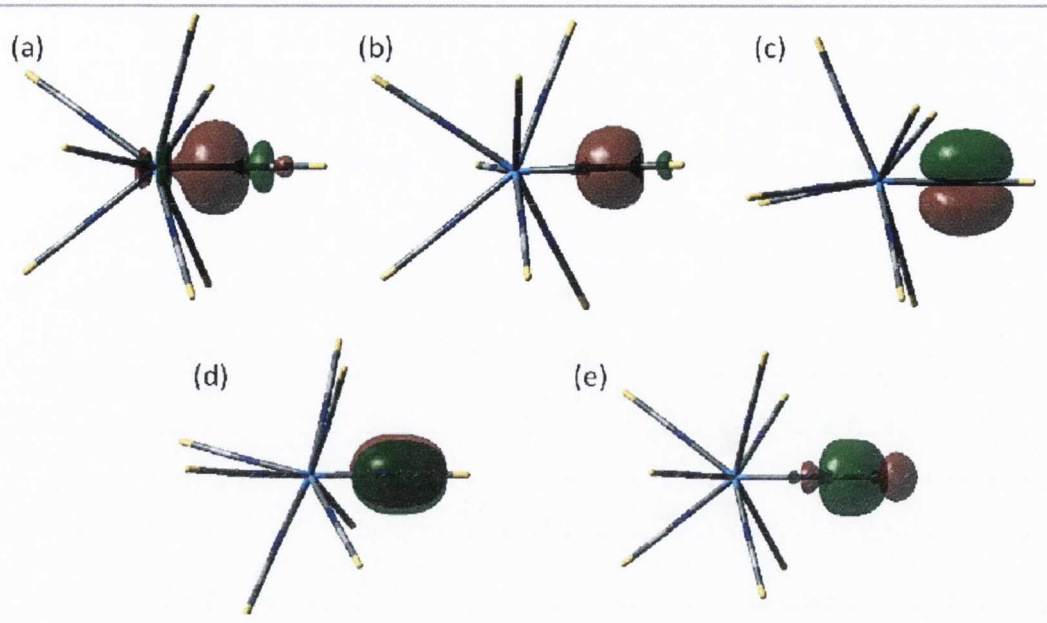

Figure 3.43: NBO analysis for **5** ion: (a) U-N σ NBO; (b) N-C σ NBO; (c) and (d) degenerate N-C π NBO; (e) C-S σ NBO

Using the same basis sets, data for two uranyl compounds was calculated (Table 3.9), with HOMO, LUMO and NBO analysis shown in Figure 3.44 and Figure 3.45. Agreement between experiment and theory for the uranyl(VI) complex is again reasonably good for both geometry and vibrational frequencies. Bond lengths and vibrational frequencies associated with thiocyanate are generally very similar to **5**, while U=O data is comparable to previous reports. Table 3.9 also contains DFT predictions for the result of $1e^-$ reduction to the uranyl(V) species. This finds significantly longer (by more than 0.2 Å) U-N bonds as well as slightly longer U=O and C-S bonds, while N-C bonds are almost unaffected by reduction. NBO analysis sheds light on these changes: charges in the uranyl(VI) and reduced complexes on U are +1.02 and +1.35, on O -0.47 and -0.65, and on NCS -0.62 and -0.82, respectively. Thus, the added electron resides mainly on O and NCS, particularly S, rather than on the metal, despite the LUMO lying on U. Moreover, the uranyl(VI) complex contains 3 U=O, 1 U-N, 3 N-C and 1 C-S bonding orbitals, which fall to 3, 0, 3 and 1 in the reduced complex, reflecting increased ionic character in the reduced complex.

	Bond Lengths (Å)				U=O vibration (cm^{-1})		N-C vibration (cm^{-1})		C-S vibration (cm^{-1})	
	U=O	U-N	N-C	C-S	IR	Raman	IR	Raman	IR	Raman
$[UO_2(NCS)_5]^{3-}$										
Expt	1.770	2.448	1.1526	1.618	920	847	2046	2072	783	810
BP86	1.800	2.497	1.184	1.646	887	811	2076	2099	795	790
$[UO_2(NCS)_5]^{4-}$										
BP86	1.836	2.702	1.181	1.669	812	761	2091	2101	738	739

Table 3.9: Calculated and experimental bond lengths and vibrational frequencies in **10**

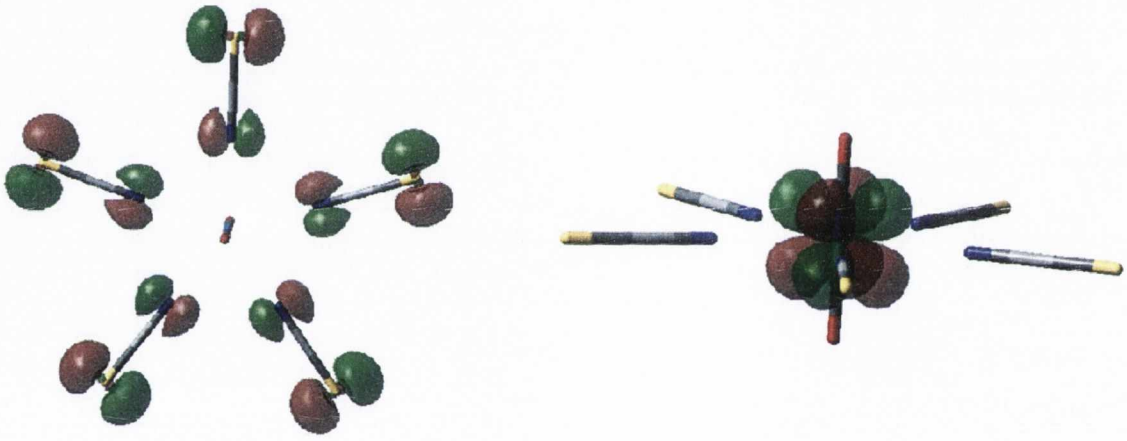

Figure 3.44: HOMO and LUMO of **10** at BP86 level of theory

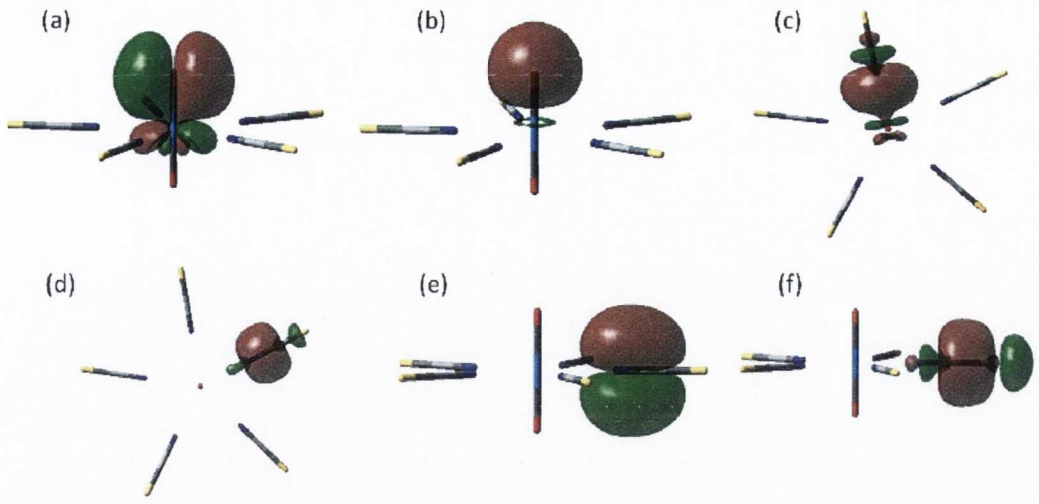

Figure 3.45: NBO analysis of **11**, (a) U-O π NBO; (b) U-O σ NBO; (c) U-N σ NBO; (d) N-C σ NBO; (e) N-C π NBO; (f) C-S σ NBO

3.6.1 Atoms in Molecules

Table 3.10 reports properties evaluated at bond critical points for An—N and the ligand N=C and C=S bonds in a series of compounds. It is worth noting that the N=C and C=S provide a good internal check of our calculations. This data indicates that all compounds studied feature predominantly ionic U-N bonds, as deduced from low values of σ, positive $\nabla^2\sigma$ and an energy density, H, close to zero. In contrast, U=O bonds have significant covalent character, while the expected covalency in the NCS ligand is reproduced, with values consistent with the resonance form found with NBO analysis. The effects of oxidation or reduction are also evident in AIM data, for instance in weakening U=O and U-N bonds in the uranyl species, or strengthening U-N bonds on oxidation of **5**.

Compound	Bond	ρ	$\nabla^2\rho$	ε	H	Bond order	Ref
9 $[UO_2(NCS)_5]^{3-}$	U-O	0.317	0.616	0.000	-0.302	1.893	this work
	U-N	0.047	0.188	0.066	-0.002	0.243	
	N-C	0.453	-0.497	0.006	-0.780	2.458	

	C-S	0.211	-0.260	0.004	-0.248	1.077	
$[UO_2Cl_4]^{2-}$	U-O	0.31	0.32	-		1.92	63
	U-Cl	0.05	0.12	-		0.53	
$[UO_2(NCS)_5]^{4-}$	U-O	0.286	0.484	0.000	-0.252	1.848	this work
	U-N	0.028	0.116	0.226	0.001	0.175	
	N-C	0.457	-0.424	0.000	-0.794	2.436	
	C-S	0.205	-0.372	0.003	-0.227	1.086	
5 $[U(NCS)_8]^{4-}$	U-N	0.047	0.200	0.320	-0.007	0.219	this work
	N-C	0.445	-0.204	0.006	-0.757	2.401	
	C-S	0.215	-0.405	0.033	-0.245	1.082	
$[U(NCS)_8]^{3-}$	U-N	0.068	0.226	0.277	-0.010	0.426	this work
	N-C	0.434	-0.586	0.010	-0.730	2.516	
	C-S	0.219	-0.268	0.014	-0.260	1.094	
$[Th(NCS)_8]^{4-}$	Th-N	0.048	0.166	0.019	-0.002	0.243	this work
	N-C	0.444	-0.672	0.006	-0.749	2.486	
	C-S	0.216	-0.388	0.058	-0.249	1.083	
$[UCl_5(THF)]^-$	U-Cl	0.072	0.165	0.090	n.r	0.75	23

Table 3.10: Bond critical point properties for selected compounds (values in a.u.)

3.7 Conclusions

The nature of the conjugated "non-innocent" thiocyanate ligands result in intense absorbance bands in the visible region of the spectrum arising from $n \rightarrow \pi^*$ and $\pi \rightarrow \pi^*$ transitions within the chromophore. Excitation into the band of the ligand chromophore (230 - 340 nm) is followed by inefficient electron transfer and subsequent de-excitation through the *f*-orbital manifold resulting in featureless broad bands in the emission spectrum. The short lived luminescence lifetime of these bands is an indication of ligand-based emission transitions arising from U(IV) species.

It was shown that luminescence spectroscopy can be used to fingerprint the +4 oxidation state of uranium in the ambiguous complex $[Et_4N][U(NCS)_5(bipy)_2]$. A re-determination of the solid state structure gives more precise bond lengths compared to those previously reported and spectroscopic and magnetic studies confirm that the bipy ligands are indeed neutral and the oxidation state of the uranium is +4. A computational study supports the assignment of oxidation state, and suggests that the bonding between the bipy and uranium centre is better described as donation from N lone pairs into empty orbitals on U, as opposed to covalency.

Furthermore, spectroelectrochemistry allows us to explore further the redox behaviour of uranium compounds with non-innocent ligands and unstable oxidation states of uranium complexes. **5** in acetonitrile shows reversible $1e^-$ electron oxidative processes suggesting a ligand based oxidation. The $2e^-$ oxidation process however suggests the formation of the radical species which rapidly recombine to form the dithiolate NCS-SCN, making the oxidation process irreversible.

Using BP86 method to support the cyclic voltammetry observations, it was confirmed that whilst the LUMO is of a *5f*-orbital character, the HOMO is ligand based and the one-electron oxidation of the uranyl thiocyanate, **10**, species was rather identical to that seen in **5**. However, the reduced species of **10** were unstable and the irreversible reduction shows only evidence of decomposition as observed in the IR and UV spectra of the SEC measurements.

The exact nature of this bonding was explored further using theoretical calculations. All compounds studied feature predominantly ionic U-N bonds, as deduced from low values of σ, positive $\nabla^2\sigma$ and an energy density, H, close to zero. In contrast, U=O bonds have significant covalent character, while the expected covalency in the NCS ligand is reproduced, with values consistent with the resonance form found with NBO analysis.

3.8 Experimental

All manipulations were carried out using standard Schlenk and glove box techniques under an atmosphere of high purity argon. Description of instrumentation is as discussed in Chapter 2. Crystals were mounted and crystal structures were resolved by Prof. Carola Schulzke (Greifswald University) (see appendex B – E). Magnetic susceptibility measurements were carried out by Dr. M unuswamy Venkatesan (TCD) and by Dr. Marco Evangelisti (ICMA-CSIC). For SEC measurements, solutions of freshly distilled acetonitrile containing 10^{-1} M [$^{n}Bu_4N$][PF_6] as the supporting electrolyte were used. The electrolyte was re-crystallised twice from absolute methanol, dried under vacuum at 80 °C overnight and stored under argon atmosphere. Electrochemical (cyclic voltammetric) measurements were undertaken with a METROHM AUTOLAB PGSTAT302N using air tight three electrode cell connected to a schlenk line, platinum microdisc electrode with a reaction surface of 0.14 mm^2 as working electrode, platinum coil electrode was used as a reference electrode and a silver coil electrode as auxiliary electrode. Internal referencing was measured versus ferrocene/ferrocenium Fc/Fc^+. Controlled-potential electrolyses within the room-temperature OTTLE cell[64] were carried out using a PA4 potentiostat (Laboratory Devices, Polná, Czech Republic). IR and UV/Vis spectral monitoring of the redox reaction was carried out with a Bruker Vertex 70v FT-IR spectrometer and a Scinco S3100 diode array spectrophotometer, respectively. The different redox steps were localized with the aid of contemporarily recorded thin-layer cyclic voltammograms.

D_3-acetonitrile was distilled over CaH_2, distilled and degassed immediately prior to use. Spectroscopic measurements used spectroscopic grade solvents, which were purchased from commercial sources and dried over molecular sieves and thoroughly degassed before use. Compounds **5**[10], **6**[11], **7**[10], **9**[46] and $[Et_4N]_4[Th(NCS)_8]$[27] were made using previously reported methods whilst all other reagents were obtained from commercial sources.

3.8.1 Synthesis of $[Bu_4N]_4[U(NCS)_8]$ (7)

To a suspension of UCl_4 (100 mg, 0.25 mmol) in acetonitrile (20 cm^3) was added NaNCS (170.75 mg, 2.11 mmol) and Bu_4NCl (291.82 mg, 1.05 mmol). The solution mixture was stirred at room temperature for 30 mins, the resulting green solution was filtered and the solvent was reduced in volume. Placement at -20 °C overnight yielded dark green crystals suitable for X-ray diffraction (240 mg, 0.16 mmol, 64%). IR (cm^{-1}): 2047, 2090 ν(CN), 783 ν(CS). RAMAN (cm^{-1}) 2090, 2056 and 2045 ν(CN), 796 ν(CS), UV-Vis/NIR (ε mol dm^{-3} cm^{-1}): (MeCN, ~10^{-4}M) 230 nm (12833.4), 475 nm (33.8), 505 nm (87.8), 573 nm (32.5), 691 nm (214), 933 nm (35), 1168 nm (127), 1584 nm (65), 1994nm (25).

3.8.2 Synthesis of $[Et_4N]_4[U(NCS)_8]$ (8)

A solution of **5** (50 mg, 0.048 mmol) in acetonitrile (10 cm^3) was exposed to UV light for a period of 4 hours, until a change in colour from green to orange was observed. Placement at -20 °C overnight yielded dark orange crystals suitable for X-ray diffraction (26 mg, 0.025 mmol, 52%). IR (cm^{-1}): 2040 ν(CN), 783 ν(CS). RAMAN (cm^{-1}) 2090 and 2047 ν(CN), 823 ν(CS), UV-Vis/NIR (MeCN, 298 K) 230, 290, 340, 475, 505, 573, 691, 933, 1168, 1584, 1994 nm.

3.8.3 Synthesis of $[Et_4N][U(bipy)_2(NCS)_5]$ (9)

To a sample of $[Et_4N]_4[U(NCS)_8]$ (200 mg, 0.16 mmol) in a dry schlenk tube was added 2,2'-bipyridine (51 mg, 0.33 mmol). Anhydrous MeCN (20 cm^3) was added and the mixture was stirred for an hour at room temperature. The solvent was reduced and left to crystallise at -30 ^0C. After 48 hours pale green crystals suitable for X-ray diffraction had formed (116.5 mg, 0.12 mmol, 75%). ^1H NMR (CD_3CN, 298K) 9.0 – 10.65 ppm (bipy); IR (cm^{-1}) 2016, 1595, 1570, 1474, 1434, 1394, 1313, 1175, 1067, 1011, 764, 735, 641, 623, 553; RAMAN (cm^{-1}) 2070, 2030, 1600, 1568, 1496, 1300, 1069, 1000, 831, 768, 652, 546, 627, 416, 350.

3.8.4 Synthesis of $Cs_3[UO_2NCS)_5]$ (11)

A solution of $Cs_4[U(NCS)_8]$ in acetonitrile was left to stand in air at room temperature. After 48 hours dark yellow crystals suitable for X-ray diffraction were collected. IR (cm^{-1}): 2104, 2020 ν(CN), 900 ν(UO), 798 ν(CS); Raman (cm^{-1}): 2095, 2060, 2040 ν(CN), 849 ν(UO), 821 ν(CS).

3.9 References

[1] a) P. K. Khopkar and J. N. Mathur, *J. Inorg. Nucl. Chem.*, 1980, **42**, 109; b) F. L. Moore, *Anal. Chem.*, 1964, **36**, 2158; c) R. Chiarizia, P. R. Danesi, G. Scibona and L. Magon, *J. Inorg. Nucl. Chem.*, 1973, **35**, 3595; d) M. Borkowski, J. Krejzler and S. Siekierski, *Radiochim. Acta.*, 1994, **65**, 99

[2] E. Metwally, A. S. Saleh and H. A. El-Naggar, *J. Nucl. Radiochem. Sci., 2005*, **6**, 119

[3] M. Borkowski, S. Lis and S. Siekierski, *J. Alloys Compd.*, 1998, **275**, 754

[4] a) S. Siekierski, *Radiochem. Radioanal. Lett.*, 1981, **48**, 169; b) M. Borkowski and S. Siekierski, *Radiochim. Acta.*, 1992, **56**, 31; c) G. R. Choppin and D. W. Barber, *J. Less-Common Met.*, 1989, **149**, 231

[5] a) A. Kirishima, T. Kimura, O. Tochiyama and Z. Yoshida, *Chem. Commun.*, 2003, 910; b) A. Kirishima, T. Kimura, R. Nagaishi and O. Tochiyama, *Radiochim. Acta.*, 2004, **92**, 705

[6] C. Danilo, V. Vallet, J. -P. Flament and U. Wahlgren, *Phys. Chem. Chem. Phys.*, 2010, **12**, 1116

[7] N. Aoyagi, K. Shimojo, N. R. Brooks, R. Nagaishi, H. Naganawa, K. Van Hecke, L. Van Meervelt, K. Binnemans and T. Kimura, *Chem. Commun.*, 2011, **47**, 4490

[8] C. E. Rowland, M. G. Kanatzidis and L. Soderholm, *Inorg Chem.*, 2012, **21**, 11798

[9] a) E. G. Arutyunyan and M. A. Porai-Koshits, Zh. Strukt. Khim., 1963, **4**, 110; b) K. W. Bagnall, D. Brown and R. Colton, *J. Chem. Soc. Dalton Trans.*, 1964, 2527

[10] R. Countryman and W. S. McDonald, *J. Inorg. Nucl. Chem.*, 1971, **33**, 2213; b) Z. M. S. Al-Kazzaz, K. W. Bagnall, D. Brown and B. Whittaker, *J. Chem. Soc. Dalton. Trans.*, 1972, 2273

[11] G. Bombieri, P. T. Moseley and D. Brown, *J. Chem. Soc., Dalton Trans.*, 1975, 1520

[12] a) W. P. Griffith and M. J. Mockford, *J. Chem. Soc., Dalton Trans.*, 1986, 1057; b) G. Folcher, H. Marquet-Ellis, P. Rigny, E. Soulic and G. Goodman, *J. Inorg. Nucl. Chem.*, 1976, **38**, 757; c) I. E. Grey and P. W. Smith, *Australian J. Chem.*, 1969, **22**, 311

[13] J. D. Rinehart and J. R. Long, *J. Am. Chem. Soc.*, **2009**, *131*, 12558

[14] J. D. Rinehart, K. R. Meihaus and J. R. Long, *J. Am. Chem. Soc.*, **2010**, *132*, 7572

[15] J. D. Rinehart and J. R. Long, *Dalton Trans.*, **2012**, *41*, 13572

[16] J. T. Coutinho, M. A. Antunes, L. C. J. Pereira, H. Bolvin, J. Marçalo, M. Mazzanti and M. Almeida, *Dalton Trans.*, **2012**, *41*, 13568

[17] M. A. Antunes, L. C. J. Pereira, I. C. Santos, M. Mazzanti, J. Marçalo and M. Almeida, *Inorg. Chem.*, **2011**, *50*, 9915

[18] D. P. Mills, F. Moro, J. McMaster, J. van Slageren, W. Lewis, A. J. Blake and S. T. Liddle, *Nat. Chem.*, **2011**, *3*, 454

[19] V. Mougel, L. Chatelain, J. Pecaut, R. Caciuffo, E. Colineau, J. –C. Griveau and M. Mazzanti, *Nat. Chem.*, **2012**, *4*, 1011

[20] F. Moro, D. P. Mills, S. T. Liddle, J. van Slageren, *Angew. Chem. Int. Edn.*, 2013, DOI: 10.1002/anie.201208015

[21] J. J. Baldoví, S. Cardona-Serra, J. M. Clemente-Juan, E. Coronado and A. Gaita-Arino, *Chem. Sci.*, 2013, **4**, 938

[22] a) B. S. Newell, T. C. Schwaab and M. P. Shores, *Inorg. Chem.*, 2011, **50**, 12108; b) S. Fortier, B. C. Melot, G. Wu, T. W. Hayton, *J. Am. Chem. Soc.*, 2009, **131**, 15512; c) J. D. Rinehart, T. D. Harris, S. A. Kozimor, B. M. Bartlett and J. R. Long, *Inorg. Chem.*, 2009, **48**, 3382; d) O. P. Lam, C. Anthon, F. W. Heinemann, J. M Connor and K. Meyer, *J. Am. Chem. Soc.*, 2008, **130**, 6567; e) G. Nocton, J. Pecaut and M. Mazzanti, *Angew. Chem. Int. Ed.*, 2008, **47**, 3040; f) Y. L. Lai, R. K. Chiang, K. H. Lii and S. L. Wang, *Chem. Mater.*, 2008, **20**, 523; g) G. Nocton, F. Burdet, J. Pecaut and M. Mazzanti, *Angew. Chem. Int. Ed.*, 2007, **46**, 7574; h) E. J. Schelter, D. E. Morris, B. L. Scott, J. D. Thompson, and J. L. Kiplinger, *Inorg. Chem.*, 2007, **46**, 5528. i) M. J. Monreal, C. T. Carver and P. L Diaconescu, *Inorg. Chem.*, 2007, **46**, 7226; j) L. Salmon, P. Thuery, E. Riviere, S. Miyamoto, T. Yamato, and M. Ephritikhine, *New J. Chem.*, 2006, **30**, 1220; k) I. Castro-Rodríguez, K. Olsen, P. Gantzel, and K. Meyer, *J. Am. Chem. Soc.*, 2003, **125**, 4565

[23] E. Hashem, A. N. Swinburne, C. Schulzke, R. C. Evans, J. A. Platts, A. Kerridge, L. S. Natrajan and R. J. Baker, *RSC Adv.*, 2013, **3**, 4350

[24] C. Danilo, V. Vallet, J.-P. Flament and U. Wahlgren, *Phys. Chem. Chem. Phys.*, 2010, **12**, 1116

[25] D. K. Palit, H. Pal, T. Mukherjee, and J. P. Mittal, *J. Chem. Soc. Faraday Trans.*, 1990, **86**, 3861

[26] D. F. de Sá, O. L. Malta, C. de Mello Donegá, A. M. Simas, R. L. Longo, P. A. Santa Cruz and E. F. Silva, *Coord. Chem. Rev.*, 2000, **196**, 165

[27] P. Charpin, M. Lance and A. Navaza, *Acta Crystallogr., Sect. C: Cryst. Struct. Commun.*, 1983, **39**, 190

[28] Photoluminescence from $[Th(PO_3C_6H_4CO_2H)F_2]$ has been reported, but these arise from the ligand. P. O. Adelani and T. E. Albrecht-Schmitt, *Inorg. Chem.*, 2010, **49**, 5701

[29] A) D. C. Sonnenberger and J. G. Gaudiello, *Inorg. Chem.*, **1988**, 27, 2747; b) R. G. Finke, G. Gaughan and R. Voegeli, *J. Organomet. Chem.*, 1982, **229**, 179

[30] C. Clappe, D. Leveugle, D. Hauchard and G. Durand, *J. Electroanal. Chem.*, 1998, **448**, 95

[31] D. E. Morris, R. E. DaRe, K. C. Jantunen and I. Castro-Rodríguez, *Organometallics*, 2004, **23**, 5142

[32] W. Kaim and J. Fiedler, *Chem. Soc. Rev.*, 2009, **38**, 3373

[33] L. P. Eremin, O. Kh. Poleshchuk. V. A. Poluboyarov, L. V. Babovskaya and A. E. Lapin., *J. Struct. Chem.*, 2003, **44**, 404

[34] A. K. Pathak, T. Mukherjee and D. K. Maity, *J. Mol. Struct. Theochem.*, 2005, **755**, 241

[35] A. K. Pathak, T. Mukherjee and D. K. Maity, *J. Mol. Struct., 2008,* **851**, 158

[36] a) V. Lyaskovskyy and B. de Bruin, *ACS Catalysis*, 2012, **2**, 270; b) W. Kaim, *Eur. J. Inorg. Chem.*, 2012, 343; c) P. Chirik, *J. Inorg. Chem.* 2011, **50**, 9737

[37] C. C. Scarborough and K. Weighardt, *Inorg. Chem.*, 2011, **50**, 9773

[38] E. König and S. Kremer, *Chem. Phys. Lett.*, 1970, **5**, 87

[39] C. C. Scarborough, S. Sproules, T. Weyhermüller, S. DeBeer and Wieghardt, *Inorg. Chem.* 2011, **50**, 12446

[40] a) A. C. Bowman, J. England, S. Sproules, T. Weyhermüller and K Wieghardt, *Inorg. Chem.*, 2013, **52**, 2242; b) A. C. Bowman, S. Sproules and K Wieghardt, *Inorg. Chem.*, 2012, **51**, 3707

[41] S. J. Kraft, P. E. Fanwick and S. C. Bart, *Inorg. Chem.*, 2010, **49**, 1103

[42] M. K. Takase, M. Fang, J. W. Ziller, F. Furche and W. Evans, *J. Inorg. Chim. Acta.*, 2010, **364**, 167

[43] a) G. Zi, L. Jia, E. L. Werkema, M. D. Walter, J. P. Gottfriedsen and R. A. Andersen, *Organometallics*, 2005, **24**, 4251; b) A. Mohammad, D. P. Cladis, W. P. Forrest, P. E. Fanwick and S. C. Bart, *Chem. Commun.*, 2012, **48**, 1671

[44] W. Ren, G. Zi and M. D. Walter, *Organometallics*, 2012, **31**, 672

[45] W. Ren, H. Song, G. Zi and M. D. Walter, *Dalton Trans.*, 2012, **41**, 5965

[46] R. O. Wiley, R. B. Von Dreele and T. M. Brown, *Inorg. Chem.*, 1980, **19**, 3351

[47] W. Zhou, A. N. Desnoyer, J. A. Bailey, B. O. Patrick and K. M. Smith, *Inorg. Chem.*, 2013, **52**, 2271

[48] E. J. Schelter, R. Wu, B. L. Scott, J. D. Thompson, T. Cantat, K. D. John, E. R. Batista, D. E. Morris, and J. L. Kiplinger, *Inorg. Chem.*, 2010, **49**, 924

[49] S. J. Kraft, U. J. Williams, S. R. Daly, E. J. Schelter, S. A. Kozimor, K. S. Boland, J. M. Kikkawa, W. P. Forrest, C. N. Christensen, D. E. Schwarz, P. E. Fanwick, D. L. Clark, S. D. Conradson and S. C. Bart, *Inorg. Chem.*, 2011, **50**, 9838

[50] E. König and S. Kremer, *Chem. Phys. Lett.* 1970, **5**, 87-90

[51] L. S. Natrajan, *Dalton Trans.*, 2012, **41**, 13167

[52] a) L. A. Seaman, G. Wu, N. Edelstein, W. W. Lukens, N. Magnani and T. W. Hayton, *J. Am. Chem. Soc.*, 2012, **134**, 4931; b) L. P. Spencer, E. J. Schelter, P. Yang, R. L. Gdula, B. L. Scott, J. D. Thompson, J. L. Kiplinger, E. R. Batista and J. M. Boncella, *Angew. Chem., Int. Ed.*, 2009, **48**, 3795; c) S. C. Bart, C. Anthon, F. W. Heinemann, E. Bill, N. M. Edelstein and K. Meyer, *J. Am. Chem. Soc.*, 2008, **130**, 12536; d) C. R. Graves, P. Yang, S. A. Kozimor, A. E. Vaughn, D. L. Clark, S. D. Conradson, E. J. Schelter, B. L. Scott, J. D. Thompson, P. J. Hay, D. E. Morris and J. L. Kiplinger, *J. Am. Chem. Soc.*, 2008, **130**, 5272;

e) C. R. Graves, A. E. Vaughn, E. J. Schelter, B. L. Scott, J. D. Thompson, D. E. Morris and J. L. Kiplinger, *Inorg. Chem.*, 2008, **47**, 11879; f) I. Castro-Rodriguez and K. Meyer, *Chem. Commun.*, 2006, 1353; g) I. Castro-Rodriguez, H. Nakai and K. Meyer, *Angew. Chem., Int. Ed.*, 2006, **45**, 2389

[53] C. E. Rowland, M. G. Kanatzidis and L. Soderholm, *Inorg. Chem.*, 2012, **51**, 11798

[54] P. K. Khulbe, A. Agarwal, G. S. Raghuvanshi, H. D. Bist, H. Hashimoto, T. Kitagawa, T. S. Little and J. R. J. Durig, *Raman Spectrosc.*, 1989, **20**, 283

[55] M. H. Brooker, C. B. Huang and J. Sylwestrowicz, *J. Inorg. Nucl. Chem.*, 1980, **42**, 1431

[56] F. H. Allen, Acta Crystallogr., *Sect. B: Struct. Sci.*, 2002, **58**, 380

[57] a) P. Thuéry and B. Masci, *Dalton Trans.*, 2003, 2411; b) P. O. Adelani, A. G. Oliver, and T. E. Albrecht-Schmitt, *Crys. Growth. Des.*, 2011, **11**, 3072 c) A. J. Locock and P. C. Burns, *J. Solid. State. Chem.*, 2003, **175**, 372

[58] D. E. Morris, *Inorg. Chem.*, 2002, **41**, 3542

[59] H. C. Hardwick, D. S. Royal, M. Helliwell, S. J. A. Pope, L. Ashton, R. Goodacre and C. A. Sharrad, *Dalton Trans.*, 2011, **40**, 5939

[60] S.-Y. Kim, H. Tomiyasu and Y. Ikeda, *J. Nucl. Sci. Technol.*, 2002, **39**, 160

[61] D. L. Clark, S. D. Conradson, R. J. Donohoe, D. W. Keogh, D. E. Morris, P. D. Palmer, R. D. Rogers and C. D. Tait, *Inorg. Chem.*, 1999, **38**, 1456

[62] a) G. Schreckenbach and G. A. Shamov, *Acc. Chem. Res.*, 2010, **43**, 19; b) L. Gagliardi and B. O. Roos, *Chem. Soc. Rev.*, 2007, **36**, 893; c) N. Kaltsoyannis, *Chem. Soc. Rev.*, 2003, **32**, 9; d) I. Kirker and N. Kaltsoyannis, *Dalton Trans.*, 2011, **40**, 124; e) M. J. Tassell and N. Kaltsoyannis, *Dalton Trans.*, 2010, **39**, 6719; f) D. Wang, W. F. van Gunsterenb and Z. Chai, *Chem. Soc. Rev.*, 2012, **41**, 5836

[63] F. Ruipérez and U. Wahlgren, *J. Phys. Chem. A.*, 2010, **114**, 3615

[64] M. Krejčík, M. Daněk and F. Hartl, *J. Electroanal. Chem.* 1991, **317**, 179

Chapter 4

Spectroscopic Properties of Uranyl(VI) Halide Complexes in Non-Aqueous Media

4.1 Introduction

One class of compound that has known covalency is the uranyl ion, $[UO_2]^{2+}$.[1] However, it has taken some time to fully elucidate the bonding in this species, which has immense importance as it is the most stable oxidation state of uranium and is prevalent in the environment and in spent nuclear fuel dissolved in aqueous nitric acid. A comprehensive understanding has come from both experiment and theory and an authoritative review by Denning summarises recent developments.[1b] The study of $[UO_2Cl_4]^{2-}$ has substantially aided in the description of the bonding in the uranyl fragment, whilst the heavier halides have been less well studied with few examples of structurally characterised $[UO_2Br_4]^{2-}$,[2] whilst $[UO_2I_4]^{2-}$ was only synthesised and unambiguously characterised in 2005.[3]

Luminescence spectroscopy of actinides has become an important measurement tool,[4] and the photophysical properties of uranyl(VI) ions in solid and aqueous solution are well understood.[5] The optical properties of $[UO_2]^{2+}$ were first investigated in yellow-green uranium containing glass and minerals.[6] The absorption profile of the ion shows ligand-to-metal charge transfer electronic transitions centred at *ca.* 420nm.[5,7] The corresponding emission profile shows up to six "hot bands" centred at *ca.* 520 nm due to ligand-to-metal charge transfer transitions involving promotion of an electron from a bonding oxygen orbital (σ_u, σ_g) to non-bonding uranium $5f_\delta$ and $5f_\phi$ orbitals.[8] They often exhibit a fine structure characteristic of the coupling of the ground state symmetric vibrational O=U=O (ν_1) mode with the $^3\Pi_u$ electronic triplet excited state.[9] Figure 4.1 shows a molecular orbital description of the uranyl ion $[UO_2]^{2+}$ which has been both experimentally and theoretically understood.[1]

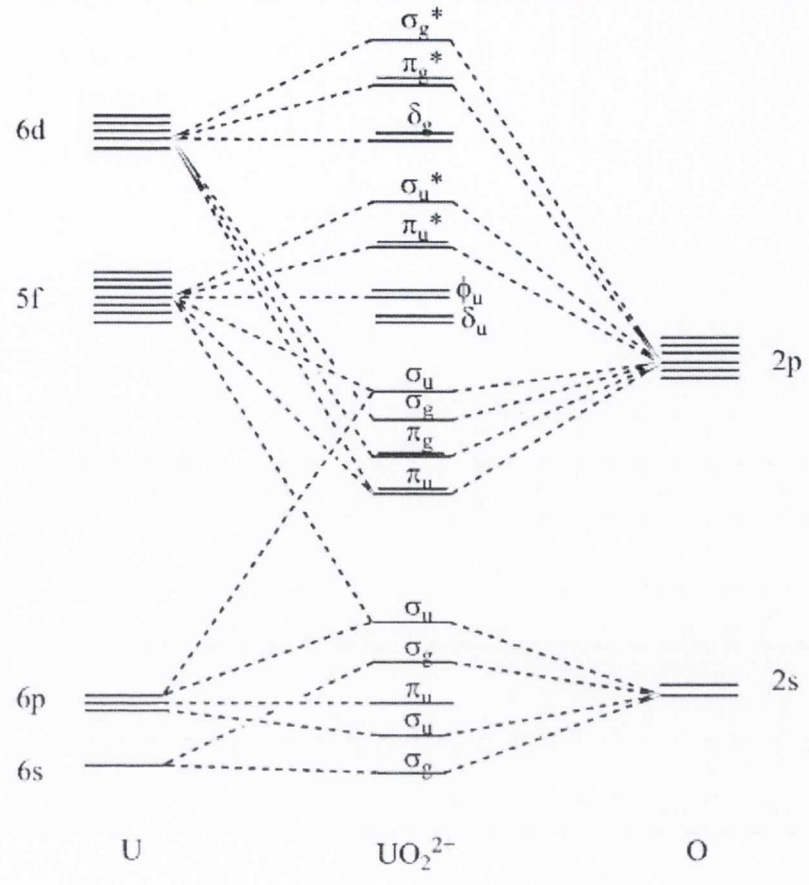

Figure 4.1: Qualitative Molecular orbital diagram for uranyl[1]

However, whilst the photophysical properties of aqueous uranyl(VI) compounds are well explored and understood,[5] there are only a few reports on the luminescence spectroscopy of uranyl(VI) ions in non-aqueous media.[10] Organic based ligands in protic solvents are usually non-emissive at room temperature.[11] The π-π^* and n-π^* absorption transitions of the organic ligands overlap significantly with the uranyl emission bands. The uranyl emission is quenched by thermally-activated back energy transfer to low-lying excited states of the ligands.[11] However, when the correct choice of chromophore containing ligand is made and the absorption envelope is restricted to the UV region, the energy gap between the organic triplet excited state and uranyl excited state should be large enough to prevent thermally activated back energy transfer and non-radiative decay processes.[12]

In Chapter 2, the photoluminescence properties of simple U(IV) compounds in non-aqueous media were reported.[13] In this chapter the synthetic utility of $[Li(THF)_4][UX_5(THF)]$ (X = Cl, Br, I), and reaction of these species with $Ph_3P{=}O$ is explored. A series of the different halide analogues of structurally characterized uranyl(VI) complexes of the type $[UO_2X_2L_2]$ (where X = Cl, Br, I and L = $OPPh_3$) are differentiated from one another by absorption and emission spectroscopy in non-aqueous media. The local coordination environment of uranyl(VI) complexes and the nature of the uranyl and ligand metal bonding in the equatorial plane are discussed.

4.2 Uranyl Complex $[UO_2X_2(O{=}PPh_3)_2]$

4.2.1 Synthesis and Structural Characterisation

$[UCl_4(O{=}PPh_3)_2]$ was structurally characterised by Brown in 1975,[14] and the reaction is thought to have been sensitive to reaction conditions. Herein, the reaction of $[Li(THF)_4][UX_5(THF)]$ (X = Br, I) with $Ph_3P{=}O$, in an attempt to synthesise the analogous tetrahalouranate species, was investigated. There are only few examples of these compounds prepared in the literature, and the electronic spectrum of $[UO_2I_4]^{2-}$ has not yet been reported.

Firstly, the reaction of $[Li(THF)_4][UCl_5(THF)]$ with $Ph_3P{=}O$ was investigated in order to examine how different Lewis bases would influence the spectroscopic and structural parameters of the U(IV) species (Scheme 4.1). Upon addition of a THF solution of $Ph_3P{=}O$ to the $[Li(THF)_4][UCl_5(THF)]$ compound a colour change from green to yellow was observed, indicating the formation of a uranyl moiety, which could have resulted due to oxidation in air. Crystallisation from acetonitrile produced $[UO_2Cl_2(OPPh_3)_2]$ (**12**) isolated as the major product, with *ca.* 10% of $[Li(O{=}PPh_3)(MeCN)_2]_2[UO_2Cl_4]$ (**13**). The former was unambiguously characterised by X-ray diffraction and matched that in the literature.[15] This reaction is reproducible when carried out under strictly

anhydrous conditions and the appearance of a peak at δ_P = 48.51 ppm in the ^{31}P NMR spectrum of the reaction mixture, indicating the formation of Ph_3PO coordinated to uranium and a peak at δ_P = 30.06 ppm, indicative of a phosphine oxide coordinated to a lithium cation. The absorption spectrum and the characteristic band at 839 cm^{-1} in the Raman spectrum and at 915 cm^{-1} in the IR spectrum confirm the formation of a $[UO_2]^{2+}$ species.

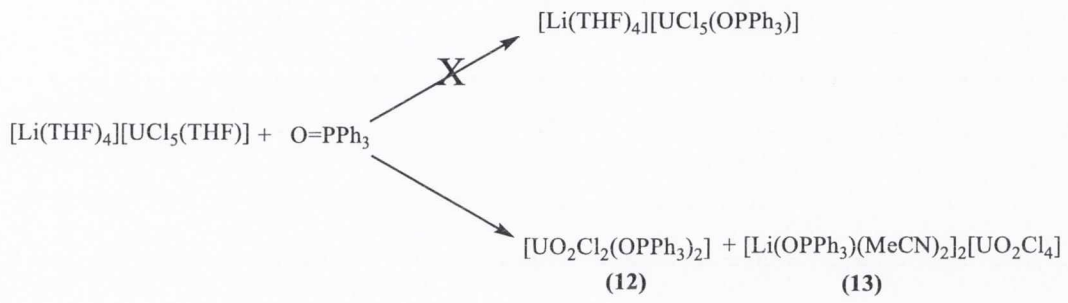

Scheme 4.1: Synthesis of **12** and **13**

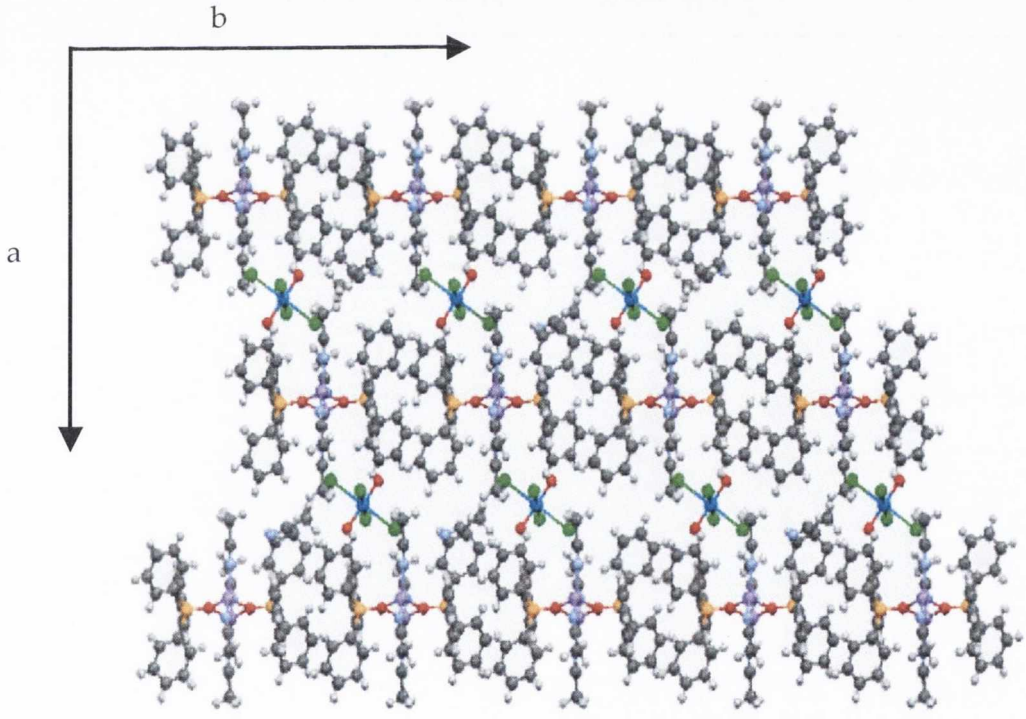

Figure 4.2: Solid state crystal structure of **13** showing packing diagram

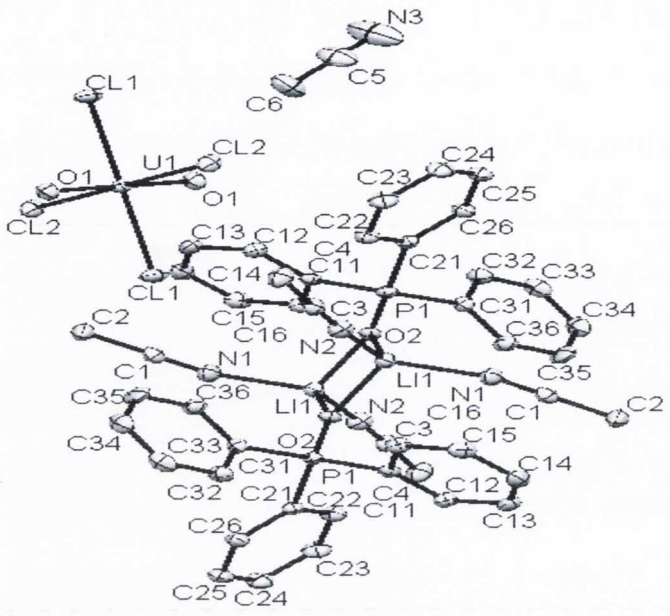

Figure 4.3: Solid state crystal structure of **13** showing symmetrical unit

U1-Cl1	2.672(1)	N2-C3	1.1399(5)	C23-C24	1.3933(5)
U1-Cl2	2.6762(8)	C1-C2	1.4574(5)	C24-C25	1.3840(3)
U1-O1	1.7730(4)	C3-C4	1.4607(7)	C25-C26	1.3963(9)
P1-O2	1.5106(4)	C11-C12	1.3948(5)	C31-C32	1.4006(3)
P1-C11	1.7946(4)	C11-C16	1.4042(7)	C31-C36	1.3926(5)
P1-C21	1.799(1)	C13-C14	1.3894(7)	C32-C33	1.3863(4)
P1-C31	1.8002(4)	C14-C15	1.3871(5)	C33-C34	1.3750(5)
O2-Li1	1.945(1)	C15-C16	1.3894(3)	C34-C35	1.3882(3)
N1-Li1	2.0087(6)	C21-C22	1.4002(3)	C35-C36	1.3955(4)
N1-C1	1.1411(4)	C21-C26	1.3963(5)		
N2-Li1	2.0164(8)	C22-C23	1.3892(9)		

Cl1-U1-Cl2	91.17	C14-C15-C16	120.43	Li1-O2-Li1	86.19
Cl1-U1-O1	90.18	C11-C16-C15	119.74	Li1-N1-C1	164.05
Cl1-U1-Cl1	180	P1-C21-C22	117.41	Li1-N2-C3	172.13
Cl2-U1-O1	89.73	P1-C21-C26	123.02	O2-Li1-O2	93.81
Cl2-U1-Cl2	180	C22-C21-C26	119.5	O2-Li1-N1	110.13
O1-U1-O1	180	C21-C22-C23	120.38	O2-Li1-N2	117.95
O2-P1-C11	110.34	C22-C23-C24	119.76	O2-Li1-N1	109.77
O2-P1-C21	109.61	C23-C24-C25	120.18	O2-Li1-N2	109.13
O2-P1-C31	110.77	C24-C25-C26	120.38	N1-Li1-N2	114.05
C11-P1-C21	109.45	C21-C26-C25	119.75	N1-Li1-O2	110.13
C11-P1-C31	107.24	P1-C31-C32	121.55	N2-Li1-O2	117.95
C21-P1-C31	109.39	P1-C31-C36	118.36	N1-C1-C2	179.3
P1-C11-C12	120.58	C32-C31-C36	120.05	N2-C3-C4	178.49
P1-C11-C16	119.07	C31-C32-C33	119.64	P1-O2-Li1	128.93

C12-C11-C16	119.58	C32-C33-C34	120.34	P1-O2-Li1	144.84
C11-C12-C13	120.05	C33-C34-C35	120.54	Li1-O2-Li1	86.19
C12-C13-C14	120.28	C34-C35-C36	119.95		
C13-C14-C15	119.91	C31-C36-C35	119.48		

Table 4.1: Bond lengths (Å) and bond angles (°) for **13**

The solid state structure of **13** is shown in Figure 4.2 and Figure 4.3 and list of bond lengths and bond angles are provided in Table 4.1. The bond lengths within the uranyl complex are as expected based upon structurally characterised examples in the literature (U=O = 1.7730(14) Å, U-Cl = 2.6721(12) and 2.6762(9) Å).[16] Whilst the $[Li(O{=}PPh_3)(solv)_2]_2$ fragment, is quite rare, it is also unremarkable with Li-O bonds of 1.922(4) and 1.945(4) Å and P=O bonds of 1.5106(14) Å; the average distances are 1.984 Å and 1.512 Å respectively.[17] The supramolecular structure consists of layers of $[UO_2Cl_4]^{2-}$ anions and $[Li(O{=}PPh_3)(MeCN)_2]_2$ cations held together by extensive C-H...O hydrogen bonds[18] to the acetonitrile (2.676 Å) and phenyl (2.575 and 2.452 Å) groups, and C-H...Cl hydrogen bonds between the acetonitrile of the anionic unit (2.937 and 2.911 Å) and phenyl groups (2.937 and 2.911 Å). Notably these C-H...Cl interactions are bifurcated hydrogen bonds, which are common in uranyl halide/ pyridinium structures.[19] The acetonitrile solvent molecules seemingly aid the assembly of this species.

Furthermore, $[PyH]_2[UO_2Cl_4].2Py$[13] (**14**) was synthesised from the oxidation of THF solution of $[Li(THF)_4][UCl_5(THF)]$ in air. The oxidation was followed by emission spectroscopy (see Chapter 2, Section 2.2.4.3) and the crystallisation from pyridine gave clear yellow crystals.

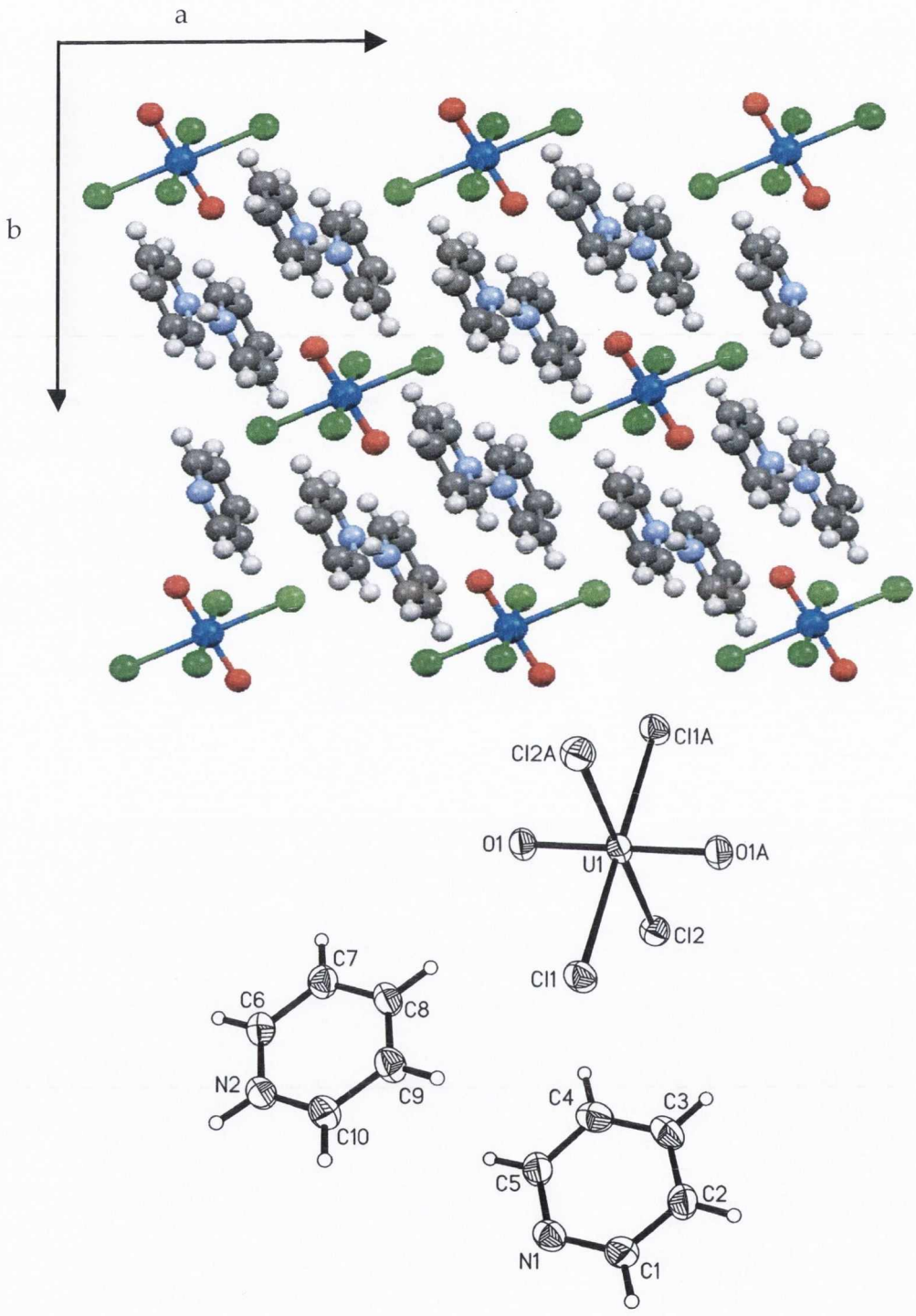

Figure 4.4: Solid state crystal structure of **14** showing packing (top) and symmetrical unit (bottom)

U1-Cl1	2.6523(7)	U1-O1	1.7740(9)	C3-C4	1.3692(7)
U1-Cl2	2.6662(8)	N1-C1	1.3266(7)	N2-C6	1.3381(6)
U1-O1	1.7740(9)	N1-C5	1.3356(7)	N2-C10	1.3387(7)
U1-Cl1	2.6523(7)	C1-C2	1.3768(4)	C7-C8	1.3788(7)
U1-Cl2	2.6662(8)	C2-C3	1.3760(7)	C9-C10	1.3763(4)

Cl1-U1-Cl2	91.12	O1-U1-O1	180	C3-C4C5	119.13
Cl1-U1-O1	90.21	Cl1-U1-Cl2	91.12	N1-C5C4	121.61
Cl1-U1-Cl1	180	Cl1-U1-O1	90.21	C6-N2C10	121.1
Cl1-U1-Cl2	88.88	Cl2-U1-O1	89.7	N2-C6C7	120.58
Cl1-U1-O1	89.79	C1-N1-C5	118.84	C6-C7C8	118.55
Cl2-U1-O1	89.7	N1-C1-C2	122.54	C7-C8C9	120.41
Cl2-U1-Cl2	180	C1-C2-C3	118.89	C8-C9C10	118.65
Cl2-U1-O1	90.3	C2-C3-C4	118.94	N2-C10C9	120.7

Table 4.2: Bond lengths (Å) and bond angles (°) for **14**

The solid state crystal structure is shown in Figure 4.4 and the bond lengths and bond angles are listed in Table 4.2. The uranyl is coordinated by four atoms of Cl and two O. The O=U=O is perfectly linear with a bond length of 1.774(4) Å and bond angle of 180°. The U-Cl bond distances are within the ionic radii (2.6523(15) Å and 2.6662(16) Å) and O-U-Cl bond angles of 90.21° and 89.79°. All values agree with those previously reported in literature for $[UO_2Cl_4]^{2-}$.[16] The supramolecular structure consists of layers of $[UO_2Cl_4]^{2-}$ anions and held together by extensive C-H...O hydrogen bonds to the pyridine (2.535 Å), and C-H...Cl hydrogen bonds between the pyridine and the uranyl (2.889 and 2.931 Å).

In an attempt to synthesise the analogous tetrahalouranate species, $[Li(THF)_4][UX_5(THF)]$ (X = Br, I) was reacted with a THF solution of $Ph_3P{=}O$. Following crystallisation from acetonitrile, $[UO_2Br_2(OPPh_3)_2]$ (**15**) (Scheme 4.2) was the only product isolated from the reaction of $[Li(THF)_4][UBr_5(THF)]$ and $Ph_3P{=}O$.

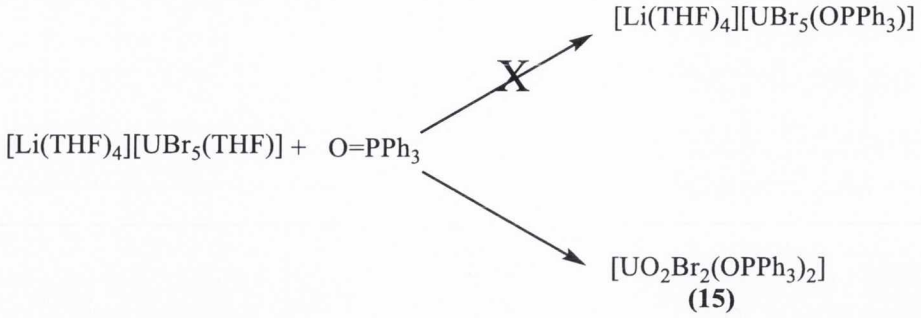

Scheme 4.2: Synthesis of complex **15**

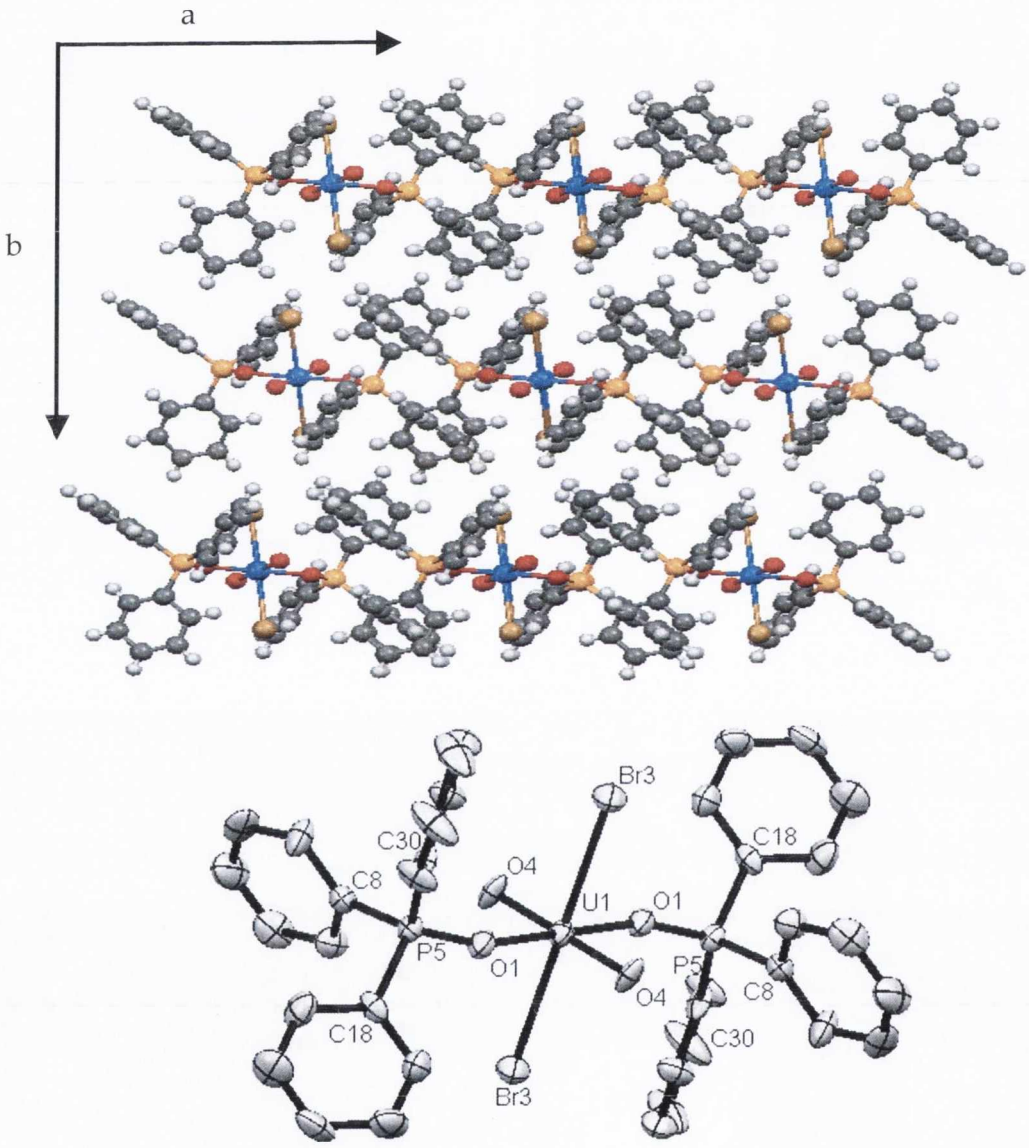

Figure 4.5: Solid state crystal structure of **15** showing packing arrangement (top) and symmetrical unit (bottom)

U1-Br3	2.8373(7)	C8-C9	1.4124(2)	C22-C65	1.3495(4)
U1-O1	2.3062(4)	C9-C10	1.4247(2)	C28-C29	1.4057(3)
U1-O4	1.7511(3)	C10-C11	1.3689(3)	C28-C62	1.3865(3)
P5-O1	1.5225(2)	C11-C12	1.3797(2)	C29-C30	1.4279(4)
P5-C8	1.7911(3)	C18-C19	1.3879(2)	C30-C60	1.3561(3)
P5-C18	1.7872(6)	C18-C22	1.4196(2)	C60-C61	1.3996(3)
P5-C30	1.7824(4)	C19-C20	1.3444(4)	C61-C62	1.4066(4)
C7-C8	1.3992(3)	C20-C21	1.4245(2)		
C7-C12	1.3682(2)	C21-C65	1.3600(2)		

Br3-U1-O1	87.73	O1-P5-C30	110.02	C19-C18-C22	117.46
Br3-U1-O4	90.84	C8-P5-C18	105.83	C18-C19-C20	120.51
Br3-U1-Br3	180	C8-P5-C30	110.2	C19-C20-C21	121.92
Br3-U1-O1	92.27	C1-P5-C30	108.42	C20-C21-C65	117.05
Br3-U1-O4	89.16	U1-O1-P5	152.47	C18-C22-C65	120.97
O1-U1-O4	89.09	C8-C7-C12	119.38	C29-C28-C62	122.44
O1-U1-Br3	92.27	P5-C8-C7	116.13	C28-C29-C30	117.37
O1-U1-O1	180	P5-C8-C9	123.15	P5-C30-C29	114.84
O1-U1-O4	90.91	C7-C8-C9	120.64	P5-C30-C60	124.18
O4-U1-Br3	89.16	C8-C9-C10	117.79	C29-C30-C60	120.84
O4-U1-O1	90.91	C9-C10-C11	119.77	C30-C60-C61	120.64
O4-U1-O4	180	C10-C11-C12	121.3	C60-C61-C62	120.59
O1-U1-O4	89.09	C7-C12-C11	120.83	C28-C62-C61	117.93
O1-P5-C8	111.21	P5-C18-C19	121.77	C21-C65-C22	122.02
O1-P5-C18	111.05	P5-C18-C22	120.68		

Table 4.3: Bond lengths (Å) and bond angles (°) for **15**

The solid state crystal structure of **15** is shown in Figure 4.5 and bond lengths and bond angles are provided in Table 4.3. The bond lengths within the uranyl fragment are as expected based upon the structurally characterised example of the chloride analogue $[UO_2Cl_2(OPPh_3)_2]$ where U=O is 1.764(9) Å, U-OP = 2.300(8) Å and U-Cl = 2.645 (5) Å. The U=O bond length in **15** is 1.7511(3) Å, the U-Br bond length is 2.8373(7) Å and U-OP bond is 2.3062(4) Å. The uranium metal centre is six coordinate, with bromide and triphenylphosphine oxide ligands lying in mutually *trans* positions about the uranium centre. The coordination octahedron is distorted and the uranyl oxo groups lie in the axial position. The U-Br bond of 2.8373(7) Å is slightly longer than the U-Cl bond in **12** (2.645 (5) Å) and similar to the U-Br bond in $[UO_2Br_2(OAsPh_3)_2]$ (2.828 (1) Å).[20]

The supramolecular structure consists of layers of $[UO_2Cl_2(OPPh_3)_2]$ held together by C-H...O hydrogen bonds between the uranyl oxygen and the phenyl ring (2.587 Å). No C-H...Br hydrogen bonds are found.

Synthesis of the uranyl(VI) iodide analogue in a similar manner did not yield tractable crystals of the iodide analogue and the reaction of $[Li(THF)_4][UI_5(THF)]$ and $Ph_3P{=}O$ followed by crystallisation from acetonitrile gave yellow crystals of $[Li(O{=}PPh_3)_4][I_3]$ (**16**) and the orange powder of what must be $[UO_2I_2(OPPh_3)_2]$ (**17**) (Scheme 4.3) as indicated by the spectroscopic properties of this compound.

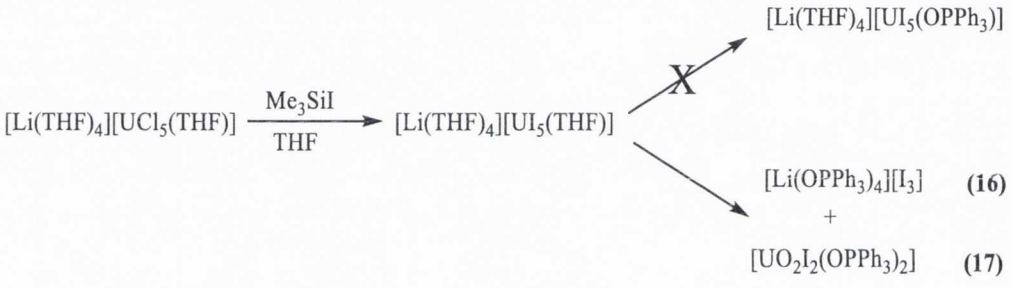

Scheme 4.3: Synthesis of complexes **16** and **17**

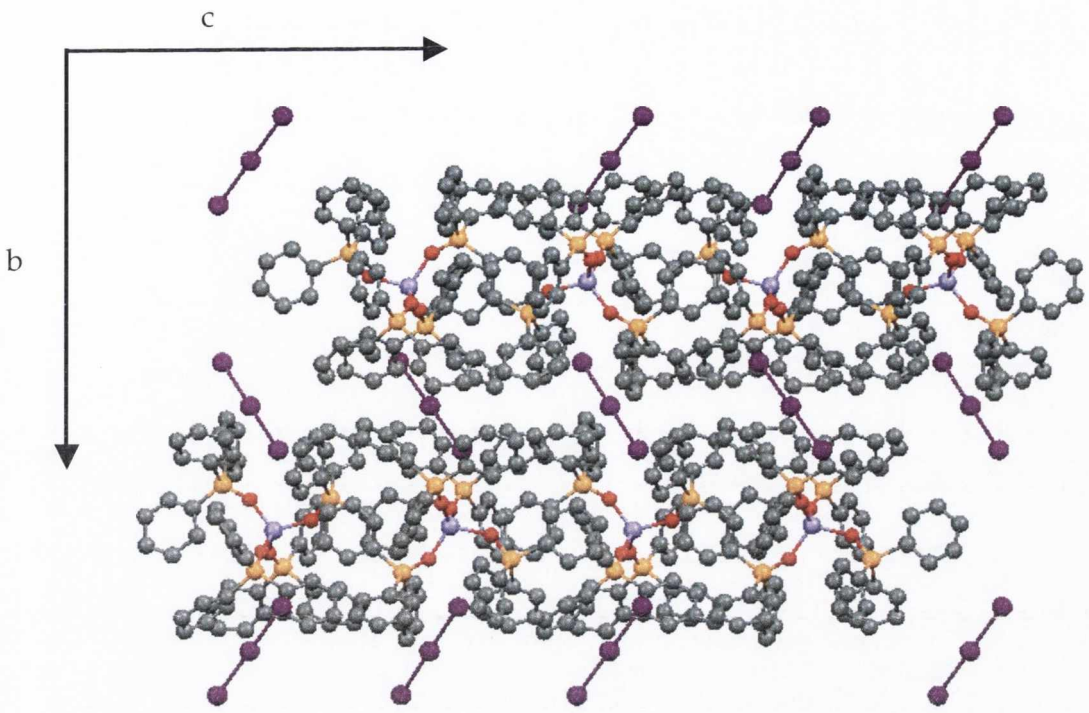

Figure 4.6: Supramolecular solid state crystal structure of **16** (purple = I, red = oxygen, orange = phosphorus, grey = carbon and lilac = Li)

P1-O1	1.482(3)	C22-C23	1.377(8)	C13-C17	1.39(1)
P1-C29	1.802(6)	C23-C24	1.36(1)	C14-C15	1.374(8)
P1-C36	1.805(7)	C43-C44	1.380(9)	C15-C18	1.37(1)
P1-C59	1.800(7)	C43-C48	1.389(8)	C16-C17	1.375(8)
O1-Li2	1.87(1)	C44-C45	1.379(6)	C16-C18	1.386(8)
C25-C26	1.373(9)	C45-C46	1.36(1)	P2-C42	1.806(6)
C25-C29	1.391(7)	C46-C47	1.37(1)	P2-C49	1.801(6)
C26-C27	1.38(1)	C47-C48	1.392(5)	P2-C56	1.798(6)
C27-C28	1.367(7)	C64-C65	1.383(9)	P2-O10	1.489(4)
C28-C30	1.376(8)	C64-C68	1.375(8)	C37-C38	1.385(9)
C29-C30	1.39(1)	C65-C66	1.37(1)	C37-C42	1.390(7)
C31-C32	1.38(1)	C66-C67	1.367(8)	C38-C39	1.39(1)
C31-C36	1.361(5)	C67-C69	1.383(8)	C39-C40	1.380(8)
C32-C33	1.351(9)	C68-C69	1.39(1)	C40-C41	1.368(9)
C33-C34	1.348(6)	P4-O2	1.487(4)	C41-C42	1.395(7)
C34-C35	1.37(1)	P4-C6	1.805(7)	C49-C50	1.398(7)
C35-C36	1.36(1)	P4-C10	1.805(6)	C49-C72	1.383(9)
C52-C59	1.390(6)	P4-C13	1.796(6)	C50-C51	1.383(8)
C52-C62	1.389(9)	O2-Li2	1.894(8)	C51-C70	1.377(9)
C59-C60	1.388(8)	C1-C2	1.38(1)	C53-C54	1.381(9)
C60-C63	1.382(9)	C1-C6	1.392(9)	C53-C55	1.386(9)
C61-C62	1.381(8)	C2-C3	1.369(7)	C54-C58	1.370(6)

C61-C63	1.372(6)	C3-C4	1.365(9)	C55-C56	1.395(5)
P3-O3	1.484(4)	C4-C5	1.38(1)	C56-C57	1.388(9)
P3-C19	1.806(6)	C5-C6	1.380(6)	C57-C58	1.377(9)
P3-C48	1.799(6)	C7-C8	1.376(6)	C70-C71	1.382(7)
P3-C69	1.796(6)	C7-C12	1.37(1)	C71-C72	1.377(8)
O3-Li2	1.86(1)	C8-C9	1.382(9)	O10-Li2	1.890(8)
C19-C20	1.382(6)	C9-C10	1.39(1)	I1-I2	2.9204(5)
C19-C21	1.38(1)	C10-C11	1.399(6)	I2-I1	2.9204(5)
C20-C24	1.385(9)	C11-C12	1.381(9)	I3-I5	2.9094(5)
C21-C22	1.372(9)	C13-C14	1.391(7)	I5-I3	2.9094(5)

O1-P1-C29	111.7(3)	C22-C23-C24	119.6(6)	C13-C14-C15	120.4(6)
O1-P1-C36	113.5(3)	C20-C24-C23	120.8(6)	C14-C15-C18	119.9(6)
O1-P1-C59	108.9(3)	C44-C43-C48	120.4(6)	C17-C16-C18	119.6(6)
C29-P1-C36	106.8(3)	C43-C44-C45	119.6(6)	C13-C17-C16	120.3(6)
C29-P1-C59	110.3(3)	C44-C45-C46	120.0(7)	C15-C18-C16	120.6(6)
C36-P1-C59	105.5(3)	C45-C46-C47	121.3(7)	C42-P2-C49	108.5(3)
P1-O1-Li2	147.1(4)	C46-C47-C48	119.5(6)	C42-P2-C56	103.9(3)
C26-C25-C29	120.9(6)	P3-C48-C43	123.4(4)	C42-P2-O10	111.8(3)
C25-C26-C27	120.1(7)	P3-C48-C47	117.4(4)	C49-P2-C56	109.9(3)
C26-C27-C28	120.0(6)	C43-C48-C47	119.2(5)	C49-P2-O10	110.0(2)
C27-C28-C30	120.0(6)	C65-C64-C68	119.7(6)	C56-P2-O10	112.5(2)
P1-C29-C25	116.9(5)	C64-C65-C66	119.9(6)	C38-C37-C42	120.3(6)
P1-C29-C30	125.3(5)	C65-C66-C67	120.4(6)	C37-C38-C39	119.9(6)
C25-C29-C30	117.9(6)	C66-C67-C69	120.5(6)	C38-C39-C40	119.6(6)
C28-C30-C29	121.1(6)	C64-C68-C69	120.4(6)	C39-C40-C41	120.9(6)
C32-C31-C36	120.8(6)	P3-C69-C67	116.7(5)	C40-C41-C42	120.2(6)
C31-C32-C33	121.1(6)	P3-C69-C68	124.4(5)	P2-C42-C37	118.2(5)
C32-C33-C34	118.2(6)	C67-C69-C68	119.0(6)	P2-C42-C41	122.6(5)
C33-C34-C35	121.3(8)	O2-P4-C6	111.3(2)	C37-C42-C41	119.1(6)
C34-C35-C36	121.0(8)	O2-P4-C10	110.0(2)	P2-C49-C50	116.9(4)
P1-C36-C31	123.9(5)	O2-P4-C13	113.4(2)	P2-C49-C72	123.3(4)
P1-C36-C35	118.4(5)	C6-P4-C10	108.6(3)	C50-C49-C72	119.9(5)
C31-C36-C35	117.6(6)	C6-P4-C13	105.9(3)	C49-C50-C51	119.3(5)
C59-C52-C62	120.1(6)	C10-P4-C13	107.4(3)	C50-C51-C70	120.4(6)
P1-C59-C52	117.3(5)	P4-O2-Li2	152.0(4)	C54-C53-C55	120.3(6)
P1-C59-C60	123.5(5)	C2-C1-C6	120.2(6)	C53-C54-C58	120.2(6)
C52-C59-C60	119.2(6)	C1-C2-C3	120.2(6)	C53-C55-C56	119.4(5)
C59-C60-C63	120.5(6)	C2-C3-C4	120.2(6)	P2-C56-C55	124.9(4)
C62-C61-C63	120.6(6)	C3-C4-C5	120.2(6)	P2-C56-C57	115.6(4)
C52-C62-C61	119.7(6)	C4-C5-C6	120.5(6)	C55-C56-C57	119.5(5)
C60-C63-C61	119.8(6)	P4-C6-C1	117.3(5)	C56-C57-C58	120.4(5)
O3-P3-C19	109.8(2)	P4-C6-C5	123.9(5)	C54-C58-C57	120.2(6)
O3-P3-C48	110.6(2)	C1-C6-C5	118.6(6)	C51-C70-C71	120.2(6)
O3-P3-C69	111.4(3)	C8-C7-C12	120.3(6)	C70-C71-C72	120.0(6)
C19-P3-C48	108.9(3)	C7-C8-C9	120.0(6)	C49-C72-C71	120.2(6)

C19-P3-C69	107.9(3)	C8-C9-C10	120.5(6)	P2-O10-Li2	143.9(4)
C48-P3-C69	108.1(3)	P4-C10-C9	117.8(4)	O1-Li2-O3	109.2(5)
P3-O3-Li2	175.9(4)	P4-C10-C11	123.3(5)	O1-Li2-O2	110.4(5)
P3-C19-C20	123.9(5)	C9-C10-C11	118.9(5)	O1-Li2-O10	107.8(5)
P3-C19-C21	117.3(5)	C10-C11-C12	119.9(6)	O3-Li2-O2	108.9(5)
C20-C19-C21	118.7(6)	C7-C12-C11	120.5(6)	O3-Li2-O10	109.2(5)
C19-C20-C24	120.0(6)	P4-C13-C14	118.9(5)	O2-Li2-O10	111.2(5)
C19-C21-C22	120.9(6)	P4-C13-C17	121.9(5)	I1-I2-I1	180.00(1)
C21-C22-C23	120.1(6)	C14-C13-C17	119.2(6)	I3-I5-I3	180.00(1)

Table 4.4: Bond lengths (Å) and bond angles (°) for **16**

The supramolecular structure of **16** consists of layers of $[Li(O{=}PPh_3)_4]$ cations and I_3 anions. Each unit cell consists of a triiodide and a lithium atom which are tetrahedrally coordinated by four $O{=}PPh_3$ molecules each. The average distance for P=O bonds is 1.487 Å and for Li-O is 1.879 Å, similar to those observed for **13**. The I-I-I bond is perfectly linear with a bond angle of 180° and a bond length of 2.9204(5) and 2.9094(5) Å.

The uranyl moiety has pronounced vibrational modes that are active in both the IR and Raman spectra. The IR and Raman spectra for complexes **12**, **15** and **17** are shown in Figure 4.7 and Figure 4.8 respectively. Albeit the small shift observed for the O=U=O in **15** compared to **12** and **17**, it is clear that there is no significant change in the vibrational profile for all three compounds. This is expected as the uranyl oxo group sits in an axial position within the distorted octahedron and is perfectly linear with O=U=O bond angle of 180.0°. The $^{31}P\{^1H\}$ NMR spectrum shown in Figure 4.9, is in accordance with the crystal structure. The $^{31}P\{^1H\}$ NMR spectrum was measured for the mixture products of complexes (**12** and **13**, **16** and **17**). It displays two resonances for the mixture complexes **12** and **13**; a resonance at 29.0 ppm corresponding to $OPPh_3$ coordinated to the uranium in **12** and a resonance at 48.0 ppm corresponding to $OPPh_3$ coordinated to Li in **13**. The $^{31}P\{^1H\}$ NMR spectrum also shows a single resonance at 28.0 ppm corresponding to the uranium coordinated $OPPh_3$ in **15** and two resonances at 50.1 ppm corresponding to $OPPh_3$ coordinated to the lithium in **16** and another resonance at 31.02 ppm corresponding to $OPPh_3$ coordinated to uranium in **17**.

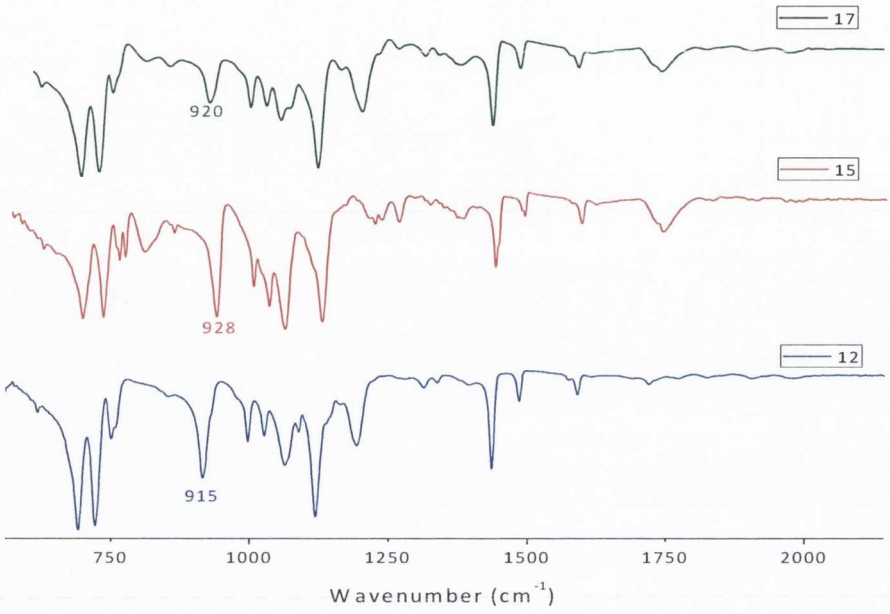

Figure 4.7: IR spectral profile for complexes **12**, **15** and **17**

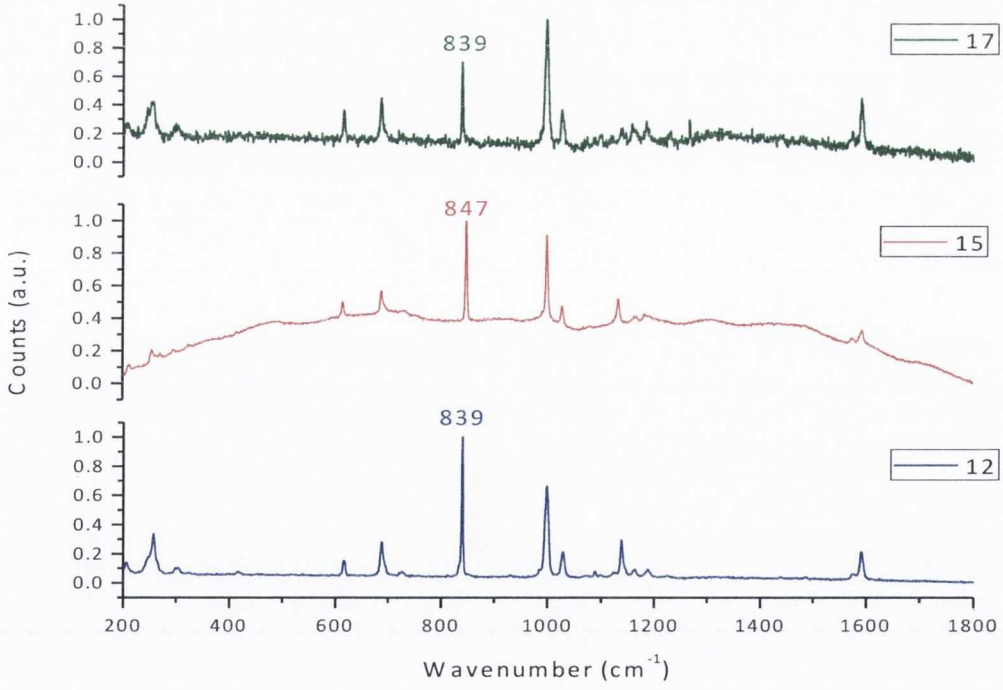

Figure 4.8: Raman spectrum of complexes **12, 15** and **17**

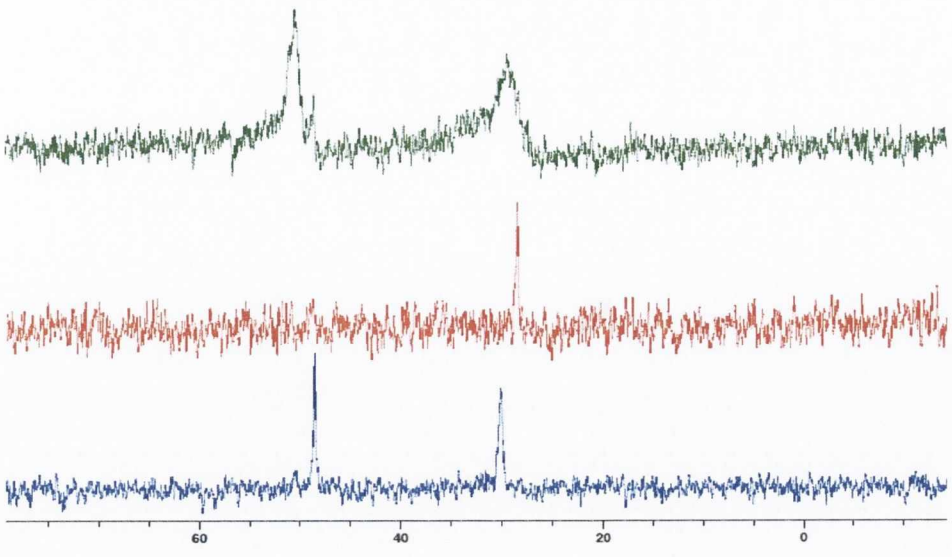

Figure 4.9: $^{31}P\{^{1}H\}$ NMR spectrum for compounds **12** and **13** (blue line), **15** (red line) and **16** and **17** (green line)

4.2.2 Photophysical Properties

The electronic absorption spectra of the complexes **12, 15,** and **17** in MeCN solutions display three main features as shown in Figure 4.10 and Figure 4.11: an intense band centred at λ_{max} = 230 nm assigned to a spin allowed ligand centred π-π^* transition within the phenyl chromophore; a broad feature ligand-to-metal charge transfer (LMCT) transition from an equatorial bound donor atom to the uranium cation at *ca.* λ_{max} = 300 nm for complex **12** which shifts to 325 nm and 350 nm for **15**, and **17** respectively; and weak transition centred at *ca.* 450 - 500 nm characteristic of the Laporte forbidden O=U=O LMCT transition with an extinction coefficient of about ε = 50 M cm^{-1}. The observed red shift for the charge transfer transition resulting from the halide-to-uranium compares reasonably well with the reported experimental and theoretical values for the halide to uranyl charge transfer in $[UO_2X_4]^{2-}$.[21] Complex **14** displays a uranyl band at λ_{max} = 250 nm and a Cl-U CT at λ_{max} = 300 nm and a well resolved O=U=O transition at λ_{max} = 460 nm (Figure 4. 10 and Figure 4.11; green line).

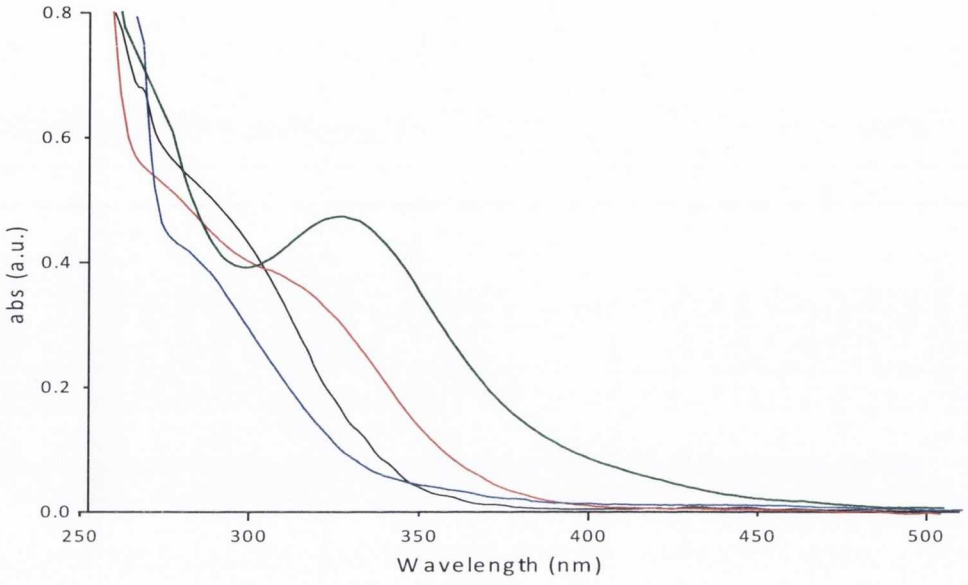

Figure 4.10: UV-Vis absorption spectra for complex **12** (blue line), **14** (black line), **15** (red line) and **17** (green line)

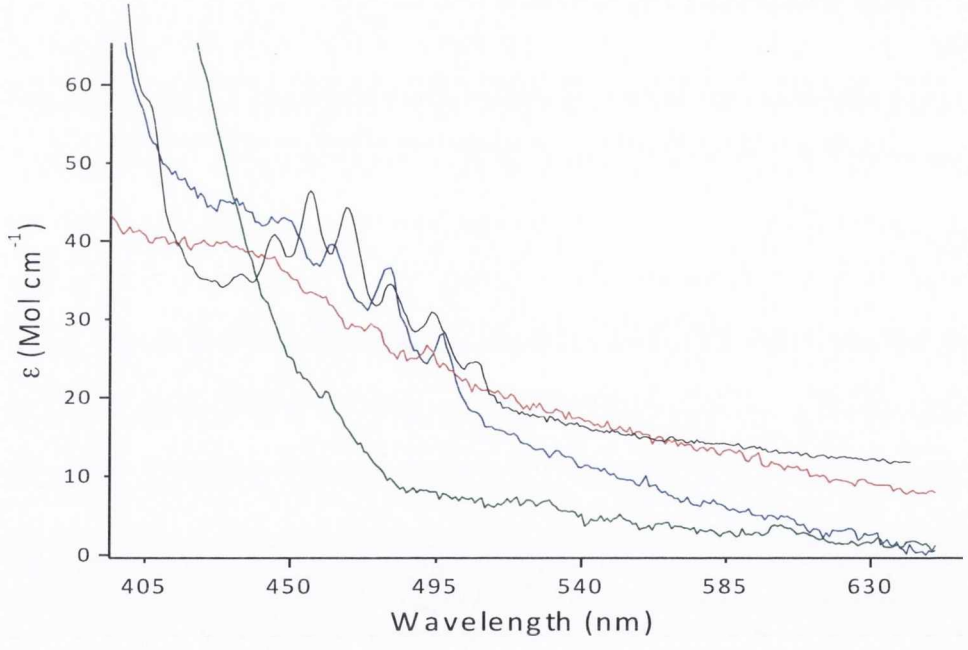

Figure 4.11: UV-Vis absorption spectra for complex **12** (blue line), **14** (black line), **15** (red line) and **17** (green line) showing the $[UO_2]^{2+}$ vibronic coupling transitions

Excitation into either of the absorption bands (between 230 and 460 nm) produces luminescence spectra which are dominated by the corresponding LMCT emission bands at *ca.* 515 nm to 520 nm as shown in Figure 4.12. The fine vibrationally resolved structure of the uranyl is an indication that non-radiative back energy transfer quenching mechanisms to the aromatic electronic excited levels have been eliminated. However, uranyl O=U=O transitions are very weak in comparison with the chromophoric absorption at λ_{max} = 230 and an increase in solution concentration activates this quenching which makes it impossible to obtain the quantum yield. It is worth noting that despite the lack of a crystal structure for complex **17** all spectroscopic properties are characteristic of the uranyl moiety and demonstrate the ability of luminescence spectroscopic technique in the characterisation and the detection of uranium complexes in the environment.

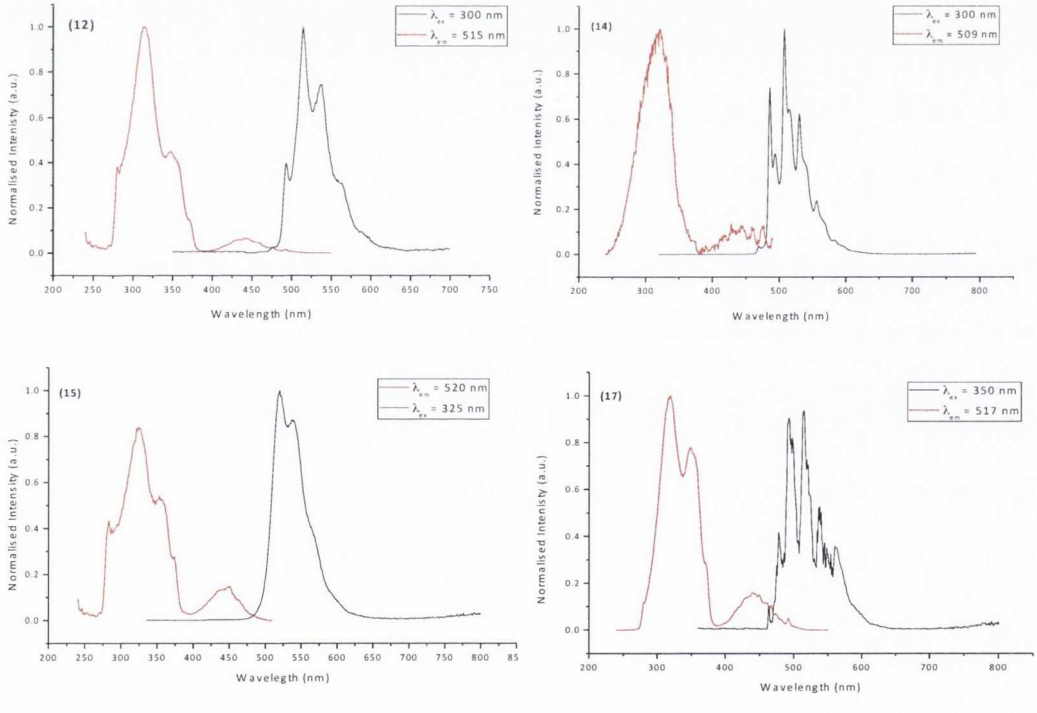

Figure 4.12: Emission (black line) and excitation (red line) profile for complexes **12**, **14**, **15** and **17** in MeCN at 298 K (λ_{ex} = 230 - 350 nm, λ_{em} = 520 nm)

As seen from Figure 4.12, the emission spectra for complexes **12, 14, 15** and **17** were almost identical and no red shift matching that reported for similar complexes was observed. For example, in the $[UO_2Cl_2L_2]$ system, a red shift in the uranyl emission in line with the increased donor strength was observed and a shift from 517 nm to 529nm to 531 nm for *trans*-$[UO_2Cl_2(Ph_3PNH)_2]$,[22] *trans*-$[UO_2Cl_2(Ph_3PO)_2]$[15] and *trans*-$UO_2Cl_2(Ph_3AsO)_2]$[22] respectively was reported.[23]. The observed red shift was postulated to signify a decrease in uranyl oxo bond order as a consequence of increased electron donation from the ancillary ligand L in the equatorial plane to the uranium centre. Interestingly, for complexes **12, 15** and **17,** the only difference observed is the small shift in the halide-to-uranium charge transfer transition in the absorption profile from 300 nm to 325 nm to 350 nm for Cl, Br and I respectively in line with the bond length of 2.645 (5) for U-Cl in **12**, 2.8373(7) Å for U-Br in **15** and 3.0665(4) for U-I in $[UO_2I_4]^{2-}$.[3]

In the emission spectra a small red shift is observed for complex **15** (520 nm) when compared to **12**, (515 nm) in MeCN that can be related to the uranyl bond strength in both complexes. This is expected as the bond length for the U=O is 1.764(9) Å, 1.7511(3), Å and 1.761(5) Å for **12**, **15** and $[UO_2I_4]^{2-}$ respectively. The observed red shift is very insignificant and is subjected to errors and instrumentation calibrations. In order to confirm this the emission profile of authentically prepared $[UO_2Cl_2(THF)_n]$[24] (n = 2, 3) was measured and showed identical emission profile to that observed for $[PyH]_2[UO_2Cl_4].2Py$. Furthermore, the obtained values for the emission bands for the complexes **12, 14, 15** and **17** were compared to those known in the literature as shown in Table 4.1 and indicate that the very insignificant difference seen in the emission profile is dependent on many different parameters. For example, whilst an emission band at 504 nm was reported for $[UO_2Cl_2(THF)_n]$ in THF the measured emission obtained for $[UO_2Cl_2(THF)_n]$ in acetonitrile is 509 nm. Similarly the emission band at 515 nm obtained for **12** in MeCN differ to that reported for **12** in DCM (529 nm).

The luminescence lifetime of all complexes were determined by the correlated single photon counting on nanosecond scale for complex **14** and microsecond scale for complexes **12, 15** and **17** following excitation at 294 nm with a nanoLED. The kinetic decay profile of all complexes was fitted to a mono-exponential decay. The luminescence lifetime for complex **14** in MeCN was measured to be 120 ns and matches the previously reported value of 150 ns for$[UO_2Cl_2(THF)_2]_2$ in THF.[15] The luminescence life times for complexes **12, 15** and **17** (Table 4.5) were measured to be *ca.* 1 μs in line with the emission lifetime for $UO_2(NO_3)_2$ in H_2O of 1.0 μs at room temperature.[25] No change in lifetime was observed for the different halide system and the uranyl LMCT lifetime is not particularly sensitive to the nature of the halide donor atoms. Table 4.5 summarises the photophysical properties of the measured complexes and compares them to the literature values.

Complex	Solvent	U-X (CT) λ_{abs} (nm)	O=U (CT) λ_{abs} (nm)	λ_{em} (nm)	τ (μs)	χ^2	Ref
14	MeCN	300	430	509	0.120	1.62	
$[UO_2Cl_2(THF)_2]_2$	THF	300		504	0.150	1.52	[15]
$[UO_2Cl_2(THF)_n]$	MeCN	300	430	509	0.220	0.98	This work
$[UO_2Cl_2(Ph_3PO)_2]$	DCM	300	428	529	1.040	1.00	[15]
12	MeCN	300	440	515	1.083	1.07	This work
15	MeCN	325	445	520	1.400	1.18	This work
17	MeCN	350	445	517	1.035	1.78	This work
$[UO_2Cl_2(Ph_3PNH)_2]$	DCM		425	531	3.460	1.10	[22]
$[UO_2Cl_2(Ph_3AsO)_2]$	DCM			517	0.870	1.06	[22]

Table 4.5: Photophysical properties of uranyl complexes measured at 298 K

4.3 Conclusions

The electronic spectra of uranyl halide complexes $[UO_2X_2(O{=}PPh_3)_2]$ (X = Cl, Br, and I) were fully analysed. The halide ligand-to-metal charge transfer transitions are in line with the bond strength of Cl, Br and I. The effect of charge transfer from the equatorial ligands on the uranyl ion is negligible and the emission resulting from the U=O ligand-to-metal charge transfer is similar for all complexes. The results obtained here compare reasonably well with existing experimental values and the discrepancies are most likely related to approximation and are subjected to errors.

4.4 Experimental

All manipulations were carried out using standard Schlenk and glove box techniques under an atmosphere of high purity argon. ^1H and $^{31}P\{^1H\}$ NMR spectra were recorded on a Burker AV400 spectrometer operating at 400.23 MHz and 162 MHz respectively, and were referenced to the residual ^1H resonances of the solvent used or exrernal H_3PO_4. Crystal were mounted and crystal structures were resolved by Dr. Thomas McCabe (TCD) and by Prof. Carola Schulzke (Greifswald University) (see appendex F – J). Uranium stocks were obtained from TCD's stocks. THF and MeCN were distilled over potassium whilst d_5-pyridine and CD_3CN, were dried over sodium, distilled and degassed immediately prior to use. Spectroscopic measurements used spectroscopic grade MeCN solvent which were purchased from commercial sources and dried over potassium and molecular sieves and thoroughly degassed before use. The starting material of $[Li(THF)_4][UCl_5(THF)]$ $[Li(THF)_4][UBr_5(THF)]$ and $[Li(THF)_4][UBr_5(THF)]$ were prepared as described in Chapter 2 whilst all other reagents were obtained from commercial sources. Spectroscopic Instrumentation are described in Chapter 2.

4.4.1 Preparation of $[UO_2Cl_2(OPPh_3)_2]$ (12)

To a solution of $[Li(THF)_4][UCl_5(THF)]$ (100 mg, 0.129 mmol) in THF was added two equivalents of triphenylphosphine oxide (72 mg, 0.257 mmol) in THF (10 cm^3) and this was stirred for 24 hours at room temperature. The resulting yellow solution was filtered and the solvent was removed under high vacuum. Dissolution in acetonitrile and placement at -30 °C overnight yielded clear yellow crystals of both **12** and **13** suitable for X-ray diffraction (56 mg, 0.09 mmol, 48.4%). ^1H NMR (400 MHz, CD_3CN, 298 K): 7.55 - 7.67; ^{31}P NMR(400 MHz, CD_3CN, 298 K): 48.51 ppm (s, Li-$OPPh_3$) and 30.07 ppm (s, U-$OPPh_3$); IR (cm-1): 1439, 1120, 1060, 1025, 995, O=U=O 919, 764, 753, 726, 690; Raman (cm^{-1}): 1589, 1572, 1487, 1440, 1190, 1164, 1137, 1088, 1028, 1000, 929, O=U=O 839, 727, 687, 617, 417, 301. 256, 207, 193

4.4.2 Preparation of $[UO_2Br_2(OPPh_3)_2]$ (15)

To a solution of $[Li(THF)_4][UBr_5(THF)]$ (100mg, 0.10mmol) in THF was added two equivalents of triphenylphosphine oxide (55.66 mg, 0.2 mmol) in THF (10 cm^3) and this was stirred for 24 hours at room temperature. The resulting yellow solution was filtered and the solvent was removed under high vacuum. Dissolution in acetonitrile and placement at -30 °C overnight yielded dark yellow crystals of **15** suitable for X-ray diffraction (41 mg, 0.042 mmol, 41.6%). ^1H NMR (400 MHz, CD_3CN, 298 K): 7.67, 7.57 ppm U-$OPPh_3$; ^{31}P NMR(400 MHz, CD_3CN, 298 K): 28.46 ppm; IR (cm^{-1}): 1439, 1120, 1050, 1025, 995, O=U=O 928, 764, 753, 726, 690; Raman (cm^{-1}): 1590, 1672, 1487, 1440, 1190, 1164, 1137, 1088, 1028, 1000, 929, O=U=O 847, 727, 687, 617, 417, 301. 256, 207, 193.

4.4.3 Preparation of $[UO_2I_2(OPPh_3)_2]$ (17)

To a solution of $[Li(THF)_4][UCl_5(THF)]$ (100 mg, 0.129 mmol) in THF (5 cm^3) was added Me_3SiI in excess (256mg, 0.128 mmol). The solution was stirred for 24 hours to give a pale yellow solution. The solvent was removed under high vacuum and the remaining orange powder was dissolved in acetonitrile (10 cm^3). To this was added 2 equivalents of $OPPh_3$ (72 mg, 0.257 mmol) in MeCN (5 cm^3) and the reaction was stirred for a further 24 hours. The resulting orange solution was filtered and the solvent was reduced in volume. Placement at -30 °C overnight yielded dark orange crystals of **16** and orange powder of **17** (19 mg, 0.018 mmol, 13.6%) ^1H NMR (400 MHz, CD_3CN, 298 K): 7.55-7.69 (m, Ar-H) 7.55, 7.67 ppm; ^{31}P NMR (400 MHz, CD_3CN, 298 K): 31.2 ppm (s, U-OPPh3) and 50.4 ppm(s, Li-$OPPh_3$); IR (cm^{-1}): 1439, 1120, 1060, 1025, 995, O=U=O 920, 764, 753, 726, 690; Raman (cm^{-1}): 1590, 1568, 1265, 1229, 1185, 1156, 1137, 1090, 1028, 1000, O=U=O 839, 687, 617, 300.2, 256.6.

4.5 References

[1] R. J. Baker, *Chem. Eur. J.*, 2012, **18,** 16258; b) R. G. Denning, *J. Phys. Chem. A*, 2007, **111,** 4125

[2] a) M. B. Andrews and C. L. Cahill, *Dalton Trans.*, 2012, **41**, 911; b) R. E. Wilson, S. Skanthakumar, C. L.; Cahill and L. Soderholm, *Inorg. Chem.*, 2011, **50**, 10748; c) N. P. Deifel and C. L. Cahill, *C. R. Chimie*, 2010, **13**, 747; d) M. –O. Sornein, M. Mendes, C. Cannes, C. Le Naour, P. Nockemann, K. Van Hecke, L. Van Meervelt, J. –C. Berthet and C. Hennig, *Polyhedron*, 2009, **28**, 1281; e) P. Nockemann, K. Servaes, R. Van Deun, K. Van Hecke, L. Van Meervelt, K. Binnemans and C. Goerller-Walrand, *Inorg. Chem.*, 2007, **46**, 11335; f) R. Bohrer, E. Conradi and U. Mueller, Z. Anorg. Allg. Chem., 1988, **558**, 119; g) G. Van den Bossche, M. R. Spirlet, J. Rebizant and J. Goffart, *Acta Crystallogr.*, 1987, **C43**, 383; h) E. Conradi, R. Bohrer and U. Mueller, *Chem. Ber.*, 1986, **119**, 2582; i) L. Di Sipio, E. Tondello, G. Pelizzi, G. Ingletto and A. Montenero, *Cryst. Struct. Commun.*, 1977, **6**, 723; j) L. Di Sipio, E. Tondello, G. Pelizzi, G. Ingletto and A. Montenero, *Cryst. Struct. Commun.*, 1974, **3**, 301; k) L. Di Sipio, E. Tondello, G. Pelizzi, G. Ingletto and A. Montenero, *Cryst. Struct. Commun.*, 1974, **3**, 297; l) Y. N. Mikhailov and V. G. Kuznetsov, Zh. Neorg. Khim, 1971, **16**, 2512; (m) Y. N. Mikhailov, V. G. Kuznetsov and E. S. Kovaleva, Zh. Strukt. Khim., 1965, **6**, 787

[3] M. J. Crawford and P. Mayer, *Inorg. Chem.*, 2005, **44**, 5547

[4] L. S. Natrajan, *Coord. Chem. Rev.*, 2012, **256**, 1583

[5] G. Meinrath, *J. Radioanal. Nucl. Chem.*, 1998, **232**, 179

[6] a) E. Gaillou, A. Delaunay, B. Rondeau, M. Bouhnik-le-Coz, E. Fritsch, G. Cornen and C. Monnier, *Ore Geol. Rev.*, 2008, **34**, 113; b) Y. Sugitani, K. Kato and K. Nagashima, *Bull. Chem. Soc. Jpn.*, 1979, **52**, 918

[7] a) C. K. Jorgensen and R. Reisfeld, *Struct. Bond.* (Heidelberg) 1982, **50**, 122; b) J. L. Sessler, P. Melfi and G. D. Pantos, *Coord. Chem. Rev.*, 2006, **250**, 816; c) R. Ghosh, J. A. Mondal, H. N. Gosh and D. K. Palit, J. Phys. Chem. A., 2010, **114**, 5263; d) G. K. Liu, *J. Phys. Chem.* A., 2011, **115**, 12419

[8] a) R. G. Denning, *J. Phys. Chem. A.*, 2007, **111**, 4125; b) F. R'eal, V. Vallet, C. Marian and U. Wahlgren, *J. Phys. Chem. A.*, 2007, **127**, 21430

[9] a) R. G. Denning, *Structure and Bonding*, 1992, **79**, 215 (Berlin); b) J. R. Plaisier, D. J. W. IJdo, C. de Mello Donega and G. Blasse, *Chem. Mater.*, 1995, **7**, 738; c) R. G. Denning, *J. Lumin.*, 2008, **128**, 1745

[10] a) Z. Hnatejko, S. Lis and Z. Stryła, *J. Therm. Anal. Calorim.*, 2009, **100**, 253; b) R. Steudtner, T. Arnold, G. Geipel and G. Bernhard, *J. Radioanal. Nucl. Chem.*, 2010, **284**, 421

[11] a) F. de Maria Ramirez, S. Varbanov, J. Padilla and J.-C. G. B¨ unzli, *J. Phys. Chem. B.*, 2008, **112**, 10976; b) T. Yayamura, S. Iwata, S. I. Iwamaru and H. Tomiyasu, *J. Chem. Soc., Faraday Trans.*, 1994, **90**, 3253; c) S. Kannan, M. A. Moody, C. L. Barnes and P. B. Duval, *Inorg. Chem.*, 2006, **45**, 9206; d) A. E. Vaughn, D. B. Bassil, C. L. Barnes, S. A. Tucker and P. B. Duval, *J. Am. Chem. Soc.*, 2006, **128**, 10656

[12] a) M. Latva, H. Takalo, V.-M. Mukkala, C.Matachescu, J. C. Rodriguez- Ubis and J. Kankare, *J. Lumin.*, 1997, **75**, 149; D. Parker, P. K. Senanayake and J. A. G. Williams, *J. Chem. Soc., Perkin Trans.*, 1998, **2**, 2129

[13] E. Hashem, A. N. Swinburne, C. Schulzke, R. C. Evans, J. A. Platts, A. Kerridge, L. S. Natrajan and R. J. Baker, *RSC. Adv.*, 2013, **3**, 4350

[14] G. Bombieri, D. Brown and R. Graziani, *J. Chem. Soc. Dalton Trans.*, 1975, 1873

[15] G. Bombieri, E. Forsellini, P. J. Day and W. I. Azeez, *J. Chem. Soc. Dalton Trans. Inorg. Chem.*, 1978, 6, 677

[16] a) D. J. Watkin, R. G. Denning and K. Prout, *Acta Cryst.*, 1991, **C47**, 2517; b) R. J. Baker, E. Hashem, M. Motevalli, H. V. Ogilvie, and A. Walshe, *Z. Anorg. Allg. Chem.*, 2010, **636**, 443

[17] Determined from a survey of the Cambridge Structural Database

[18] The most recent IUPAC definition of a hydrogen bond states that "*in most cases, the distance between H and Y are found to be less than the sum of their van der Waals radii*": E. Arunan, G. R. Desiraju, R. A. Klein, J. Sadlej, S. Scheiner, I. Alkorta, D. C. Clary, R. H. Crabtree, J. J. Dannenberg, P. Hobza, H. G. Kjaergaard, A. C. Legon, B. Mennucci and D.

Nesbitt, *J. Pure Appl. Chem.*, 2011, **83**, 1637. According to this criterion, H···Y distances of less than 2.72 Å for a C-H...O and 2.95 Å for C-H...Cl are classed as hydrogen bonds.

[19] a) N. P. Deifel and C. L. Cahill, *Cryst. Eng. Comm.*, 2009, **11**, 2739; b) M. B. Andrews and C. L. Cahill, *Dalton Trans.*, 2012, **41**, 3911

[20] F. J. Arnaiz, M. J. Miranda, R. Aguado, J. Mahia, M. A. Maestro, *Polyhedron.*, **2000**, *20*, 3295

[21] F. Ruiperez and U. Wahlgren, *J. Phys. Chem. A.*, 2010, **114**, 3615

[22] M. J. Sarsfield, I. May, S. M Cornet, and M. Helliwell, *Inorg. Chem.*, 2005, **44**, 7310

[23] M. P Redmond, S. M. Cornet, S. D. Woodall, D. Whittaker, D. Collison, M. Helliwell, and L. S. Natrajan, *Dalton Trans.*, 2011, **40**, 3914

[24] M. P. Wilkerson, C. J. Bunrs, R. T. Paine and B. L. Scott, *Inorg. Chem.*, 199, **38**, 4156

[25] a) H. D. Burrows, *Inorg. Chem*, 1990, **3**, 139; b) H. D. Burrows and T. Kemp, *Chem. Soc. Rev.*, 1974, **3**, 139; c) C. G¨orller-Walrand and K. Servaes, *Helv. Chim. Acta*, 2009, **92**, 2304; d) R. Ghosh, J. A. Mondal, H. N. Gosh and D. K. Palit, *J. Phys. Chem. A*, 2010, **114**, 5263; e) R. Nagaishi, Y. Katsumura, K. Ishigure, H. Aoyagi, Z. Yoshida, T. Kimura and Y. Kato, *J. Photochem. Photobiol., A*, 2002, **146**, 157; f) S. J. Formosinho, H. D. Burrows, M. G. M. Miguel, M. E. D. G. Azenha, I. M. Saraiva, A. Catarina, D. N. Ribeiro, I. V. Kholyakov, R. G. Gasanov, M. Bolte and M. Sarakhad, *Photochem. Photobiol. Sci.*, 2003, **2**, 569; g) M. E. D. G. Azenha, H. D. Burrows, S. J. Formosinho, M. G. M. Miguel, A. P. Daramanyan and I. V. Kholyakov, *J. Lumin.*, 1991, **48–49**, 522

Appendix **A**

Crystal data and structure refinement for complex **1**

Identification code	**1**
Empirical formula	C20 H40 Cl5 Li O5 U
Formula weight	782.74
Temperature	108(2) K
Wavelength	0.71073 Å
Crystal system, space group	Orthorhombic, P/ bca
Unit cell dimensions	a = 15.812(3) Å $\alpha = 90^{o}$
	b = 18.378(4) Å $\beta = 90^{o}$
	c = 20.363(4) Å $\gamma = 90^{o}$
Volume	5917(2) $Å^3$
Z, Calculated density	8, 1.741 Mg/m^3
Absorption coefficient	5.903 mm^{-1}
F(000)	3032
Crystal size	0.30 x 0.20 x 0.10 mm^3
Theta range for data collection	2.43 to 31.43°
Limiting indices	-22<=h<=22, -26<=k<=26, -29<=l<=29
Reflections collected / unique	184530 / 9498 [R(int) = 0.0722]
Completeness to theta = 31.43	96.9 %
Absorption correction	Semi-empirical from equivalents
Max. and min. transmission	0.9800 and 0.5136
Refinement method	Full-matrix least-squares on F^2
Data / restraints / parameters	9498 / 0 / 289
Goodness-of-fit on F^2	1.413
Final R indices [I>2sigma(I)]	R1 = 0.0761, wR2 = 0.1499
R indices (all data)	R1 = 0.0795, wR2 = 0.1512
Largest diff. peak and hole	2.470 and -2.727 e. $Å^{-3}$

Appendix **B**

Crystal data and structure refinement for complex **7**

Identification code	**7**
Empirical formula	C75H150N14S8U
Formula weight	1742.6
Temperature	100(2) K
Wavelength	1.54178 Å
Crystal system, space group	Orthorhombic, P c a 21
Unit cell dimensions	a = 26.3721(9) Å $\alpha = 90^{o}$
	b =17.9946(6) Å $\beta = 90^{o}$
	c = 19.9695(7) Å $\gamma = 90^{o}$
Volume	9476.6(6) $Å^3$
Z, Calculated density	1, 31.221 g/cm^3
Absorption coefficient	6.797 mm^{-1}
F(000)	3672
Crystal size	0.30 x 0.20 x 0.10 mm^3
Theta range for data collection	4.02 to 66.96°
Limiting indices	-29<=h<=31, -21<=k<=21, -22<=l<=23
Reflections collected / unique	14001 [R(int) = 0.0391]
Completeness to theta = 31.43	97.5 %
Absorption correction	direct method
Max. and min. transmission	0.9800 and 0.5136
Refinement method	Full-matrix least-squares on F^2
Data / restraints / parameters	14001 / 1 / 901
Goodness-of-fit on F^2	1.322
Final R indices [I>2sigma(I)]	R1 = 0.0377, wR2 = 0.0844
R indices (all data)	R1 = 0.0413, wR2 = 0.0860
Largest diff. peak and hole	2.529 and -1.294 $e.Å^{-3}$

Appendix **C**

Crystal data and structure refinement for complex **8**

Identification code	**8**
Empirical formula	C88 H200 N12 S8 U
Formula weight	1921.11
Temperature	293(2) K
Wavelength	0.71073 Å
Crystal system, space group	Orthorhombic, P c a 21
Unit cell dimensions	a = 11.4650(5) Å $\alpha = 90^{o}$
	b = 11.4650(5) Å $\beta = 90^{o}$
	c = 22.9311(9) Å $\gamma = 90^{o}$
Volume	3014.2(2) $Å^3$
Z, Calculated density	2, 2.117 Mg/m^3
Absorption coefficient	3.047 mm^{-1}
F(000)	2064
Crystal size	0.30 x 0.20 x 0.05mm^3
Theta range for data collection	1.78 to 25.08°
Limiting indices	-13<=h<=13, -7<=k<=10, -24<=l<=26
Reflections collected / unique	5234 / 815 [R(int) = 0.0267]
Completeness to theta = 25.08	99.1 %
Refinement method	Full-matrix least-squares on F^2
Data / restraints / parameters	815 / 0 / 46
Goodness-of-fit on F^2	1.658
Final R indices [I>2sigma(I)]	R1 = 0.0458, wR2 = 0.1397
R indices (all data)	R1 = 0.0458, wR2 = 0.1397
Largest diff. peak and hole	3.400 and -1.246 $e.Å^{-3}$

Appendix **D**

Crystal data and structure refinement for **9**	
Identification code	**9**
Empirical formula	C33 H36 N10 S5 U
Formula weight	971.05
Temperature	100(2) K
Wavelength	1.54178 Å
Crystal system, space group	Monoclinic, P 21/c
Unit cell dimensions	a = 14.2687(6) Å $\alpha = 90^{o}$
	b = 18.5947(9) Å $\beta = 103.810(2)^{o}$
	c = 15.3116(7) Å $\gamma = 90^{o}$
Volume	3945.1(3) $Å^3$
Z, Calculated density	4, 1.635 Mg/m^3
Absorption coefficient	14.354 mm^{-1}
F(000)	1904
Crystal size	0.30 x 0.20 x 0.10 mm^3
Theta range for data collection	3.189 to 66.942^{0}
Limiting indices	-17<=h<=16, -22<=k<=21, -14<=l<=17
Reflections collected / unique	20737 / 6619 [R(int) = 0.0448]
Completeness to theta = 25.000	90.0 %
Refinement method	Full-matrix least-squares on F^2
Data / restraints / parameters	6619 / 0 / 441
Goodness-of-fit on F^2	1.131
Final R indices [I>2sigma(I)]	R1 = 0.0416, wR2 = 0.1047
R indices (all data)	R1 = 0.0420, wR2 = 0.1052
Largest diff. peak and hole	2.267 and -2.180 e. $Å^{-3}$

Appendix **E**

Crystal data and structure refinement for complex **11**

Identification code	**11**	
Empirical formula	C80 Cs48 N80 O40 S80 U10	
Formula weight	15475.36	
Temperature	293 K	
Wavelength	0.71073 Å	
Crystal system, space group	monoclinic, c/ 2c	
Unit cell dimensions	a = 19.669(4) Å	$\alpha = 90^{o}$
	B = 17.792(4) Å	$\beta = 99.65(3)^{o}$
	c = 23.396(5) Å	$\gamma = 90^{o}$
Volume	8071(3) $Å^3$	
Z, Calculated density	1, 3.184 Mg/m^3	
Absorption coefficient	13.902 mm^{-1}	
F(000)	6752.0	
Theta range for data collection	1 to 25.000	
Limiting indices	-23<=h<=23, -21<=k<=21, -27<=l<=27	
Reflections collected / unique	53707 / 7099 [R(int) = 0.0333]	
Completeness to theta = 25.000	99.7%	
Max. and min. transmission	0.6610 and 0.1900	
Refinement method	Full-matrix least-squares on F^2	
Data / restraints / parameters	7120 / 0 / 412	
Goodness-of-fit on F^2	1.084	
Final R indices [I>2sigma(I)]	R1 = 0.0531, wR2 = 0.1333	
Data R indices (all data)	R1 = 0.0531, wR2 = 0.1333	

Appendix **F**

Crystal data and structure refinement for **13**

Identification code	**13**
Empirical formula	C48 H48 Cl4 Li2 N6 O4 P2 U
Formula weight	1228.57
Temperature	108(2) K
Wavelength	0.71073 Å
Crystal system, space group	Triclinic, P-1
Unit cell dimensions	a = 9.5374(19) Å α= 114.91(3)°
	b = 12.329(3) Å β = 93.92(3)°
	c = 13.578(3) Å γ = 108.10(3)°
Volume	1339.2(5) Å 3
Z, Calculated density	1, 1.523 Mg/m^3
Absorption coefficient	3.335 mm^{-1}
F(000)	606
Crystal size	0.50 x 0.45 x 0.40 mm
Theta range for data collection	1.70 to 31.18°
Limiting indices	-13<=h<=13, -17<=k<=17, -18<=l<=19
Reflections collected / unique	12900 / 6805 [R(int) = 0.0184]
Completeness to theta = 25.00	90.9 %
Absorption correction	Numerical
Max. and min. transmission	0.6610 and 0.1900
Refinement method	Full-matrix least-squares on F^2
Data / restraints / parameters	6805 / 0 / 307
Goodness-of-fit on F^2	1.081
Final R indices [I>2sigma(I)]	R1 = 0.0193, wR2 = 0.0560
R indices (all data)	R1 = 0.0193, wR2 = 0.0560
Largest diff. peak and hole	0.682 and -1.651 e. $Å^{-3}$

Appendix **G**

Crystal data and structure refinement for **14**

Identification code	**14**
Empirical formula	C20 H22 Cl4 N4 O2 U
Formula weight	730.25
Temperature	108(2) K
Wavelength	0.71073 Å
Crystal system, space group	Triclinic, P-1
Unit cell dimensions	a = 8.4466(17) Å α = 111.85(3)°
	b = 9.1058(18) Å β = 91.90(3)°
	c = 9.865(2) Å γ = 115.10(3)°
Volume	621.0(2) $Å^3$
Z, Calculated density	1, 1.953 Mg/m^3
Absorption coefficient	6.988 mm^{-1}
F(000)	346
Crystal size	0.30 x 0.20 x 0.05 mm
Theta range for data collection	2.71 to 31.36°
Limiting indices	-11<=h<=10, -12<=k<=12, -11<=l<=14
Reflections collected / unique	6237 / 3306 [R(int) = 0.0434]
Completeness to theta = 25.00	95.7 %
Absorption correction	Numerical
Max. and min. transmission	1.0000 and 0.4796
Refinement method	Full-matrix least-squares on F^2
Goodness-of-fit on F^2	1.050
Final R indices [I>2sigma(I)]	R1 = 0.0415, wR2 = 0.1060
R indices (all data)	R1 = 0.0418, wR2 = 0.1062
Largest diff. peak and hole	1.432 and -4.142 e. $Å^{-3}$

Appendix **H**

Crystal data and structure refinement for **15**

Identification code	**15**	
Empirical formula	C72 H60 Br4 O8 P4 U2	
Formula weight	1972.78	
Temperature	150(2) K	
Wavelength	0.71073 Å	
Crystal system, space group	Orthorhombic, P2(1)/c	
Unit cell dimensions	a = 9.2695(19) Å	$\alpha = 90°$
	b = 10.430(2) Å	$\beta = 97.91(3)°$
	c = 18.221(4) Å	$\gamma = 90°$
Volume	1, 1744.9(6) $Å^3$	
Density (calculated)	1.877 Mg/m^3	
Absorption coefficient	7.070 mm^{-1}	
F(000)	940	
Crystal size	0.30 x 0.30 x 0.20 mm^3	
Theta range for data collection	2.94 to 24.99°	
Index ranges	-11<=h<=11, -12<=k<=12, -21<=l<=21	
Reflections collected / unique	17097 / 3022 [R(int) = 0.1519]	
Completeness to theta = 24.99°	98.4 %	
Absorption correction	Semi-empirical from equivalents	
Max. and min. transmission	0.5023 and 1.0000	
Refinement method	Full-matrix least-squares on F^2	
Data / restraints / parameters	3022 / 0 / 205	
Goodness-of-fit on F^2	1.150	
Final R indices [I>2sigma(I)]	R1 = 0.1019, wR2 = 0.2766	
R indices (all data)	R1 = 0.1176, wR2 = 0.2991	
Largest diff. peak and hole	4.587 and -2.642 e. $Å^3$	

Appendix **I**

Crystal data and structure refinement for **16**

Identification code	**16**
Empirical formula	$C_{72}H_{60}I_3LiO_4P_4$
Formula weight	1500.72
Temperature	293(2) K
Wavelegnth	0.71073 Å
Crystal system, space group	monoclinic, P 1 21/c 1
Unit cell dimensions	a = 16.4991(9) Å α= 90°
	b = 23.63236(12) Å β = 123.690(2)°
	c = 23.0801(9) Å γ = 90°
Volume	6612.3(6) $Å^3$
Z, Calculated density	4, 1.508 g/cm^3
Absorption coefficient	1.562 mm^{-1}
F(000)	2984
Crystal size	0.050 x 0.200 x 0.300 mm^3
Theta range for data collection	1.48 to 20.44
Limiting indices	-16<=h<=16, -23<=k<=23, -22<=l<=22
Reflections collected / unique	53707 / 6568 [R(int) = 0.0333]
Completeness to theta = 25.000	99.08%
Refinement method	Full-matrix least-squares on F^2
Data / restraints / parameters	6568 / 0 / 751
Goodness-of-fit on F^2	1.070
Final R indices [I>2sigma(I)]	R1 = 0.0288, wR2 = 0.06285578
Data R indices (all data)	R1 = 0.0387, wR2 = 0.0678
Largest diff. peak and hole	0.879 and -0.500 $eÅ^{-3}$

Appendix J

List of Publications:

Synthesis, Structure and Photophysical Properties of $[UO_2X_2(O=PPh_3)_2]$ (X = Cl, Br, I). E. Hashem, T. McCabe, C. Schulzke and R. J. Baker. Dalton Trans., Accepted 2013

DOI: 10.1039/C3DT52480A

Fingerprinting the Oxidation State of U(IV) by Emission Spectroscopy. E. Hashem, G. Lorusso, M. Evangelisti, T. McCabe, C. Schulzke, J. A. Platts and R. J. Baker. *Dalton Trans.*, 2013, **42**, 14677 – 14680

DOI: 10.1039/C3DT52151F

Emission Spectroscopy of Uranium(IV) Compounds: A Combined Synthetic, spectroscopic and Computational Study. E. Hashem, A. N. Swinburne, C. Schulzke, R. Evans, J. A. Platts, A. Kerridge, L. Natrajan and R. J. Baker. *RSC Adv.*, 2013, **3** (13), 4350 - 4361

DOI: 10.1039/C3RA22712J

A Study of the Reactivity of Secondary Phosphanes with Radical Sources: A New Dehydrocoupling Reaction. R. J. Baker and E. Hashem. *Helvetica Chimica Acta.* 2010, **93**, 1081-1085

DOI: 10.1002/hlca.201000114

The Coupling of Pyridine and Dichloromethane Mediated by UO_2Cl_2. R. J. Baker, E. Hashem, M. Motevalli, H. V. Ogilvie, and A. Walshe. *Z. Anorg. Allg. Chem.* **2010**, *636*, 443–445

DOI: 10.1002/zaac.200900342